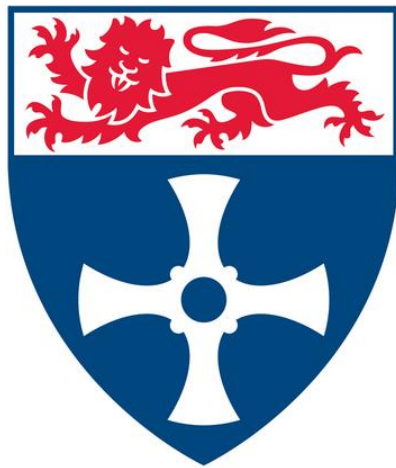


IMPROVING THE TORQUE QUALITY OF A MODULATED POLE MACHINE



NABEEL AHMED

A thesis submitted for the degree of

Engineering Doctorate

Newcastle University 2016

School of Electrical and Electronic Engineering

ABSTRACT

Nabeel Ahmed: Improving the Torque Quality of a Modulate Pole Machine

(Under the supervision of Dr. Glynn Atkinson and Dr. Nick Baker)

The research work carried out in this thesis is collaboration between Newcastle University and Höganäs AB, Sweden.

A topology, termed ‘Separate Phase MPM’ was initially developed by Newcastle University and Höganäs where the machine takes advantage of mutual flux paths in order to increase the torque density of the machine, however had high cogging torque and back EMF harmonic content. The work presented in this thesis was carried out with an overall aim to minimise the cogging torque and back EMF harmonics in the Modulated Pole Machine (MPM) topology aimed toward electric bicycles.

Various techniques are proposed and verified in this thesis to reduce the magnitude of unwanted voltage and torque harmonics, providing a smoother riding experience. Finite Element Analysis was carried out using Infolytica MagNet® on various design techniques which ultimately stemmed in 24 motor prototypes being constructed and tested during this PhD. The measured results are compared with each other to approve the technique that provides the optimum motor performance.

It is shown that the peak cogging torque is reduced by 90% while the back EMF harmonics are diminished too, with a minor 2% reduction in mean back EMF. The efficiency and peak torque of the optimum motor is 8% and 10% higher, respectively, when compared with the base motor used in this study.

ACKNOWLEDGEMENT

This work has been carried out under the kind supervision of Dr. Glynn Atkinson and Dr. Nick Baker, University of Newcastle upon Tyne, U.K. I am thankful for their most sincere and valuable guidance, benevolence and cooperation during whole of my research. Their continued interest and support contributed a lot to make this research a success.

I am heartily grateful also to all the Höganäs team; especially Dr. Jamie Washington, Dr. Lars Sjöberg, Dr. Cristofaro Pompermaier and Dr. Lars-Olov Pennander for their constructive suggestions, precious assistance, encouragement and help at every stage of this research work.

I express my deep gratitude to all the technicians, the laboratory staff, the tutors and the receptionists at the School of Electrical, Electronic and Computer Engineering and Höganäs AB for providing me all the facilities to successfully complete this project.

I extend my thanks to Professor Barrie Mecrow, Head of The School of Electrical and Electronic Engineering at Newcastle University, for providing me this opportunity, and to all those teachers who contributed towards the elevation of my knowledge in Engineering up to the level that I could accomplish my research and degree in the present form.

I would like to thank my parents and brothers for giving me time and space to complete my research which sometimes meant returning home late in nights. None of this would have been possible without the support of my family, who at every step guided and believed in me. I dedicate this PhD to my mother, it was her dream to see me as a PhD doctor and I have no shame in admitting that without her motivation, love and affection, I could not have completed this work. A special thanks to my Father who has been my backbone throughout my life and have raised me to this stage in life where I could have completed my PhD.

And lastly, I would like to thank my best friend, Hira Saqib for her moral support at times when I needed it the most. It would not have been possible to go through this journey without her presence, backing and prayers.

Table of Contents

1 Introduction

1.1 Project Background.....	1
1.2 Modulated Pole Machines.....	2
1.3 Objective of this Thesis	4
1.4 Structure of the Thesis	5
1.5 Published work.....	6

2. Literature Review

2.1 Introduction.....	7
2.2 First generation of Electrical Machines	9
2.3 Second generation of Electrical Machines	12
2.3.1 Single sided machines.....	13
2.3.2 Double sided machines	15
2.3.3 Multi-Phase Machines	18
2.4 General properties of Transverse Flux Machines	19
2.5 Soft magnetic composite – MPM	20
2.5.1 Production of SMC Somaloy	20
2.5.2. Properties	22
2.6 Material Hybrid Machines	24
2.7 Cogging torque.....	26
2.8 Literature Review Summary	28

3. Base Machine Torque Quality

3.1 The Base machine for comparison.....	30
3.2 Base machine performance	34
3.3 Problem Statements	37
3.3.1 Cogging Torque	37

3.3.2 Factors affecting cogging torque	39
3.3.3 Back EMF	40
3.3.4 Torque Ripple	40
3.4 Summary	42
4. Design Investigation	
4.1 FEA – Mesh Sensitivity Analysis	44
4.2 FE Models vs. Prototypes	45
4.3 Tooth tip span alteration and combinations	47
4.4 Reduction of cogging torque and torque ripple	56
4.5 Conclusion	59
4.6 Pitching the Stator components	60
4.7 Cogging Torque	61
4.8 Back EMF	65
4.9 Combination of tooth span and pitching techniques	68
4.10 Pole Piece Designs	73
4.5 Conclusion	78
5. Construction and Assembly of Prototypes	
5.1 Introduction	81
5.2 Stator Construction	84
5.2.1 Laminations	84
5.2.2 SMC Stator components	87
5.2.3 The SMC Core-back	89
5.2.4 Shaft mounted Hub	90
5.2.5 The Shaft	91
5.2.6 Coils	92
5.3 Stator Assembly	94
5.4. Rotor types and Assembly	96
5.5 Final Assembly	98
6. Testing of Prototypes - harmonic effects	
6.1 Measurement setup – Test benches	99
6.11 Cogging Torque test bench	99
6.12 Dynamometer test bench	100

6.2 Cogging Torque	103
6.2.1 Laminate Stators	103
A) Base Rotor (R1)	103
B) Convex pole pieces – R4.....	105
C) Wave Direction Pole pieces – R5	106
D) Split Rotor (R2)	107
6.2.2 SMC Stators	109
A) SMC stator chamfered teeth (S5)	109
B) SMC 6 th and 12 th pitched Stator (S6)	113
6.2.3 Summary Cogging Torque.....	115
6.3 Back EMF	120
6.3.1 Laminate Stators (S1 to S4)	121
A) Basic rotor (R1)	121
B) Convex Rotor (R4).....	122
C) Wave direction (R5).....	123
D) Split Rotor (R2)	124
6.3.2 SMC Stators (S5 to S7).....	126
6.3.3. Back EMF Summary.....	129
7. Performance measurements	
7.1. Torque Speed Envelope	132
7.1.1: Laminate Stators	132
7.1.2 SMC Stators	134
7.1.3 Summary	137
7.2 Efficiency	138
7.2.1 Laminated Stators	139
7.2.2 SMC Stators	139
7.2.3 Summary – Efficiency vs. Torque	141
7.3. Conclusion	142
8. Combined Phase MPM	
8.1 Combined Phase vs. Separate Phase MPM.....	146
8.2 Induced back EMF.....	147
8.3 Cogging Torque	150

8.4 Torque Ripple	152
8.5 Combination of tooth spans	153
8.6 Conclusion	159
9. Summary and Conclusions	
9.1 Background	160
9.2 Design and Construction	161
9.3 Future work recommendations	164
9.4 Published work	167
References	170
Appendix A – Stator component	184
Appendix B – The Shaft	186
Appendix C – Cogging Torque Test Bench Rig Drawings	187
Appendix D – Motor Test Bench Rig drawings	188
Bearing Shield – Cable Side	189
Bearing Shield – Coupling Side	190
Pole piece designs	191

List of Figures

Chapter 1

Figure 1. 1: Illustration of the MPM used in the rear wheel of Höganäs electric bike	2
Figure 1. 2: Two pole section of a single phase showing a complete magnetic circuit from (1) to (7)	3
Figure 1. 3: Illustration of changing the pole number of a modulated pole machine and its 'global' coil linking the flux of every pole.....	4
Figure 1. 4: Simplified CAD drawing of the previously constructed MPM.....	5

Chapter 2

Figure 2. 1: Mordey's electric generator (left) in 1890 and another rotor topology (right) [1]	9
Figure 2. 2: Diagram of Tesla's high frequency generator [36].....	11
Figure 2. 3: Diagrams from patent of E. F. W. Alexanderson showing 100 kHz alternator [40]	12
Figure 2. 4: A single sided modulated pole machine arrangement designed by Weh [42]	14
Figure 2. 5: Magnet utilisation in a single sided Modulated Pole machine by M. Bork et al [45]; solid rotor (left), separated rotor parts (right).....	15
Figure 2. 6: A double sided MPM with flux concentrating rotor in a zero torque position; rotor iron pieces and U cores are aligned [41]	16
Figure 2. 7: Various Claw pole Modulated Pole Machines	17
Figure 2. 8: Two examples of multiple phase MPMs; Mecrow's [69] multiple phase MPM (left), Cros's [72] hybrid multiphase MPM (right).....	19
Figure 2. 9: Schematic of Somaloy powder (SMC particles) with lubricant coating [73]	21
Figure 2. 10: Three steps involved in compacting the powder [74].....	21
Figure 2. 11: Illustration of operating induction level of Somaloy as a function of operating frequency in comparison with steel sheets and ferrites.	23
Figure 2. 12: : Comparison of resistivity of Somaloy with different materials.	24
Figure 2. 13: Jack et al [80] Material Hybrid machine made from compacted iron powder and laminations....	26

Chapter 3

Figure 3. 1: CAD model of the base machine assembled 3-phase stator	30
Figure 3. 2: CAD model of the base machine rotor	31
Figure 3. 3: Finite Element axial view of a three-phase MPM with axial separation.....	32
Figure 3. 4: Static Torque characteristics of the base machine design prototype over two pole pitches (28.8 mechanical degrees).....	34
Figure 3. 5: Back EMF of all three phases of the base machine design taken under no load conditions with the rotor rotating at 200rpm.....	36
Figure 3. 6: Torque waveform of the base machine design prototype over two pole pitches (28.8 mechanical degrees) when supplied with 20A	37
Figure 3. 7: The cogging torque of a Single Phase MPM over one electrical cycle [133]	39

Chapter 4

Figure 4. 1: 3DFE solid model of a two-pole segment of the MPM.....	47
Figure 4. 2: Illustration of the tooth span of an MPM (where x is 160° span, x' is 120° span, y is magnet thickness off 3.9mm, s is the pole span off 4° , m is the magnet height off 3.5mm and z is the pole piece height off 4.3mm).....	48
Figure 4. 3: Magnitude of cogging torque harmonics in the three-phase MPM with varying tooth span	48
Figure 4. 4: Harmonic content of cogging torque with changes in tooth span	50
Figure 4. 5: Cogging torque of the three-phase MPM with 130° and 170° spans.	50
Figure 4. 6: Variation in back EMF waveform with tooth span.....	51

Figure 4. 7: A tooth span of 180° (right) covering a significant area of rotor magnet causes an increased flux leakage between the tooth and the magnet compared to a tooth span of 120° (left).....	52
Figure 4. 8: Harmonic content of back EMF waveform with tooth span.	53
Figure 4. 9: Torque ripple as a percentage of average torque.....	54
Figure 4. 10: Three-phase torque waveform for 130° and 170° tooth span.....	54
Figure 4. 11: Cogging torque waveforms for a 120° and 180° span machine	55
Figure 4. 12: Harmonic content of cogging torque with a combination of tooth spans	56
Figure 4. 13: Illustration of the two tooth span combinations; combination 1 on left, combination 2 on right...	57
Figure 4. 14: Cogging torque waveform with a combination of tooth spans	58
Figure 4. 15: Illustration of pitching angle Ω	60
Figure 4. 16: Illustration of a 2 pole pairs fully pitched MPM (left) and a MPM pitched by 30° electrical (right)	61
Figure 4. 17: Comparison of cogging torque waveforms for fully pitched and 6th pitched models of MPM.....	62
Figure 4. 18: Illustration of a 2 pole pairs MPM pitched by 15° and 30° electrical (6th and 12th harmonic)	63
Figure 4. 19: Cogging Torque waveforms comparison of 6th pitched and 6th &12th pitched models	64
Figure 4. 20: Cogging Torque harmonic contents of 6th pitched and 6th &12th pitched models (6 th and 12 th harmonics zoomed in for the two new models).....	64
Figure 4. 21: Back EMF waveforms for the three phases of the fully pitched model.....	66
Figure 4. 22: Comparison of Phase B back EMF waveforms for fully pitched and 6th and 12th pitched models, 5 th and 7 th harmonics displayed	67
Figure 4. 23: Comparison of fundamental, fifth and seventh harmonic for Phase B of a fully pitched and 6th and 12th pitched models (per unit fully pitched model)	67
Figure 4. 24: Variations in peak cogging torque and its harmonics as tooth span is varied while pitched for 6th harmonic.....	69
Figure 4. 25: Variations in back EMF harmonics as tooth span is varied while pitched for 6th harmonic.....	70
Figure 4. 26: Cogging Torque waveforms for the base design machine (130° tooth span fully pitched), 130° tooth span and 6th pitched lamination and combination of three tooth spans with 6th pitching (TSC + 6 th pitched).....	71
Figure 4. 27: Back EMF waveforms for inner phase of the base design machine (130° tooth span and fully pitched) and combination of tooth spans with 6th pitching	71
Figure 4. 28: Comparison of the original unmodified machine with the machine made of a stator with combination of tooth span and pitching	72
Figure 4. 29: Various Pole designs under investigation to reduce the harmonic content in cogging and back EMF waveforms.....	75
Figure 4. 30: Comparison of percentage peak cogging torque and back EMF for various pole designs per unit of base machine model (unmodified pole piece).....	76
Figure 4. 31: Comparison of cogging torque waveforms for the unmodified, convex and direction 5 pole piece designs	77
Figure 4. 32: Comparison of harmonics of the unmodified, convex and direction 5 pole piece designs per unit of base pole design	78
Figure 4. 33: Comparison of cogging torque and its harmonics for various techniques investigated in this section (base design, combination of three tooth spans, 6th and 12th pitched laminations, laminations made of combination of tooth spans and 6th pitched, modified pole pieces of convex and direction 5 type)	79
Figure 4. 34: Comparison of mean back EMF, its harmonics and average Torque for various techniques investigated in this section (base design, combination of three tooth spans, 6th and 12th pitched laminations, laminations made of combination of tooth spans and 6th pitched, modified pole pieces of convex and direction 5 type).....	80

Chapter 5

Figure 5. 1: Gluing jig placed in the oven for heat treatment with lamination stack inserted; four bolts and the spacers visible too	84
Figure 5. 2: Wire Eroding jig with glued laminations bolted between two plates.....	85
Figure 5. 3: Base stator - Single tooth span unpitched lamination – S1	85
Figure 5. 4: Lamination made of combination of 3 tooth spans – S2.....	86
Figure 5. 5: Lamination made of 3 tooth spans combination and 6th pitched – S3	86
Figure 5. 6: 6th and 12th pitched lamination – S4.....	86

Figure 5. 7: CAD illustration of SMC stator component with new type of coil exit	87
Figure 5. 8: CAD illustration of new SMC stator component, coil sandwiched between two stator components	87
Figure 5. 9: CAD Illustration of SMC chamfered teeth – S5.....	88
Figure 5. 10: 6th and 12th pitched SMC stator component – S6.....	88
Figure 5. 11: Core-back prototype manufactured from SMC, notches and slot visible – lamination compressed and fitted too.....	89
Figure 5. 12: Central hub of the machine fitted over the shaft.....	90
Figure 5. 13: Prototype representation of the shaft and central hub displaying the exit holes, threaded end, bearing seat and coil exits	91
Figure 5. 14: Prototype coil showing 17 turns.....	92
Figure 5. 15: Prototype lamination, coil and core-back fitted together, coil exiting through the lamination and core-back slots, Nomex providing insulation between coil and laminations.....	93
Figure 5. 16: Machine Stator during assembly	95
Figure 5. 17: Stator coil wires soldered and second end cap screwed to press the stator components	95
Figure 5. 18: View of the complete stator assembly.....	95
Figure 5. 19: Different views of simple rotor consisting magnets and pole pieces and end plates	96
Figure 5. 20: Split Rotor prototype	96
Figure 5. 21: Rotor with a cut of 0.04mm for increased air gap in inner phase	97
Figure 5. 22: CAD models of Convex (top) and wave direction (bottom) pole piece designs	97
Figure 5. 23: Prototype rotor with convex pole pieces.....	97
Figure 5. 24: CAD version of machine assembly showing the stator components, rotor, shaft and inner hub....	98

Chapter 6

Figure 6. 1: Cogging Torque test bench.....	100
Figure 6. 2: Motor Test Bench.	101
Figure 6. 3: Instrument rack for the motor test bench.....	102
Figure 6. 4: Comparison of cogging torque waveforms of four laminate stator types with simple rotor.....	103
Figure 6. 5: Comparison of cogging torque waveforms of four laminate stator types with rotor R4.	105
Figure 6. 6: Comparison of cogging torque waveforms of four stator types with R5.....	106
Figure 6. 7: Comparison of cogging torque waveforms of stators S1 and S2 with rotors R1 and R2.....	107
Figure 6. 8: Comparison of cogging torque waveforms for S1R1 (base model) and S5R1	109
Figure 6. 9: Comparison of cogging torque waveforms for S5R1, S5R4 and S5R5	110
Figure 6. 10: Comparison of cogging torque waveforms for S5R1, S5R2 and S5R3	111
Figure 6. 11: Comparison of cogging torque waveforms for S5R1 and S7R1.....	111
Figure 6. 12: Comparison of cogging torque waveforms for the two SMC stators	113
Figure 6. 13: Comparison of cogging torque waveforms for S6 with R1, R2, R4 and R5.....	114
Figure 6. 14: Comparison of peak cogging torque per unit of base model for all the motors tested	115
Figure 6. 15: Comparison of 2nd harmonic of peak cogging torque per unit of base model for all the motors tested.....	116
Figure 6. 16: Comparison of 4th harmonic of peak cogging torque per unit of base model for all the motors tested.....	117
Figure 6. 17: Comparison of 6th harmonic of peak cogging torque per unit of base model for all the motors tested.....	118
Figure 6. 18: Comparison of 12th harmonic of peak cogging torque per unit of base model for all the motors tested.....	118
Figure 6. 19: Harmonic content for the base and optimised motor designs.....	119
Figure 6. 20: Illustration of back EMF waveforms of phase 2 for four laminated stators with R1.....	121
Figure 6. 21: Variation in back EMF waveforms with different laminated stators with R4.....	122
Figure 6. 22: Variation in back EMF waveform with four laminated stators and R5	123
Figure 6. 23: Variation in back EMF waveform with two laminated stators and R2.....	124
Figure 6. 24: Illustration of back EMF waveforms for S5 with different rotors.....	126
Figure 6. 25: Variations in Back EMF waveforms for S6 and four rotors	127
Figure 6. 26: Comparison of mean back EMF per unit of base model for all the motors tested.....	129
Figure 6. 27: Comparison of 5th harmonic of mean back EMF per unit of base model for all the motors tested	130

Figure 6. 28: Comparison of 7th harmonic of mean back EMF per unit of base model for all the motors tested	131
--	-----

Chapter 7

Figure 7. 1: Illustration of Torque Speed envelope for S3 with R1, R4 and R5	133
Figure 7. 2: Illustration of Torque Speed envelope for S4 with R1, R4 and R5	134
Figure 7. 3: Illustration of Torque speed curves of S5 with different rotors	135
Figure 7. 4: Illustration of back Torque speed waveforms for S6 with different rotors	136
Figure 7. 5: Summary of all motors for Peak torque produced per unit of a 40 Nm motor (S1R1).	137
Figure 7. 6: Efficiency vs. Torque waveforms of S3 (left) and S4 (right) with R1, R4 and R5	139
Figure 7. 7: Efficiency vs. Torque curves for S5 with R1, R2, R3, R4 and S7 with R1	140
Figure 7. 8: Efficiency vs. Torque curves for S6 with with R1, R2, R3 and R4	140
Figure 7. 9: Summary of efficiency of all motors in the study	141

Chapter 8

Figure 8. 1: Axial view of a separate phase MPM (top) and a combined phase MPM (bottom)	146
Figure 8. 2: Three dimensional FE comparison of the induced back EMF in one coil of the SP and CP machines	148
Figure 8. 3: Harmonic content of back EMF waveform with tooth span for SP and CP topologies.	148
Figure 8. 4: Harmonic contents of inner and outer coils EMF (7th harmonic zoomed in)	149
Figure 8. 5: Three dimensional FE no-load flux linkage for phase A of the SP and CP machines	150
Figure 8. 6: Magnitude of cogging torque harmonics in the three-phase MPM with varying tooth span	151
Figure 8. 7: Comparison of peak cogging torque for SP and CP topologies	152
Figure 8. 8: Comparison of torque ripple for SP and CP topologies.....	153
Figure 8. 9: Illustration of tooth span combinations for reducing 7th harmonic in back EMF	154
Figure 8. 10: Back EMF waveforms for 120°, 180° and the resultant waveform of summing the two together	155
Figure 8. 11: Harmonic content of back EMF waveforms from a combination of tooth spans with 7th harmonics zoomed in.....	155
Figure 8. 12: Cogging torque waveforms for a 120°, 150°, 180° and combination of tooth span	156
Figure 8. 13: Comparison of 2nd and 4th harmonic content of cogging torque waveforms for 120°, 150° and 180° span with combination of tooth span.....	157
Figure 8. 14: Assembled stator; Separate Phase MPM (left) and Combined Phase MPM (right).....	159

Chapter 9

Figure 9. 1: Comparison of the optimum currents and the sinusoidal currents	165
Figure 9. 2: Comparison of cogging torque harmonics for sinusoidal and profiled current waveforms shown in Figure 9.1	166

List of Tables

Chapter 3

<i>Table 3. 1: The major dimensions of the separate phase motor</i>	33
<i>Table 3. 2: Static Torque harmonic content of the base machine design (as a percentage of rated torque)</i>	35
<i>Table 3. 3: Harmonic content of back EMF waveforms for the three phases</i>	36
<i>Table 3. 4: Comparison of peak Voltages of the base machine</i>	36
<i>Table 3. 5: Misalignment of the three phases of the base machine (electrical degrees)</i>	37
<i>Table 3. 6: Summary of various base machine output values to be compared to newer topologies</i>	42

Chapter 4

<i>Table 4. 1: Illustration of 6th and 12th harmonics being the main ones contributing to the overall cogging torque</i>	49
<i>Table 4. 2: Tooth Combinations – Number of teeth of each span</i>	57
<i>Table 4. 3: Summary of different combinations of tooth span (Combination 1 comprises of three tooth spans while Combination 2 is made up of two different tooth spans – details of each combination presented in Table 4.2)</i>	59
<i>Table 4. 4: Comparison of the major harmonic in the fully pitched, 6th pitched and 6th &12th pitched models (percentage reductions from the fully pitched model)</i>	65
<i>Table 4. 5: Comparison of the three phases back EMF harmonic content of the fully pitched model</i>	66

Chapter 5

<i>Table 5. 1: Combination of prototype stators and rotors</i>	82
--	----

Chapter 6

<i>Table 6. 1: Comparison of Peak cogging torque and its harmonic content for laminate stators and simple rotor</i>	104
<i>Table 6. 2: Comparison of Peak cogging torque and its harmonic content for four laminated stators and R4</i> . 105	
<i>Table 6. 3: Comparison of Peak cogging torque and its harmonic content for four laminated stators and R5</i> . 107	
<i>Table 6. 4: Comparison of Peak cogging torque and its harmonic content for two laminated stators with R1 and R2</i>	108
<i>Table 6. 5: Comparison of base model with the best solution of laminated stator</i>	108
<i>Table 6. 6: Comparison of Peak cogging torque and its harmonic content for S5 with five type of rotors and S7 with R1</i>	112
<i>Table 6. 7: Comparison of Peak cogging torque and its harmonic content for for S6 with R1, R2, R4 and R5</i> . 114	
<i>Table 6. 8: Comparison of Cogging Torque of the base motor and the most optimised motor</i>	119
<i>Table 6. 9: Harmonic content of back EMF waveform for laminated stators with R1</i>	121
<i>Table 6. 10: Harmonic content of back EMF waveform for laminated stators with R4</i>	122
<i>Table 6. 11: Harmonic content of back EMF waveform for laminated stators with R5</i>	124
<i>Table 6. 12: Harmonic content of back EMF waveform for laminated stators with R2</i>	125
<i>Table 6. 13: Harmonic content of back EMF waveform for S5 with various rotors and S7 with R1</i>	127
<i>Table 6. 14: Harmonic content of back EMF waveform for S6 and four rotors</i>	128

Chapter 7

<i>Table 7. 1: Peak Torque produced by each laminated motor.....</i>	<i>134</i>
<i>Table 7. 2: Peak Torque produced by each SMC motor.....</i>	<i>136</i>
<i>Table 7. 3: Measured results for all motors tested in this thesis compared against the base motor (S1R1).....</i>	<i>143</i>
<i>Table 7. 4: Comparison of base design with the most optimised motor, consisting of SMC 6th and 12th pitched stator and convex pole shaped rotor pole pieces; percentage difference between the important parameters shown.....</i>	<i>145</i>

Chapter 8

<i>Table 8. 1: Tooth Combinations – Number of teeth of each span.....</i>	<i>156</i>
<i>Table 8. 2: Comparison of base model with 120° tooth span and the model using combinations of tooth span</i>	<i>158</i>

Chapter 9

<i>Table 9. 1: Comparison of results of the base motor with the most optimised motor made</i>	<i>163</i>
---	------------

1. Introduction

This three year PhD was sponsored by Höganäs AB of Sweden. Höganäs is a company specialising in the production of metal powders. It was part of the sponsorship that the research student visits Höganäs Sweden at least once a year to carry out practical research activities in the highly advanced Höganäs laboratories. These research visits to the company were aimed to help the student understand and implement the practical aspects of research while gaining vital industrial experience.

1.1 Project Background

Metal powders are used in thousands of applications, products and solutions that are part of our everyday lives. Höganäs utilizes this vast market and develops new or better products by pushing the limits of metal powders. One such powder is Soft Magnetic Composite (SMC), the internationally recognised name for pressed and heat-treated metal powder components with three-dimensional (3D) magnetic properties. Somaloy® is the Höganäs brand for SMC materials, offering a wide material portfolio to fulfil the requirements of different electromagnetic applications such as electric motors, fast switching actuators or inductor cores for power electronics. A detailed discussion on SMC will be presented in Chapter 2.

The Electromagnetic Applications Department of Höganäs AB and a previous Engineering Doctorate funded student manufactured a new electrical machine topology using SMC. This electrical machine was termed a ‘Modulated Pole Machine’ (MPM) and was used as a motor in the front or rear wheel of a Höganäs electric bicycle, shown in Figure 1.1. This electrical assisted bicycle aids the rider by providing extra power and making the journey significantly easier.

The previous student (Dr. Jamie Washington [133]) developed a machine topology that provides a high torque at low rotation speed using Soft Magnetic Composites. This topology however had a high cogging torque and back EMF harmonics which introduced jerkiness and

vibrations into the ride and Höganäs want to minimise these effects to enhance the rider experience.



Figure 1. 1: Illustration of the MPM used in the rear wheel of Höganäs electric bike

1.2 Modulated Pole Machines

Modulated Pole Machines (MPMs) are a well-known machine topology, the use first suggested in the 1890s [1] with further recent development beginning in the 1980s with Weh [2]. The term “Modulated Pole Machine” captures all machine types where the field generated by a coil is guided or “modulated” into a multi-pole field, by a toothed iron structure placed either side of it, where the number of poles are equal to the number of guiding teeth. This is a property exploited by a number of machine types such as Transverse Flux [2-5] and Claw Pole [6-8] machines.

These machine types are considered as viable options for electric and hybrid propulsion applications due to their ability to produce high power densities. Many automotive companies and manufacturers employ their R&D to focus on projects producing efficient and cost effective designs [9 – 13].

MPMs refer to structures where the armature only takes flux from one side of the surface mounted magnets and a return flux path is provided in the form of an iron core-back. The flux path of a two-pole section of a Transverse Flux Machine is illustrated in Fig. 1.2. Flux from the magnets (1) is grouped and directed into the ‘north’ pole piece (2), navigating axially,

crossing the air gap into tooth (3). It then returns around the core back (4), via the opposite tooth (5) placed at an angle of 180° electrical, crossing the air gap to the 'south' pole piece (6) this time and across the magnet to completely enclose the coil (7) and complete the magnetic circuit.

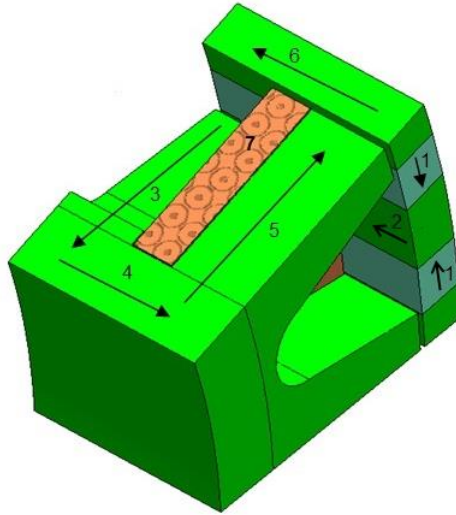


Figure 1. 2: Two pole section of a single phase showing a complete magnetic circuit from (1) to (7)

MPMs are known for their ability to produce a high torque density (up to five times that of conventional machine geometries) relative to their volume. This is made possible by utilising 3D flux paths as well as the decoupled nature of electrical and magnetic circuits in MPMs; if all other factors remain the same an increase in pole number leads to an increase in the overall magneto motive force (MMF) of the machine. This is due to the fact that the MMF of the coil is seen across all of the poles, no matter how many there are.

When a constant current density and outer diameter are considered, the magnetic and electric loading in a conventional machine is determined by the choice of tooth width and slot area respectively. This means that changing one will vary the other; the fine balance between the two will be disturbed as they share the same cross sectional space.

By comparison, MPM's advantage lies in the fact that the coil and tooth do not occupy the same plane, resulting in the magnetic and electrical loadings to be set largely independent of each other [2], giving greater flexibility of design and hence benefit with regard to high pole numbers when designing MPMs [14]. As the pole number increases, the flux per pole reduces by the same proportion, but as the coil links the flux of every pole, the flux linking the coil is unchanged as shown by figure 1.3.

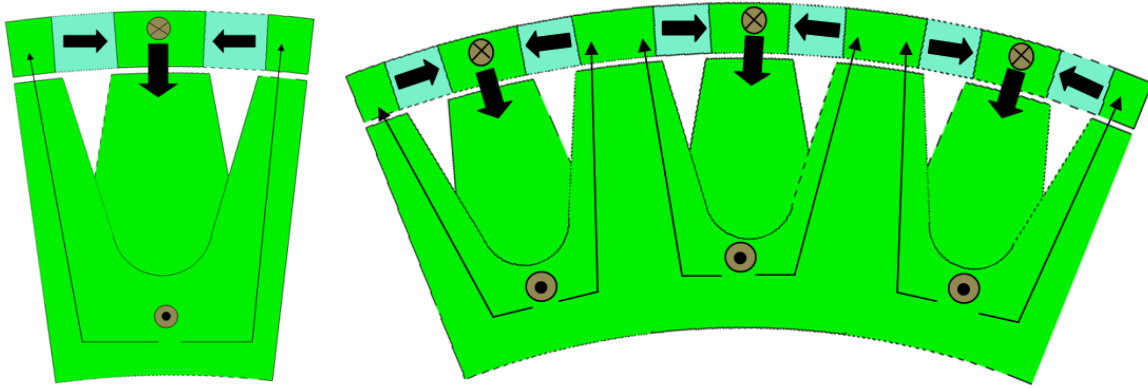


Figure 1. 3: Illustration of changing the pole number of a modulated pole machine and its 'global' coil linking the flux of every pole

As the Magneto-Motive Force (MMF) of the coil is seen across every pole of the machine, this high pole number allows for a greater electrical loading and therefore an increase in torque for a given volume [6] with relatively low winding losses [2, 8, 15].

High pole numbers cause high electrical frequency, resulting in a reduction in drive and machine efficiency. In addition, complex construction is required to fully harness three-dimensional magnetic fields [16]. Resulting machines tend to have high leakage fluxes and low power factor [17] caused by high armature reactance. MPMs are particularly suited to applications where low speed and high torque is required; for example electric traction [18, 19] and renewable energy generation [20, 21].

Two common problems of MPM are the high harmonic content of back EMF and cogging torque and the torque ripple [3, 21]. Both create undesirable noise and vibrations and hence reducing their magnitude is important. This thesis proposes several novel techniques where it is shown that cogging torque, torque ripple and harmonic content can all be significantly reduced without a significant effect on the overall torque output.

1.3 Objective of this Thesis

Despite intensive research effort in the recent years focusing on transverse flux permanent magnet modulated pole machines, high cogging torque still presents a major drawback [3]. The aim of this thesis is to reduce the cogging torque and the harmonic content of the back EMF waveform in the previously mentioned Modulated Pole Machine; shown in Figure 1.1 and 1.4. Several techniques will be implemented and prototypes will be constructed to test, validate and improve the torque quality of the machine as well as the overall technology.

1.4 Structure of the Thesis

Chapter 2 will present the literature review of the work done in this field previously with an aim to build on it. Chapter 3 will discuss the base machine design of the machine constructed previously and provides the problem statements of the thesis. Chapter 4 will look deeper into the design investigation of the novel techniques that will be used to reduce the unwanted harmonics in the cogging torque and back EMF. Analysis will be provided on the design rule for cogging torque, back EMF and their harmonics by carrying out Finite Element analysis (FEA) using the software MagNet™. Construction of the prototypes will be shown in Chapter 5 while Chapter 6 and 7 will provide a detailed study into the results and verification of prototypes. Chapter 8 will provide implementation of one novel technique onto a ‘Combined Phase’ (second generation) topology of this motor type while Chapter 9 will be the concluding chapter.

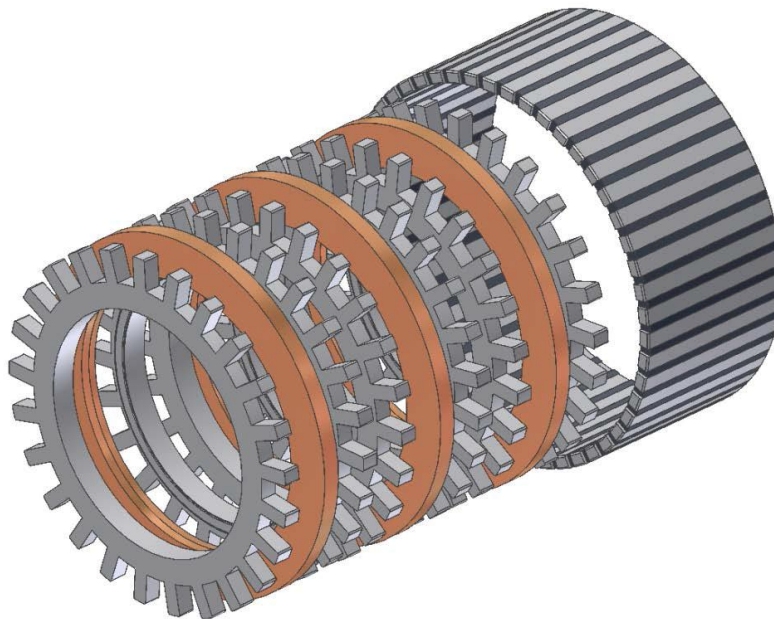


Figure 1. 4: Simplified CAD drawing of the previously constructed MPM

1.5 Published work

Following is a list of published work stemmed from the research carried out during this PhD.

1. Ahmed, N; Atkinson, G. J. ; Baker, N. J. ; Sjöberg, L. **“Flux Switching Modulated Pole Machine topologies which offer greater mechanical simplicity”**, Electrical Machines and Drives Conference (IEMDC), 2013 IEEE International on, pp. 354 – 358, May 2013
2. Ahmed, N; Washington, J. ; Atkinson, G. J. ; Baker, N. J. **“Reduction of cogging torque and torque ripple in Modulated Pole Machines by geometrical changes”**, Power Electronics, Machines and Drives (PEMD 2014), 7th IET International Conference on, pp. 1 – 6, April 2014.
3. Ahmed, N; Atkinson, G. J. ; Baker, N. J. ; Sjöberg, L. **“Reduction of Cogging Torque and back EMF harmonics in Modulated Pole Machine by variations in Tooth span,”** Electrical Machines and Drives Conference (IEMDC), 2015 IEEE International on, May 2015
4. Nabeel Ahmed, Glynn Atkinson. **“Low Ripple TFM feasibility study for BAFCO”**, January 2016. The Big Ass Fan Corporation (BAFCO) requested that Newcastle University carry out a feasibility on two TFM topologies, the aim being to produce feasible designs with high efficiency and low torque ripple.
5. Nabeel Ahmed, *Cristofaro Pompermaier, Jamie Washington, Lars Sjöberg.* **“Reduction of Cogging Torque in Transverse Flux Machines by Stator and Rotor Pole Shaping”**, *IEEE Energy Conversion Congress and Expo, Sept 18-22, Milwaukee, WI, USA.*

This PhD produced various novel design techniques to reduce the cogging torque and back EMF harmonic. 24 motor variants were constructed and tested to approve these techniques and ultimately one optimum motor was chosen that reduced the peak cogging torque by 90%; the efficiency and peak torque of the optimum motor is 8% and 10% higher, respectively, when compared with the base motor used in this study.

2. Literature Review

2.1 Introduction

Electrical machines can be thought of as a conversion device from electrical energy to kinetic energy; a two-way mutual link is formed by the magnetic field. The energy is temporarily stored in the magnetic field before being converted. It is important to note that apart from the flow of current, the reaction in the electrical system is inductions of an EMF while the product of this and current gives the rate of electrical energy conversion.

The key to unified machine theory is the principle of increasing the stored magnetic energy. In order to increase the flux and the stored energy, a force of attraction will act to bring the poles together to minimise the reluctance of the air gap in the magnetic circuit.

Magnetic systems try to optimise the stored energy by distorting the magnetic core either by closing air gaps or by aligning poles. The former is associated with forces of attraction and the latter with forces of alignment. Rotating machines are based on the force of alignment principle.

When the poles are not situated opposite one another, there is a lateral force of alignment to attract poles towards each other, or align laterally to achieve greater stored magnetic energy i.e. when the poles are in contact with the maximum area of contact. This lateral movement of poles increases the area of air gap, hence reducing the reluctance. It should however be noted that this force does not necessarily act in the direction of the lines of flux.

In 1890 [1], W. M. Mordey suggested a design which consisted of a hoop coil surrounded by numerous U and I shaped laminated iron cores with a wound field rotor. A machine where a ring coil creates a two pole field and guides this by an iron structure into a multi-pole arrangement is known as Modulated Pole Machine (MPM) [22]. The coil at this multi-pole arrangement links together the flux from individual poles creating a multiplex of poles and hence the MMF of the coil can be seen across every pole. This concept allows increasing the

specific torque by increasing the magnetising field strength which is achieved by increasing the pole number without actually changing the volume or speed of the machine [24 - 27].

Two forms of MPMs are Transverse Flux (TF) and Claw Pole (CP) machines which have been around since the late 19th century. TF machines were first put forward by Weh in his two papers [2, 24] in the 1980s in which he explains that the flux ‘transverses’ the direction of the rotor for a part of the magnetic circuit. TF and CP machines have flux paths that are 3D and hence their construction using 2D laminations is difficult. However due to the recent emergence of soft magnetic composites, research is being carried out in this area and new topologies have come into existence.

MPMs ability to provide high torque density (for direct drive systems), low current density yet high electrical loading [6] by merely having a high pole number, makes it a very useful machine. These can offer as high as five times the torque density of conventional radial machine geometries [2] as the magnetic and electrical circuits are effectively decoupled. This is due to the availability of adjusting the coil slot and iron in the teeth independently as they do not share the same plane, hence changing the pole number has no effect on the area available for the winding. This is opposite to radial machines where the area of the slot is decreased as the iron and coil share the same plane and hence the available space for iron decreases, reducing the magnetic loading.

Having a high pole number presents problems like complex and complicated construction while large amount of stray and fringing fluxes in the stator produces poor power factor. Moreover, high cogging torque and subsequently a high torque ripple presents another common disadvantage in such machines. These problems are addressed in this thesis and solutions are provided to reduce the effect of these.

MPMs have been used to manufacture propulsion systems for buses [17, 10] ships [23], railways [24], wind turbine generators [25 – 28] and wave energy converters [20, 29, 30]. This literature review will provide an overview of the linear and rotating machine designs as well as the history and development of MPMs. Moreover, a detailed review is presented of the Soft Magnetic Composite and its production, properties and use in manufacturing of machines such as MPMs.

2.2 First generation of Electrical Machines

The growing interest in electrical machines, power and its distribution led to various inventions and many patents being filed in the late 19th century and early 20th century. One of the early patents granted to W. M. Mordey in 1890 for an electric generator can be classified as the backbone of today's transverse flux machine as it had the same constructional and operational conceptual properties [1].

Figure 2.1 (left) shows the inner rotor design as proposed by Mordey, composed of a simple ring coil enclosed by I and K components spread out circumferentially around the machine. In order to reduce the eddy current losses, the iron segments are designed to provide a flux path that has similar reluctance whether the rotor aligns with I or K component; change in flux in the rotor is reduced hence the magnetic circuit should appear to be the same [1].

The pole number of the machine is quantified by the number of teeth on the rotor and is equivalent to the number of iron segments. This meant that an increase in the number of sections led to an increased number of electrical cycles for a coil in one full rotation of the rotor.

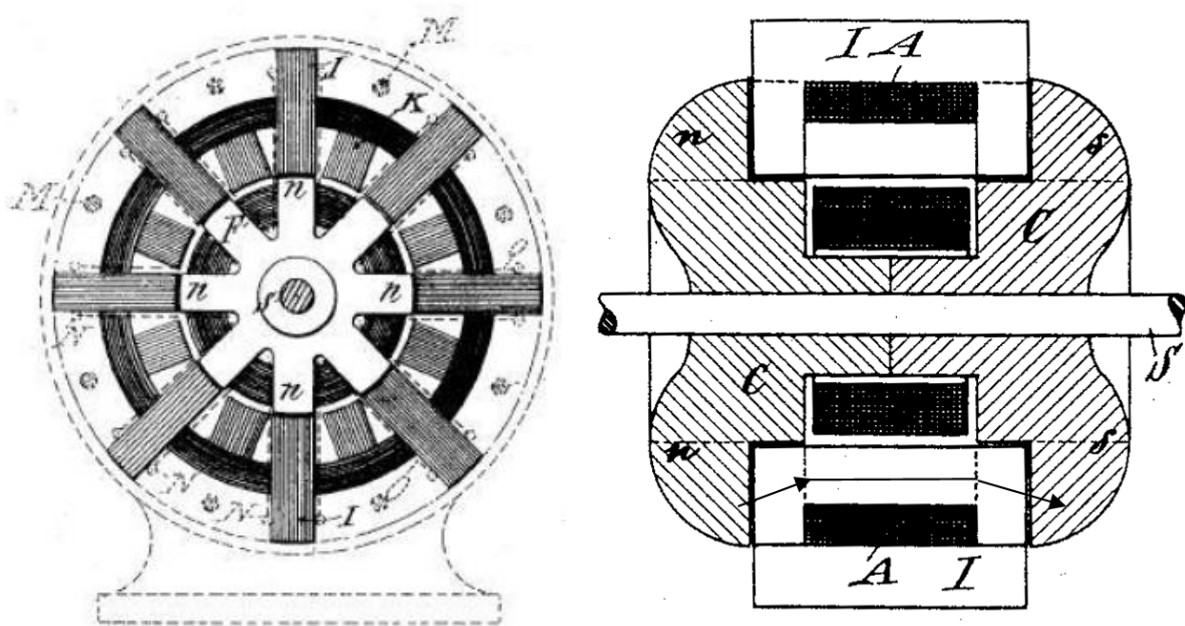


Figure 2. 1: Mordey's electric generator (left) in 1890 and another rotor topology (right) [1]

There are many other rotor topologies offered too and one such design is presented in figure 2.1 (right). It can be seen from this that there is an iron core, C which is referred to as a 'magnet', mounted on a shaft S and wound with a field coil to create the field distribution

shown. Upon inspecting the design in figure 2.1 (left), the flux path can be seen to start from the top ‘north’ pole making its way into the U core piece, along the core-back, down the other side of the U core into the bottom ‘south’ pole of the rotor and returning back to the ‘north’ pole through the rotor iron.

Rotor parts labelled K in figure 2.1 are referred to as ‘magnetic short circuiting pieces’ as these does not link the coil as they are aligned with an inner U core, therefore not contributing to the output. This concept is quite common in modern machines as these are merely added to avoid stray fields that may occur in the parts of rotor that are not used to link the coil.

Other patents that use flux paths similar to MPMs include Nicola Tesla’s high frequency generator in 1891 [31], Ernest Alexanderson’s 100 kHz alternator in 1911 [32] and Robert Lundell’s claw-pole alternator in 1960 [34]. Tesla’s generator, shown in Figure 2.2, consists of an iron ‘C’ core labelled ‘N’, contains a homopolar winding labelled ‘I’ while the triangular surface within the air gap produces an assembly of poles. An alternating voltage is induced when the rotating winding is wound (as shown in Figure 2.2 right) and placed between the triangular air gap of the stator.

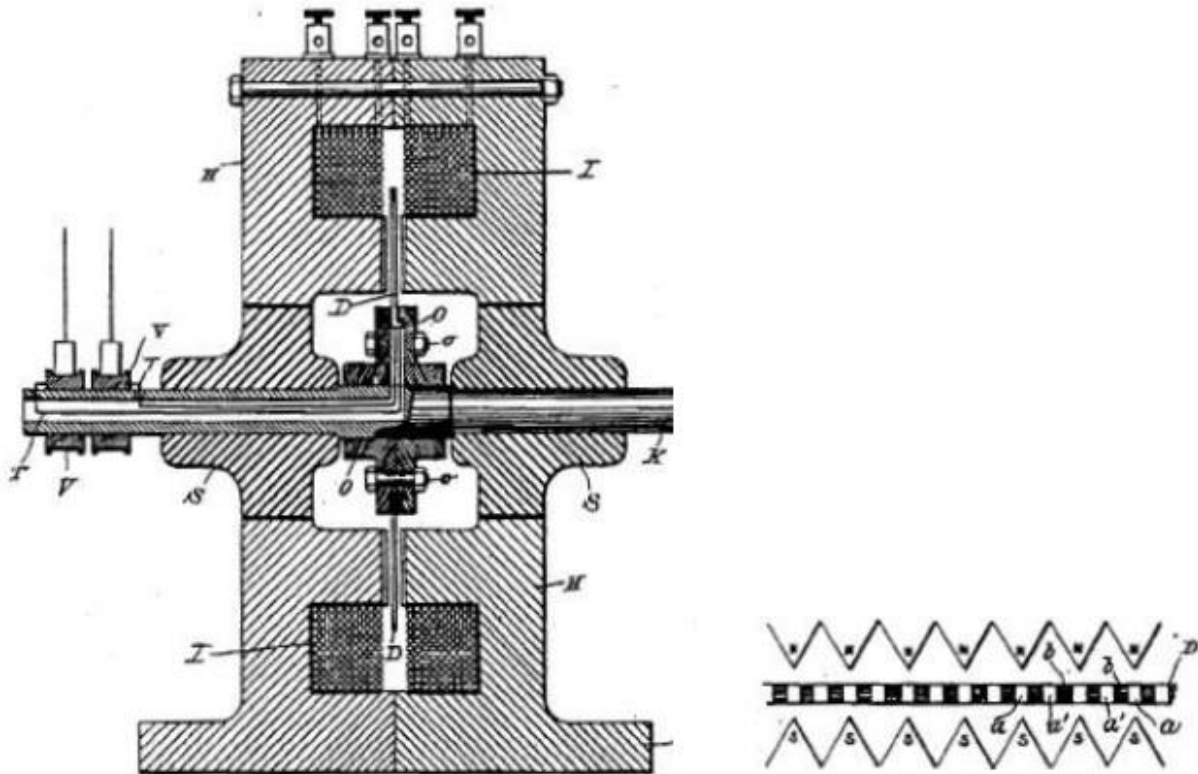


Figure 2. 2: Diagram of Tesla's high frequency generator [36]

A few years later, Ernest F. W. Alexanderson built a 100 kHz alternator [32] for radio communications, shown in Figure 2.3. The concept of this machine is similar to the double sided machine (which will be described later in this chapter) and William Stanley's 1887 invention of producing fluctuating magnetic field [33, 34].

It is seen from Figure 2.3 (right) that the armature coil (6) is integrated into the stator (1) and a 'solid magnetic inductor' rotor (5) is used to create an alternating field by placing it in between two laminated rings. These rings are separated by two air gaps positioned in the circumferential/radial plane.

The flux path of this can be described as being perpendicular to that of an MPM. The field created by the stator coil passes through one ring, crosses the first air gap in the rotor, across the second air gap into the second ring and finally around the core-back to the original ring completing a full magnetic circuit.

Figure 2.3 (left) shows a cut out of rotor; zigzag winding (9) is shown held between two clamps (4). A high strength non-magnetic material (7) is used to fill the gaps between the rotor

windings in order to give the rotor a smooth finish ultimately reducing the windage which can often cause problems at the high speeds at which this machine works.

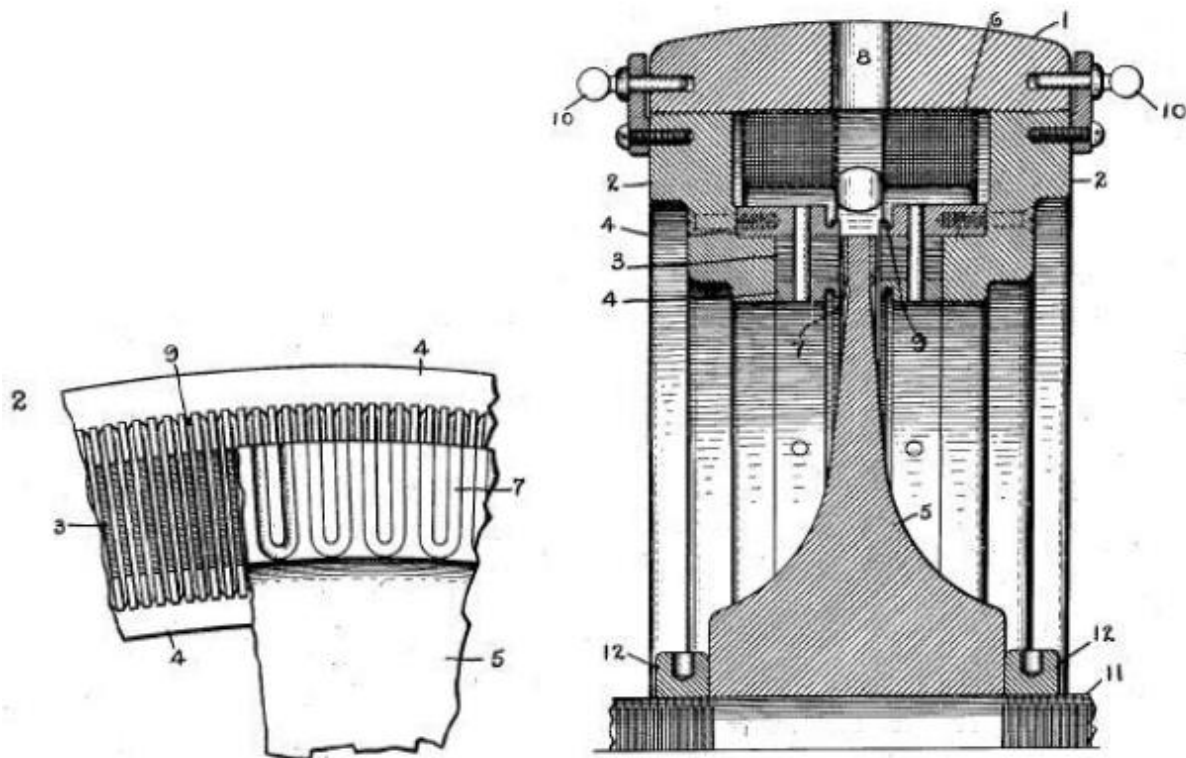


Figure 2. 3: Diagrams from patent of E. F. W. Alexanderson showing 100 kHz alternator [40]

The Lundell ‘claw-pole’ alternator was patented 49 years later and can be regarded as one of the most profound examples of a modern modulated pole machine and formed the basis of the modern day automotive alternator. Robert Lundell was the pioneer inventor of the iron core like structure, modulating flux for a single dc stator winding; this idea was developed by General Electric in 1902. Lundell’s technique was further revised and got used to form the modern day automotive alternator [35] once the silicon diodes were introduced. However, the introduction of affordable silicon components meant the birth of silicon thyristors, which replaced the induction alternators bringing them to an end.

2.3 Second generation of Electrical Machines

In the last twenty-five to thirty years, with the introduction of higher energy density magnets [36], availability of rare earth magnets for a realistic cost, semiconductors replacing valves and the development of materials such as soft magnetic composites, attention turned back to MPMs with its popularity touching skyline. There was an increasing curiosity with research being

carried out more than ever before to figure out the result of replacing field windings by permanent magnets. This paved the way to many papers being published presenting different topologies for MPMs out of which was one published by H. Weh in 1986 presenting a MPM which formed the base of current day machines [2]. He realised the path of the flux transverse the direction of motion of motor and hence named the machine ‘transverse flux machine’ which is the name used today for such types of machine.

In [2], Weh puts forward the need to develop new soft magnet materials to avoid saturation, increased tooth widths were needed in conventional machines which in turn reduced the size available for the coil. Therefore to keep the electrical loading the same, higher current density and cooling was required [2].

This was one of the main reasons why MPMs became popular as this type of machine allows increasing the number of pole numbers without reducing the space for the coil due to the electrical and magnetic circuits being decoupled from each other. This meant that one does not need to reduce the electric loading to increase the magnetic loading. Conductor losses in MPMs were also reduced due to high current loading as each pole saw the whole coil MMF and hence high current densities were not required.

All these features meant that there were many designs created amongst which were single sided modulated pole machines (SSMPM), double sided modulated pole machines (DSMPM) as well designs with combined stators. A few designs from the literature are discussed in the following sub sections.

2.3.1 Single sided machines

In a Single sided modulated pole type of machine, flux is taken from one side of the magnet (mounted on the surface) by the armature and returned via the iron core-back via a return flux path. The most relevant arrangement to explain a single sided modulated pole machine is shown in figure 2.4 where several U shaped laminated iron cores, spaced two pole pitches apart, enclose the ring shaped winding. The purpose of this arrangement is to direct the flux around the coil across the air gap, up to the rotor where the magnets efficiently alternate the direction of the magnetising circuit [37]. The return path for the flux to return from the rotor is provided by an iron segment situated below the magnets.

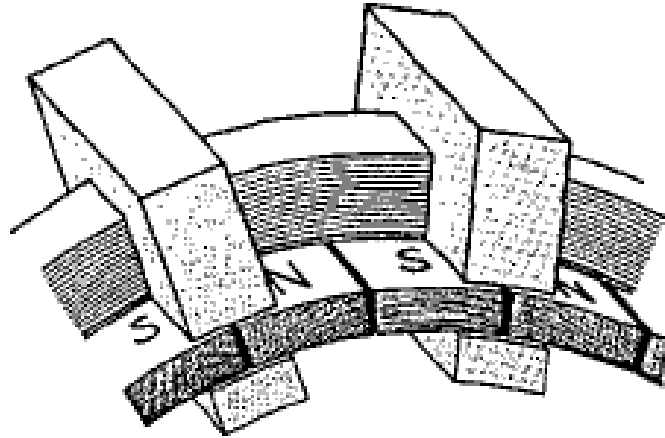


Figure 2. 4: A single sided modulated pole machine arrangement designed by Weh [42]

It was also noted by Arshad et al [38] that the topology presented in Figure 2.4 only utilises half the coil and uses only half the magnet material at any one time, which leads to stray fields.

To tackle these issues, Mordey provided a solution by implementing magnetic short circuiting bars [39] which were used by Bork et al [40] and many other machine users [2, 39] to guide the flux from unused magnets. Bork not only used Mordey's solution but also took this one step further by removing the iron link between the magnet; shown in Figure 2.5. The removal of iron from the rotor reduced the overall cost and weight of the machine as well as reducing eddy currents in the magnets, which are big advantages in machine manufacturing. It was seen that the main flux path links all the magnets however the presence of two air-gaps which the field must cross, an increase in current density for a given torque and reduced available area for the winding [41] reduces the extent of the initial advantage.

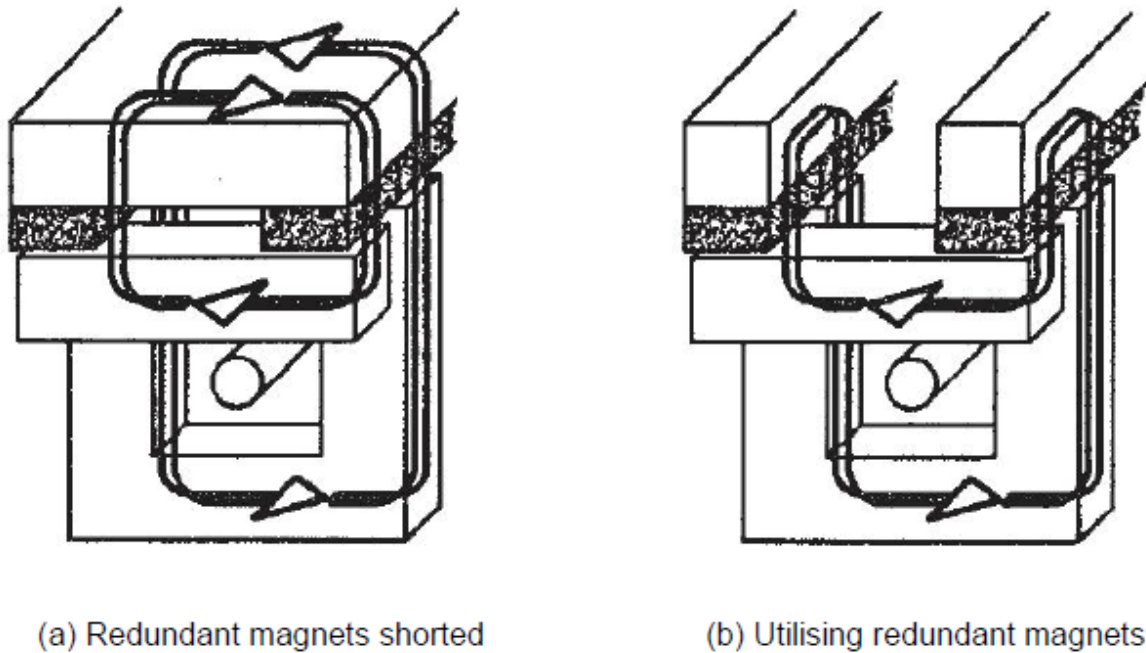


Figure 2. 5: Magnet utilisation in a single sided Modulated Pole machine by M. Bork et al [45]; solid rotor (left), separated rotor parts (right)

A big problem in single sided MPMs is the high armature leakage due to iron cores being in close proximity of each other and hence the reluctance of these is very close to the reluctance of the air gap. High armature leakage means low power factor, at times as low as 0.35 [41].

2.3.2 Double sided machines

There are many benefits of a double sided machine over a single sided one, the main one being the doubling in force density [8]. In a double sided machine, several U cores and the coil usually covers the rotor from both sides [2, 33]. These rotors can be surface mounted [2, 37, 42, 43], where currents in the coils flow in opposite directions or flux concentrated [24, 33, 42-45], where current flows in the same direction in coils, as shown in Figure 2.6.

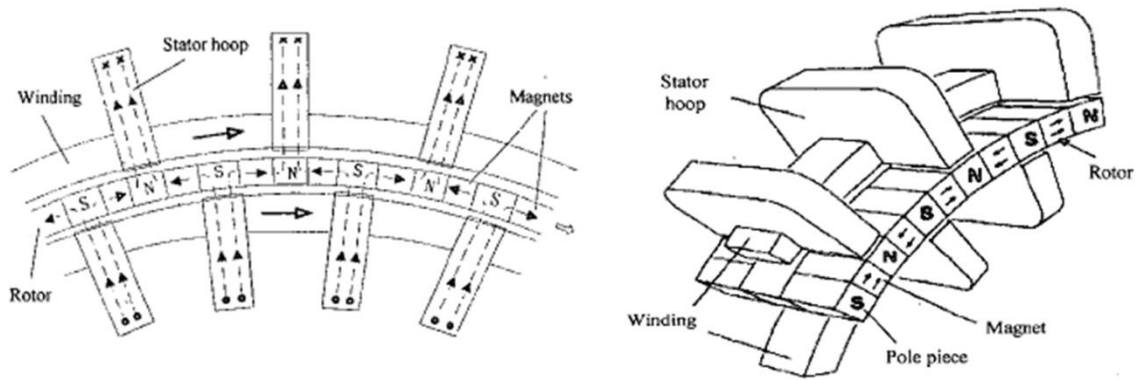


Figure 2. 6: A double sided MPM with flux concentrating rotor in a zero torque position; rotor iron pieces and U cores are aligned [36]

The double sided machine concept was first brought into existence by Weh [2] by simply removing the magnet core back in figure 2.5a and replacing it with a second stator in an aim to achieve 100% magnet utilization. The concept of removing the magnetic short circuiting bars in the stator was the back bone of Weh's paper [46] in which he explained the idea of using a flux concentrated rotor so both sides of the magnets can be used at all times.

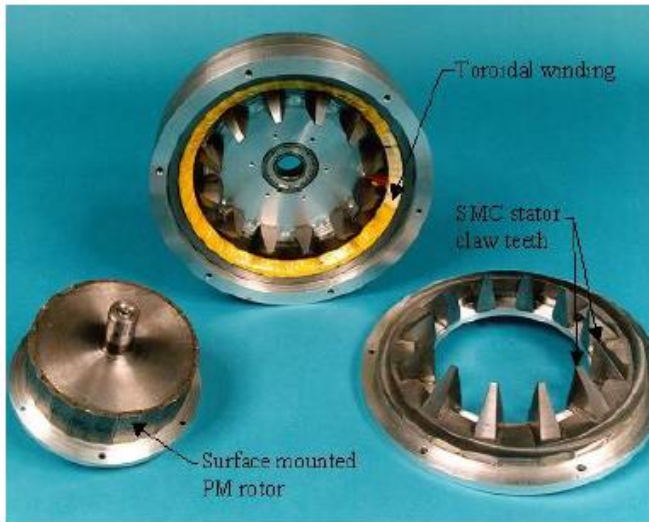
This flux concentration causes the flux density of the air gap to be greater than the residual value of the magnet which provided it, providing a huge advantage to the overall performance of the machine. This benefit, united with better magnet utilization and a stator made up on modulated pole topology, delivers high force densities with much better power factors.

There were many ideas and machines that were manufactured to reduce the redundancy of magnets; one such machine was built by Jack et al [47] and tested by Madison [48] shown in Figure 2.7a. This was similar to the machine developed by McLean, a claw pole machine (CPM), shown in Figure 2.7c [49] in which he took full advantage of SMC's isotropic permeability by introducing a surface mounted magnet rotor and a claw pole structure in the armature stator. CPMs have been used in cars [50], stepping motors such as hard drives and digital cameras [51, 52] and recently in an induction motor made from SMC [53]. Mclean showed that torque is not just dependent on peak flux density and electrical loading (and the machine constant [49]), but also on the number of poles.

Figure 2.7c shows Mclean's double rotor single stator axial field claw pole machine [49] where the claw pieces are split, half pointing inwards and half pointing outwards to direct the magnet's flux linking the coil. The machine proved advantageous when compared against conventional machines however it also had its disadvantages such as high stator leakage, poor power factor

and high core losses [47]. Overall, the machine topology presented by Mclean was unusual for a claw pole machine because of its axial design; more common are the radial type machines found in [6, 47].

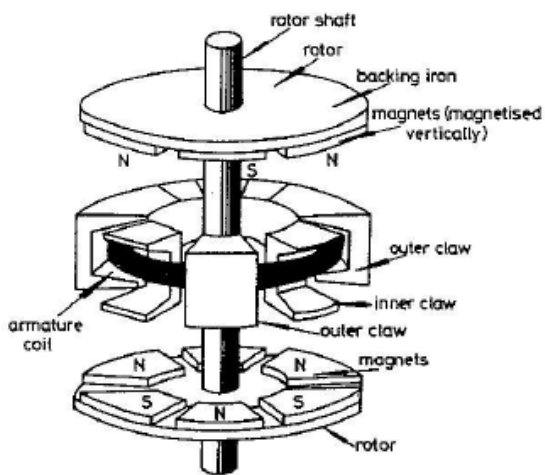
The machine design by Jack et al [47] provided a close complex structure of claw teeth which



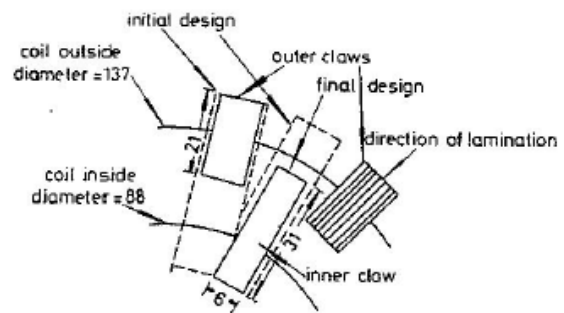
(a) Jack's single sided 'claw pole' MPM [47]
machine [54]



(b) Dickinson's optimised machine [54]



(c) McLean's general topology [58]



(d) McLean's method to allow iron claws to be laminated

Figure 2. 7: Various Claw pole Modulated Pole Machines

resulted in high amount of armature flux reducing the power factor, a low torque density of 3.3

Nm/kg for active material; however the simple structure of the armature eased the manufacturing.

Dickenson et al [9, 54], on the other hand, increased the pole number to 50 in order to optimise the design, by changing the claw topology to reduce the armature flux which resulted in a torque density of 9.3 Nm/kg; the machine design is shown in Figure 2.7b.

Other advantages of a double sided MPM include high torque densities as shown by Mecrow et al [3] where the machine was built out of SMC and achieved a torque density of 12.35 Nm/kg, torque per unit volume of 45.3 kNm/m³; compared to 28.3 kNm/m³ for a single sided design. The downside of a DSMPM when compared to a SSMPM is the complex construction [3] though the power factor shows improvement as the amount of armature leakage is lowered. Use of SMC material is recommended for double sided MPM as pointed out by Guo et al [55] due to eddy currents in the laminated material.

It can thus be concluded that double sided topologies offer higher power producing capabilities compared to single sided topologies: however they are more complicated to manufacture. In order to find a good compromise between performance and simplicity, a claw pole transverse flux permanent magnet machine is often considered by researchers [6, 56].

2.3.3 Multi-Phase Machines

The concepts, designs and topologies presented so far all consisted of single phase synchronous machines. The simplest way to design a multiphase machine is by stacking multiple machines in series displaced by an appropriate angle to produce a smooth net output. There are many examples of such machines such as Mecrow et al's [57] and others such as [53, 58, 59] which uses the technique to integrate variations in an induction machine's stator, while Cros et al [60] have a hybrid machine comprising a conventional and modulated pole machine, presented in Figure 2.8.

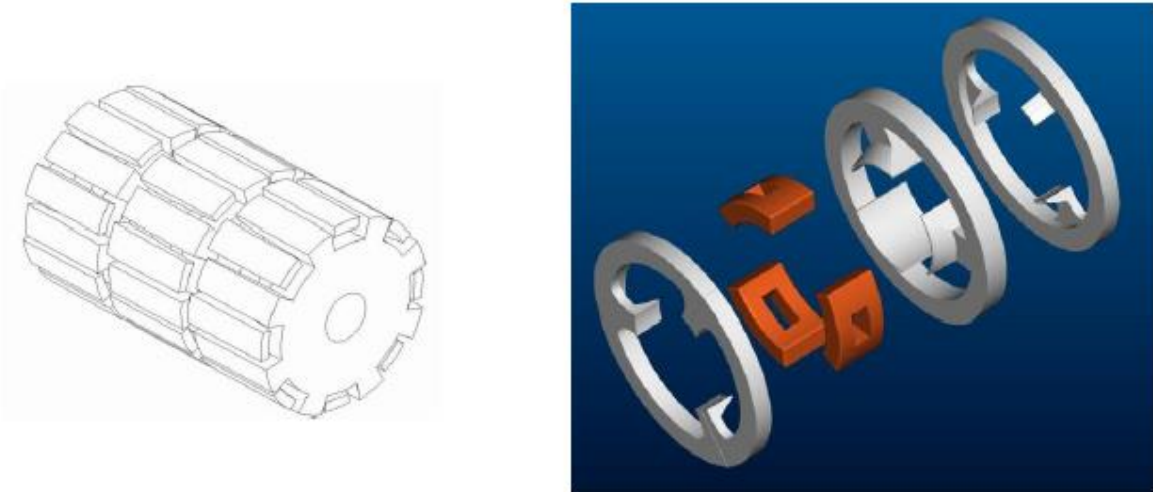


Figure 2. 8: Two examples of multiple phase MPMs; Mecrow's [57] multiple phase MPM (left), Cros's [60] hybrid multiphase MPM (right)

2.4 General properties of Transverse Flux Machines

There are many advantages of TFM topology over the classical longitudinal concept; the main ones being the increase in pole numbers does not reduce the MMF per pole therefore producing higher power densities if needed. Secondly, there is a lot more design freedom as the magnetic flux and the coil geometry can be varied without compromising on the dimensions of either giving a higher torque/volume ratio. Moreover the armature coil is very simple and the total conductor length is relatively short. Last but not the least, the control method is simplified due to magnetic decoupling as the phases in a TFM are magnetically independent.

On the other hand, the reasons that can prevent companies from manufacturing mass production of TFM comprises of low power factor, three dimensional magnetic fields causing complex and complicated construction. This means that the use of lamination is replaced by the use of isotropic materials like soft magnetic composite materials as well as 3D numerical design tools, increasing the production costs significantly. However, for critical applications where the demand revolves around the performance and the compactness of machine, TFMs fulfil the criteria perfectly.

TFM designs can be based around three concepts. The first design is when there is an active rotor i.e. the exciting permanent magnets are placed on the rotor. The second concept is when the rotor is passive i.e. the exciting permanent magnets are on the stator. The third concept of

a TFM is when the permanent magnets are replaced by an electrically excited reluctance motor. These three concepts can either be single sided or double sided, though single sided are easier to manufacture and have better prospects in practical applications.

There have been various designs and prototypes recently developed in the field of TFMs investigating regarding the geometries and their characteristics. To conclude, TFMs have a higher torque/volume ratio when compared to conventional ones, but because of three dimensional flux paths, the topologies require the use of isotropic materials like soft magnetic composites, as well as 3D numerical design tools.

2.5 Soft magnetic composite – MPM

Most of the early MPMs were manufactured using laminated steel to offer the flux path to link the coil of the machine [1-2] however advancements in materials such as soft magnetic composite and 3D design techniques made research into flux switching MPMs more feasible and offered commercial viability for this machine type. Many complex designs and complex shapes can now be made out of SMC which were difficult or impossible to make via stamping the laminations.

Soft Magnetic Composites (SMC) is the internationally recognised name for pressed and heat-treated metal powder components with three-dimensional (3D) magnetic properties. Somaloy[®] is Höganäs brand for SMC materials. The Somaloy technology offers a wide material portfolio to fulfil the requirements of different electromagnetic applications such as electric motors, fast switching actuators or inductor cores for power electronics.

2.5.1 Production of SMC Somaloy

Höganäs Somaloy is a high purity water atomized iron powder with very thin inorganic surface insulation. The iron powder is coated with insulation of 50 – 200 micro-meter in diameter combined with a binder or lubricant, as shown in Figure 2.9. The addition of additives, lubricants and coating depends on the application; for electric motors, Somaloy 700HR would be coated with 5P (phosphate) where for power electronic applications, Somaloy 700HR would only require a coating of 1P. Moreover, the size of the fraction, microstructure and processing parameters for heat treatment solely depend on the application.

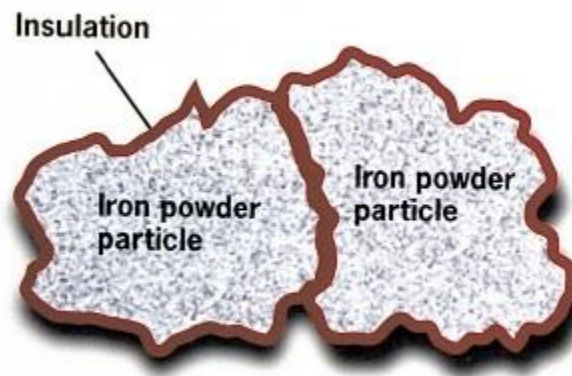


Figure 2. 9: Schematic of Somaloy powder (SMC particles) with lubricant coating [73]

The properties and performance of the SMC material depends upon the mix and the method of compaction, the atmosphere it is compacted under and the amount of pressure applied. Compaction takes place after the addition of necessary lubricants and additives; three steps involved in the compaction cycle [62] are shown in Figure 2.10. The first step is crucial as filling determines the homogeneity of the compacted component in terms of density. The performance of the material at a given frequency is determined by the size of the particles in the initial mix; the smaller the particles, the better the performance at high frequencies and vice versa [49].

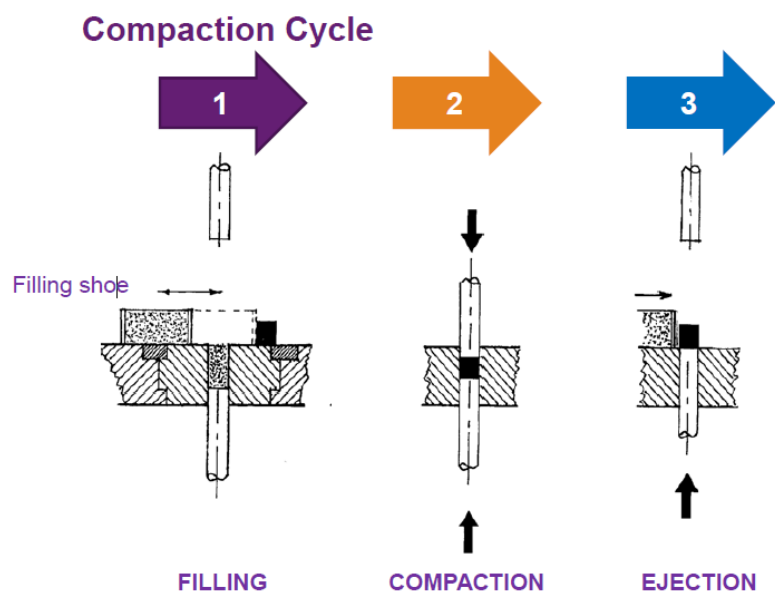


Figure 2. 10: Three steps involved in compacting the powder [62]

Secondly, the pressure applied during compaction is important as this determines the gaps between the particles. Higher pressure means small gaps between the particles leading to higher permeability and saturation flux density [62]. The process of compaction causes poor magnetic performance and high hysteresis losses due to the stresses created in the material [49] and hence the components need to be heat treated under high temperatures to remove the lubrication from compaction and to improve the performance of the finished component.

Although laminations require less processing and hence are cheaper and quicker to manufacture, SMC's ability to easily assemble the finished shape is of greater benefit [63]. Other benefits of SMC include a smoother shape of the end product which saves on further machining, an increased fill factor due to reduced requirement for slot insulation, a compact size, smaller thermal barriers and shorter end windings than laminated machines [64].

2.5.2. Properties

SMC has a lower density and permeability than magnetic steel due to the insulation layer described earlier and asymmetrical shape of particles leading to gaps in the material. SMC has a density ranging between $7300 - 7550 \text{ kg/m}^3$ whereas laminations have densities higher than 7600 kg/m^3 . The relative permeability of SMC is usually around 500 to 800 while laminations have permeability in numerous thousands (7500 for Transil 315); these comparisons can be seen in [65]. Because of the lower permeability of SMC, the performance of the machine can be lowered [62] and hence it cannot be a direct replacement for laminations especially in induction or switched reluctance machine which require high permeability (to minimise the magnetising currents) due to smaller air gaps.

The main advantage of SMC comes when the machine to be designed has complex three dimensional shapes, requiring 3D flux paths. One such example is presented in [66] where the magnets are positioned in order to provide flux to a radial and axial machine's air gap; this would not have been made possible with laminations. It is easier to use powder and engineer shapes that are otherwise not possible with laminations, ultimately saving space and material; one such example of an axial flux machine is presented in [67].

The positioning of Somaloy in terms of resistivity and operating induction level makes it a desirable candidate for electric motor application. Somaloy falls between the operating frequency of ferrites and steel sheets with wider operating induction level for the given frequency, as shown by figure 2.11. SMC also has higher resistivity with fewer alloying

elements as shown in figure 2.12; it was shown in [68] that SMC has an approximate value of $150\mu\Omega\text{m}$ compared to $0.16\mu\Omega\text{m}$ for laminations.

Other benefits of SMC include iron loss, at low frequencies it is comparable to low quality laminated steels [49] however it is much better at higher frequencies. This is due to the insulation around each iron particle, as shown in figure 2.9, eddy currents find it difficult to circulate around the material. It is therefore preferred to use SMC in high frequency applications such as drive fed machines. It is discussed in [49, 69, 70] that there is a point where SMCs act superior to the conventional machines due to the fact that hysteresis losses increase linearly with frequency while eddy current losses increase with frequency squared.

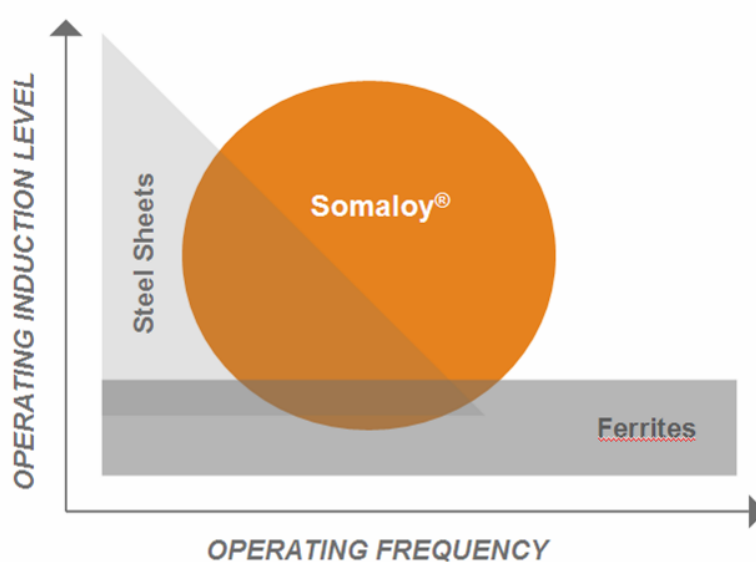


Figure 2. 11: Illustration of operating induction level of Somaloy as a function of operating frequency in comparison with steel sheets and ferrites.

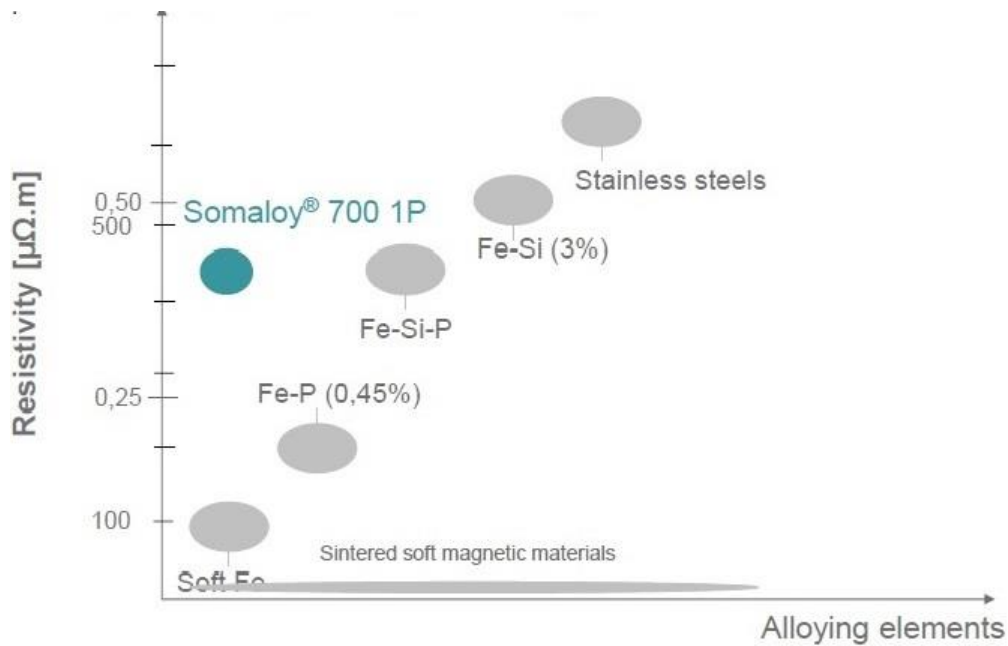


Figure 2. 12: : Comparison of resistivity of Somaloy with different materials.

It can hence be concluded that although laminations are a good manufacturing material, SMC behaves better in many aspects, especially when the machine designs are complex requiring 3D flux paths and high frequency operations. In order for laminations to compete at high frequencies, the losses needs to be reduced by making them thinner and introducing additives such as silicon that have high resistivity. This however would increase the cost of manufacturing process [63, 71] which will put laminates to another disadvantage as SMCs frequency operation is not affected by the manufacturing process.

2.6 Material Hybrid Machines

It is difficult to press large size shapes of SMC and sometimes therefore many smaller SMC pieces needs to be connected together to make a final shape of a large machine, as was the case in [3]. Using this technique however causes a compromise on the permeability and isotropic properties of the machine.

The solution to such problems is hybrid machines, where both laminates and SMC are used. Laminates are used where there is a need of radial component of field such as the teeth and SMC is used to fulfil 3D field requirements such as the core back and the pole pieces. This brings into practice the best properties of both materials as well as reducing the component

count and overall size of individual pieces, ultimately reducing the manufacturing cost of the machine.

There have been many instances when this technique has been used, such as in [67] shown in Figure 2.12 where Jack et al combines SMC teeth and laminated strip-punched core back to produce a hybrid axial machine. Pinguey [22] and Amreiz [72] both produced stator teeth from bent laminations while the core back is manufactured from SMC, exploiting its 3D flux carrying properties. Pinguey's machine features the MPM concept while Amreiz construction method of producing stator teeth from laminated strips wastes very little material. The laminations are used to create flux paths with higher permeability while the rotor contains the SMC flux producing blocks.

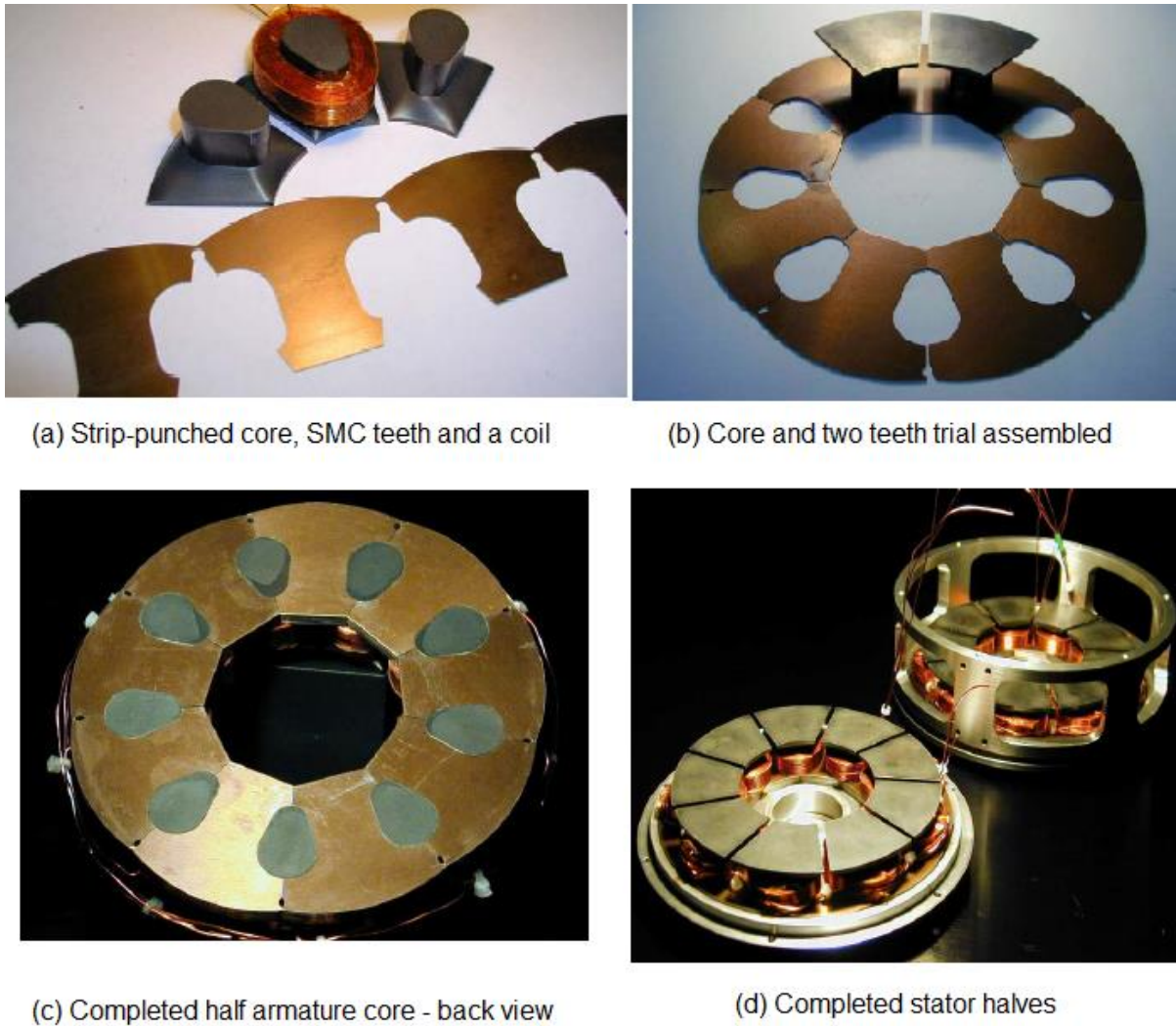


Figure 2. 13: Jack et al [67] Material Hybrid machine made from compacted iron powder and laminations

2.7 Cogging torque

Cogging torque in an electrical motor is produced exclusively due to the interaction between the permanent magnets on the rotor and the teeth on the stator, which have a tendency to align such that the reluctance seen by the rotor is minimised. It is position dependant and hence depends on the number of magnetic poles and the teeth on the stator.

In a MPM, there are an equal number of rotor poles and stator teeth (poles) and hence the number of positions where the rotor will find this position of low reluctance will be equal to the number of poles. In the case of this these, the MPM discussed is 50 poles, hence there are possible 50 positions where production of cogging torque can take place. It was shown in [86-89] that a suitable selection of slot/pole combinations with a high common multiple can

decrease the cogging torque produced by a conventional machine; this however is not true for MPM.

Although an MPM has equal numbers of stator teeth and rotor poles, these still line up twice in positions of low reluctance per electrical cycle. During one electrical cycle the rotor lines up in the d-axis twice (at 180° and 360°) and twice in q-axis (at 90° and 270°) and hence a large amount of rated torque is in fact the cogging torque [52, 90]. Moreover, improper designing of the machines can also cause a high cogging torque, sometimes as high as 25% of the rated torque; though many commercial machines, the value of cogging torque usually ranges around 5% to 15% [3].

Another factor influencing the performance of the machine is the torque ripple which is not just made up of the cogging torque, but the harmonic content in the back EMF waveform too. It is vital to consider this, especially when the application demands a low torque ripple, as machines of this type can show a high harmonic content especially on load as was shown in [77]. It is vital that in high performance applications, the cogging torque of the machine does not exceed 1% to 2% of the rated torque and therefore detailed analysis and computation techniques are required to design optimal machines which meet the specifications.

Phases of an MPM usually consist of three identical stator sections stacked axially and separated by a gap for magnetic isolation to reduce the mutual coupling between adjacent phases. Each of these three phases produces their own cogging torque [78] which is summed together on the shaft to create the resultant cogging torque for the whole machine. This allows for the possibility of reducing cogging torque by appropriate phase alignments and orientation.

It was shown in [79] that most of the even harmonics in a three phase MPM cancel out, leaving only the 6th and 12th harmonics and hence techniques to reduce these will be investigated in this thesis. It was also shown that cogging torque for a SSMPM is usually significantly lower than that of DSMPM, as was discussed earlier in the section.

There have been many literature publications on axial [80] and radial [81-83] PM machines however not many can be used directly in flux switching PM machines. Techniques that can reduce cogging torque include skewing the stator stack or magnets [84-86], using fractional slots per pole, optimising the magnet pole arc or width, shaping stator tooth tips [86], notching of teeth [87-88] and modulating the drive current waveform to compensate the torque ripple from a control viewpoint [89]. These techniques however are either difficult for some

topologies, adds to the complexity of the machine or reduce the motor's back-EMF therefore reducing the resultant running/useful torque.

It is also suggested in [90] that the cogging torque can be computed by calculating the co-energy around the edges of the magnet in proximity to the nearest tooth and slot opening. A limited amount of research work is conducted to reduce the noise and vibrations in the machine [91-93], however due to the emerging interest in this field on part of the manufacturer, progress is being made to address the problem of cogging torque in much more detail.

2.8 Literature Review Summary

A brief history into the literature of modulated pole machines and soft magnetic composite was presented in this section. Topologies such as single sided, double sided and multiphase modulated pole machines were discussed, ultimately leading towards material hybrid designs as these are of particular interest to this thesis.

It was shown that early modulated pole machines such as the one designed by Mordey mainly consist of solid laminated steel while the field was provided by a coil carrying current. However, the renewed research and availability of strong permanent magnets have reintroduced the modulated pole machines concept, especially in applications where high torque density is required. On the other hand, material hybrid machines use a combination of high permeability laminated steel and soft magnetic composite to make use of two kinds of field; one that travels in the plane and other that harness three-dimensional nature.

A brief review on soft magnetic composite discussed the material's production process, its isotropic and thermal properties, and its ability to produce three-dimensional flux paths that are ideal for modulated pole machines. It was also argued that these have a lower permeability than laminated steels mainly due to the compaction process; the non-magnetic gaps created between the adjacent iron powders that make up the composite.

Lastly, the problem of cogging torque was highlighted and reducing this is the main aim of this thesis. Various techniques are presented in the literature to reduce the cogging effect, however most of them either alter the machine parameters, give rise to complex manufacturing or decrease the useful torque. These ultimately either increase the cost of the machine or reduce the performance.

3. Base machine Torque Quality

The modulated pole machine (MPM) is well known for torque density; however the quality of torque is generally poor, with cogging and ripple exceeding 10% of rated torque. In this chapter a base machine is presented and analysed, against which all subsequent design development and analyses are compared. The chapter concludes with a set of suggestions to improve the torque quality of the MPM.

In this chapter the operation of the previously designed separate phase MPM design is presented along with the problems that were highlighted in the design. These problems will be discussed and solutions will be outlined to improve the torque quality of the machine.

3.1 The Base machine for comparison

The stator of the machine, described in [117] is shown in Figure 3.1 and forms the base design for this study. The stator is made up of six pressed SMC toothed sections enclosing three hoop coils made from rectangular cross section copper wire. The phases are separated by 2mm thick aluminium rings to reduce the mutual coupling between the phases.

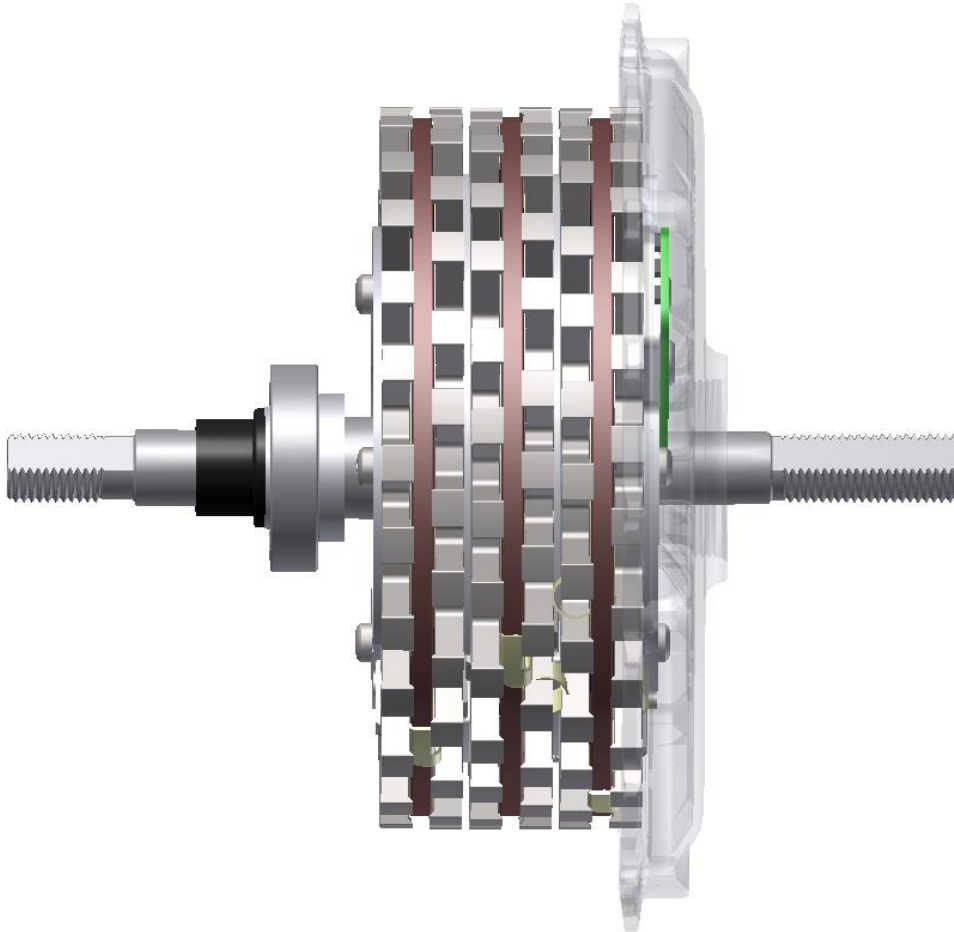


Figure 3. 1: CAD model of the base machine assembled 3-phase stator

The rotor consists of fifty pole pieces made from pressed SMC (Somaloy® grade 3P) while the magnets are made from Neodymium grade N35; the pole pieces and magnets are alternately arranged in an aluminium hub, as shown in Figure 3.2.

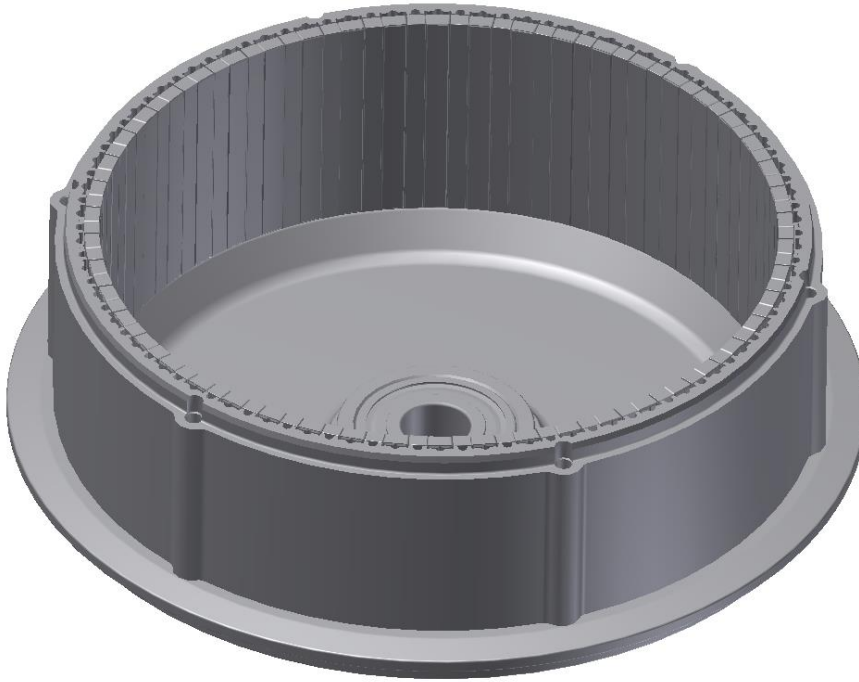


Figure 3. 2: CAD model of the base machine rotor

An axial view of the three phase MPM arrangement is shown in Fig. 3.3. It consists of three identical stator sections separated by a gap to reduce the mutual coupling between adjacent phases. Phase A consists of two laminate toothed rings (Tooth 1 and 1') placed at an electrical angle of 0° and 180° respectively enclosing coil A. Phase B is similar to Phase A except that the Tooth 2 is moved by 120° from Tooth 1 while Tooth 2' is 180° from Tooth 2. Phase C's Tooth 3 is 240° from Tooth 1 and hence completes a balanced three phase arrangement.

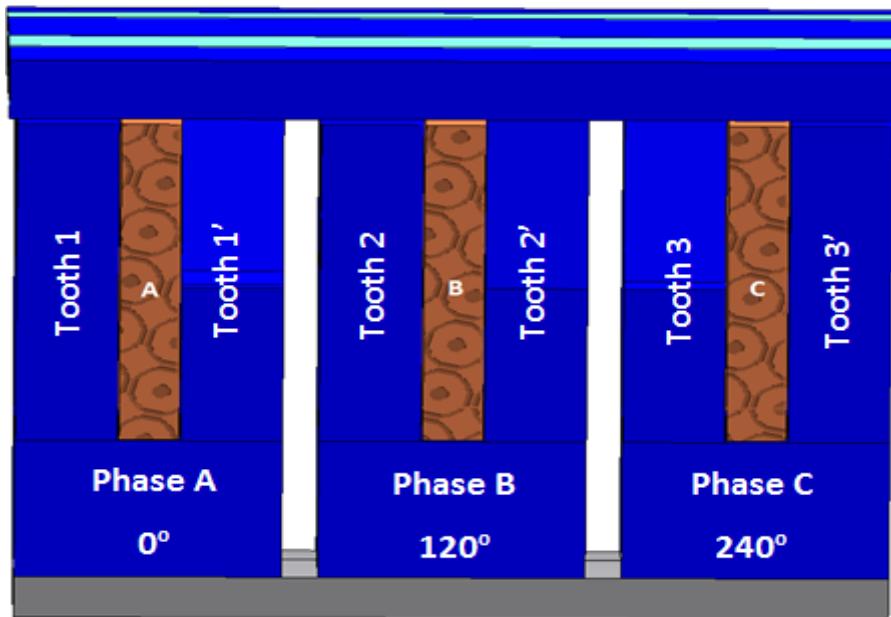


Figure 3. 3: Finite Element axial view of a three-phase MPM with axial separation

The coils are made from rectangular cross section copper wire and are 3.3mm wide axially while the phases are separated by 2 mm thick aluminium rings; the separation reduces the mutual coupling between phases, whilst the aluminium rings ensure the correct angular position of the adjacent stator phases, table 3.1 gives the major dimensions of the machine. Figure 3.1 shows the CAD view of the stator arrangements along with the shaft, bearing and a rotor end cap.

Table 3. 1: The major dimensions of the separate phase motor

Stator Tooth sections (axial length)	5.95 mm
Coil Width	3.3 mm
Coil Outer Diameter	146 mm
Coil Inner Diameter	114 mm
Number of turns on Coil	17
Phase separation gap	2 mm
Phases	3
Poles	50
Magnets	50
Magnet Dimensions	3.9mm x 3.5mm x 49.6mm
Outer Diameter	159.2 mm
Inner Diameter	103.7 mm
Axial Length	49.6 mm
Stator Core-back Depth	5 mm
Air gap	0.4 mm

3.2 Base machine performance

The cogging torque and back EMF waveforms of the base machine are presented in Figures 3.4 and 3.5 respectively. These results form the base performance for all subsequent analysis.

The cogging torque measurements of the base machine is shown in Figure 3.4. This test was carried out with zero current using the test bench shown in Figure 6.1.

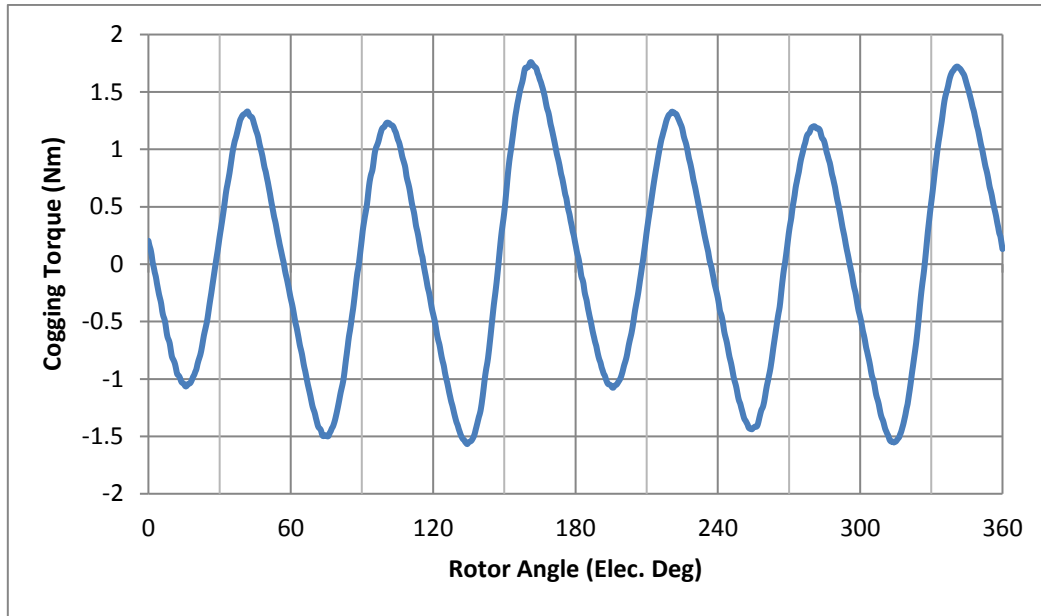


Figure 3. 4: Static Torque characteristics of the base machine design prototype over two pole pitches (28.8 mechanical degrees)

It is seen that the base machine has a peak cogging torque of 1.76Nm, which is 12.6% of the rated torque, and as such is too high. Harmonic decomposition of this waveform yields a high 6th harmonic content and significant second, fourth and twelfth harmonics, these are presented in Table 3.2.

Table 3. 2: Static Torque harmonic content of the base machine design (as a percentage of rated torque)

Peak Cogging Torque	12.57%
1st harmonic	1.57%
2nd harmonic	1.67%
3rd harmonic	0.19%
4th harmonic	1.25%
5th harmonic	0.14%
6th harmonic	10.41%
7th harmonic	0.10%
8th harmonic	0.12%
9th harmonic	0.11%
10th harmonic	0.34%
11th harmonic	0.02%
12th harmonic	1.41%
13th harmonic	0.11%
14th harmonic	0.04%
15th harmonic	0.07%
16th harmonic	0.12%

In figure 3.5, the no-load back EMF is shown for the three phases. In this waveform, there is a significant 5th and 7th harmonic, which is found to be greatest in Phase B, the central of the three coils. The harmonic components are presented in Table 3.3. These harmonics are undesirable and subsequent work will describe the efforts to reduce and remove them.

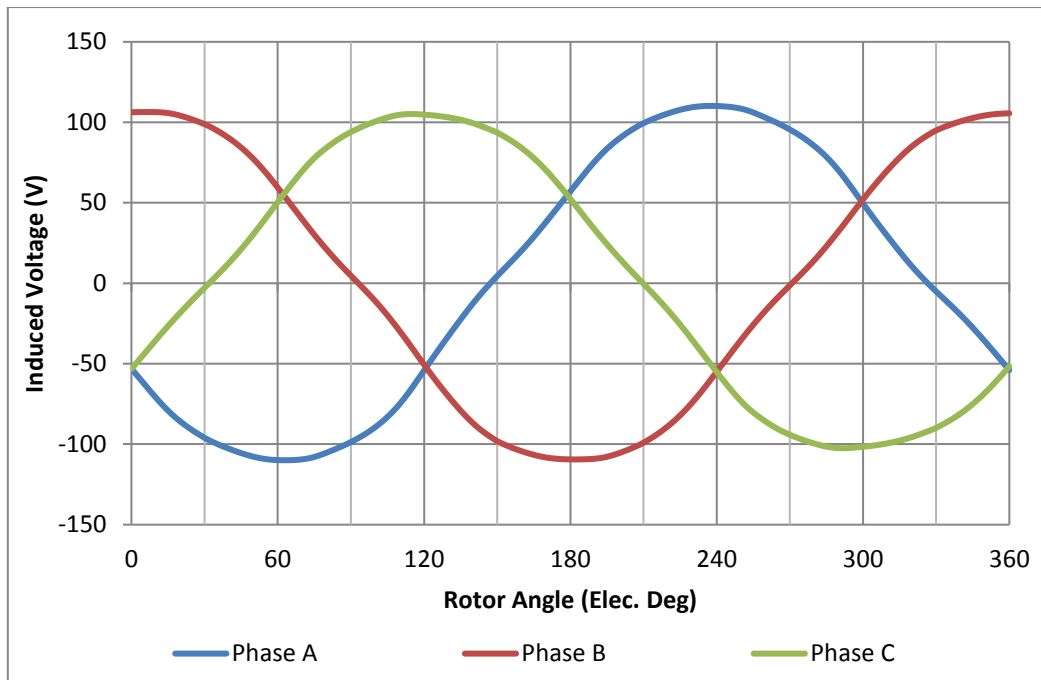


Figure 3. 5: Back EMF of all three phases of the base machine design taken under no load conditions with the rotor rotating at 200rpm.

Table 3. 3: Harmonic content of back EMF waveforms for the three phases

Harmonics	Phase A	Phase B	Phase C
Fundamental	110.57	110.94	110.07
5 th	2.75	3.20	2.46
7 th	1.07	0.86	0.84

The central phase (B) shows a higher peak voltage than the two outer phases (A and C) as seen from Table 3.4. In addition to this imbalance, there is a slight mis-alignment in the electrical angle of the three phases, as shown in Table 3.5. The three waveforms can be regarded as close to 120° electrical; phases A and B are misaligned by 1.85 electrical degrees, indicating the circumferential displacement of the stator phases can affect the phase voltages, as seen from Figure 3.4.

Table 3. 4: Comparison of peak Voltages of the base machine

Base Design	Phase A	Phase B	Phase C	Mean
Peak back EMF (V)	109.46	110.19	109.01	109.55

Table 3. 5: Misalignment of the three phases of the base machine (electrical degrees)

	Phase AB	Phase AC	Phase BC
Electrical angle	120	240	120
Misalignment (elec. Deg)	121.85	242.92	120.78

Transient torque analysis was also carried out in Finite Element Analysis; the machine was supplied with 20 Amperes of current while the rotor was rotated two pole pitches. It can be seen from Figure 3.6 that the average torque produced at 20A is approximately 14 Nm with a very high torque ripple of 25%.

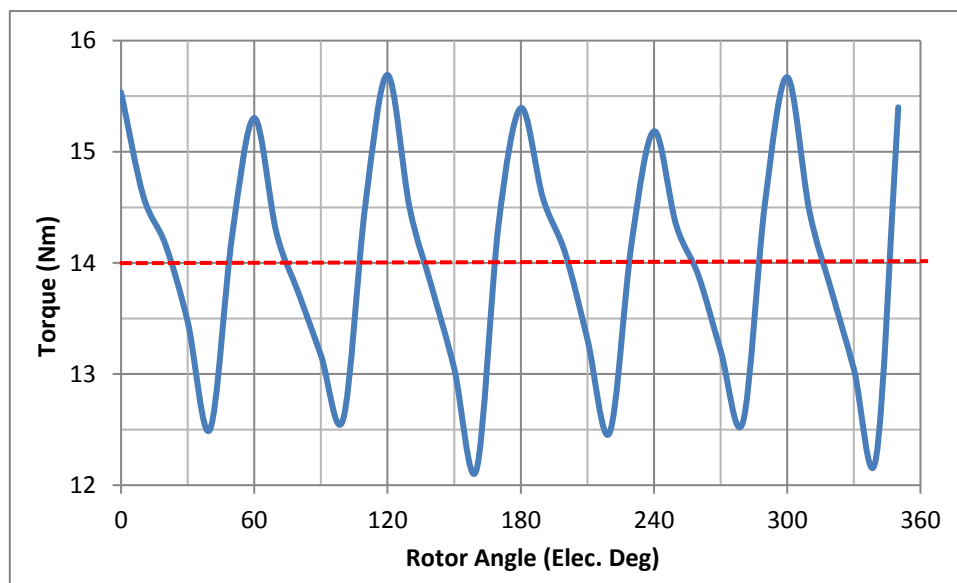


Figure 3. 6: Torque waveform of the base machine design prototype over two pole pitches (28.8 mechanical degrees) when supplied with 20A

3.3 Problem Statements

The machine model presented in section 3.2 is treated as the base design and all the newer techniques and topologies were compared against this model. The three problems that are encountered in this design are the high peak cogging torque and its harmonic, the back EMF and its harmonics and the high torque ripple. The aim of this thesis is to provide solutions to reduce these undesired cogging, back EMF harmonics and the ripple without altering most of the machine parameters that were presented in Table 3.1.

3.3.1 Cogging Torque

Interaction between the rotor permanent magnets and the stator slots of a PM machine give rise to an undesirable component for the operation of the motor known as Cogging torque. MPMs

display a large amount of cogging torque [30, 94] and this can be a substantial proportion of the rated torque. This cogging torque coupled with a high torque ripple is detrimental to the performance for an application where low torque ripple is a necessity [1]. Because MPMs have the same number of rotor and stator poles, the number of positions where the rotor will find a stable low reluctance position is equal to the number of these poles and hence is not ideal from the cogging point of view.

It is seen from Table 3.2 that there is a high peak cogging torque and its harmonics present in the machine. It is important to reduce cogging torque as it introduces jerkiness, vibration; noise and torque ripple in the user's experience of the machine. There have been many techniques that can reduce the cogging torque however these also reduce the back EMF resulting in reduced average torque. There are techniques [30-31] that decrease the cogging torque produced by a conventional machine; these however, are not applicable to an MPM.

There are numerous techniques mentioned previously in Chapter 2 as well in recently published literature which can be implemented to reduce cogging torque in both, axial and radial type permanent magnet machines. These include skewing the poles [95 – 97] or the magnets [97], segmenting the magnet [98, 99], shifting the magnet [100], optimising the slot openings [111] and the pole arc coefficient [101 – 102]. Moreover, the authors in [103 – 104] present a possible method of teeth pairing, while [105 – 108] provides teeth notching as a technique to reduce the cogging torque in flux switching permanent magnet machines, though only suitable for machines with odd numbers of rotor [105]. Authors in [109] present a dual rotor axial field flux switching PMM whose cogging torque is reduced by approximately 77% with simply increasing the rotor pole width and adopting a fan shaped rotor pole.

Other techniques that are previously developed in literature to minimise the cogging torque magnitude of conventional MPMs consist of two major classes: 1) generating a supply current which produces an opposing torque ripple to the cogging torque [112] and 2) optimising machine size and parameters [113 – 116]. These include slot number and pole number combination, stator slot widths, radial air gap length and magnet thickness, pole arc to pole pitch ratios and skewing of slots in the stator or magnets in the rotor.

Although the MPM has equal number of stator teeth and rotor poles, these still line up twice in positions of low reluctance per electrical cycle. When moving through one electrical cycle, the rotor passes through the aligned and unaligned position twice. These positions are explained [28] and the graph of this cogging torque is shown in figure 3.7.

Fig. 3.7 shows the cogging torque created by a Single Phase MPM over one electrical cycle. The rotor starts in the d-axis, passes the q-axis at 90° , and crosses the negative d-axis at 180° , followed by q-axis at 270° and finally d-axis at 360° . These five are the zero torque positions for this machine type shown in figure 3.6.

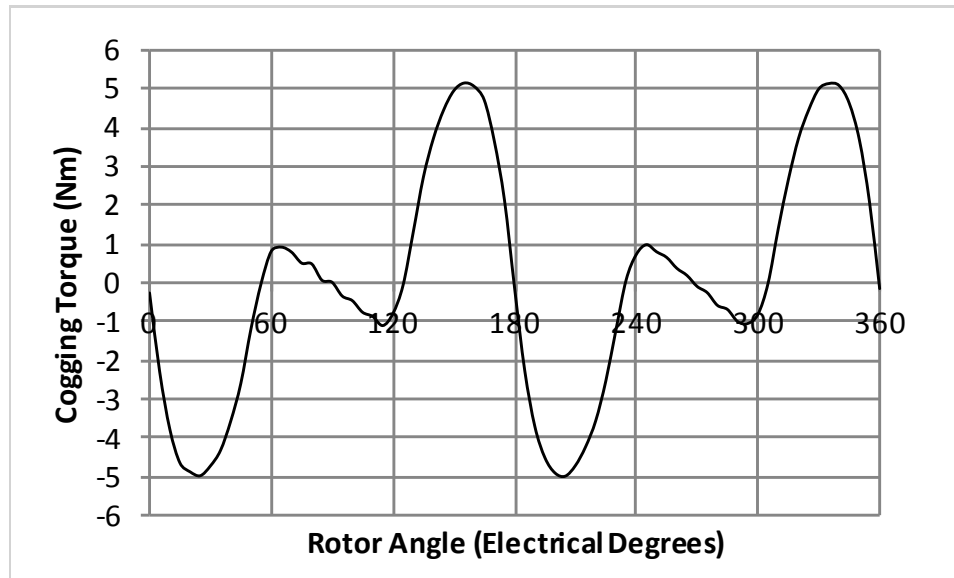


Figure 3. 7: The cogging torque of a Single Phase MPM over one electrical cycle [133]

Torque ripple is a combination of the cogging torque and the harmonic content in the back EMF waveform. It was shown in [30] that when such machines are used on load, there is a high harmonic content and hence MPM is not ideal for low torque ripple applications.

3.3.2 Factors affecting cogging torque

Cogging torque is largely affected by machine design issues and manufacturing related variables. These include magnet strength, slot width, manufacturing irregularities such as placement of magnets in the rotor and other manufacturing impact on materials (such as quality of SMC or stamping the laminations). The precision required in placing magnets in the rotor requires more attention than the dimension of the magnets itself, as it has a greater influence on the cogging torque, as previously been investigated [117].

Magnet strength is an important characteristic as it determines the air gap flux which in turn determines the magnitude of cogging torque. Factors such as temperature and initial charging of magnets also affect the flux density and hence the cogging torque.

Slot width is used to maximise the torque generation and is usually equal to the tooth width (at least in conventional designs). This is beneficial from output point of view but it is important to remember that it is the interaction between the magnets and slot opening that affects the cogging torque. It could be said that a zero slot opening will have zero cogging torque though a minimum opening has to be provisioned for winding placements. The key is to determine this minimum slot opening while maximising the torque output while placing magnetic wedges in the slot opening to reduce cogging torque; though this may increase the manufacturing cost.

Two other factors that affect the cogging are the manufacturing of stator laminations and the rotor eccentricity in the machine. Stator laminations isotropy is affected by punching, stamping, grain orientation, and method of stacking, using welds, holes and bolts and other forms of interlocking as these introduce anisotropies resulting in reduction of cogging cycles and hence increasing the cogging torque. Secondly, the rotor eccentricity in the machines is affected by the manufacturing tolerances and imperfections in the bearing which not only contribute to the unbalanced radial forces but also constraints the cogging cycles.

The priority of the new topologies is to reduce this peak cogging torque and its harmonics in order to provide smoother riding experiences for the rider.

3.3.3 Back EMF

The counter (back) electromotive force or the voltage produced against the current which induces it is an important indicator on machine's working capabilities and also on how well the prototypes are configured.

Three important features are to be considered when testing for back EMF for new topologies; the mean back EMF of the three phases, the harmonic content in the back EMF waveforms and the alignment of the three phases.

3.3.4 Torque Ripple

Torque ripple is the peak-peak torque expressed as a percentage of the average torque;

$$\text{Torque Ripple} = \frac{\text{Maximum Torque} - \text{Minimum Torque}}{\text{Average Torque}} \times 100\%$$

The torque ripple of this machine type is not just made up of the cogging torque but the harmonic content in the back EMF waveform and reluctance ripple due to inductance variations contributes too. It is vital to consider this especially when the application demands a low torque ripple as machines of this type can show a high harmonic content especially on load as was

shown in [30]. It has been previously stated that torque ripple can also be present/increased due to magnetic saturation [118, 119] as it enlarges the original three sources of torque ripple. There have been many instances in the previous literature where skewing the rotor and stator is used to minimise the cogging torque and back EMF harmonics in order to reduce the torque ripple [120 - 125].

Torque ripple can be caused by cogging torque, the interaction between the air gap flux harmonics and the MMF as well as mechanical imbalances. In order to reduce the torque ripple, the interference between the MMF and air gap flux harmonics must be analysed. It is known that this factor is influenced by changes in the geometry of the machine design; hence varying these should have an effect.

3.4 Summary

The main problems highlighted in this section were cogging torque, back EMF harmonics and therefore high torque ripple. It is important to keep in mind that a machine with a low cogging torque might have a high torque ripple whereas a machine with a high cogging torque might have a low torque ripple. This is due to the fact that the torque ripple due to the interaction between the MMF and air gap flux harmonics can compensate or increase the cogging torque in different cases. Magnitudes of these are presented in table 3.6 and the thesis is aimed at producing novel ways that can reduce these magnitudes while increasing or at least keeping the mean back EMF and average torque the same.

Table 3. 6: Summary of various base machine output values to be compared to newer topologies

Peak Cogging Torque	1.76 Nm
2 nd harmonic cogging torque	0.23
4 th harmonic cogging torque	0.17
6 th harmonic cogging torque	1.46
12 th harmonic cogging torque	0.52
Mean back EMF	109.55 V
5 th harmonic back EMF	3.20
7 th harmonic back EMF	0.86
Torque Ripple (%)	25
Average Torque at 285 rpm	14 Nm

4. Design Investigations

This chapter introduces techniques that can improve current Modulated Pole machines (MPM) by reducing the cogging torque, back EMF harmonics and the torque ripple. All the techniques were first simulated using 3D Finite Element methods with Infolytica MagNet software; results and comparisons are presented in this chapter.

It is seen previously that only one phase of a multiphase MPM is modelled when using finite element analysis. This is due to the fact that there is a magnetic isolation for each phase for most part due to the separation of both rotor and stator. However in this thesis, the finite element analysis is conducted on models that represent all three phases. This is because the machines modelled in this thesis use the same rotor where the three phases share some magnet between them, as shown in figure 4.1. This extra magnet increases the flux linkage of all phases of the SPMPM when compared to modelling a single phase machine. This was investigated previously (in) [117].

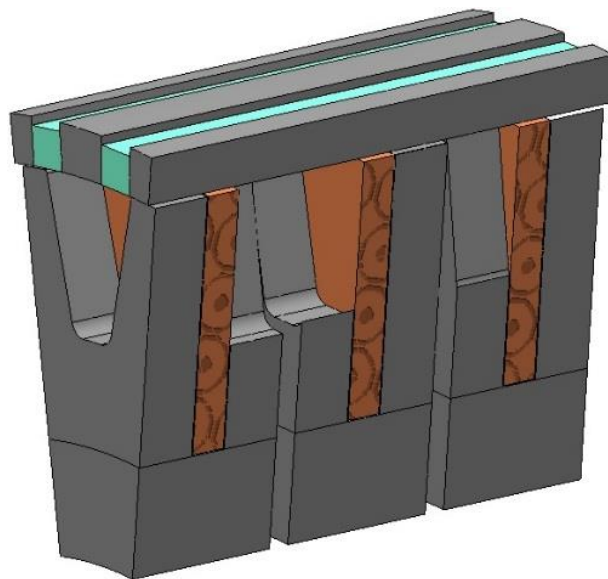


Figure 4. 1: FEA geometry of one pole-pair

Due to periodic nature, there was no need for a full fifty poles finite element model rather a two poles of each machine was modelled with an even periodic boundary condition applied to the edge of the models. This reduced the computational time required for the models to solve as the models were not as complex as would be for a 50 poles model and therefore reducing the number of elements it contains. The two pole geometry for FEA is shown in Figure 4.1.

4.1 FEA – Mesh Sensitivity Analysis

There is a lot of work that is purely theoretical based on outcomes from 3D FEA. It is important to verify the sensitivity of the solution mesh as it is considered the most valuable part for torque quality analysis in this thesis. A mesh is used in FEA to segment the model of the machine into many small parts which are termed elements. These elements are of first or second order tetrahedrons with their specific set of equations which when solved provide the solution of the magnetic fields in the model.

The initial analysis in this thesis are all based on FE solutions. These are extremely sensitive to the size of mesh especially in the regions such as air gap. This is because of the large changes in the magnetic fields and stored energies. For the solution to be considered valid, it is vital that the mesh of the FE solution is within reasonable bounds.

A mesh sensitivity analysis was conducted where in the mesh size was reduced until the change in d-axis flux or peak torque became very small (due to finer mesh) i.e. less than 1%. Reducing the mesh more than this would considerably increase the computation time without much improvement in accuracy of the results.

Machine's air gap was the key region where mesh refinement would have the biggest effect as most energy is stored here and field changes direction the most. Due to this reason, air gap mesh was kept significantly denser than other regions in the machine. The maximum element size in the air gap was limited to 0.4mm, the model contained over 60,000 elements.

Air gap was split into four section. These were named stator air box, stator slip, rotor slip and rotor air box. The rotor and stator air boxes extend into the air gap by 0.1mm to make sure that they clear any stator or rotor components that have acute edges. This is very important as these are the areas where there are very high errors in the field, in fact a right angled corner would tend towards a field with an infinite flux density at that point.

The torque calculated in MagNet™ by the Maxwell Stress method along a surface with such field irregularities would lead to a highly inaccurate calculation [136]. Hence extending the rotor and stator air boxes into the air gap and assigning a material known in MagNet™ as virtual

air which is not used to denote separation between bodies removes the problem caused by the field errors at component edges. This is known as virtual air shell [136].

So the model is split in four section; rotor air box, rotor slip, stator slip and stator air box. Rotor and stator slips are in the air gap regions therefore applying a fine mesh to these regions only as they benefit from it the most. It also allows for a boundary condition to be placed upon the surface of the static slip region, shown in Figure 4.2; this is required for proper operation of the model when static three dimensional models are solved.

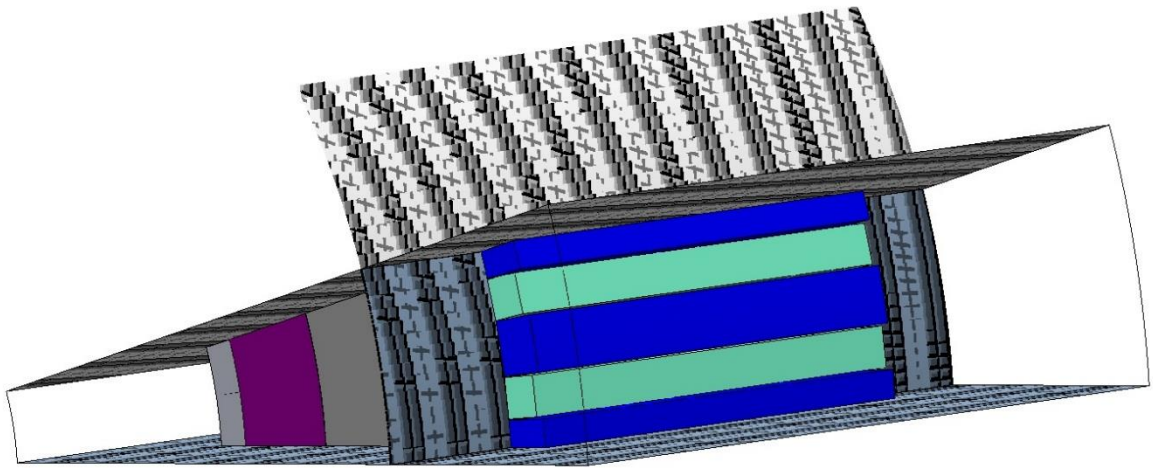


Figure 4. 2: Periodic boundary condition for a 2 pole section of MPM

4.2 FE Models vs. Prototypes

Work done previously [117] showed that there are some known differences between the FE models and the final prototypes that can be included in the adjusted FE models. These differences were:

- An increased air gap due to excessive machining of the stator to remove high points from construction. These were measured by clocking the teeth while holding them in a lathe and were in the range of +/-0.05mm.
- A construction gap between the SMC core-backs and the inner diameter of the stator laminations. This exists as there must be some clearance to be able to fit the laminations over the SMC core-backs and also because of the tolerances that occur in manufacturing, this was expected to be in the range of 0.025mm – 0.1mm [117].
- There can be gaps between the rotor poles and magnets which is a difficult problem as these gaps are non-uniform and are not easy to measure.

Although the effect of these gaps is averaged out on the measured back EMF, there is also the possibility that the tolerance in the angular placement of the magnets and pole pieces could create a ‘pitching’ effect, which may also reduce the magnitude of the fundamental EMF and some harmonics.

There was analysis carried out [117] where such gaps were introduced in the FE models to notice the effect of these. It was concluded that a gap of 0.05mm will be introduced between the stator laminations and SMC core-back and a 0.2mm gaps between rotor poles and magnets gives a reasonable correlation however air gap was kept at 0.4mm. It was understood that if there are any variances between the FE and prototype results, these are mainly due to the differences listed above. Illustration of these gaps is shown in Figure 4.3.

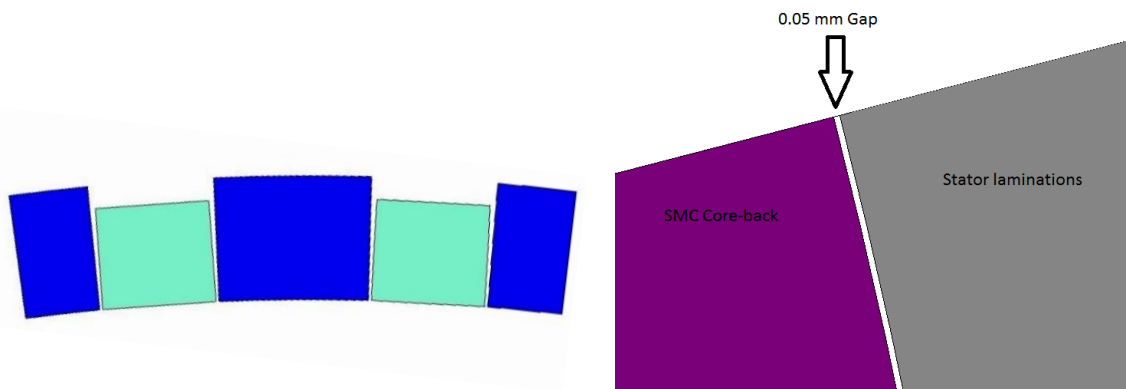


Figure 4. 3: Illustration of gaps between rotor poles and magnets (left) and SMC core-back and stator laminations (right)

A parameterised model of a three-phase machine was created where all dimensions and machine parameters can be altered (diameter, axial length, pole number, tooth span, magnet size, pitching angle, MMF...). To reduce computing time (which can be quite considerable for a 3DFE simulation) a two-pole segment of the machine is simulated and an even magnetic symmetry applied. A view of the 3DFE solid models is shown in Figure 4.4.

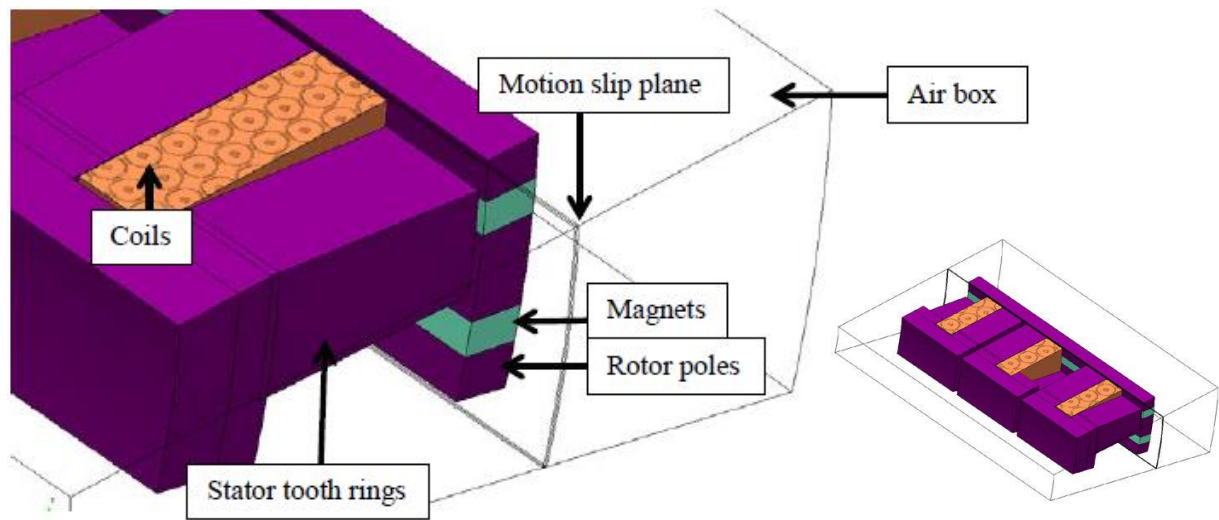


Figure 4. 4: 3DFE solid model of a two-pole segment of the MPM showing rotor and stator airboxes and slip regions

Experiments and verifications are carried out on a number of prototypes in Chapters 6 and 7.

A variety of techniques were discussed in chapter two to reduce cogging torque, however this chapter focuses on some novel methods that have minimal effect on the torque producing capability of the machine.

The design techniques presented in this chapter comprise of ‘Combination of Tooth spans’, ‘Tooth Pitching’, and ‘Designing pole pieces with different shapes’. All of these techniques are aimed to reduce the cogging torque, back EMF harmonics and torque ripple, whilst having a minimal effect on overall torque production.

4.3 Tooth tip span alteration and combinations

The parameter of interest in this section is the stator tooth span as shown in Fig. 4.5; this will be varied and the effect on cogging torque, back EMF harmonics and torque ripple is assessed. It is a much more predictable way of tuning the torque and EMF harmonics as the ratio of pole span to tooth span is merely changed by varying the tooth span and keeping magnet thickness the same; rotor pole span stays constant. This also means that there will be less of an impact on the magnitude of the fundamental back EMF as the magnets are unaltered. Varying this dimension has a minimal influence on the mass, and torque production ability of the machine in the range applicable for this machine.

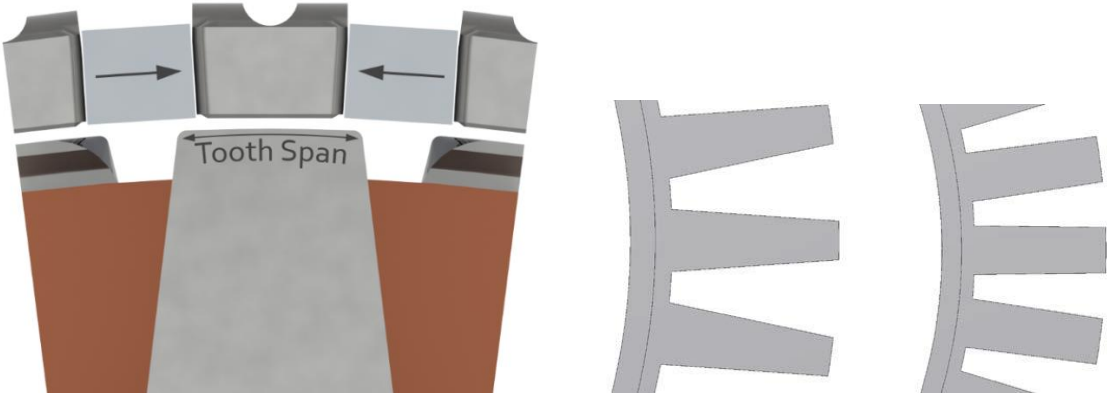


Figure 4. 5: Illustration of the tooth span of an MPM, tooth span changes applied: 120° span (left) and 180° span (right)

The tooth span was varied between 120° and 180° electrical and the Finite Element simulations for each were carried out. Figure 4.6 show the change in magnitude of the important 6th (T_{c6}) and 12th (T_{c12}) harmonics along with the peak cogging torque value corresponding to each span.

The peak cogging torque of the base design with a 130° tooth span was found to be 1.76Nm. A trend was observed, as the tooth span increased towards 170°, the cogging torque decreased to 0.42Nm. This is a significant reduction in peak cogging torque; figure 4.7 presents these two waveforms.

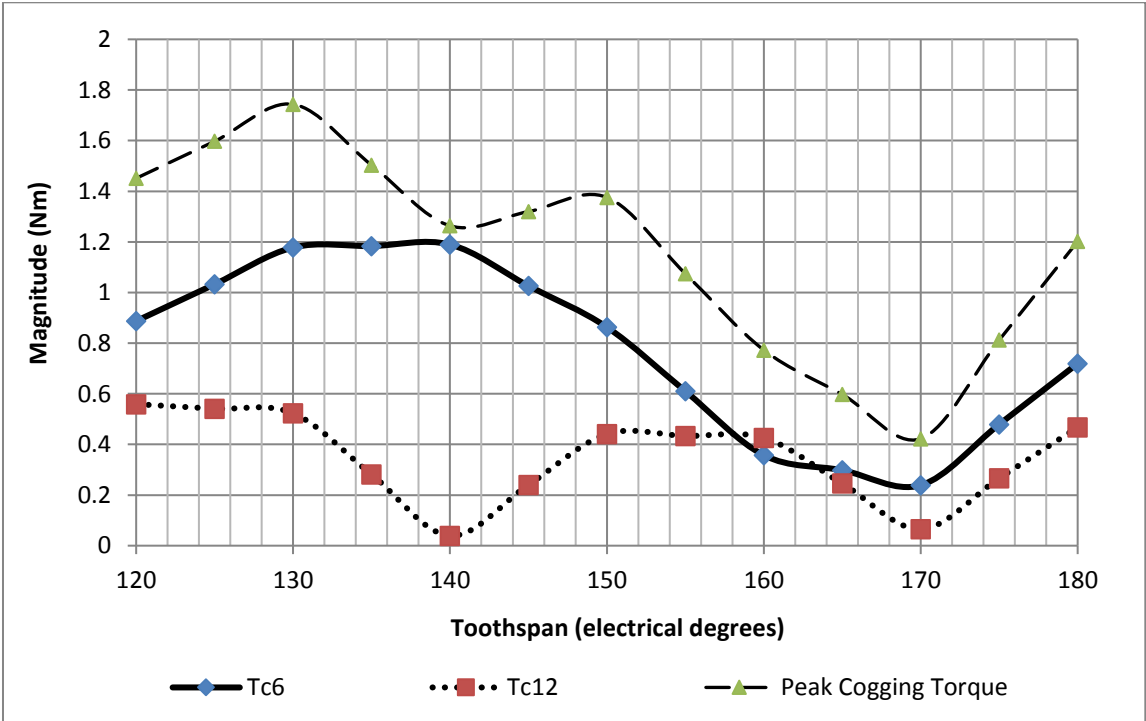


Figure 4. 6: Magnitude of cogging torque harmonics in the three-phase MPM with varying tooth span (FE analysis)

It is also evident from Figure 4.6 that T_{c6} is cyclic with its maxima at a tooth span of 135° and minima at a tooth span of 170° . T_{c12} is also cyclic however there are two cycles repeated within the tooth span range studied in this section. The two minimums of this trend are observed at a tooth span of 140° and 170° .

There is a pattern seen in Figure 4.6, the peak cogging torque is in fact just the summation of T_{c6} and T_{c12} , this is shown in Table 4.1. Adding T_{c12} for each tooth span gives a number that is very close to the actual peak cogging torque noticed for that tooth span, percentage difference is nearly zero for various tooth spans especially 120° and 160° . The only noticeable difference is for the tooth span of 170° , however that is mainly due to the values being quite small and hence a small difference makes a big percentage difference.

This meant that almost all the other harmonics contributed very little to the overall cogging torque of the machine for these tooth spans. Figure 4.7 presents a complete representation of all the harmonics in the range of tooth spans investigated and it is clearly seen that T_{c6} and T_{c12} are the main ones present.

Table 4. 1: Illustration of 6th and 12th harmonics being the main ones contributing to the overall cogging torque

Tooth Span (Elec. Deg)	6th harmonic	12th harmonic	Sum of 6th and 12 th harmonics	Peak Cogging Torque (Nm)	Percentage Difference
120	0.8873	0.5589	1.4462	1.4511	0.34%
130	1.1778	0.5233	1.7011	1.7434	2.43%
140	1.1894	0.0392	1.2286	1.2636	2.77%
150	0.8630	0.4411	1.3041	1.3756	5.20%
160	0.3573	0.4260	0.7833	0.7835	0.02%
170	0.2389	0.0655	0.3044	0.4225	27.95%
180	0.7195	0.4675	1.1870	1.2017	1.23%

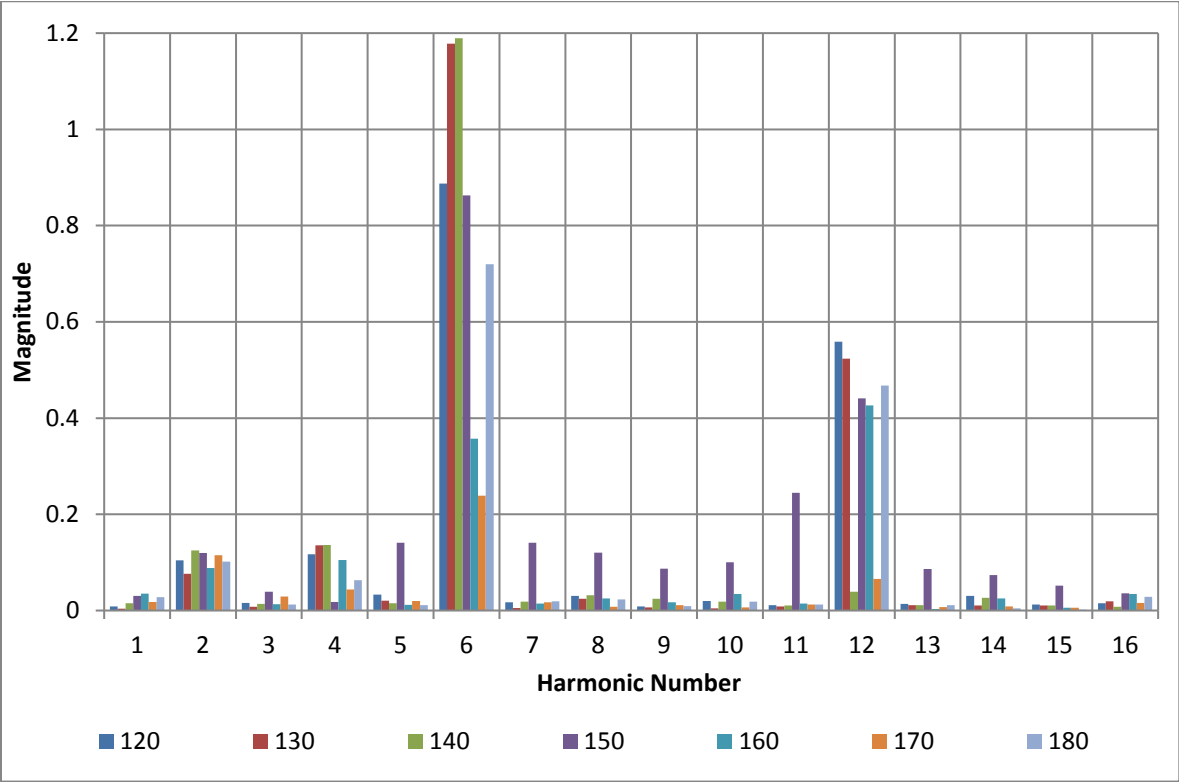


Figure 4. 7: Harmonic content of cogging torque with changes in tooth span

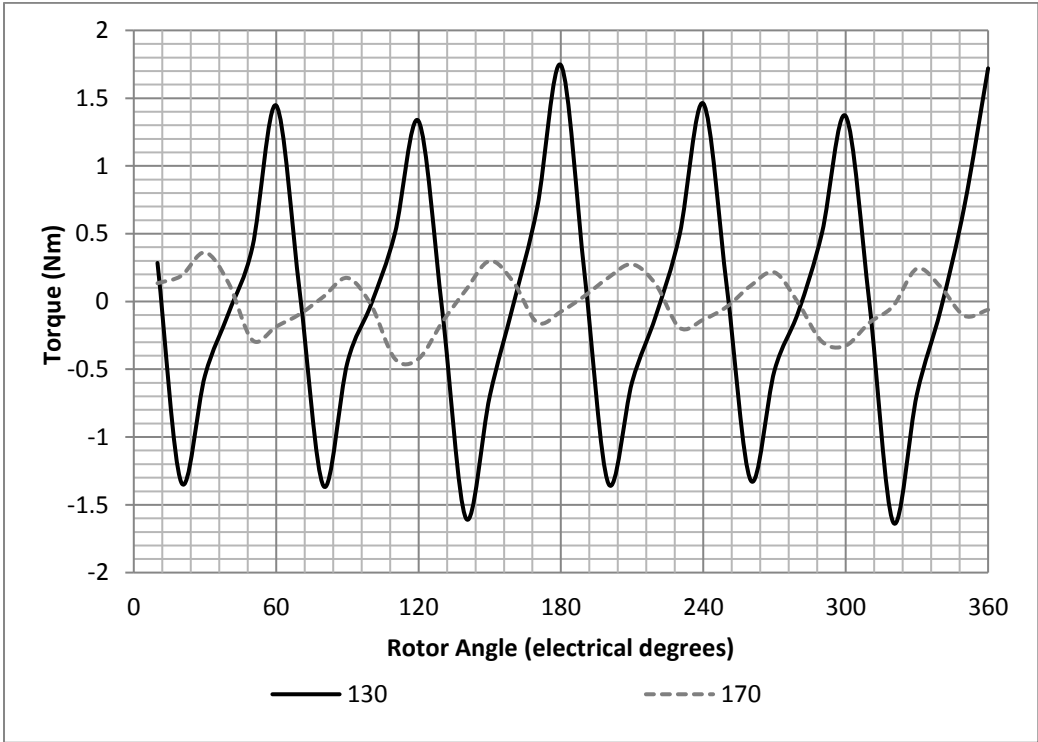


Figure 4. 8: Cogging torque of the three-phase MPM with 130° and 170° spans.

Torque ripple can be caused by cogging torque, the interaction between the air gap flux harmonics and the MMF as well as mechanical imbalances. In order to reduce the torque ripple,

the interference between the MMF and air gap flux harmonics are analysed. It is known that this factor is influenced by changes in the geometry of the machine design; hence varying tooth span should have an effect.

It was observed that similar to the cogging torque harmonics, changes in the tooth span also vary the back EMF harmonic content. Figure 4.9 shows the shape of the back EMF waveform for three different tooth spans, while Figure 4.11 shows the change in the major harmonics; with tooth spans from 120° to 180° . The three phases are connected in a star configuration, hence the triplen harmonics cancel.

It can be seen that as the tooth span changes, the harmonic magnitude is cyclic with clear minima and maxima. A span of 130° gives the lowest harmonic content with the 5th (E_{f5}) almost cancelled while a 170° span maximised the 5th and 7th harmonic (E_{f7}). This is exactly opposite to what we see in Figure 4.2 as the tooth span of 170° gives the lowest cogging torque and tooth span of 130° gives nearly the highest.

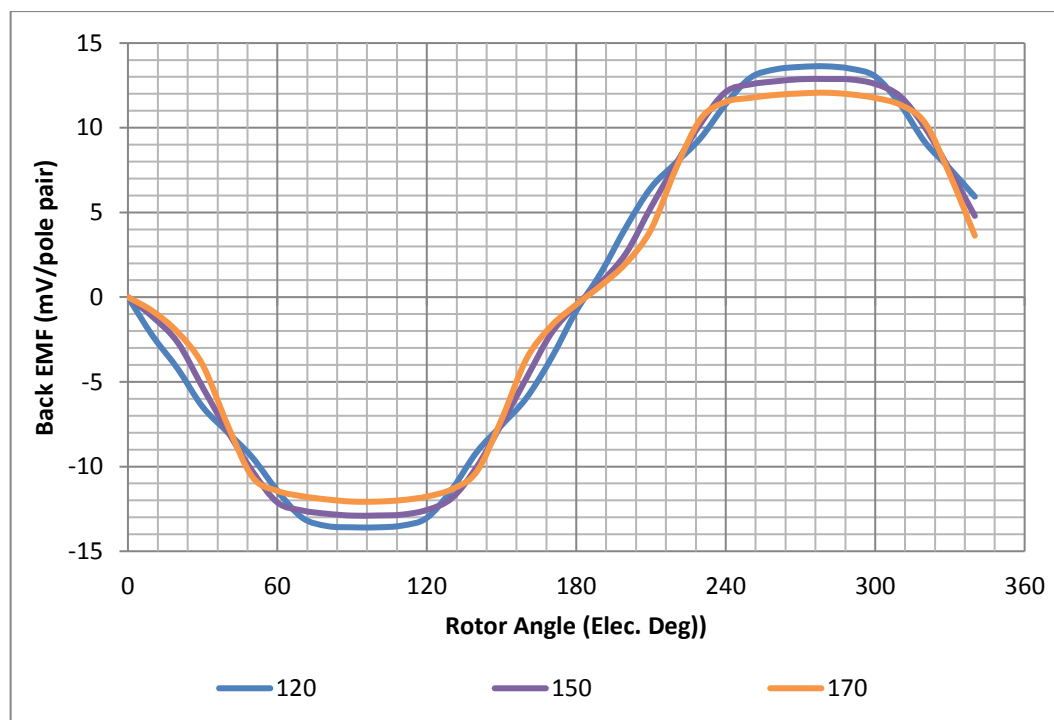


Figure 4. 9: Variation in back EMF waveform with tooth span

It can hence be concluded that a machine with low cogging torque will most probably have a high E_{f5} and a machine with high cogging torque will most likely have a low E_{f5} . This is mainly due to the fact that the back EMF harmonics can sometimes compensate/increase the cogging torque; lowest cogging torque solution will not be the best solution for harmonic content.

The significant drop in the fundamental as the tooth span increases is due to the stator tooth spanning more of the magnet and creating a magnetic short circuit. Wide tooth spans provide a low reluctance path for magnet flux where there is a short gap and hence aids the flux in travelling from one side of the magnet to the other without linking the coil, as shown by Figure 4.10.

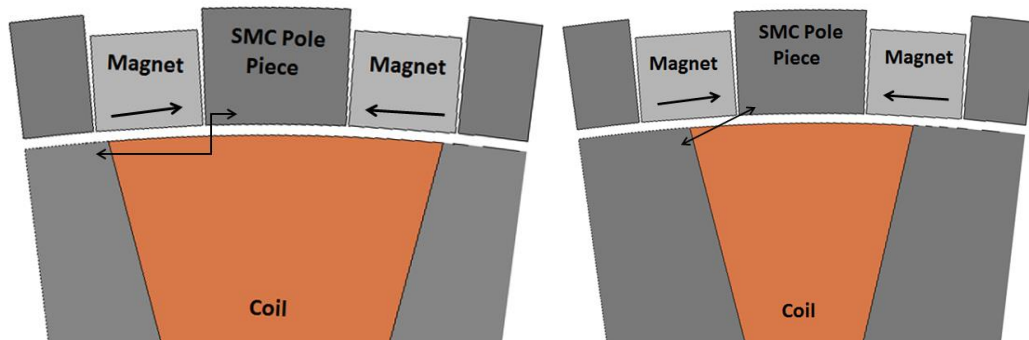


Figure 4. 10: A tooth span of 180° (right) covering a significant area of rotor magnet causes an increased flux leakage between the tooth and the magnet compared to a tooth span of 120° (left)

There is unfortunately a trade off when using tooth span to reduce the harmonics in the back EMF, and that is the effect it has on cogging torque. If the tooth span is changed the position at which the poles come into line with the teeth change, which will affect the rate of change of reluctance as seen by the rotor, and hence the cogging torque.

Figure 4.6 shows the cogging torque (non-energised coils) waveforms for the same range of tooth spans as that used in the study of back EMF. It can be seen that the optimal cogging torque is achieved at the tooth span of 170°, a position where harmonic content of the back EMF waveform is not ideal.

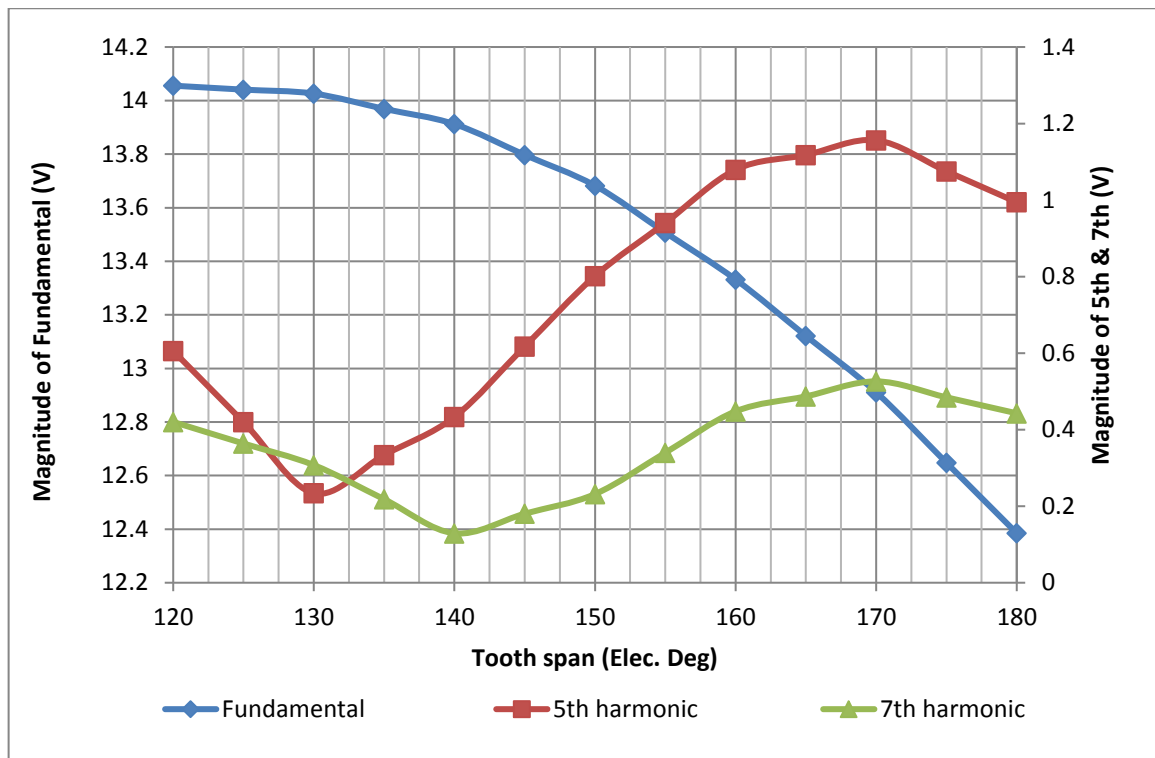


Figure 4. 11: Harmonic content of back EMF waveform with tooth span.

Both back EMF harmonics and cogging torque contribute to torque ripple. The effect of tooth span on the overall torque ripple has been analysed. A sinusoidal current with a peak value of 20A was applied to the three phase machine over the same range of tooth spans (120° to 180°); the torque ripple for each tooth span is shown graphically in Fig. 4.12.

It is seen that the span of 170° gives the lowest torque ripple which matches the position of lowest cogging torque found earlier (Figure 4.6). The torque ripple as a percentage of full load torque is reduced significantly from 25.5% for a 130° span to 17.1% for a 170° span, the mean torque drops by 8%, as would be expected due to the drop in the fundamental component of back EMF as shown in Figure 4.8. The two waveforms for the base 130° design and the 170° span tooth are shown in Fig. 4.13.

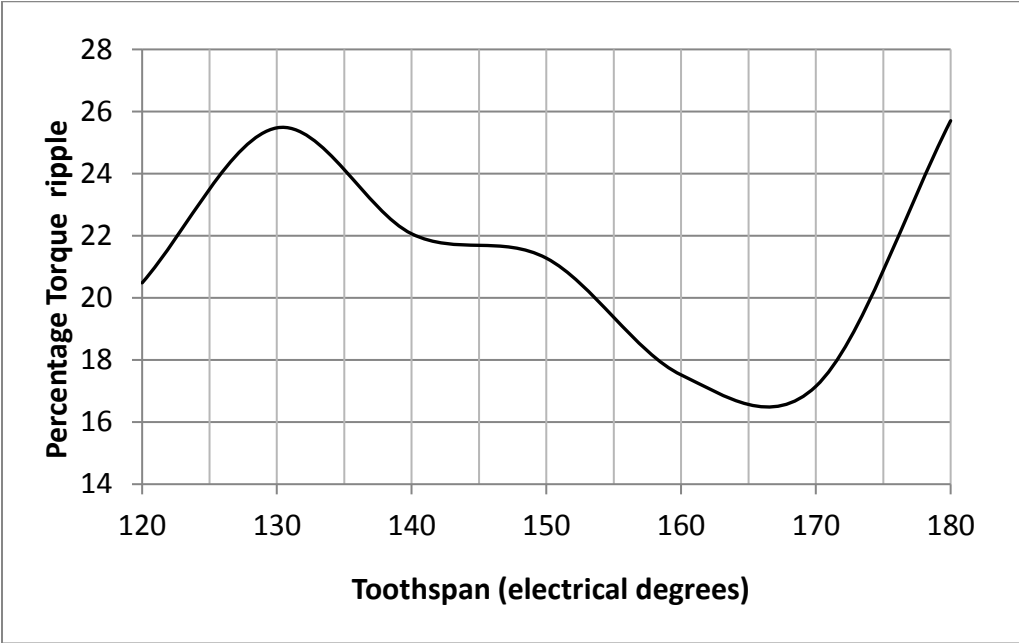


Figure 4. 12: Torque ripple as a percentage of average torque

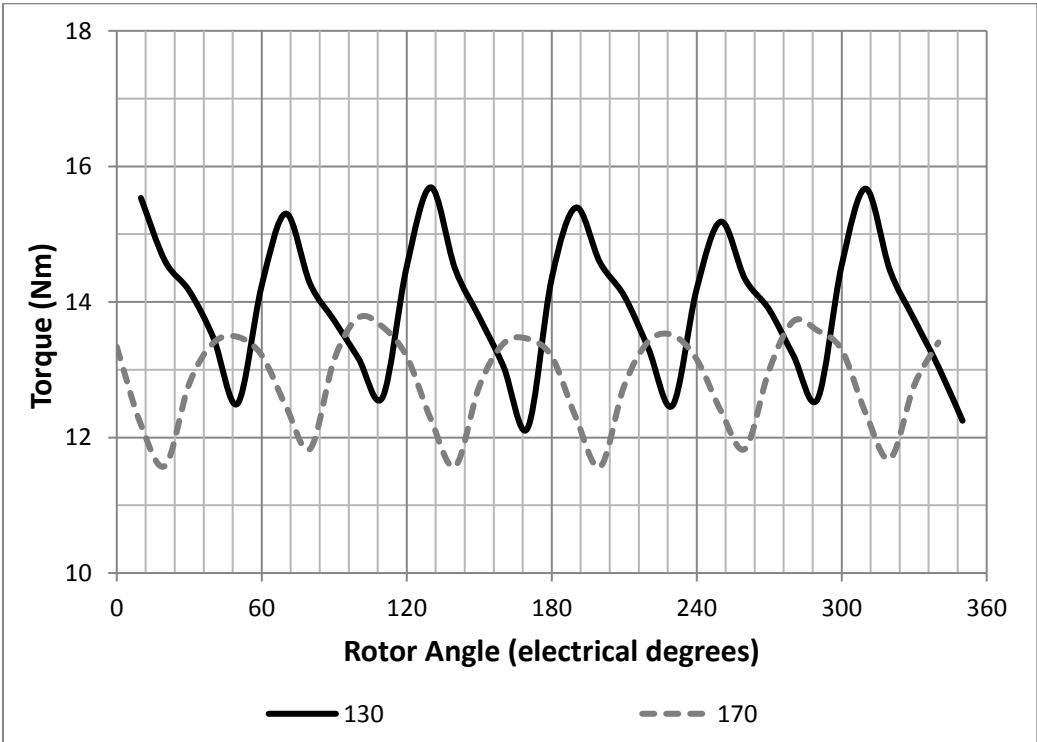


Figure 4. 13: Three-phase torque waveform for 130° and 170° tooth span

It was proposed that by applying a variety of tooth spans to the 25 tooth stator, the cogging torque and torque ripple of the machine can be reduced. Various spans could be selected in a way to attenuate certain harmonics.

This is achieved by summing the cogging torque waveforms off 120° and 180° span shown in Fig. 4.14, as these are in anti-phase and hence undergo destructive interference, reducing the resultant torque ripple. Also, it can be seen from Fig 4.6 that the T_{c6} for tooth spans between 120° to 150° is in anti-phase to tooth spans between 170° to 180° and hence the reduction in torque. Fig 4.6 also shows that T_{c12} changes phase twice between 120° and 180° and hence will be in phase. This means that the summing of waveforms in Fig 4.14 will result in T_{c6} being reduced while T_{c12} will be averaged for the two waveforms.

To test this logic, a FE simulation was created where the machine model was designed where twelve teeth were of a 120° span and the other thirteen were a 180° tooth span. Fig 4.15 presents the harmonic content of the resulting cogging torque waveforms. It is evident that the T_{c6} was subject to destructive interference and was greatly attenuated whilst T_{c12} experienced little change as it was in phase and resulted in being averaged out between the two tooth spans.

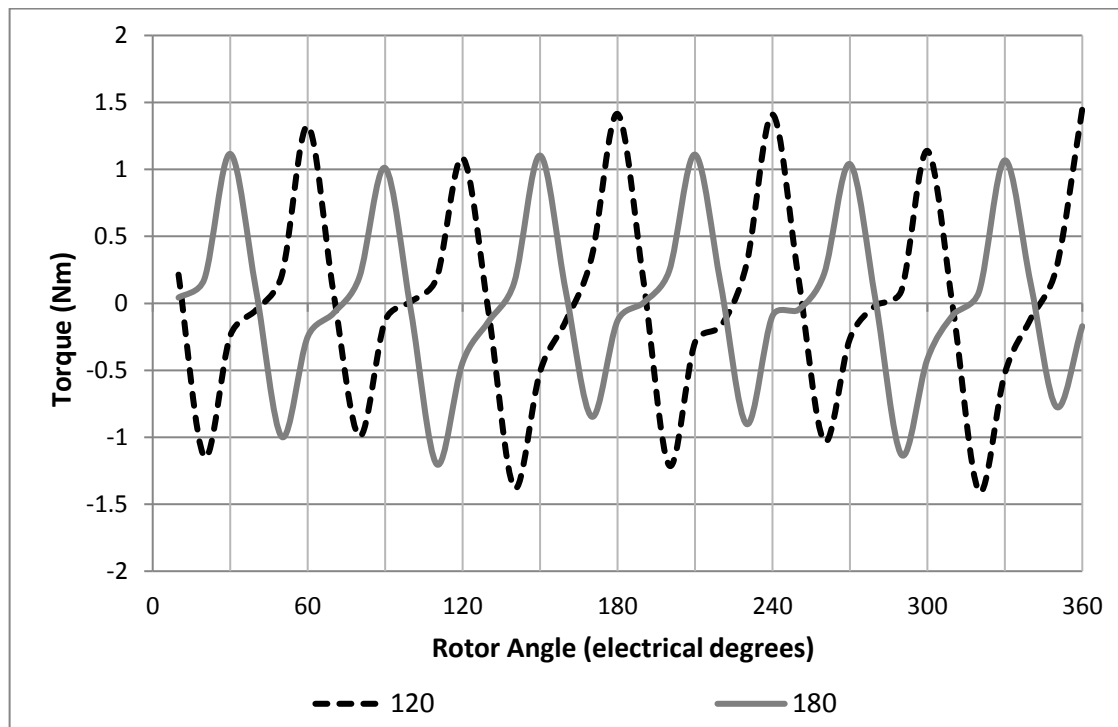


Figure 4. 14: Cogging torque waveforms for a 120° and 180° span machine

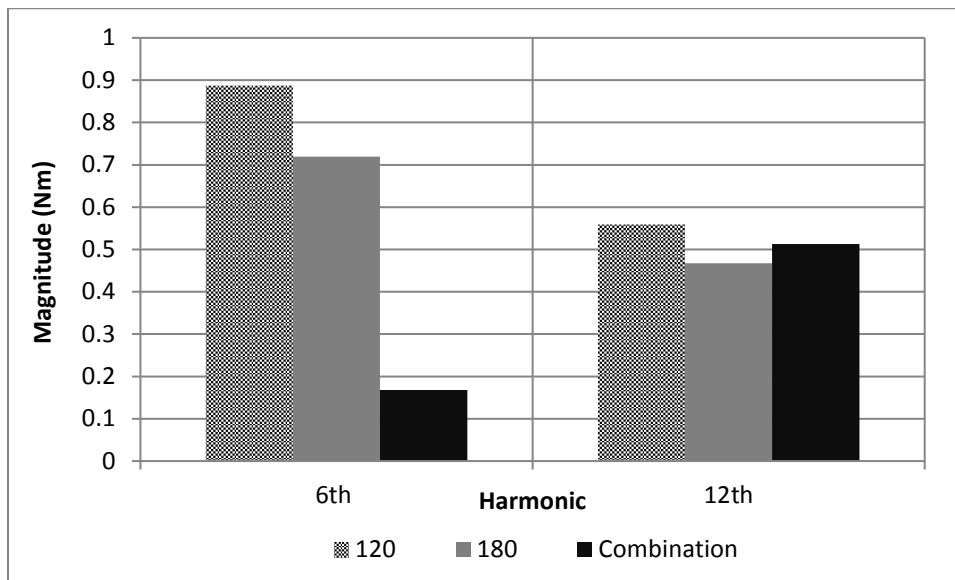


Figure 4. 15: Harmonic content of cogging torque with a combination of tooth spans

The above results paved the way for modelling a machine with a combination of tooth spans in order to investigate the effect of this on cogging torque and torque ripple. Fig. 4.15 also shows that adding the effect of two teeth with different spans together is possible, except for the points at which teeth of two differing spans intersect.

To verify the findings in Figure 4.15, a 3DFE simulation of a MPM with various spans was created. The 3DFE model showed that there was indeed a slight difference due to the intersection of the different tooth spans around the stator circumference. As the proportional of stator circumference affected by the intersection of difference tooth spans is small, the influence on overall torque is negligible. It was also a concern that the differing tooth spans would results in unbalanced magnetic forces; however the initial results suggest this is not the case [35].

4.4 Reduction of cogging torque and torque ripple

As the tooth span is a continuous variable, there are an infinite number of tooth span combinations available, however it is important to find an optimum combination which is a good compromise between cogging torque, torque ripple and back EMF harmonic reduction. There were many combinations of tooth spans available to reduce the cogging torque and torque ripple. Various calculations were carried out in Excel to reduce the peak cogging torque, the two best combinations are shown in Table 4.2.

The machine has 25 pole pairs, hence 25 stator teeth per stator half; there are only a few possible ways this machine could have been modelled to keep the periodic boundary conditions. Periodic

conditions in Finite Element are vital as these reduce the solution time of the model by reducing the mesh density of the model.

Table 4. 2: Tooth Combinations – Number of teeth of each span

Name	140° Tooth Span	150° Tooth Span	180° Tooth Span	Total teeth
Combination 1	6	7	12	25
Combination 2	0	14	11	25

Fig 4.16 shows the stator half for combination 1 where in 12 teeth are of 180° span, 7 teeth are of 150° span and 6 teeth are of 140° span. Both combinations were simulated and the resulting waveform was compared to the base design (a 130° span) and a 170° span (as it provided the lowest cogging torque harmonics and the lowest torque ripple).

These new combinations reduced the peak cogging torque and the torque ripple; Fig. 4.17 and Table 4.3 depict this improvement.

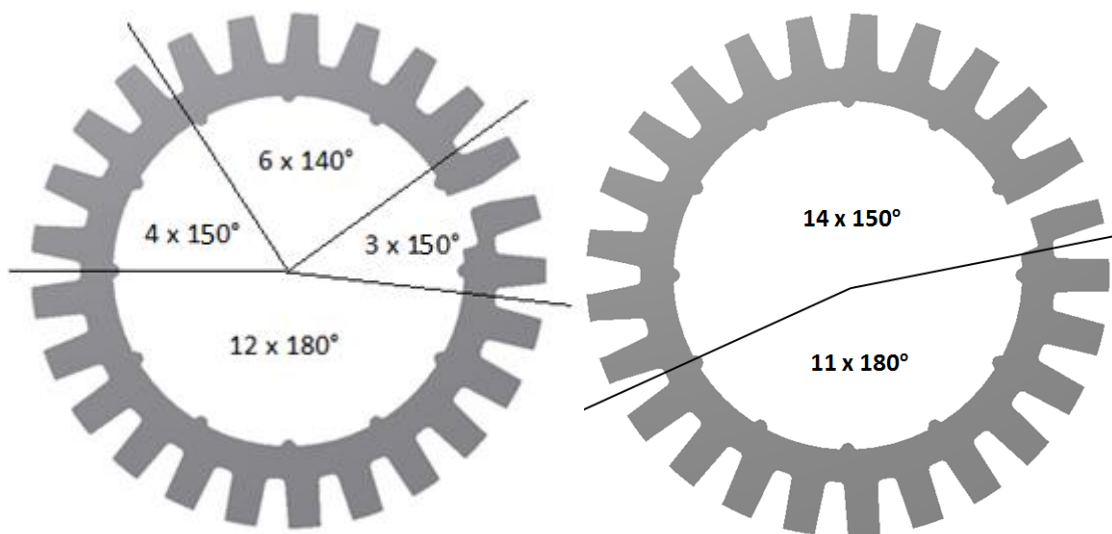


Figure 4. 16: Illustration of the two tooth span combinations; combination 1 on left, combination 2 on right

Combination one has the lowest cogging torque at 0.37Nm peak, a reduction of 79% from a span of 130° and 12% from that of 170°. In terms of torque ripple, combination one provides the best outcomes with a ripple of only 2.02%; decreasing by 92% from that of the base model with a tooth span of 130°. The peak cogging torque of combination two is higher than

combination one though this can be accounted for the fact that the cogging torque cancels the ripple introduced due to harmonic content.

Table 4.3 also shows the reduction in average torque for the new combinations and it is evident that there is a little reduction. This comes from the reduction in the fundamental harmonic content of the back EMF waveform when higher tooth spans are used as was shown in Fig 4.8. Even though the average torque produced by combination two is reduced by 2.1% in comparison to the base design this still corresponds to a torque per kg of active mass of 3.83Nm/kg.

It can be seen that while combinations 1 and 2 reduce the peak cogging torque and torque ripple, the back EMF harmonics, especially E_{f5} , increases when compared to the 130° tooth span. It is important that a combination of tooth span chosen not only reduces the cogging torque and ripple but also the back EMF harmonics.

There are many combinations of spans that can reduce the ripple and cogging torque, though for simplicity and ease of production of a component, the choice has been limited to three.

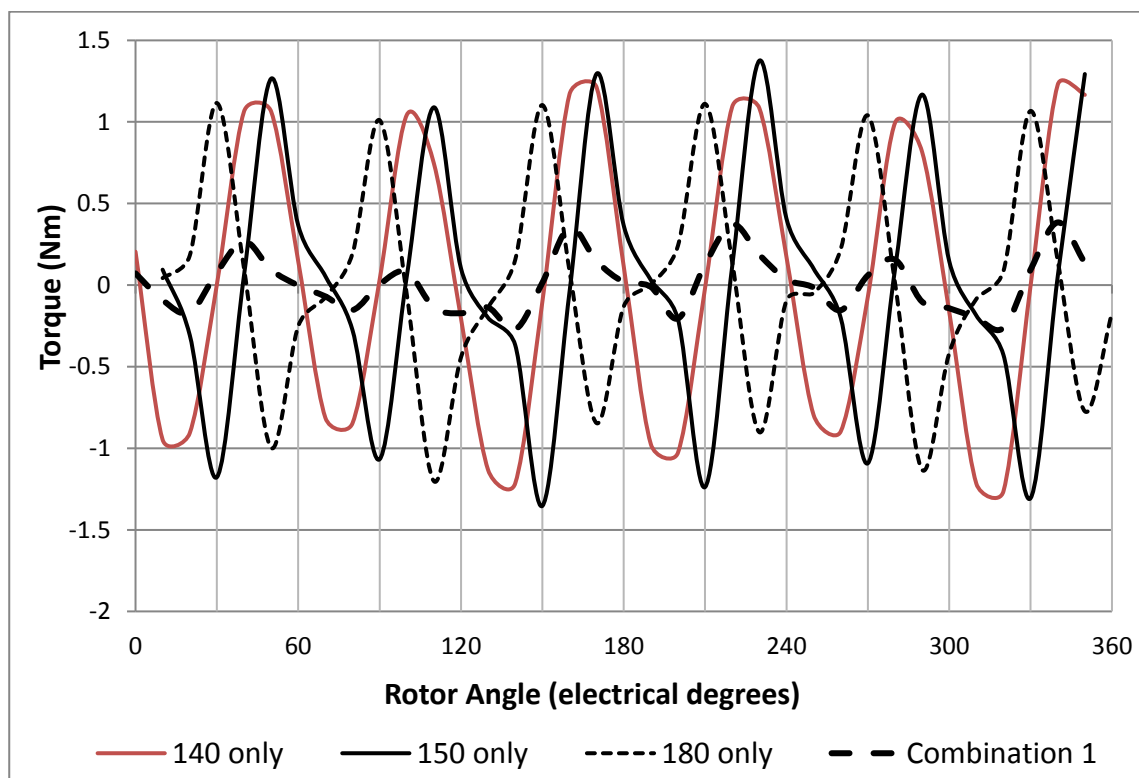


Figure 4. 17: Cogging torque waveform with a combination of tooth spans

Table 4. 3: Summary of different combinations of tooth span (Combination 1 comprises of three tooth spans while Combination 2 is made up of two different tooth spans – details of each combination presented in Table 4.2)

Combination	Peak Cogging (Nm)	T_{c6}	T_{c12}	Torque Ripple (%)	Change in Torque (%)	E_{f5}	E_{f7}
All 130° (Base)	1.76	1.46	0.52	25.4	0	0.234	0.31
All 170°	0.42	0.24	0.07	17.1	8.06	1.16	0.53
Combination 1	0.37	0.19	0.06	2.02	1.98	0.87	0.19
Combination 2	0.39	0.18	0.10	4.06	2.08	0.97	0.24

4.5 Conclusion

This section explored the possible reduction of cogging torque and torque ripple in a three-phase Modulated Pole Machine. An analysis was carried out to distinguish the optimum tooth span for the machine between 120° and 180°. It was concluded that the 170° span gave the lowest cogging torque and torque ripple while a 140° provided the lowest non-fundamental harmonic content for the back EMF.

It was examined that the cogging torque and overall torque ripple could be reduced by changing a simple stator dimension, the tooth span. Two simple combinations were modelled and investigated; it was found that the peak cogging torque could be reduced by a further 79% by having a combination of three tooth spans. This combination reduced the torque ripple on load to 2.02% of the average torque with only a 2% reduction in the average torque.

Depending on the choice of application, the final combination choice of tooth spans can be made; combination one will provide the lowest peak cogging torque and the minimum torque ripple. It can be seen that more the combination of tooth spans, the lower the cogging and ripple; combination 1 made up of three different tooth spans performs better than combination 2 which comprises of only two different tooth spans. This method could be further expanded to tune the machine output torque with other and additional combinations.

4.6 Pitching the Stator components

The technique of pitching the coils is used in conventional radial flux machines to minimise winding harmonics. In radial machines, the coils are separated by the same electrical degree as the pole pitch in order to achieve voltages that are opposite polarity under south and north pole and hence can be summed together to give twice the conductor-induced EMF when connected in series. However if the coil pitch is different to the pole pitch, the resultant induced EMF is reduced as it has a phase shift other than the pole pitch. This is usually accounted by an attenuation factor known as the pitch factor which is represented by equation 4.1 where n is the n th harmonic and Ω is the coil pitch angle, as illustrated in Figure 4.18.

$$k_p = \sin\left(n\frac{\Omega}{2}\right) \quad (4.1)$$

A harmonic can be cancelled by choosing a coil pitch with a pitch factor equal to zero e.g. a coil pitch of 72° would eliminate the 5th harmonics (while there will be no triplen harmonics in star connected windings).

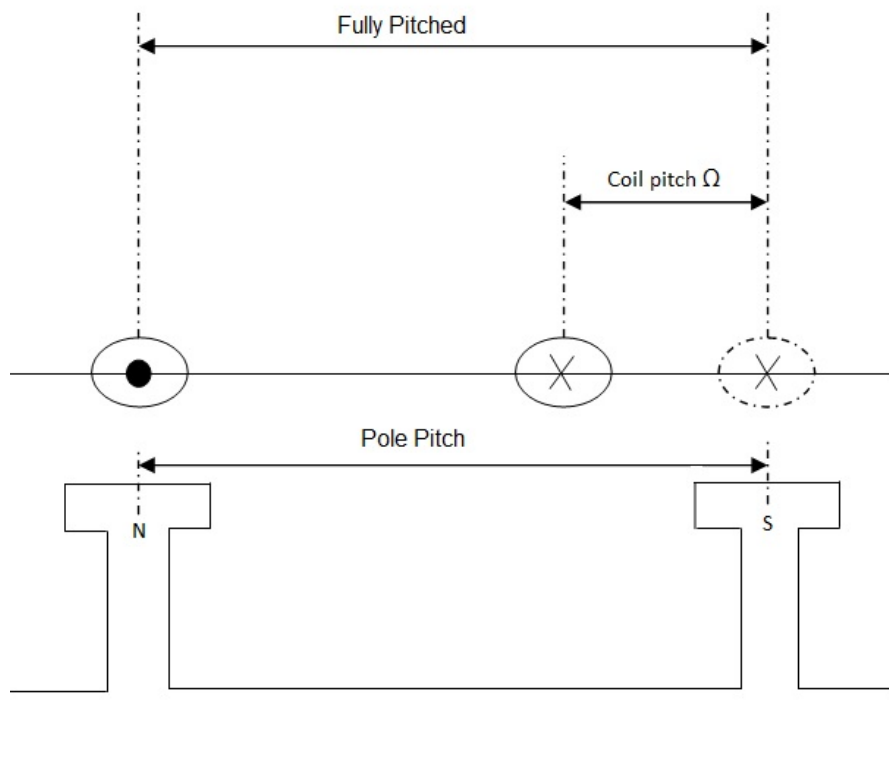


Figure 4. 18: Illustration of pitching angle Ω

In radial machines, the number of pole and slot numbers determine the number of angles that the windings can be pitched by. If the slots are increased while the pole numbers are kept constant, slots angles would decrease and hence more flexibility for pitching is available; though increasing the complexity.

4.7 Cogging Torque

In a MPM, each phase has a simple hoop coil which cannot be pitched in the same way as a radial machine. The stator structure modulates the simple 2 pole field of the hoop coil to a multi-pole field, dictated by the number of stator tooth per stator half.

There is freedom in the position of these stator teeth around the circumference so by offsetting teeth either side of the centre line, as shown in figure 4.19, the MPM is capable of pitching. These pitching angles would change the position at which the teeth overlap the poles and hence will have an effect of the cogging torque produced by the machine.

In a fully pitched version of a 50 pole MPM, the stator teeth are displaced by 14.4° mechanically, this equates to 360° electrical (two pole pitches). In the same way as a radial machine, this amplifies or attenuates harmonics of EMF and torque.

Equation 4.2 combines the pitch angle, θ_{pitch} and harmonic number where n is the harmonic to be cancelled.

$$\theta_{pitch} = \frac{180}{n} \quad (4.2)$$

Previously, Figure 4.6 showed the cogging torque was dominated by the 6th and 12th harmonics. If we consider the T_{c6} ; equation 4.2 suggests a pitching angle, $\theta_{pitch} = 30^\circ$, will cancel T_{c6} . To apply this to the MPM, the stator teeth would alternate at $+30^\circ$ and -30° electrical from the tooth centre.

For a 50 pole machine, this equates to a $\pm 1.2^\circ$ mechanical offset as shown in Figure 4.19.

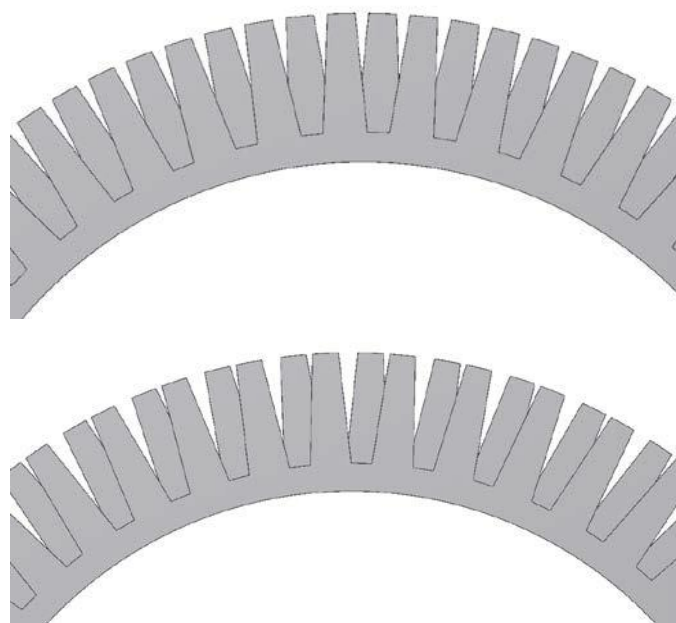


Figure 4. 19: Stator phase front elevation (coil removed) with 0 pitch (left) and 30 pitch (right)

As the teeth are shifted by $\pm 30^\circ$ electrical, the flux enclosed by the coil is also shifted by $\pm 30^\circ$ per pole pair. However, overall total flux linkage is not affected by the phase shift, as the sum of two sections of a coil sum to zero.

The tooth pitching technique was tested in a 3DFE simulation. The base machine had its teeth shifted by $\pm 30^\circ$ electrical to minimise T_{c6} . Figure 4.20 shows the effect on total cogging torque, it is clear that the magnitude is greatly reduced, and harmonic analysis shows a reduction in T_{c6} of 94%.

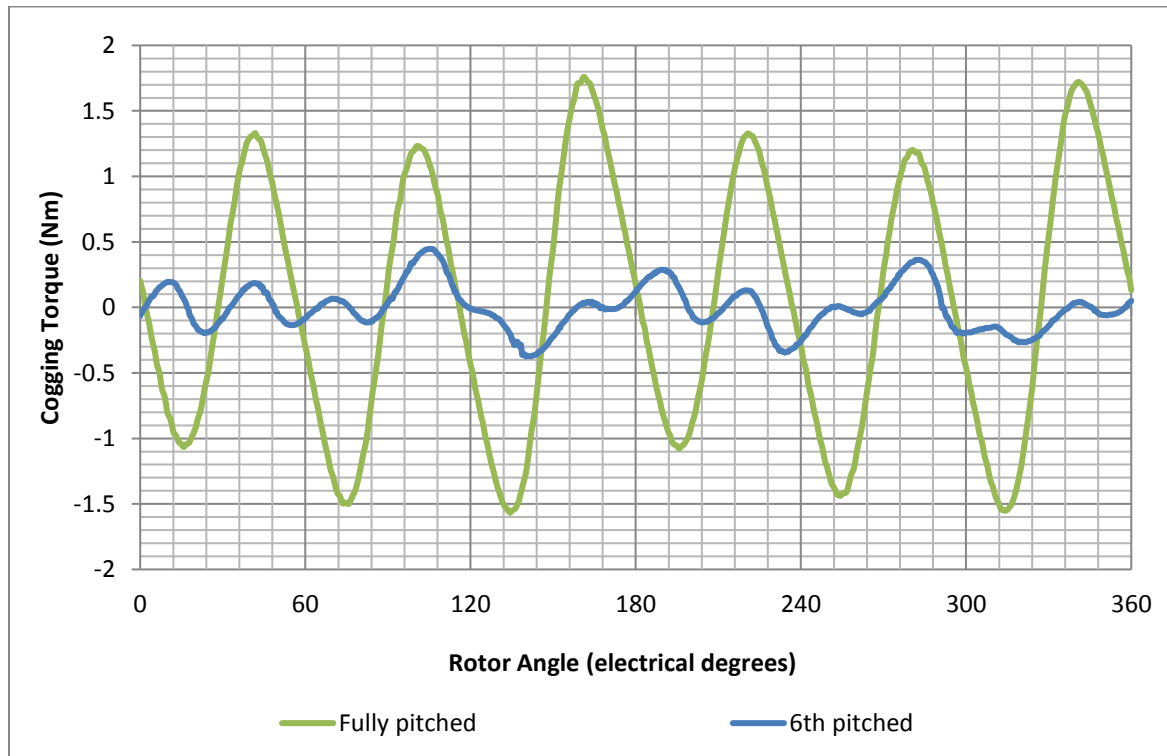


Figure 4. 20: Comparison of cogging torque waveforms for fully pitched and 6th pitched models of MPM

With a feasible technique to reduce T_{c6} , T_{c12} was also tested by introducing a pitching angle of 30° and 15° electrical.

Tooth pitching to minimise a pair of harmonics requires two pitching angles to be introduced which requires modelling at least 4 pole pairs of the MPM and is shown in Figure 4.21. The cogging torque waveforms for the 6th pitched and 6th and 12th pitched machines are shown in Figure 4.22. It is seen that the peak cogging torque is further reduced from 0.45 Nm to 0.42 Nm. This is a 76% reduction from the base model.

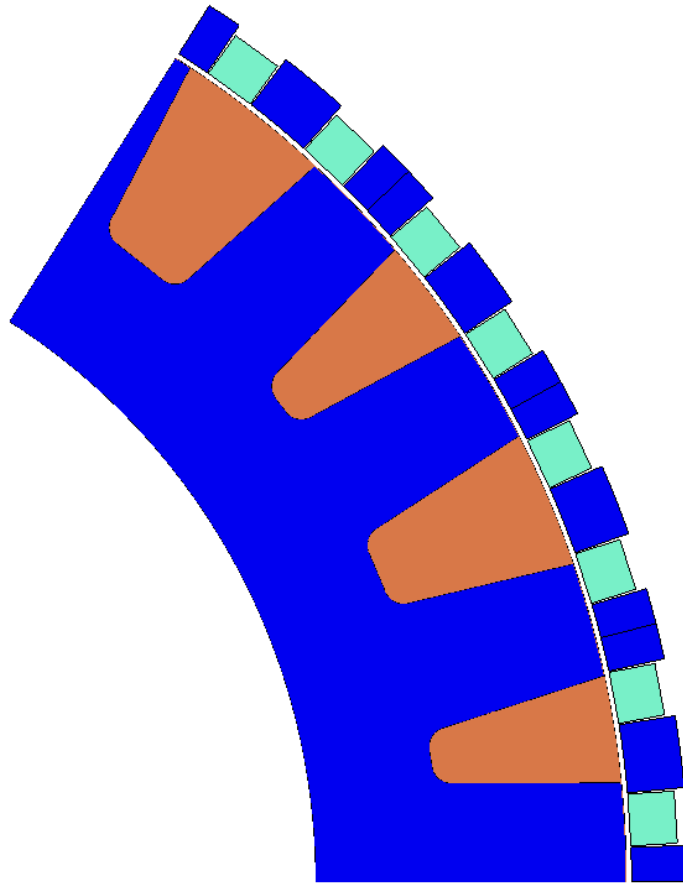


Figure 4. 21: Illustration of a 2 pole pairs MPM pitched by 15° and 30° electrical (6th and 12th harmonic)

Harmonic analyses of both models are shown in Figure 4.20 and it can be seen that T_{c6} and T_{c12} are greatly attenuated. Table 4.4 shows a comparison of the harmonic contents in the kind of models presented in this section.

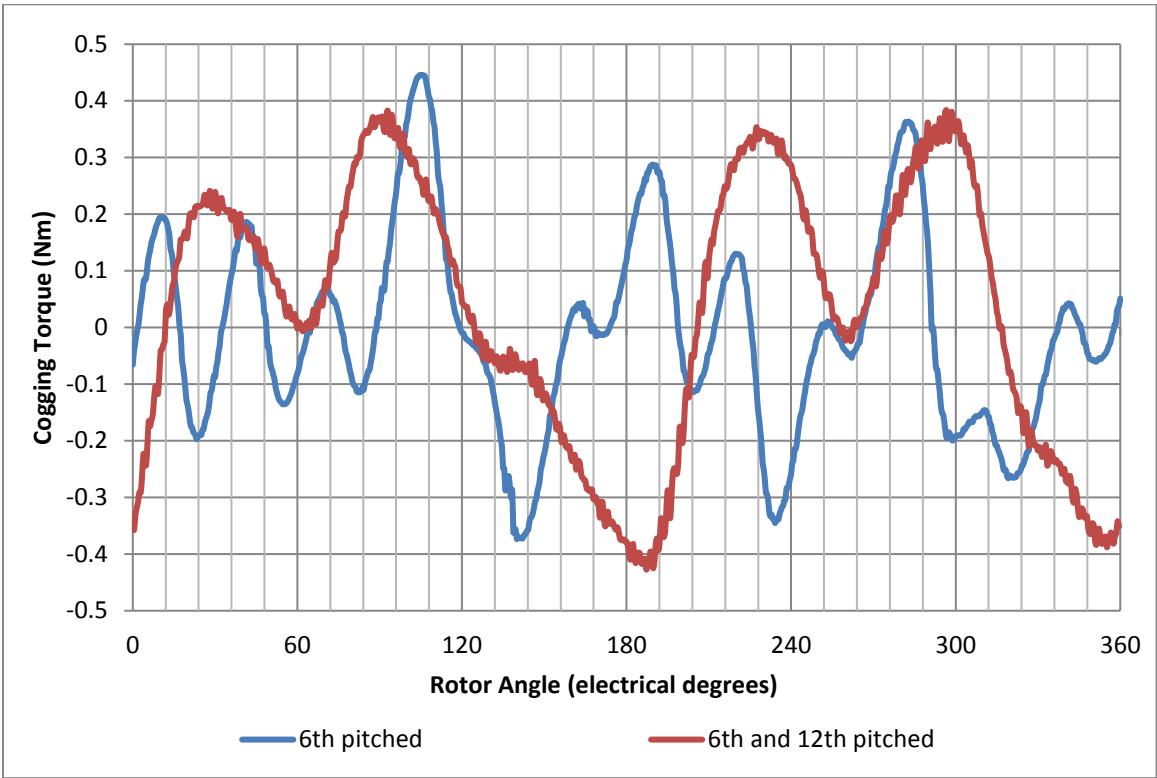


Figure 4. 22: Cogging Torque waveforms comparison of 6th pitched and 6th &12th pitched models

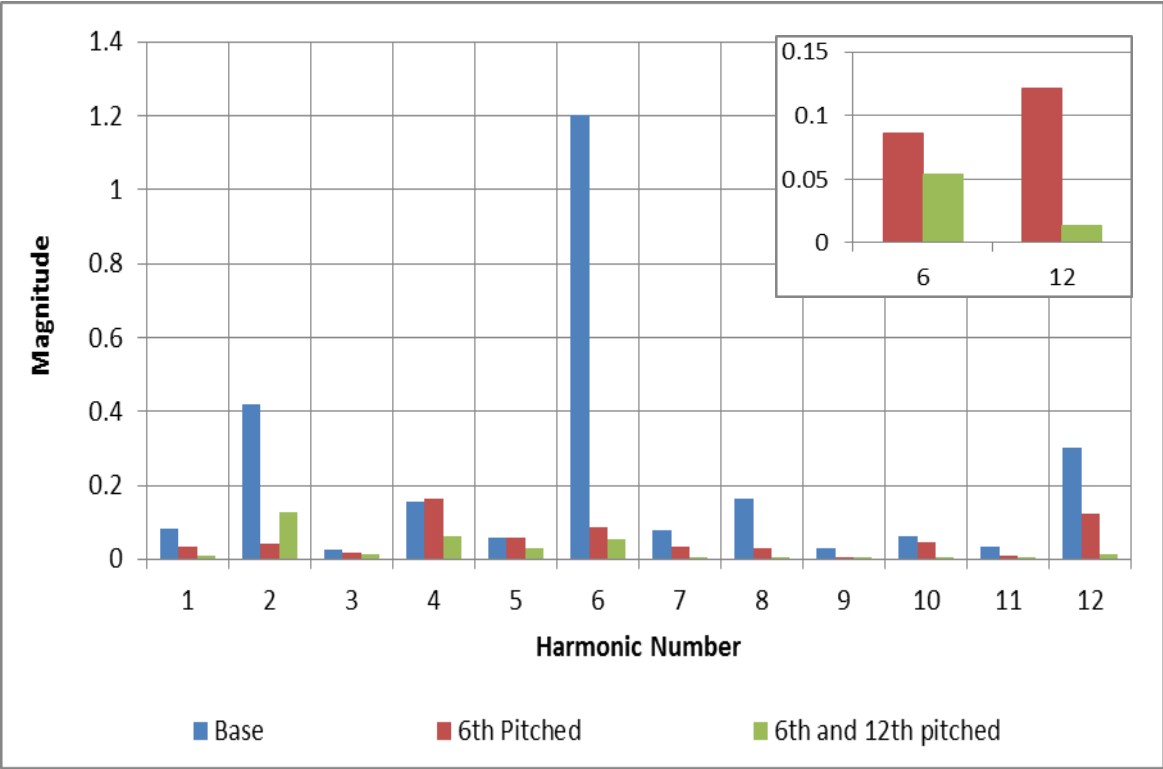


Figure 4. 23: Cogging Torque harmonic contents of 6th pitched and 6th &12th pitched models (6th and 12th harmonics zoomed in for the two new models)

Table 4. 4: Comparison of the major harmonic in the fully pitched, 6th pitched and 6th &12th pitched models (percentage reductions from the fully pitched model)

Harmonic Number	Fully Pitched (Base)	6th Pitched	6th and 12th pitched
T_{c2}	0.230	0.040 (82.60)	0.128 (44.35)
T_{c4}	0.170	0.163 (4.12)	0.064 (62.35)
T_{c6}	1.462	0.086 (94.12)	0.054 (96.31)
T_{c12}	0.522	0.122 (76.63)	0.013 (97.51)

4.8 Back EMF

The 3 phase EMF waveforms of the fully pitched machine are shown in Figure 4.24 with the harmonic content in Table 4.5. The fundamental harmonic in all three phases are similar however there is a large 5th and 7th harmonic component which ought to be reduced. The majority of the harmonics are present in the inner phase of the machine hence Phase B is compared for the fully pitched and 6th and 12th pitched models and presented in Figure 4.25. It can be seen that the 5th and 7th harmonic are suppressed. Figure 4.26 shows the changes in 1st, 5th and 7th harmonics with the pitching angles.

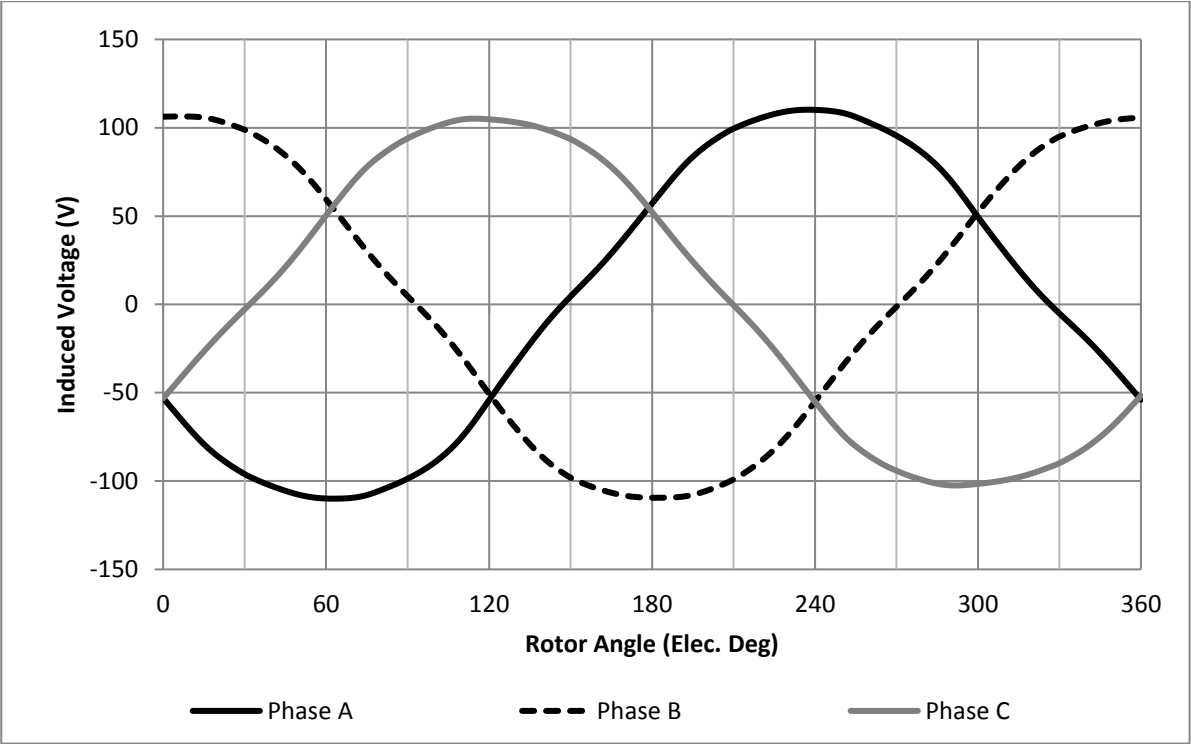


Figure 4. 24: Back EMF waveforms for the three phases of the fully pitched model

Table 4. 5: Comparison of the three phases back EMF harmonic content of the fully pitched model

Harmonic Number	Phase A	Phase B	Phase C
1	110.94	110.57	110.76
2	2.47	2.29	2.47
3	1.86	0.24	1.70
4	0.17	0.25	0.12
5	2.75	3.20	2.46
6	0.21	0.23	0.26
7	0.86	1.07	0.84
8	0.22	0.10	0.25
9	0.28	0.16	0.34
10	0.08	0.01	0.07
11	0.05	0.02	0.03
12	0.12	0.01	0.11
13	0.22	0.11	0.14
14	0.05	0.02	0.06
15	0.09	0.05	0.07
16	0.05	0.01	0.06

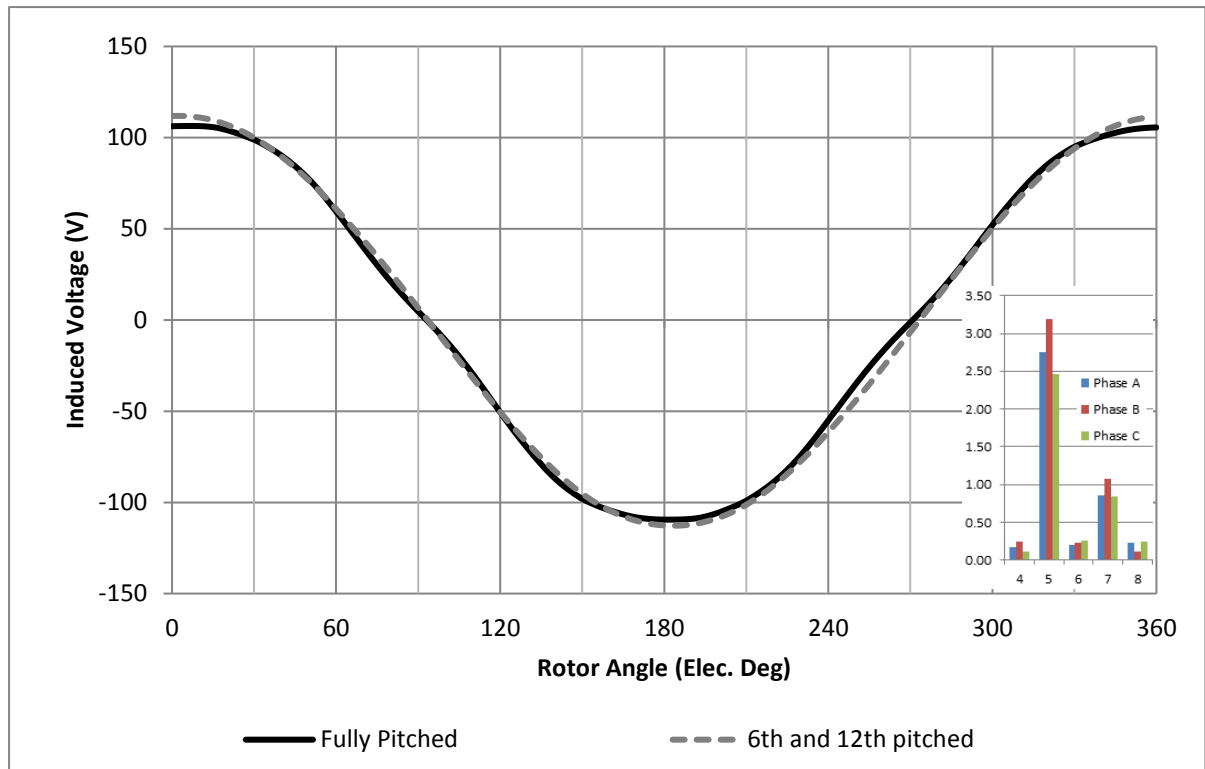


Figure 4. 25: Comparison of Phase B back EMF waveforms for fully pitched and 6th and 12th pitched models, 5th and 7th harmonics displayed

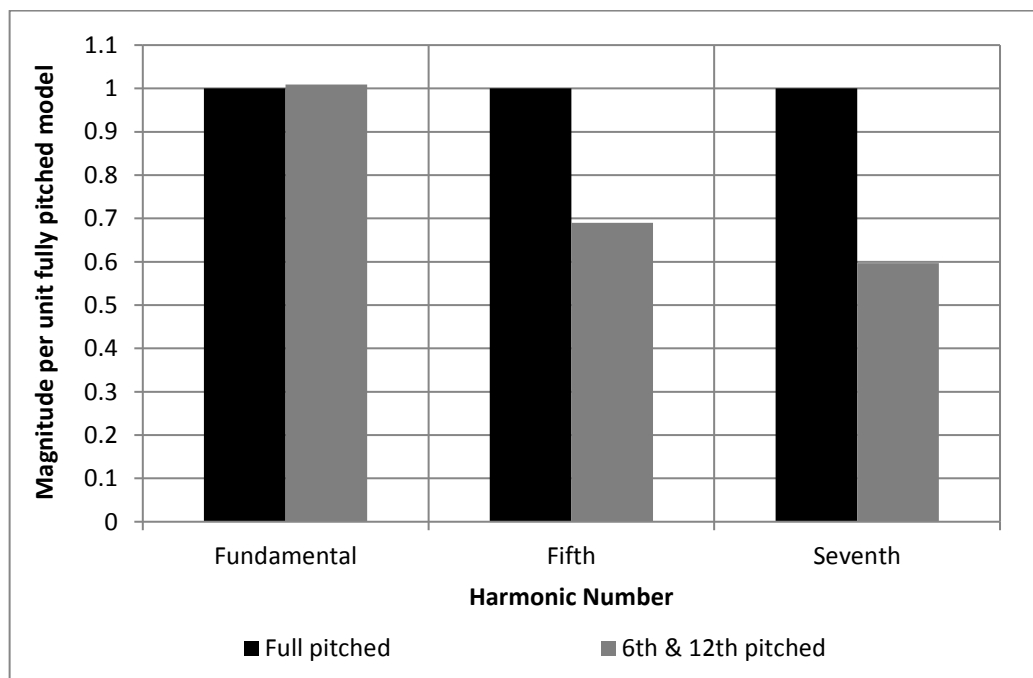


Figure 4. 26: Comparison of fundamental, fifth and seventh harmonic for Phase B of a fully pitched and 6th and 12th pitched models (per unit fully pitched model)

It can be concluded that the pitching technique suppress unwanted cogging torque harmonics as well as back EMF harmonics, and presents much smoother waveforms. Pitching angles of 15° and 30° electrical were tested to see if these reduce T_{c6} and T_{c12} in cogging torque as well as the E_{f5} and E_{f7} ; the results in Table 4.4 and Figure 4.22 proves that these angles work.

4.9 Combination of tooth span and pitching techniques

It is seen in this chapter thus far that combination of tooth spans and applying a pitching angle reduces the cogging torque and back EMF harmonics. However it is found that a solution that works well to reduce the cogging torque might not be the best solution to reduce the back EMF harmonics too. In order to find out one solution that can solve both problems and reduce the harmonics content further, an investigation will be carried out to see if a combination of solutions can be applied to reduce the harmonics in both, back EMF and cogging torque, to produce a better solution and balance in the machine.

The two significant harmonics in the back EMF are the E_{f5} and E_{f7} hence the machine was pitched for the 6th harmonic, as a good compromise for both E_{f5} and E_{f7} . The tooth span is then varied between 120° and 180° electrical to evaluate the effect it has on E_f and T_c .

Figure 4.27 presents the peak cogging torque and T_{c6} and T_{c12} normalised to the 130° tooth span. It seems that a tooth span of 170° provides the lowest peak cogging torque and a reasonable T_{c6} while T_{c12} is almost eliminated. However it's equally important to see the effect a tooth span of 170° and 6th pitched stator has on back EMF waveform and its harmonics; this is presented in Figure 4.28.

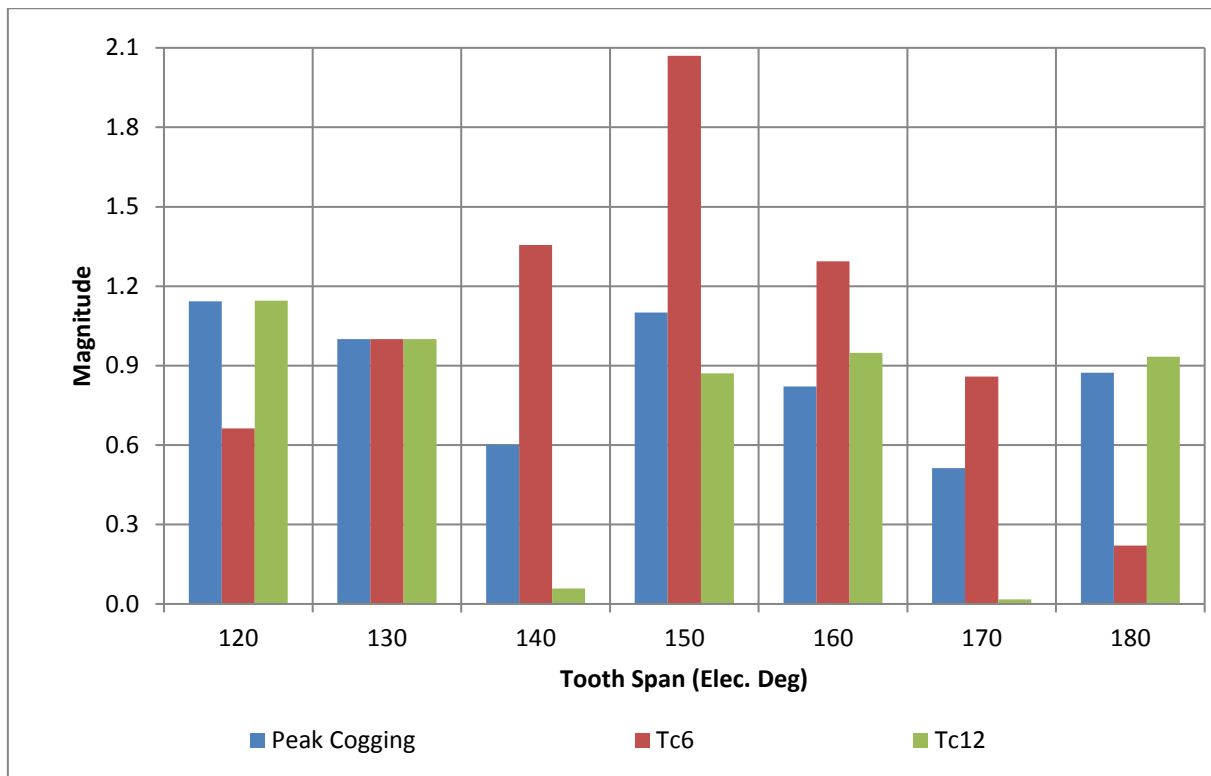


Figure 4. 27: Variations in peak cogging torque and its harmonics as tooth span is varied while pitched for 6th harmonic

A tooth span of 170° gives rise to 5th harmonic in back EMF and is seen as the highest with in the tooth span range investigated. The 1st and 7th harmonics are comparable to the others. In order to achieve the best solution for cogging torque and back EMF, a combination of techniques will be applied where in a combination of 6th pitched tooth spans will be modelled.

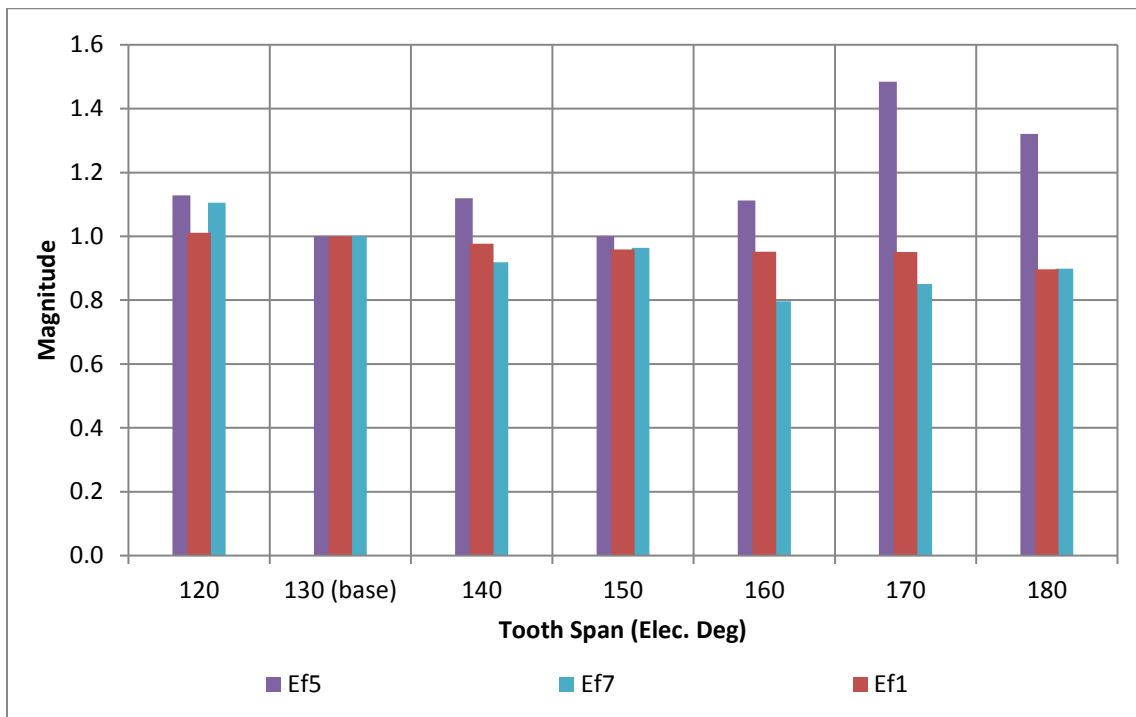


Figure 4. 28: Variations in back EMF harmonics as tooth span is varied while pitched for 6th harmonic

Various combinations of tooth span were investigated that could offer a good solution for improved cogging torque and EMF harmonics. The most appropriate combination was six teeth of 140° span, seven teeth of 150° span and 12 teeth of 170° span. The cogging torque produced by this combination is shown in figure 4.25 and is compared with the original unmodified machine and 6th pitched machine. The peak cogging torque is reduced from 1.74 Nm to 0.40 Nm for this combination of techniques.

Back EMF waveform for the inner phase of the machine is compared for the original unmodified machine and the machine with combination of tooth spans and pitching technique, shown in Figure 4.29. The harmonic content of this machine is much lower and the waveform is smoother than before. Combining the tooth span and introducing pitching reduces the cogging torque by a considerable percentage. It shows that the techniques work the best when combined together.

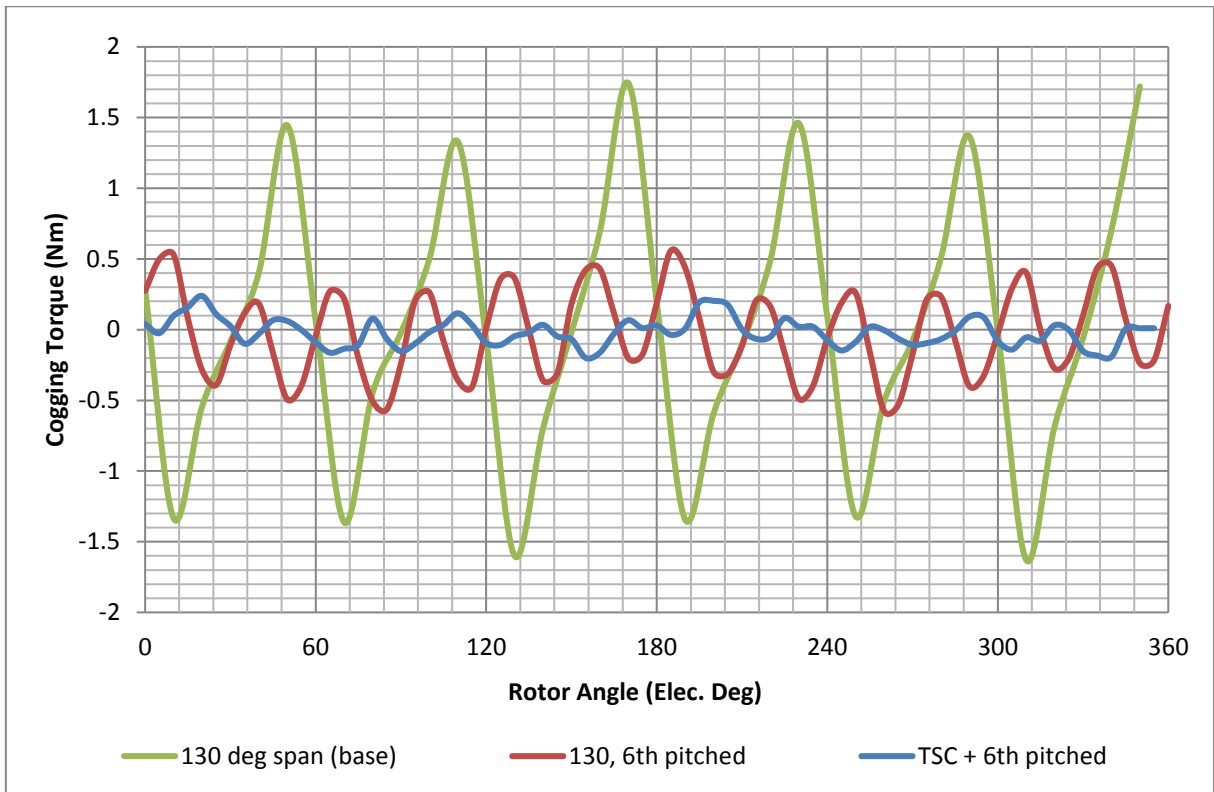


Figure 4.29: Cogging Torque waveforms for the base design machine (130° tooth span fully pitched), 130° tooth span and 6th pitched lamination and combination of three tooth spans with 6th pitching (TSC + 6th pitched)

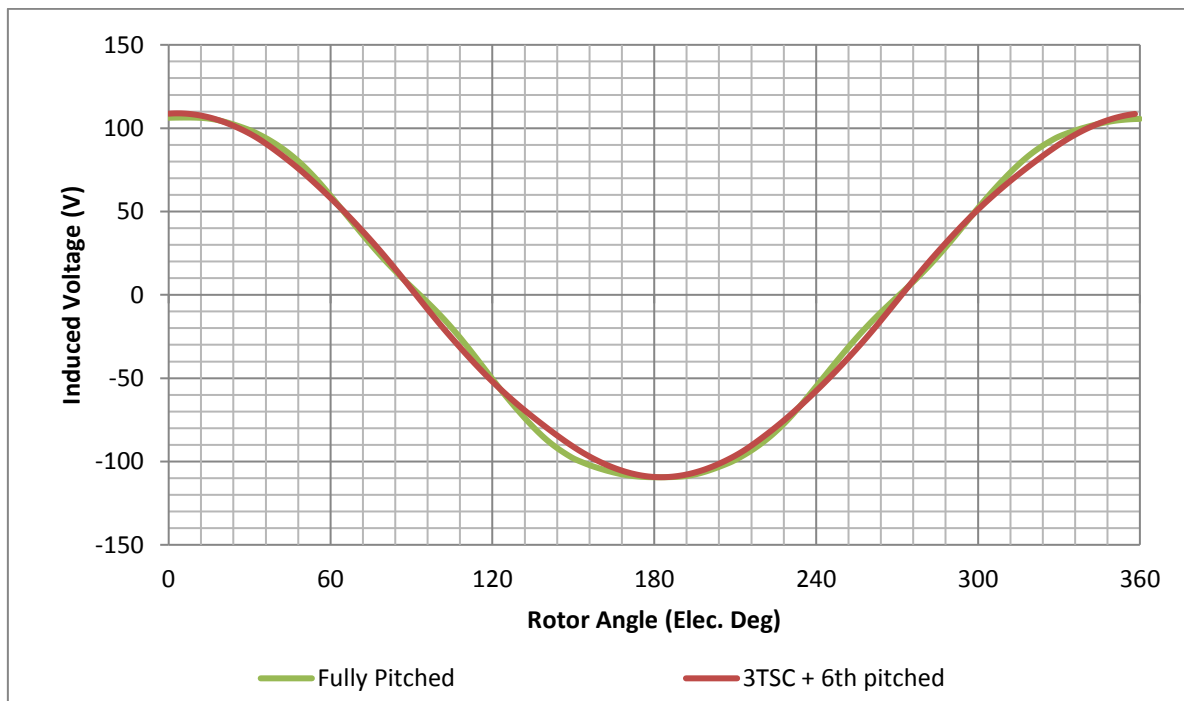


Figure 4.30: Back EMF waveforms for inner phase of the base design machine (130° tooth span and fully pitched) and combination of tooth spans with 6th pitching

Figure 4.31 compares the base machine with the machine made of a combination of tooth spans and pitching; the results are per unit value of the original machine. There is a substantial reduction in cogging torque (by 77%) and T_{c6} (by 83%) and T_{c12} (by 87%) harmonics while the E_{f5} and E_{f7} are also reduced significantly, by 75% and 70% respectively. A 2% reduction in E_{f1} is encouraging as it is not a big price to pay for huge reductions in the unwanted harmonics of cogging and back EMF.

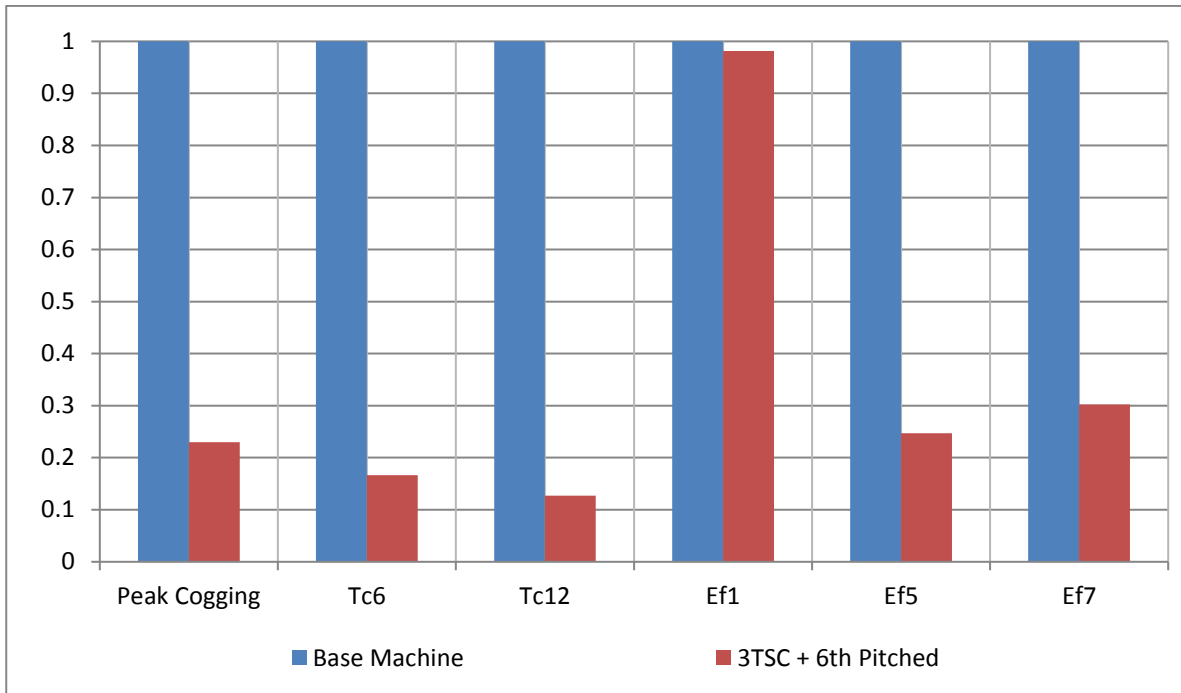


Figure 4. 31: Comparison of the original unmodified machine with the machine made of a stator with combination of tooth span and pitching

4.10 Pole Piece Designs

The influence of tooth span and tooth pitching has been investigated in this chapter thus far and it has been shown that altering these parameters can help to reduce the unwanted harmonics. Both these parameters are altered on the stator; however the focus now turns to the rotor.

Cogging torque is produced as a result of rotor's tendency to align with stator poles to minimise reluctance even when no current is applied in the coils. Cogging torque can be investigated by focusing on the magnetic interaction and the reluctance change between the coil and the magnets which means that cogging torque can be determined by air gap flux and the variation of reluctance in the magnetic circuit with the rotating displacement. It is easier for the rotor to align itself with stator at some positions than others and this tendency causes vibrations and speed ripples, particularly at low speed, which need to be reduced [126 – 129]. Cogging torque can predominantly be produced due to fringing fields in the magnet poles interpole [130] and hence the side of the pole facing the air gap is vital.

There have been many methods in literature where cogging torque is reduced by rotor redesigning in both radial and axial type PM machines [82, 83, 89, and 131]. There has also been methods such as rotor axis teeth pairing [132], harmonic current injection into the excited winding to compensate the torque ripple resulting from cogging torque [89], teeth notching [108, 133], pole flanging [133] and adopting a fan-shaped rotor pole [111].

In this section, the pole piece designs are investigated and various proposals are presented to see the influence of these on the cogging torque and back EMF. The pole pieces were located in the rotor and shapes of these are altered while the stator is kept unchanged. The pole piece side facing the air gap has an influence on cogging torque and the new shapes have this side redesigned and optimised in Finite Elements. The effect of these designs on the back EMF and cogging torque have been examined in this section.

The designs were created to reduce T_{c6} and hence the pole pieces with wave direction feature are 6th frequency, shown in Figure 4.32. These were designed to cancel/reduce the effect of 6th harmonic by destructive interference, pole piece waveforms are in antiphase with T_{c6} .

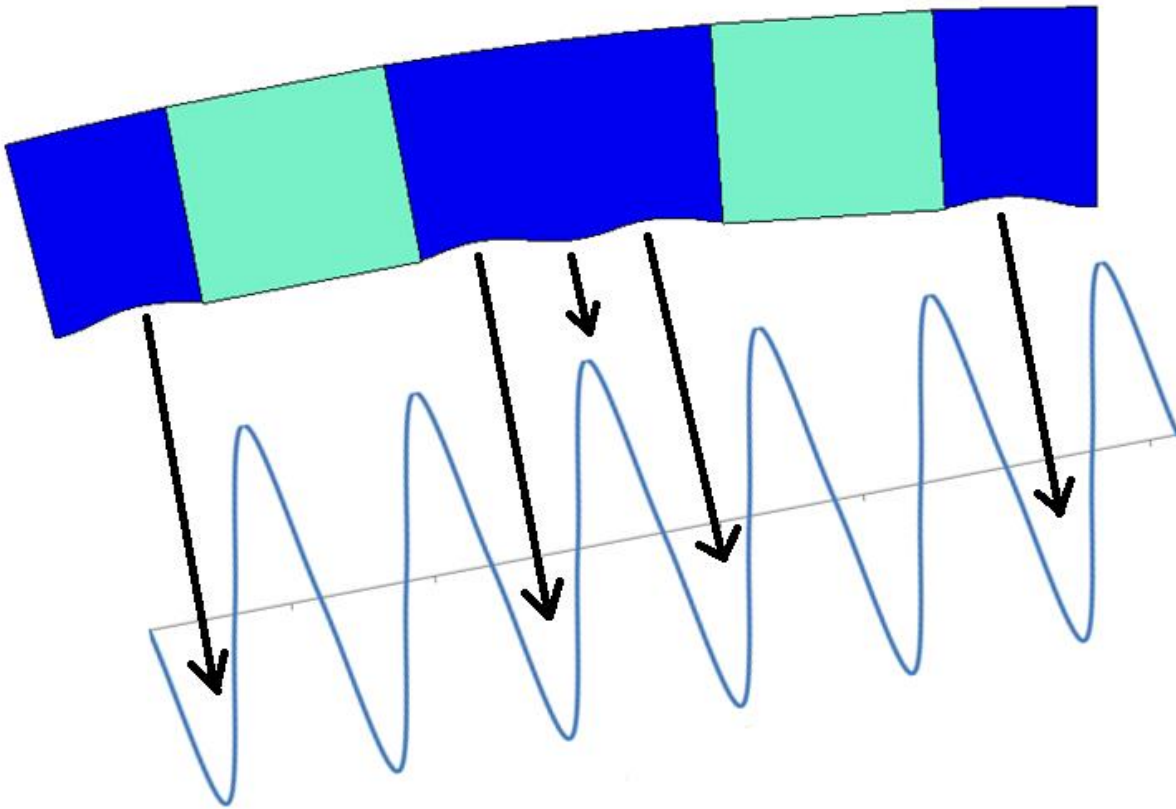


Figure 4. 32: Illustration of wave direction pole pieces design to accommodate the 6th harmonic waveforms of cogging torque

Other designs shown have features such as notches, concave, convex, gradient and claw base structures which help to reduce the cogging torque harmonics too. The simulated results are shown in Figure 4.34 and 4.35.

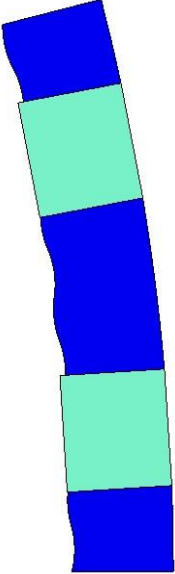
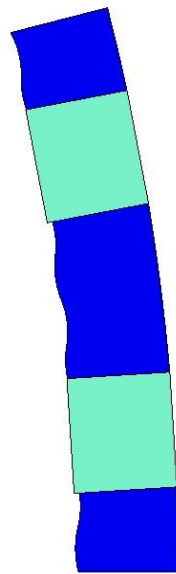
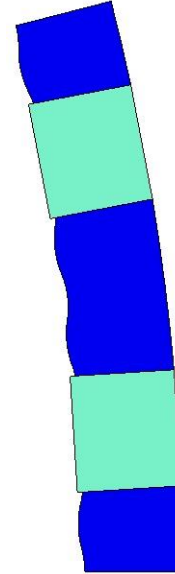
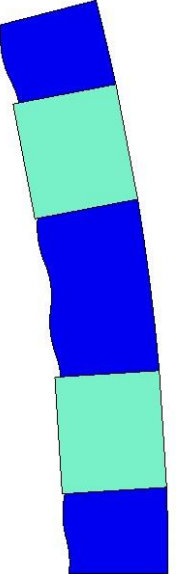
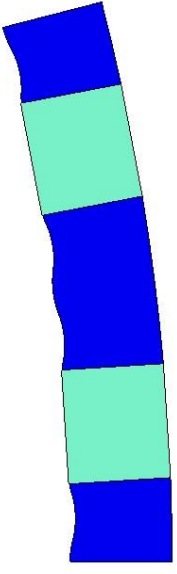
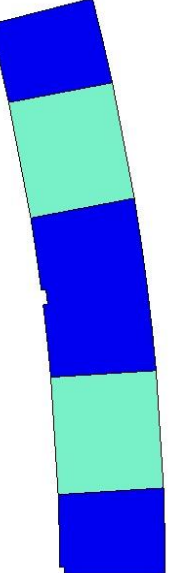
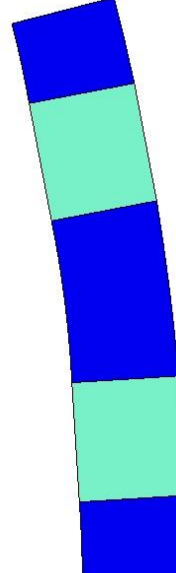
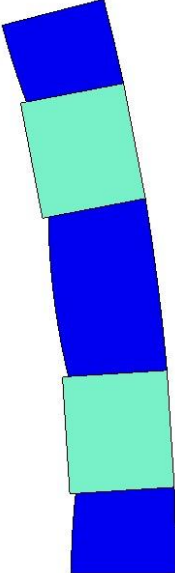
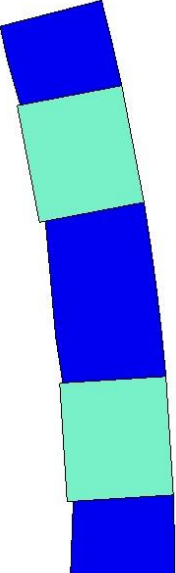
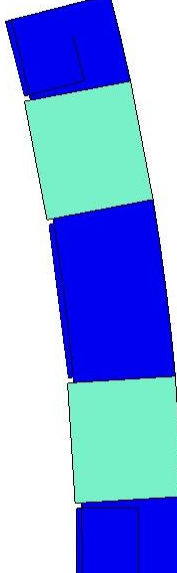
6 th harmonic Wave Direction 1	6 th harmonic Wave Direction 2	6 th harmonic Wave Direction 3	6 th harmonic Wave Direction 4	6 th harmonic Wave Direction 5
				
Notch (0.2mm and 0.5mm)	Concave (0.1mm)	Convex (0.2mm)	Gradient (0.2mm)	Claw Base
				

Figure 4. 33: Various Pole designs under investigation to reduce the harmonic content in cogging and back EMF waveforms

There are several designs that reduced the peak cogging torque, particularly pole piece named ‘Direction 5’, ‘Convex’ and ‘Claw’ pole piece designs, as seen from Figure 4.34. Peak cogging torque for direction 5 design is reduced by 56% of the base design while convex 0.2 mm shape reduces the cogging torque by 39%. This figure also presents the percentage back EMF for all these pole designs and most of these produce nearly the same as base machine pole piece design. The two pole piece shapes that stand out are the ‘Gradient 5’ and ‘Convex 0.2mm’ as these have 100% back EMF as the base design. Claw pole designs are good options too however their manufacturing can be a little demanding and requires a new tool to be made first; the pressing is not as straight forward. It is therefore decided that the two modified pole piece designs to be taken forward for manufacturing are ‘Gradient 5’ and ‘Convex 0.2mm’; these will be used to construct a prototype rotor and compared against base unmodified pole piece rotor.

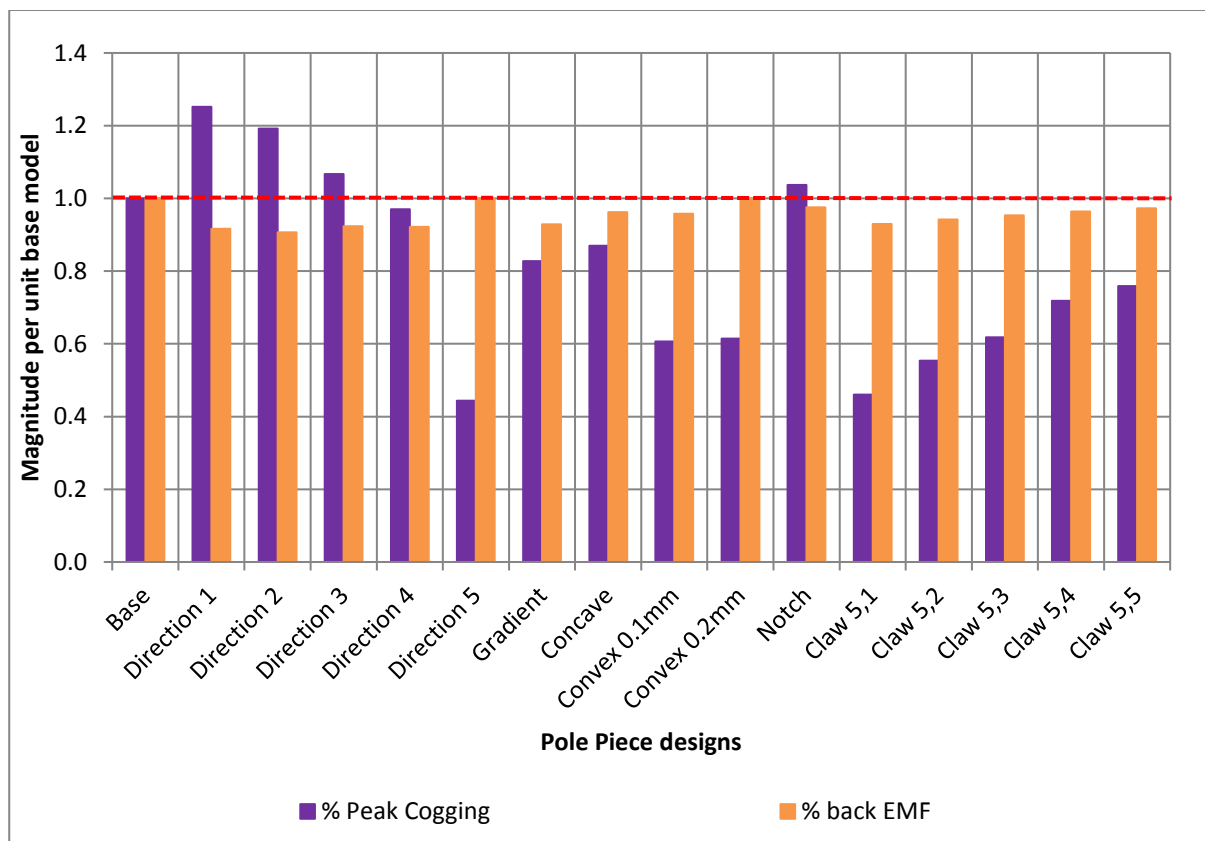


Figure 4. 34: Comparison of percentage peak cogging torque and back EMF for various pole designs per unit of base machine model (unmodified pole piece)

The cogging torque waveforms for these two pole piece designs are compared to the unmodified pole shape and are displayed in Figure 4.35. The harmonic content of these two newer pole piece’s designs are much lower than the unmodified pole piece shape. The 6th and 12th harmonics that made up most of the cogging torque in the unmodified pole pieces are reduced significantly. Figure 4.36 shows the T_{c6} being reduced by 51% and T_{c12} down to 17% of the

base design for convex shaped pole piece. Wave direction 5 also suppresses T_{c6} by 64% while T_{c12} is reduced by 6%. This also proves that the wave direction feature which was designed to reduce T_{c6} works well in achieving the purpose.

As well as the harmonics, these two pole piece designs reduce the harmonic content in back EMF too. Figure 4.36 shows that the convex pole piece shape reduces E_{f5} by 37% while wave direction 5 pole piece reduces E_{f5} almost to zero. This is a huge benefit in using such pole piece designs as not only are the cogging torque reduced, back EMF harmonics are also eliminated.

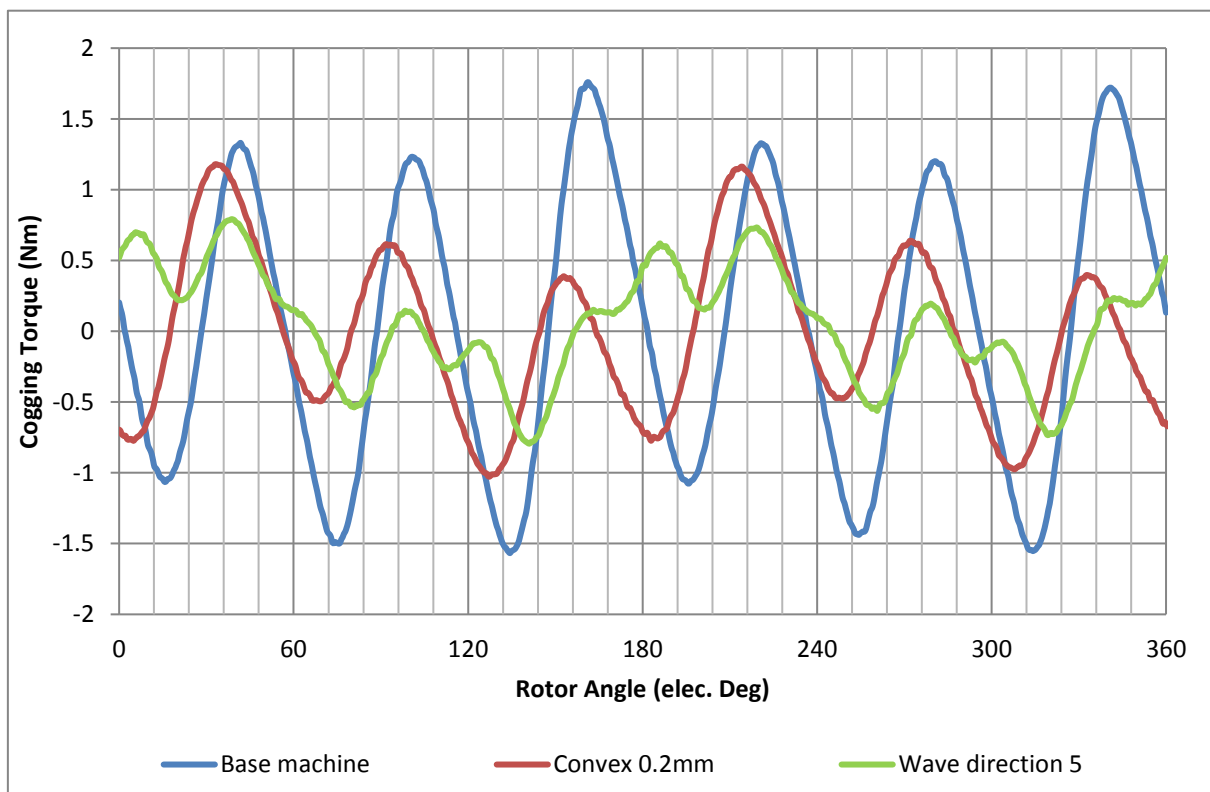


Figure 4. 35: Comparison of cogging torque waveforms for the unmodified, convex and direction 5 pole piece designs

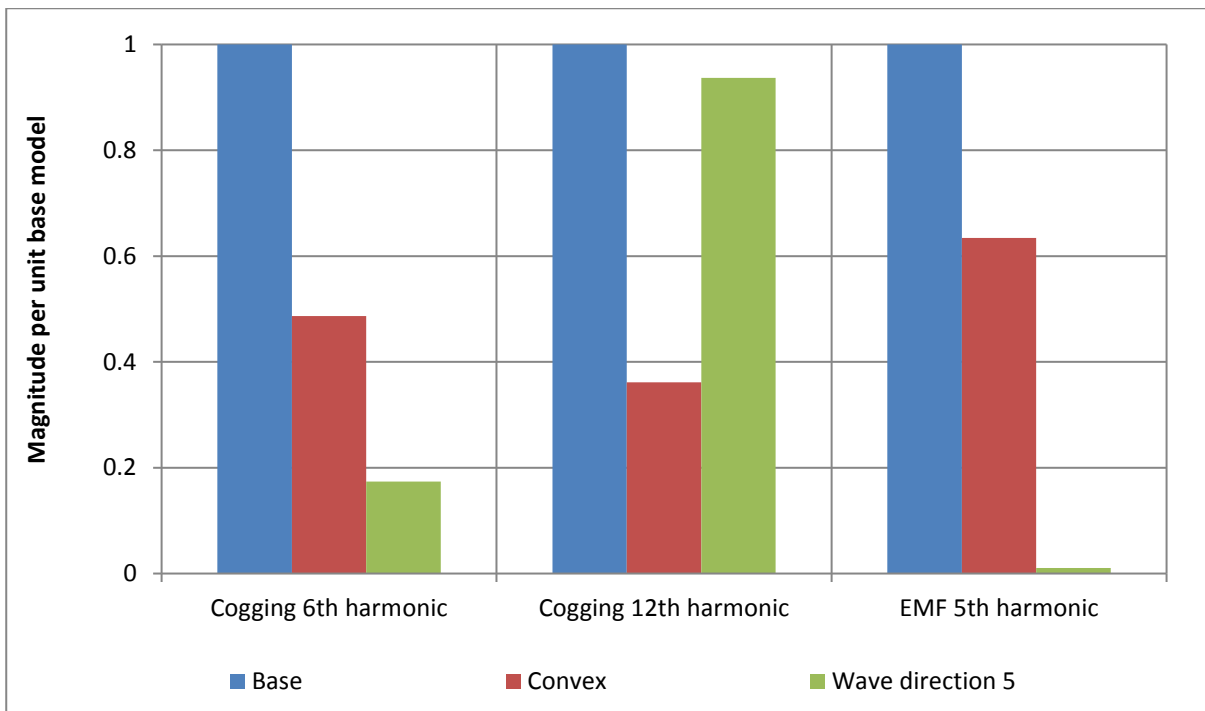


Figure 4. 36: Comparison of harmonics of the unmodified, convex and direction 5 pole piece designs per unit of base pole design

In this section, various new rotor pole piece shapes were presented and two designs were selected based on a good compromise between reductions of cogging torque and back EMF harmonics. These designs will be manufactured and prototype results will be obtained to see how these compare with the Finite Element results with further tests conducted to see the performance of the overall machine in terms of average electromagnetic torque production, efficiency of the machine with these new pole piece rotors and a full analysis on cogging torque and back EMF. These measured results and analysis will be presented in Chapter 6.

4.5 Conclusion

Various techniques were investigated in this section and it was shown that these techniques can be used to reduce the cogging torque and back EMF harmonic by a significant amount. A selection of combination of tooth spans, pitching angles and modified pole pieces are all novel techniques applied to this MPM, figures 4.37 and 4.38 shows the comparison of these with the base model.

It is seen from the FE studies that combining the tooth spans, pitching the teeth and specific pole shapes can reduce the peak cogging torque (Figure 4.37) greatly, especially when the stator laminations are pitched for 6th and 12th harmonic. There are major reductions in T_{c6} and T_{c12} and in some cases these are reduced to nearly zero.

Laminations made of a combination of three tooth spans and 6th pitched also show promising results. The peak cogging torque of this lamination is down to 21% of the base design while its second and fourth harmonics are also very low, though the T_{c6} and T_{c12} are a little higher than 6th and 12th pitched lamination.

Modified pole piece rotors also depict a low cogging torque however their second harmonics are higher than the base design which makes these not so reasonable. However, it is important to see the effect of these techniques on the back EMF and torque production ability of the machine; these are presented in figure 4.37.

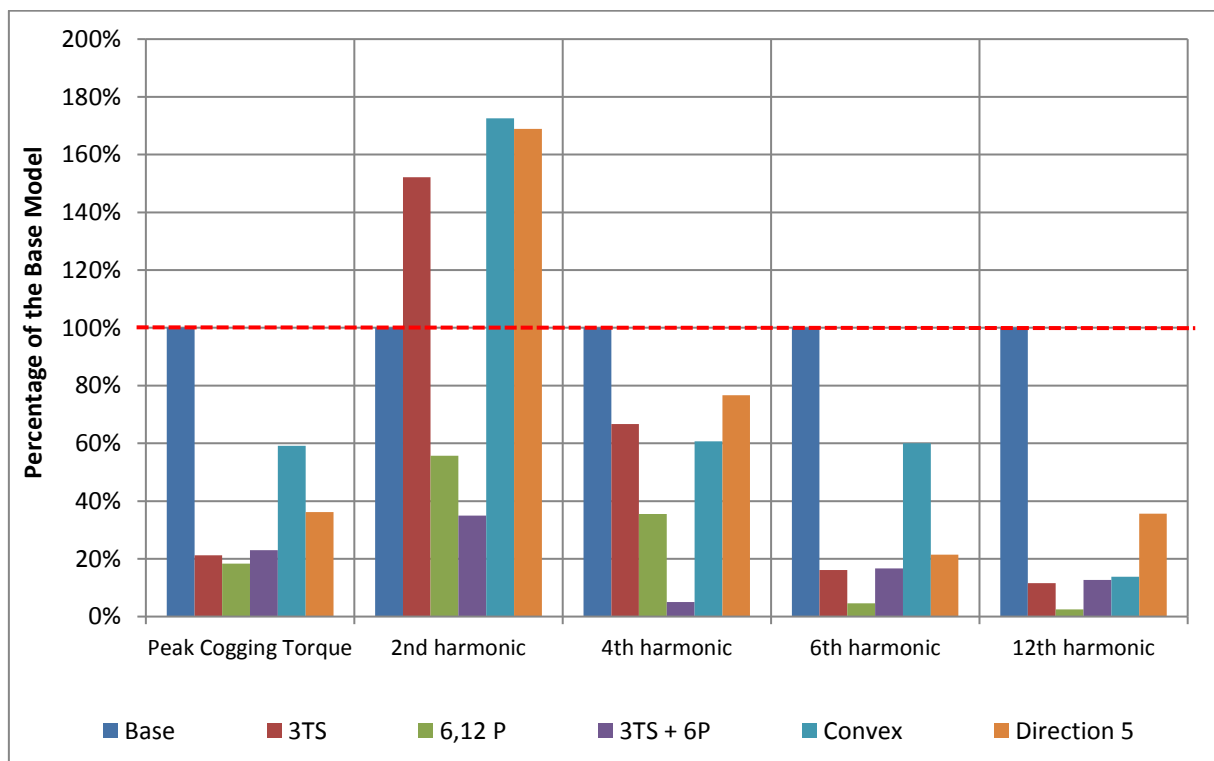


Figure 4. 37: Comparison of cogging torque and its harmonics for various techniques investigated in this section (base design, combination of three tooth spans, 6th and 12th pitched laminations, laminations made of combination of tooth spans and 6th pitched, modified pole pieces of convex and direction 5 type)

It was explored that the second and fourth harmonics were mainly caused due to the mutual coupling taking place between the stator phases and hence two rotors were manufactured to reduce these effects. These rotors consisted of split magnets and poles, affectingly creating a rotor for each phase and was termed ‘split rotor’ while another rotor was manufactured where in the inner phase magnets and rotors were cut to increase the air gap. These rotors and their effect on the techniques will be presented in chapter 6 and 7.

Mean back EMF across all six designs seems quite consistent however there is a large discrepancy between the E_{f5} and E_{f7} . The 6th and 12th pitched design produces the highest E_{f5}

and E_{f7} however the smallest T_{c6} and T_{c12} . Lamination made of three tooth spans and 6th pitching shows the best results; E_{f5} and E_{f7} are reduced by 75% while the cogging torque harmonics are very low relative to the base model. The average torque production for this kind of lamination is also the highest; 120% of the base model, and hence can be regarded as the best.

However it should be noted that there is not much of a difference between the mean back EMF and average torque produced between the six machines.

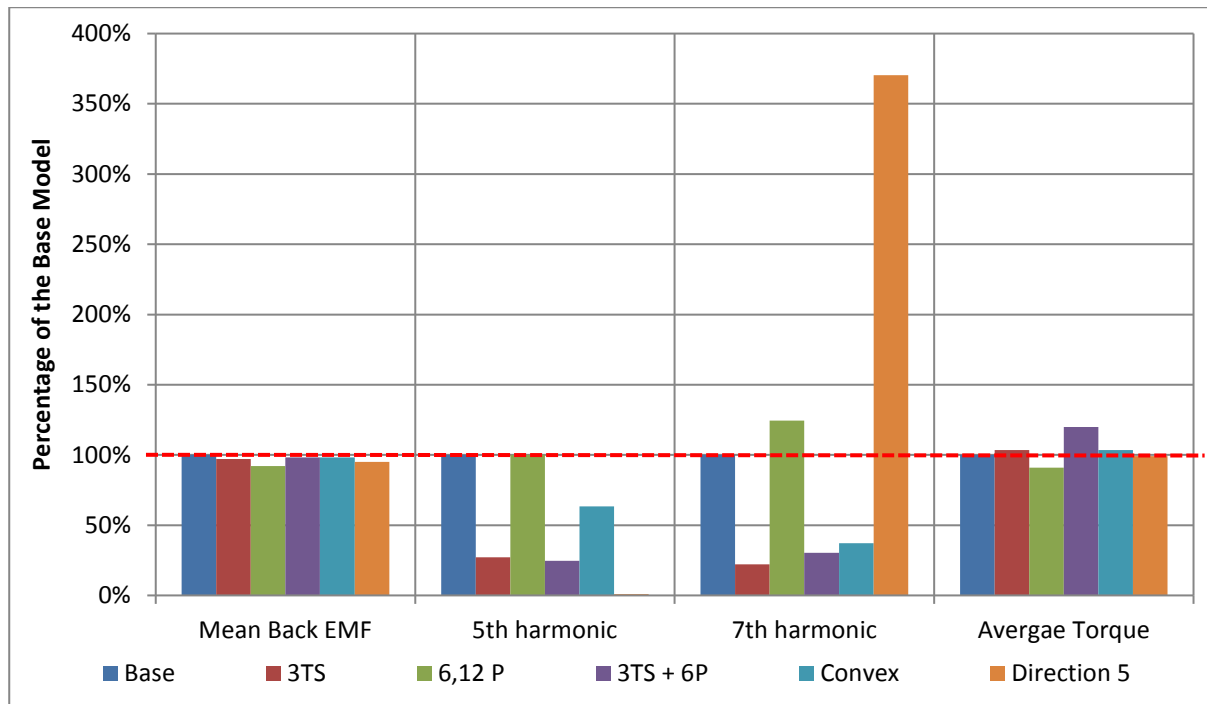


Figure 4. 38: Comparison of mean back EMF, its harmonics and average Torque for various techniques investigated in this section (base design, combination of three tooth spans, 6th and 12th pitched laminations, laminations made of combination of tooth spans and 6th pitched, modified pole pieces of convex and direction 5 type)

These methods have shown that it is possible to reduce the cogging while keeping the back EMF and torque production similar to the best machine, while the number of components to be made and assembled is kept the same too. These methods were manufactured and prototypes were constructed; construction of these is shown in the following chapter while the measured test results are presented in chapter 6.

5. Construction and Assembly of prototypes

5.1 Introduction

This chapter details the manufacturing and assembling of the prototype machines. The machines are constructed from laminates and SMC as explained in Chapter 2. Laminates aid the radial component of magnetic field in the stator teeth while SMC allows for 3D flux movement through the core-back.

Six different types of stator components were manufactured; each using one or more techniques and material to suppress the cogging torque. These six stators are described as following:

1. S1: Single tooth span unpitched stator made up of laminates – basic stator used for comparison
2. S2: Laminate stator made of 3 tooth span combinations
3. S3: Stator made up of 3 tooth spans combination and 6th pitched laminations
4. S4: 6th and 12th pitched stator laminations
5. S5: Stator made of SMC, single tooth span unpitched chamfered teeth
6. S6: 6th and 12th pitched stator made of SMC
7. S7: The same stator as S5 however the phase gaps increased by 0.1mm each.

Five different rotor types were also constructed that were used with all the six stators one at a time to find the best machine with least cogging torque. These rotors are:

1. R1: Basic rotor used for comparison – simple 50 poles and 50 magnets
2. R2: The basic rotor (R1) was ‘split’ into three sections to provide a rotor section for each phase
3. R3: The basic rotor (R1) was machined in the inner phase region to increase the air gap as seen by the flux

4. R4: Rotor made up of ‘Convex’ types of pole pieces
5. R5: Rotor made up of ‘Wave direction’ types of pole pieces

It was made sure that the dimensions of each component, the size of the overall machine as well as the number of components in the machine are kept the same in each case so the comparison is valid. These dimensions are shown in Table 5.2. The measurements from these combinations of stators and rotors are then compared to the base machine in a matrix table shown in Table 5.1, where each unfilled box represents a machine type.

Due to time constraints, not every stator-rotor combination was assembled. The machines that were tested are presented by grey-filled boxes in table 5.1. Measured test results of these 25 motors are presented in chapters 6 and 7.

Table 5. 1: Combination of prototype stators and rotors

Stator/Rotor combination	R1	R2	R3	R4	R5
S1	BASE MODEL				
S2					
S3					
S4					
S5					
S6					
S7					

Table 5. 2: Major dimensions that were kept the same in all 25 prototypes

Pole pairs	25
Stator outer radius	73 mm
Stator core radial length	5 mm
Rotor radial length	3.5 mm
Coil slot width	3.3 mm
Coil radial length	14 mm
Stator sweep	5.95 mm
Phase gap	2 mm
Core-back radial length	10 mm
Air gap	0.4 mm
Pole radial length	4.3 mm
Machine diameter	155.4 mm
Number of turns on coil	17

5.2 Stator Construction

This section will describe the construction of stator components.

5.2.1 Laminations

The stator laminations are M270-50A grade electrical steel, which was supplied in 300mm x 600mm sheets. The wire erosion machine at Newcastle University has an operable area of 200mm x 200mm, hence these lamination sheets were cut to fit. Each laminate is 0.5mm thick, therefore ten laminations glued in a stack of 5.6mm (0.1mm being made by the glue in between the sheets) for each stator side. This stack is pressed between two steel plates (as shown in Figure 5.1) to force excessive glue out between the layers and give a high stacking factor. This compressed stack is then heated to 180° C for 3 hours to get the glue to its highest strength.



Figure 5. 1: Gluing jig placed in the oven for heat treatment with lamination stack inserted; four bolts and the spacers visible too

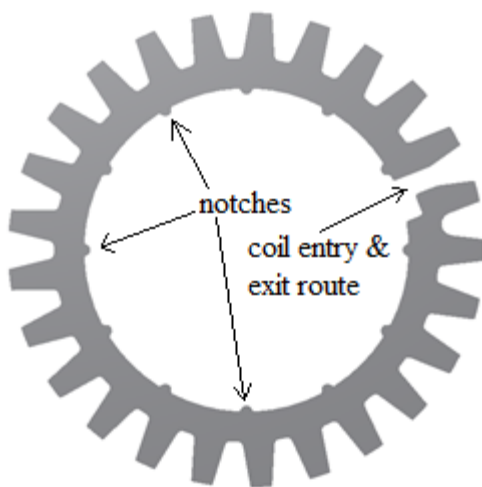
The glued lamination stacks were then wire eroded to an accuracy of +/- 0.01mm. All six stacks are placed between two aluminium plates, as shown in Figure 5.2, and cut as one using the wire erosion machine. The stacks were passed through three cuts; first one for the inner diameter, second for the outer diameter while the last cut removed the small tabs that were holding the stacks from falling out during the process.



Figure 5. 2: Wire Eroding jig with glued laminations bolted between two plates

The end product of wire erosion is the laminations shown in Figure 5.3. There are four variants of laminated stators plus two SMC variants. In all cases the diameter is kept the same. Each lamination has the same location features to help in locate itself in the inner hub according to the required electrical displacements which were 0° , 180° , 120° , 300° , 240° and 60° . There are 12 notches on the lamination displaced by 30° mechanical which help to locate the laminations to complete the three phase topology.

The opening in the lamination is to provide an entry and exit route for the coil from the outer diameter, beneath the core-back via the central shaft to exit the machine. This feature also helps to reduce circulating eddy currents.



Lamination shown in Figure 5.3 was used as the base stator model. The lamination is made from single tooth span of 130° electrical and was fully pitched. All the other stators (S2 to S6) were compared against still stator model.

Figure 5. 3: Base stator - Single tooth span unpitched lamination – S1

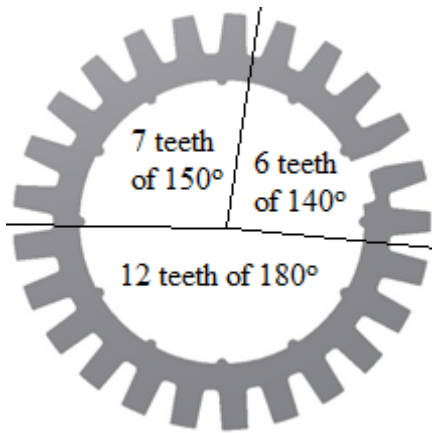


Figure 5. 4: Lamination made of combination of 3 tooth spans – S2

Another lamination variant with combinations of three tooth spans is shown in Figure 5.4. There were many combinations of tooth spans that were made and Finite Element models were created however this tooth span combination provided the least cogging torque for this technique, as discussed in Chapter 4. This lamination had 6 teeth of 140° , 7 teeth of 150° and 12 teeth of 180° . Stator assembled from this lamination was termed S2.

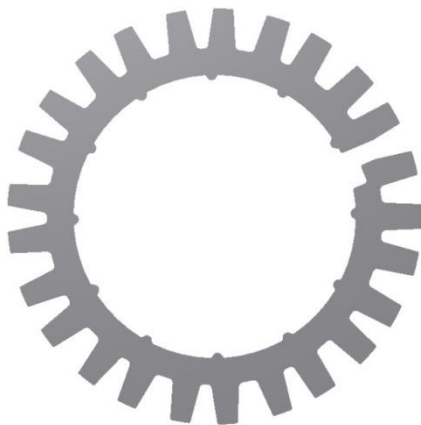


Figure 5. 5: Lamination made of 3 tooth spans combination and 6th pitched – S3

FE analysis showed that S2 would still have a high 6th harmonic in cogging torque. The lamination shown in Figure 5.5 was machined to reduce this unwanted harmonic by using the same three tooth span combination as S2 however introducing 6th pitching in the stator teeth. The stator assembled from this lamination was termed S3.

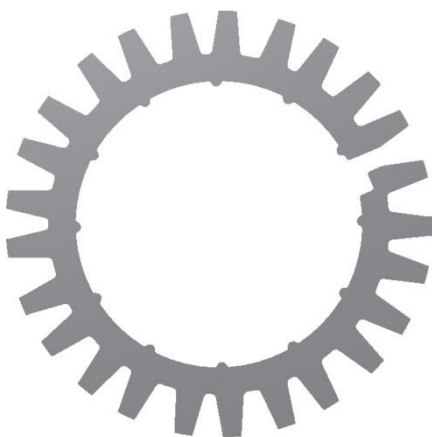


Figure 5. 6: 6th and 12th pitched lamination – S4

A fourth set of laminations were machined that consisted of single tooth span, same as that in the base machine presented in Figure 5.3 but pitched for 6th and 12th harmonic. This lamination had single tooth span is shown in Figure 5.6. Stator assembled from this lamination was termed S4.

5.2.2 SMC Stator components

There were two stators that were made from SMC stator components instead of laminate steel. These stator components had the same diameter and design parameters except the fact that there was no cut in the laminations and the coil exit route was a little different; shown in Figure 5.7 and 5.8 (and its technical drawings in Appendix A).

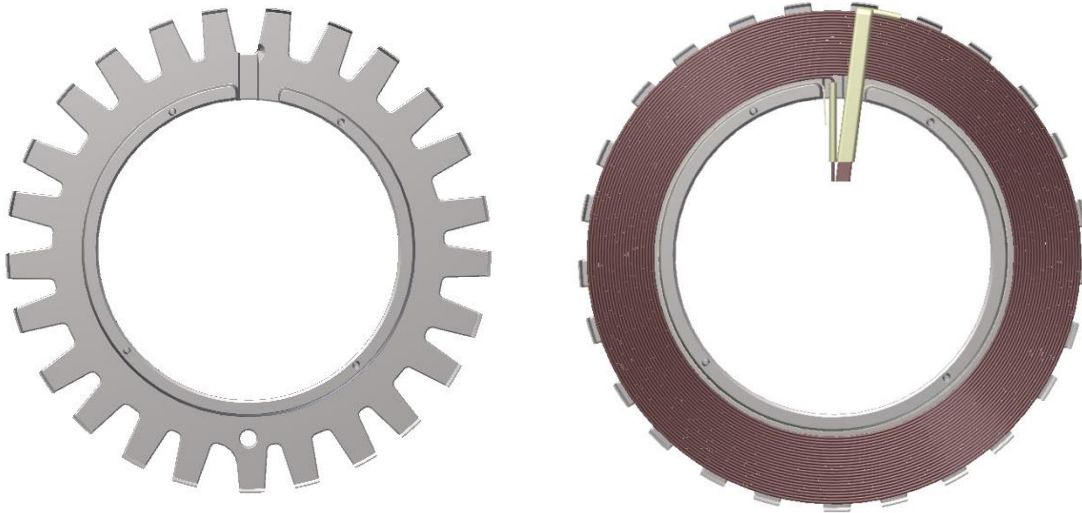


Figure 5. 7: CAD illustration of SMC stator component with new type of coil exit

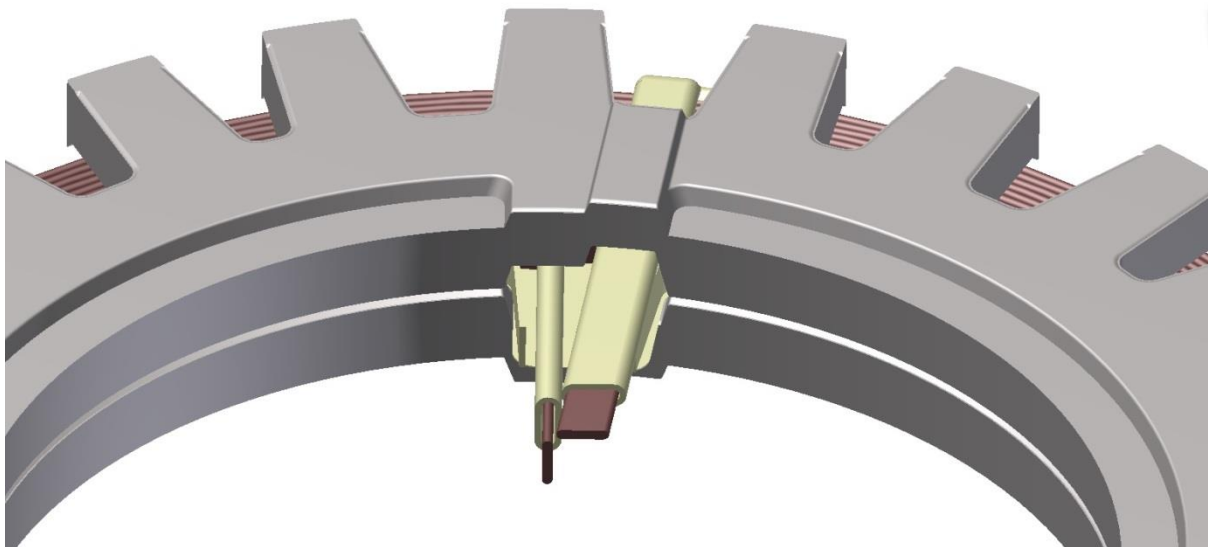


Figure 5. 8: CAD illustration of new SMC stator component, coil sandwiched between two stator components

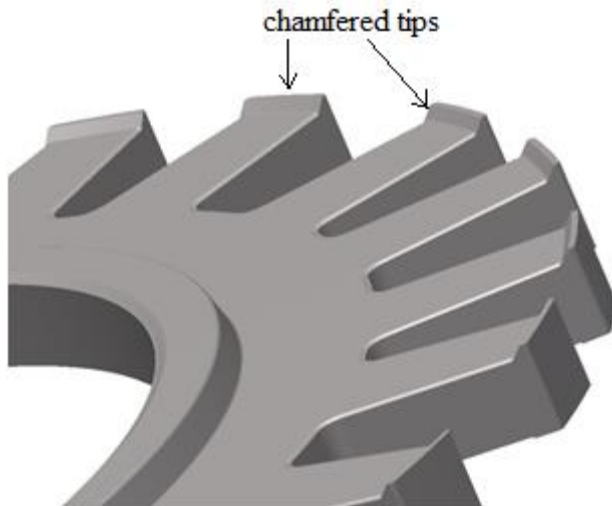


Figure 5. 9: CAD Illustration of SMC chamfered teeth – S5

A fifth set of stator components were manufactured; these were made from SMC with a single tooth span, same as that in base machine shown in figure 5.3 however the teeth were chamfered. This design feature showed signs of reducing the cogging torque in FE modelling. This design is shown in Figure 5.9. The stator assembled from this was termed S5.

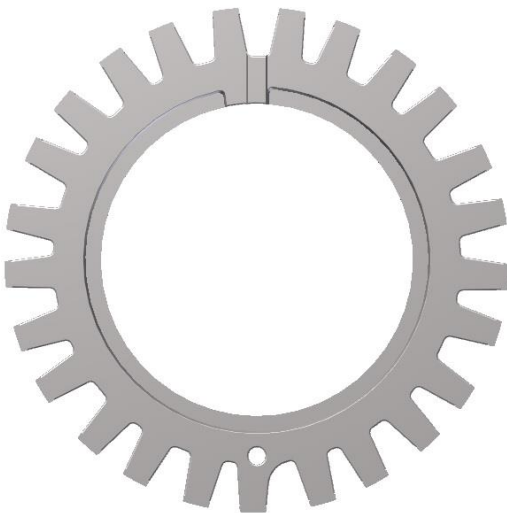


Figure 5. 10: 6th and 12th pitched SMC stator component – S6

This stator component, shown in Figure 5.10, was manufactured from SMC and pitched for 6th and 12th harmonic, similar to stator S4. The tooth tips were not chamfered and new type of coil exit slot, as described in Figure 5.8 was implemented. The stator assembled from this was termed S5.

Lastly, a stator was assembled which consisted of SMC fully pitched single tooth span stator components however the phase gaps in the stator was increased by 0.1mm. This made the inner phase of stator weaker: the effect of mutual coupling between the phases was examined. This stator was termed S7.

5.2.3 The SMC Core-back

The core-back ring was manufactured from an SMC ring provided by Höganäs AB in a pre-heated state to provide better mechanical strength and fixed characteristics compared to untreated SMC. Three identical core-backs were used in each machine, one for each phase and with locating points to align laminations.

The core-backs and the laminations have the same cross-section in the compression direction and hence one tool was used in producing these parts. The axial length of the core-backs was decided to be 14.7mm; this was made up of 5.6mm x 2 for two laminations stacks plus 3.3mm for coil and 0.2mm for associated insulation. The core-back included a 7mm deep slot through which the coil exit into the stator hub through the laminations cut, shown in Figure 5.11.



Figure 5. 11: Core-back prototype manufactured from SMC, notches and slot visible – lamination compressed and fitted too.

5.2.4 Shaft mounted Hub

The hub is made from aluminium which is wire eroded and machined to locate on the shaft, as shown in Figure 5.12. This hub determines alignment of the stator phases at 0° , 120° and 240° and provides a connection between the shaft and the stator parts such as coils, laminations and insulations while aligning the coils and its exit slots with the slots in core-backs and laminations as described before. This hub is machined to accommodate the wire and coil connections making sure there is enough space for these to be compressed within.

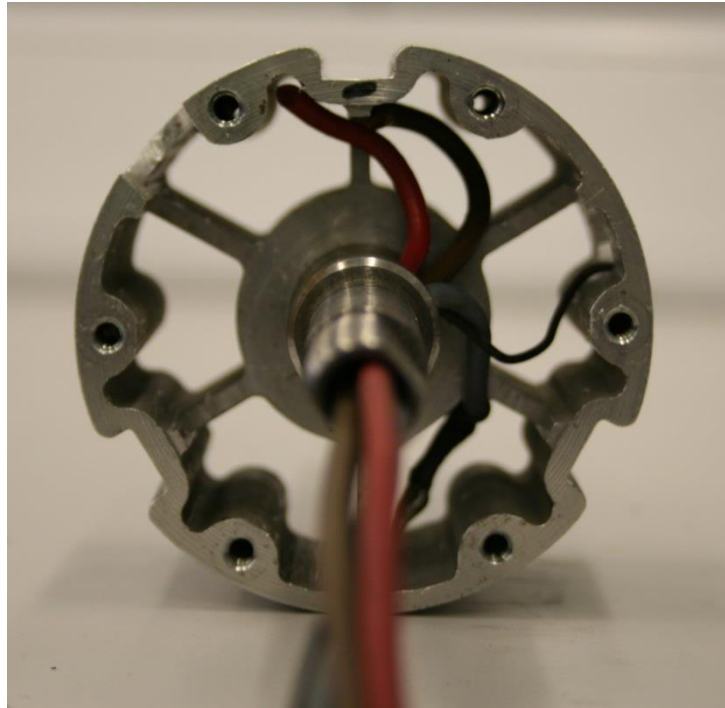


Figure 5. 12: Central hub of the machine fitted over the shaft

5.2.5 The Shaft

The shaft was machined from nonmagnetic stainless steel to a diameter of 21mm and this has the hub heat shrunk to fit. There are two bearing seats at either end for the end caps of the rotor and the shaft ends are threaded to lock on to the forks of the bicycle. The hub mounted on the shaft is shown in Figure 5.13, with the dimensional drawings in appendix B.

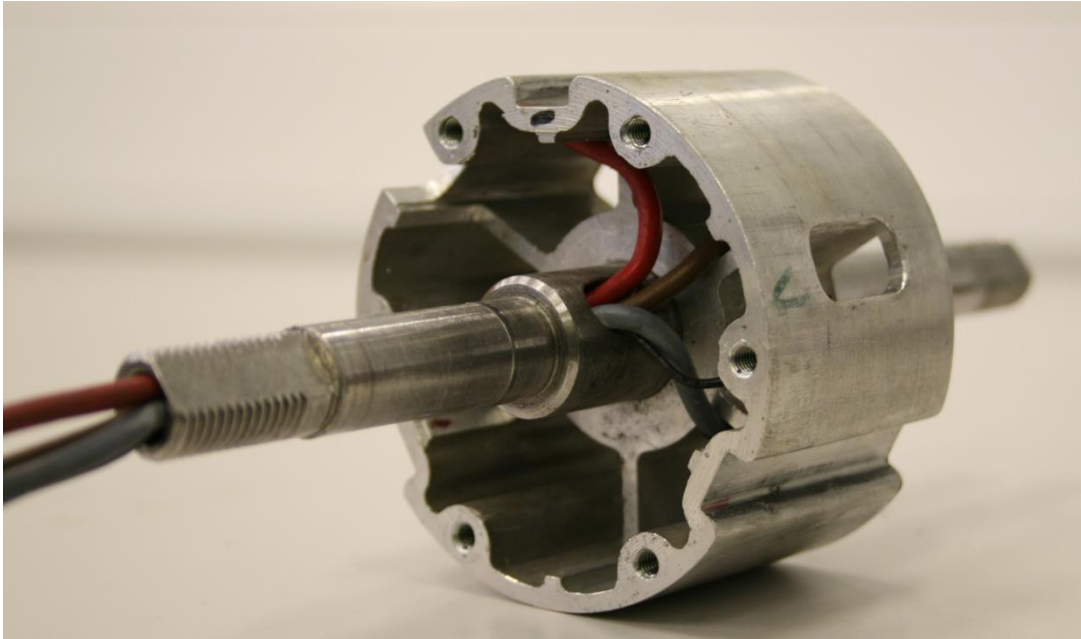


Figure 5. 13: Prototype representation of the shaft and central hub displaying the exit holes, threaded end, bearing seat and coil exits

5.2.6 Coils

The coils are made from 3mm x 1mm rectangular copper insulated wire and have 17 turns. A complete coil is shown in Figure 5.14.



Figure 5. 14: Prototype coil showing 17 turns

The coils were placed between the two lamination stacks to form a single stator phase. 0.1mm thick Nomex™ insulation is used between the lamination and coil, while extra insulation is in place around the coil bends at the entry and exit points. This arrangement is shown in Figure 5.15.

The slot fill factor of the base machine was 66%, a conservative value which exceeded 80% with rectangular wire in the new produced machines, coil shown in Figure 5.14.



Figure 5. 15: Prototype lamination, coil and core-back fitted together, coil exiting through the lamination and core-back slots, Nomex providing insulation between coil and laminations

5.3 Stator Assembly

The stator consists of 14 components which are assembled in the following order:

1. Central hub heat shrunk on shaft.
2. Sensor and power lines passed through shaft centre (as shown in Figure 5.13).
3. Stator end plate made of aluminium screwed on one end of the central hub.
4. The first core-back slid on the central hub followed by the first lamination stack, rotated by 180 degrees (six notches) from the opening in the core-back.
5. Coil, sandwiched by Nomex insulation, was placed in such a way as to allow the coil ends to pass through the core-back slot into the central hub.
6. The next lamination is placed so that it is in line with the slot in the core-back and allows the coil ends to pass through the lamination cut.
7. Another aluminium separator of 2mm thickness is placed to complete first phase of the machine, as shown in Figure 5.16 (left).
8. Phase two core-back is rotated by 120° and placed over the aluminium separator and the laminations, coil and insulation are placed in the same fashion as explained earlier, however rotated.
9. The first lamination of phase two is also rotated by 120° from the first and sits opposite to the coil exit slot in the core-back.
10. The fourth lamination rotated by 120° from the second lamination and placed such that its cut is on top of the coil exit slot.
11. A second phase separator is put on top of this fourth lamination to complete the second phase, as shown in Figure 5.16 (right).
12. Third core-back is placed rotated by a further 120° from the second core-back to complete the three phase arrangement.
13. Same steps are repeated to place the fifth and sixth laminations enclosing the third coil and insulations.
14. The coils were iron soldered with the wires and heat shrunk into the central hub space.

15. A second endplate is screwed on top to complete and press the stator assembly together as shown in Figure 5.17 while a complete stator is shown in Figure 5.18.

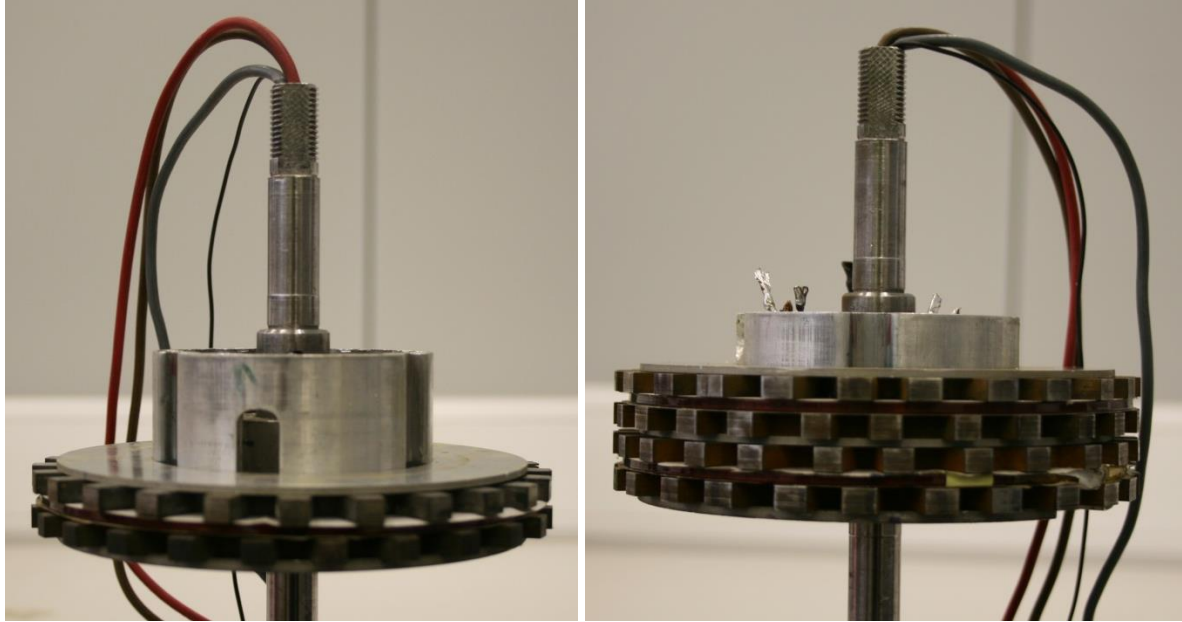


Figure 5.16: Machine Stator during assembly

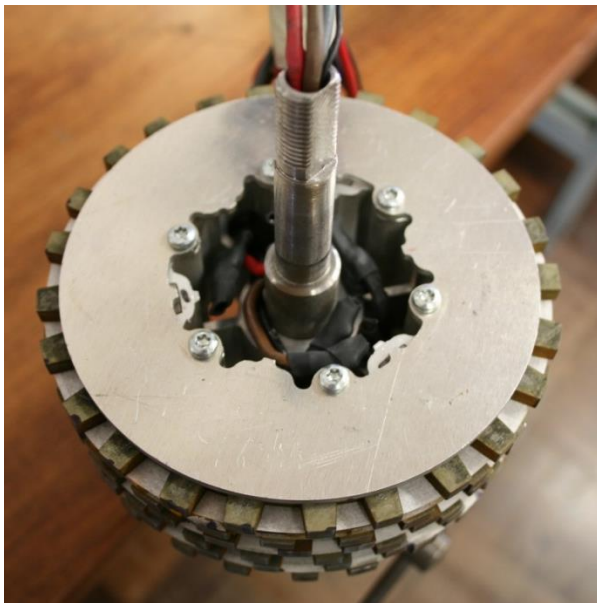


Figure 5.17: Stator coil wires soldered and second end cap screwed to press the stator components

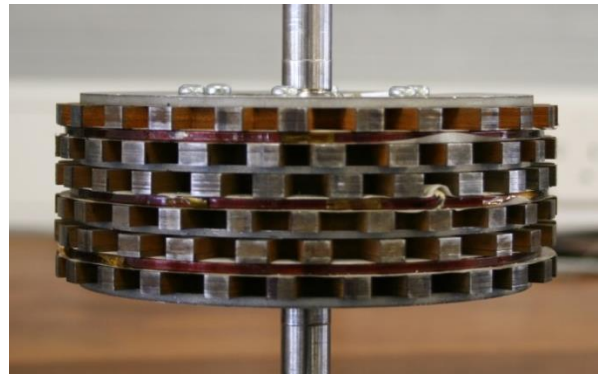


Figure 5.18: View of the complete stator assembly

5.4. Rotor types and Assembly

There are five types of rotor manufactured to reduce cogging torque as shown in Table 5.1.



The base design for all comparison is from a Höganäs Electric bicycle (shown left) and was termed R1. The 50 magnets and 50 pole pieces are glued onto an aluminium hub which has features to help locate the components. The pole pieces are Somaloy 3P and the magnets are NdFeB N35SH grade. The aluminium plates have the bearings and enclose the armature; these are shown in Figure 5.19. A single rotor was used throughout as slight

variations do occur between two different rotors.



Figure 5. 19: Different views of simple rotor consisting magnets and pole pieces and end plates



The Finite Element analysis showed that there is coupling between stator phases via the rotor pole pieces. Splitting the rotor into three separate sections axially allows for this affect to be experimentally analysed. This split rotor is shown in Figure 5.20 and was termed R2.

Figure 5. 20: Split Rotor prototype



Figure 5. 21: Rotor with a cut of 0.04mm for increased air gap in inner phase

An alternative to complete axial separation of the rotor is an increased air gap aligned with the central phase. A FE analysis study was carried out which showed a groove of 0.44mm provided the optimum solution for reducing the mutual coupling in this machine and hence a prototype with a 0.04mm cut in the inner phase was created, shown in Figure 5.21. This rotor is termed R3.



Figure 5. 22: CAD models of Convex (top) and wave direction (bottom) pole piece designs

Lastly, variable air gap was imposed on rotor pole pieces. The effect of rotor pole shaping on the air gap face was investigated. FE analyses suggested two topologies to reduce cogging; a convex and wave property; rotors using each were constructed; these are shown in Figure 5.22. Rotor assembled using Convex pole pieces was termed R4 and rotor assembled from Wave direction pole pieces was termed R5.



Figure 5. 23: Prototype rotor with convex pole pieces

5.5 Final Assembly

Figure 5.24 shows an unmounted machine assembly. The rotor and stator are separately assembled and then aligned in the lathe. The stator is slowly inserted into the rotor; one end cap is screwed onto the rotor and is held in the jaws of a lathe while the other end cap and the rotor is held in a tailstock and slowly introduced into the stator. The stator aligns itself into the rotor, the shaft locates in the bearing and the endcap is rotated to fit the screw holes in the rotor hub.

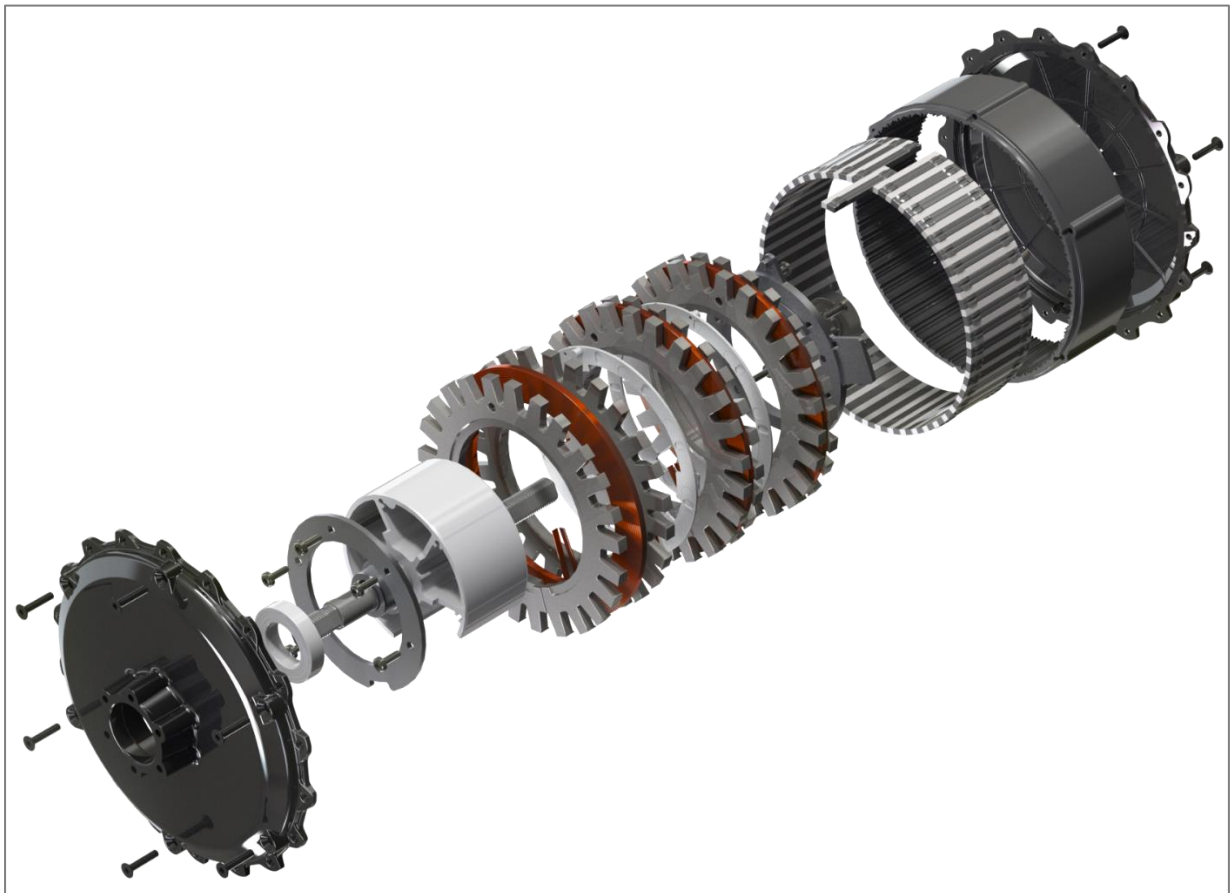


Figure 5. 24: CAD version of machine assembly showing the stator components, rotor, shaft and inner hub

6. Testing of Prototypes – harmonic effect

After construction of all the prototypes, a variety of measurements were taken for each motor so that comparisons can be made and the best combination of stator and rotor can be chosen. Cogging torque, back EMF, speed-torque and efficiency were measured for each machine. Results for cogging torque and back EMF are presented in this chapter while Chapter 7 discusses the torque-speed-efficiency performance.

This chapter is divided into four parts:

- Details of the test benches
- Cogging torque measurement and analysis
- Back EMF measurements and analysis
- Summary of design analysis for cogging and EMF – the optimum machine

Two test rigs were used to carry out the measurements; these test rigs are shown in Figure 6.1 and 6.2 while their drawings are shown in Appendix C and D. Both of the rigs were equipped with high precision instruments to provide reliable and repeatable results. LabVIEW was used to control, acquire data and process the measured values. Both test rigs are based at Höganäs.

6.1 Measurement setup – Test benches

There were two test benches used to carry out the measurements detailed above. These are:

- A cogging torque test rig, figure 6.1
- A motor performance test rig, figure 6.2

6.1.1 Cogging Torque test bench

The cogging torque test bench is equipped with an absolute encoder from Heidenhain with 25 bits resolution and rated accuracy $\pm 20''$. A torque transducer from HBM with Rated torque of 20 N and accuracy class 0.2 is used to measure the torque. A small motor rotates the machine under testing until one complete mechanical revolution. The data is recorded using National

Instruments CompactRIO and two modules, one for the torque and other of the position. The torque output from the transducer is a voltage (± 10 V), hence a voltage module with 24 bits resolution, ± 10 V is used (NI 9239). For the position, a dedicated module from SEA is used to read the digital data by means of the protocol EnDat 2.2 from the encoder (SEA 9510). 20,000 measurements per revolution were taken, equating to 900 per electrical cycle or one per 0.45° electrical.

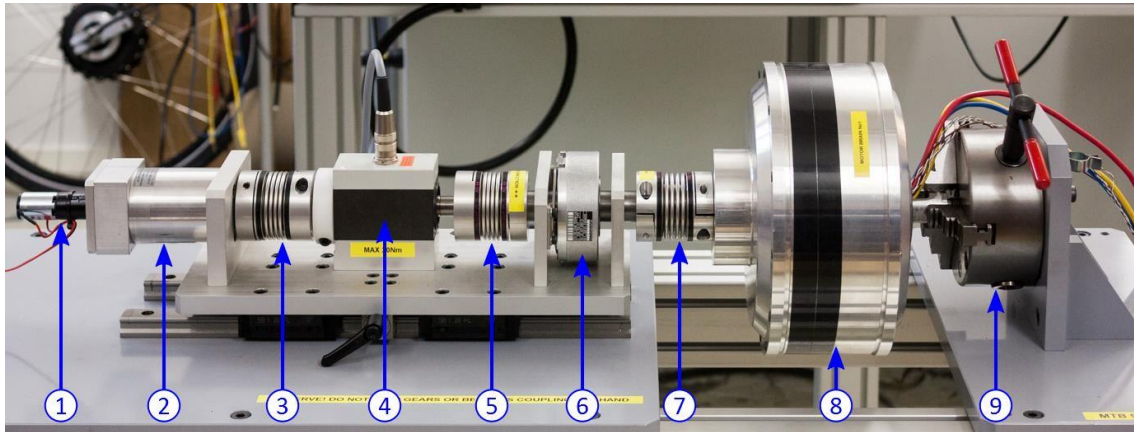


Figure 6. 1: Cogging Torque test bench.

The cogging torque test bench consists of the following components;

1. DC motor and planetary gearhead (Maxon A-max 22, 12 V, 6 W, 7 mNm and Maxon GP 22 A, reduction 84.1)
2. Planetary Gearhead (Wittenstein Alphira 060-2, reduction 100:1)
3. Coupling (R+W)
4. Torque transducer (HBM T20WN, Rated torque 20 Nm, Accuracy class 0.2)
5. Coupling (R+W)
6. Absolute Encoder (Heidenhain ECN 125, 25 bits, accuracy $\pm 20''$)
7. Coupling (R+W)
8. Machine under test
9. Lathe Chuck (Fuerda)

6.12 Dynamometer test bench

The Dynamometer Test Bench uses a drive motor to rotate the test motor as a local at a precise speed and torque. This load is equipped with a 4-quadrant control driver, which regenerates load power back to the grid. The torque measurement is with a 200Nm HBN torque transducer

from HBM; rated torque 200 Nm. An external encoder was used as the prototype motor does not have embedded position sensors. Figure 6.2 shows the test bench.

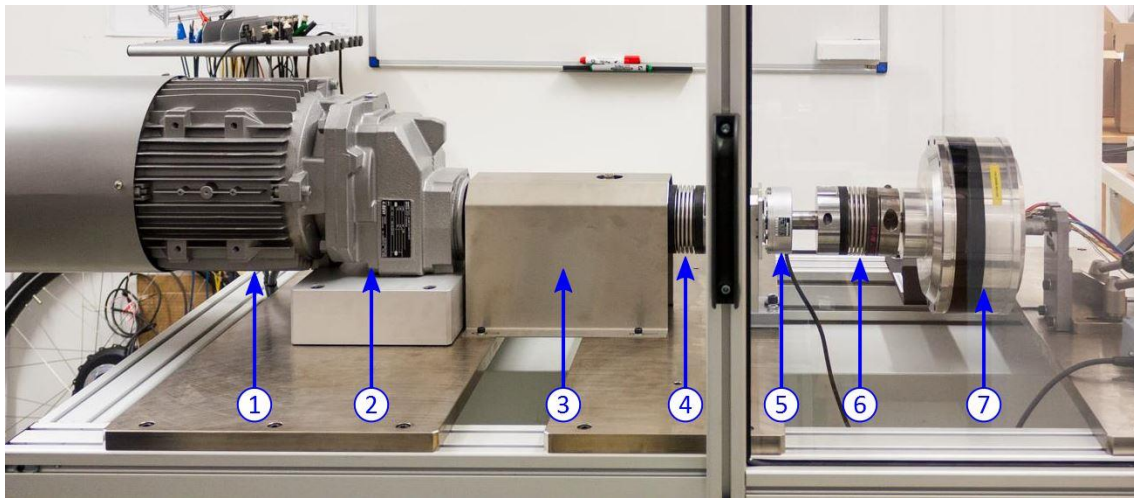


Figure 6. 2: Motor Test Bench.

1. 4-quadrant torque control driver and Induction motor (motor drive: VFD-C2000, Induction Motor: Watt Drive 1060 rpm, 5.5 kW, 50 Nm)
2. Gearhead (Watt Drive HU 60E70 133S4, 456 rpm, 115 Nm, ratio 2.33)
3. Torque transducer (HBM T20WN, Rated torque 200 Nm, Accuracy class 0.2)
4. Coupling (R+W)
5. Incremental Encoder (Heidenhain ERN 120, 5000 lines, accuracy 1/20 of grating period)
6. Coupling (R+W)
7. Machine under test

The signals are acquired using the high precision power analyser from Yokogawa, with power accuracy of $\pm 0.02\%$. Due to the current limitation of the power analyser, a HITECH current transducer was used. LabVIEW plus National Instruments modules are used to acquire and process data. The measurement and analysis rig is shown in figure 6.3.



Figure 6. 3: Instrument rack for the motor test bench.

1. Power analyser (Yokogawa WT3000, power accuracy of $\pm 0.02\%$)
2. Current Transducer (HITEC Power Protection, MACC-PLUS , Current Ratio 1000:1)
3. CompactRIO for control and data acquisition (National Instrument, modules: NI RIO 9148, NI 9229, NI 9269, NI9401, NI 9472, NI 9481)
4. Power Supply (Elektro Automatik GmbH EA-PS 8080-40, 0..80 V, 0..40 A, 0..1000 W)

6.2 Cogging Torque

In this section, cogging torque analysis is separated into the laminates and SMC stators, conjunction with each of the five rotors. Where possible, measured and FE results are compared for satisfaction of the analysis. Any variations are down to the factors discussed earlier i.e. the mesh sensitivity or the mechanical tolerances in the prototypes.

6.2.1 Laminate Stators

The four laminated stators were tested with each of the five rotors. In each test, the rotor was rotated in the clockwise direction and then in anticlockwise direction. Average cogging torque is then calculated from both which ensures hysteresis, back lash or any frictional or test bench features do not affect the measurements.

A) Base Rotor (R1)

Figure 6.4 shows the measured cogging torque for the four stators and the base rotor.

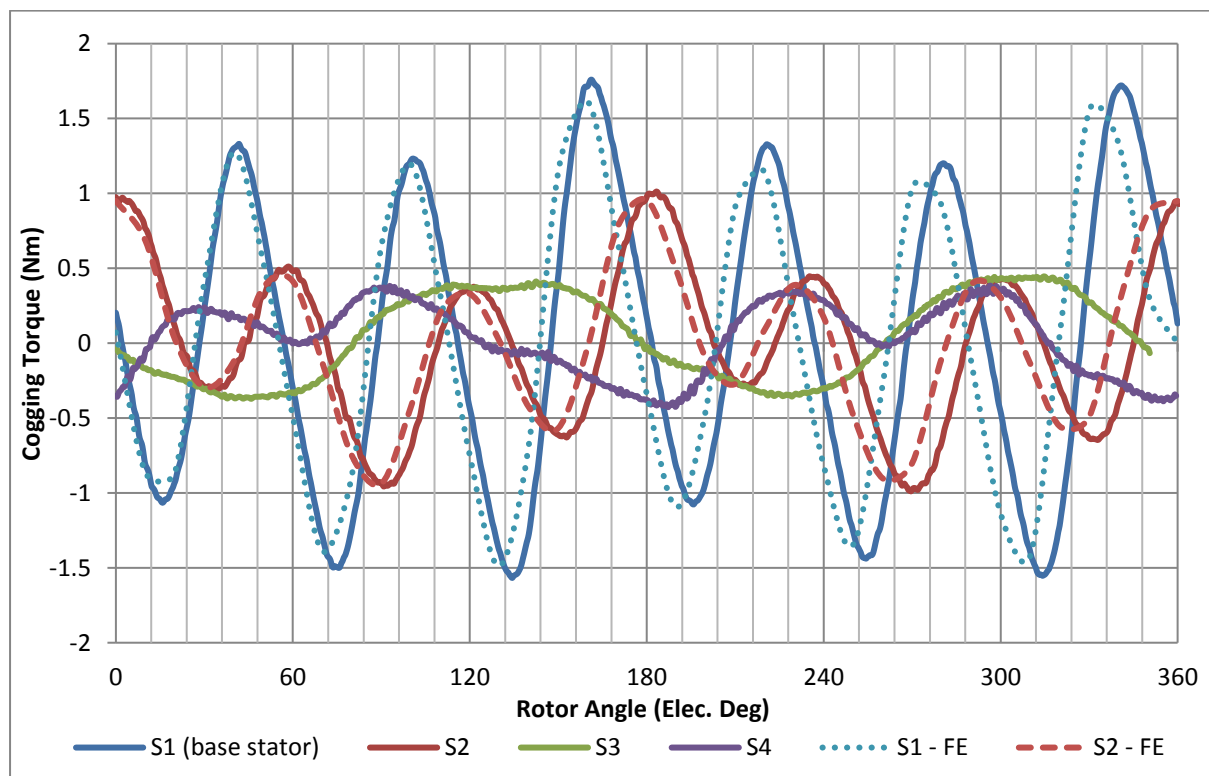


Figure 6. 4: Comparison of cogging torque waveforms of four laminate stator types with simple rotor

It is evident that the peak cogging torque is reduced for all three stators when compared to the basic stator design. There is a reduction in peak cogging torque and all harmonics for all the stators except for the T_{c2} of S2 and S3. The magnitude of T_{c2} present in these two is greater

than the base stator (S1) as seen from table 6.1. FE waveforms are of a similar magnitude and phase adding clarity to the mechanical prototyping and measurement excellence.

S3 reduce the peak cogging torque but still has a large T_{c6} (43% of the base model) however S4 reduces the T_{c6} by 97%. This shows that the pitching and tooth span combination works well and fulfils the purpose for which it was designed.

S4 reduces the peak cogging torque by 75% while the T_{c6} and T_{c12} are also reduced by 97% and 95% respectively. This by far is the best solution for peak cogging torque and its entire harmonics; at least when used in conjunction with R1. Table 6.1 presents the results for four laminated stator types when combined with basic rotor type.

Table 6. 1: Comparison of Peak cogging torque and its harmonic content for laminate stators and simple rotor

Base Rotor (R1)					
Stator types	Peak Cogging Torque (Nm)	2 nd harmonic	4 th harmonic	6 th harmonic	12 th harmonic
S1	1.76	0.23	0.18	1.46	0.20
S2	1.01	0.35	0.12	0.63	0.03
S3	0.45	0.38	0.04	0.04	0.01
S4	0.43	0.13	0.06	0.05	0.01

B) Convex pole pieces – R4

The same four stators were tested with the rotor R4, figure 6.5 compares these waveforms.

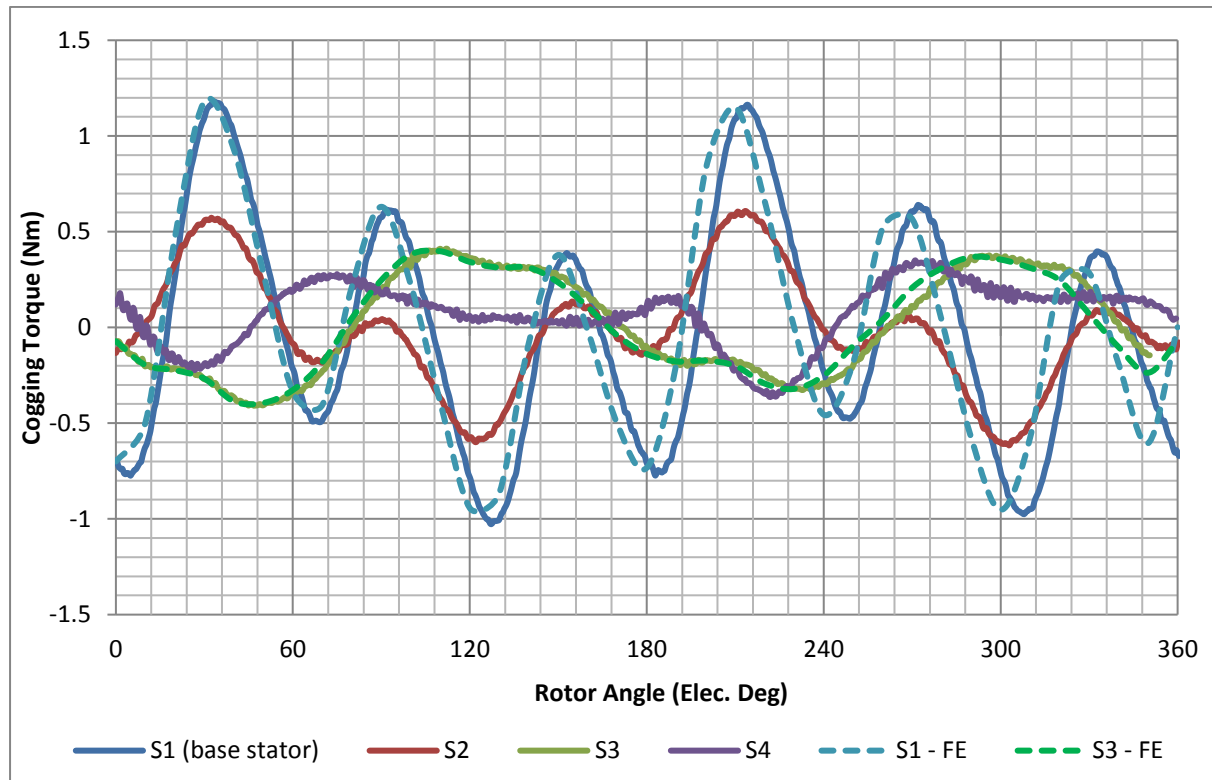


Figure 6. 5: Comparison of cogging torque waveforms of four laminate stator types with rotor R4.

The effect of convex pole pieces is evident; peak cogging torque of all the stators are reduced further when compared to the peak cogging torque with R1. Peak cogging torque of the base model (S1, R1) is reduced from 1.76 Nm to 1.18 Nm with S1, R4 motor. Table 6.2 shows the cogging torque and its harmonics for all four laminate stators with R4.

Table 6. 2: Comparison of Peak cogging torque and its harmonic content for four laminated stators and R4.

Convex Rotor (R4)					
Stator types	Peak Cogging Torque	2 nd harmonic	4 th harmonic	6 th harmonic	12 th harmonic
S1	1.18	0.40	0.11	0.71	0.07
S2	0.62	0.39	0.03	0.25	0.01
S3	0.41	0.27	0.06	0.03	0.01
S4	0.36	0.06	0.04	0.03	0.00

It is evident again that S4 has the biggest effect; the reductions in the harmonics and the peak cogging torque are the largest. S4 reduces the peak cogging torque by 70%, T_{c2} by 85%, T_{c4} by 65%, T_{c6} by 96% and T_{c12} by 100%. These percentage reductions are the largest in all four (S1 to S4) stators.

C) Wave Direction Pole pieces – R5

Thirdly, S1 - S4 were tested for cogging torque with R5, figure 6.6 presents the waveforms. The effect of using this rotor is a reduction of 33% in peak cogging torque for S1; however it causes an increase in peak cogging torque when compared with S2R4, S3R4 and S4R4. These increases are mainly due to the increased T_{c2} and T_{c6} content of these stators (Table 6.3) when compared to the results in Table 6.2.

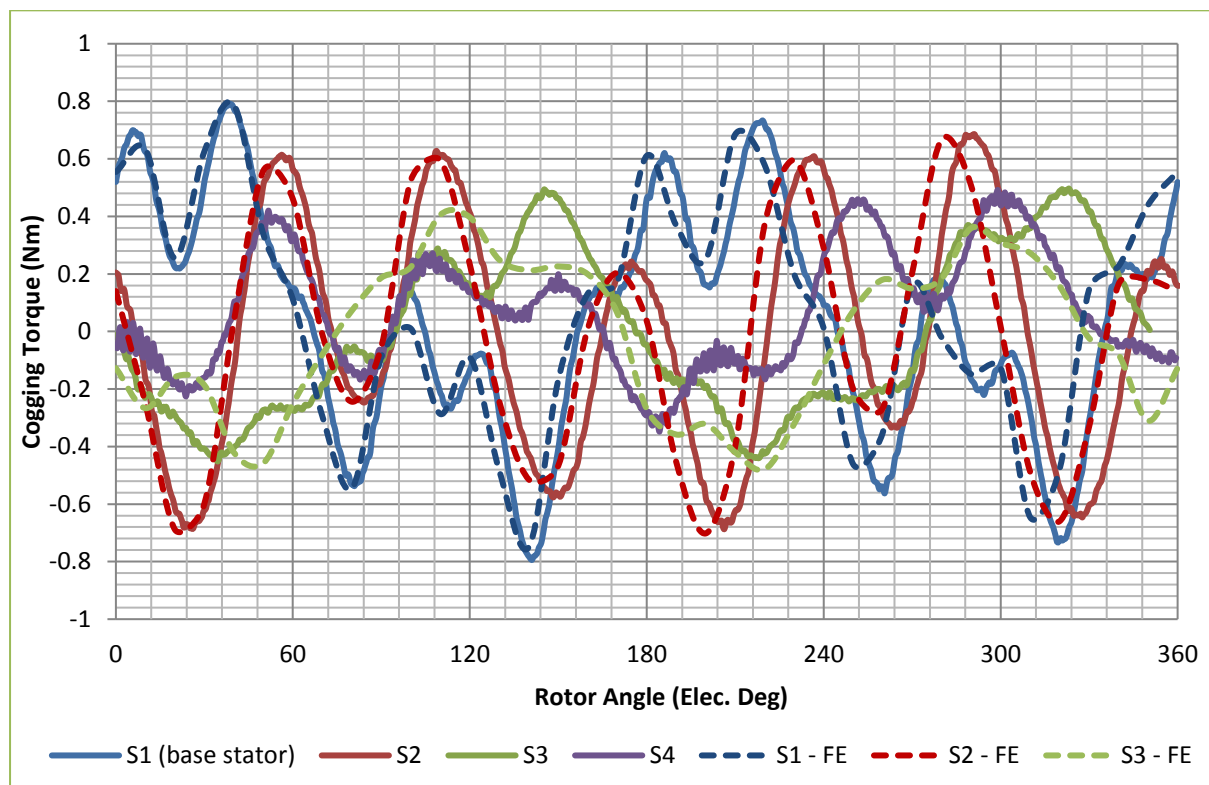


Figure 6. 6: Comparison of cogging torque waveforms of four stator types with R5.

Comparing the stators with S1 in terms of the R5, it is evident that all stators cogging torque is reduced as well as its harmonics. S2 has the lowest reduction due to its T_{c6} nearly double when compared to the S1. It can be concluded that R5 works best with S4 however the level of cogging present is higher when S4 was used with R4. The variations in S3's measurement and FE results is due to the complexity of combining tooth spans and pitching techniques however the deviation is not extreme.

Table 6. 3: Comparison of Peak cogging torque and its harmonic content for four laminated stators and R5.

Wave direction (R5)					
Stator types	Peak Cogging Torque	2 nd harmonic	4 th harmonic	6 th harmonic	12 th harmonic
S1	0.79	0.39	0.14	0.25	0.19
S2	0.69	0.24	0.03	0.51	0.03
S3	0.50	0.36	0.03	0.04	0.03
S4	0.49	0.09	0.04	0.05	0.00

D) Split Rotor (R2)

It could be seen from results in Tables 6.1, 6.2 and 6.3 that T_{c2} in all stators with the three rotors is comparatively high. It was known from [117] that this harmonic occurs mainly due to the mutual coupling taking place between the three phases of the motor and hence R2 was machined; a simple rotor (like R1) was split in three sections to reduce this effect. This rotor was only tested with S1 and S2. Figure 6.7 compares the cogging torque waveforms of S1R2, S2R2, S1R1 and S2R1.

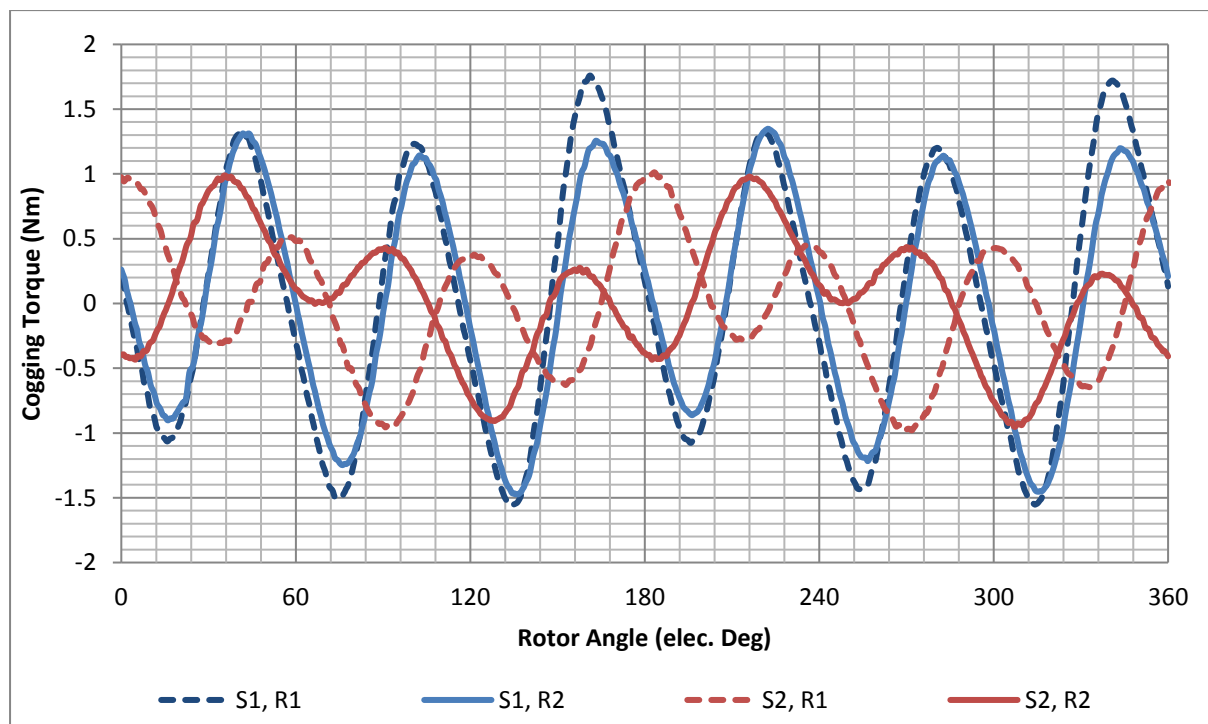


Figure 6. 7: Comparison of cogging torque waveforms of stators S1 and S2 with rotors R1 and R2.

It can be seen from figure 6.7 and table 6.4 that the peak cogging torque for both S1R2 and S2R2 is reduced when compared to these stators used with R1. The sole purpose of using this rotor was to reduce T_{c2} appearing due to mutual coupling between the stator phases. This purpose seems to be achieved as table 6.4 shows the T_{c4} , T_{c6} and T_{c12} for both stators have decreased however T_{c2} has increased by a small amount.

Moreover the peak cogging torque present in these two stators is still significantly higher than that produced when these stators were used with R4 and R5. It can therefore be concluded that although splitting the rotor will reduce the harmonics, it does not provide the best solution. Furthermore, manufacturing such rotors are not feasible as component count is increased; there are three times the components as that of R1.

Table 6. 4: Comparison of Peak cogging torque and its harmonic content for two laminated stators with R1 and R2.

Split Rotor (R2)					
Stator types	Peak Cogging Torque	2 nd harmonic	4 th harmonic	6 th harmonic	12 th harmonic
S1	1.47	0.26	0.12	1.23	0.11
S2	0.99	0.48	0.05	0.48	0.02
Simple Rotor (R1)					
S1	1.76	0.23	0.18	1.46	0.20
S2	1.01	0.35	0.12	0.63	0.03

It can be concluded that the best solution achieved by the laminated stator family for reduction of cogging torque is by using the stator pitched for 6th and 12th harmonic (S4) partnering with the convex type of modified pole pieces rotor (R4). Table 6.5 conclude the comparisons.

Table 6. 5: Comparison of base model with the best solution of laminated stator

Stator types	Peak Cogging Torque (Nm)	2 nd harmonic	4 th harmonic	6 th harmonic	12 th harmonic
S1R1	1.76	0.23	0.18	1.46	0.20
S4R4	0.36	0.06	0.04	0.03	0.00

6.2.2 SMC Stators

This family of stators are manufactured from Soft Magnetic Composite material instead of laminations. There are two stators under this family; stator with chamfered teeth (S5) and stator pitched for 6th and 12th harmonic of cogging torque (S6). Both these stators were tested with all the rotors that first family of stators were tested with to see the effect these have on them.

A) SMC stator chamfered teeth (S5)

S5 was tested first with R1 and is compared with the S1R1 (base model). Figure 6.8 compares the cogging torque waveforms for the two machines. It is apparent that S5 diminishes the peak cogging torque from 1.76 Nm to 0.86 Nm which is a major improvement in the torque quality of the machine. This improvement can be credited down to the chamfered feature introduced in the stator; Finite Element analysis predicted this as seen from Figure 6.8.

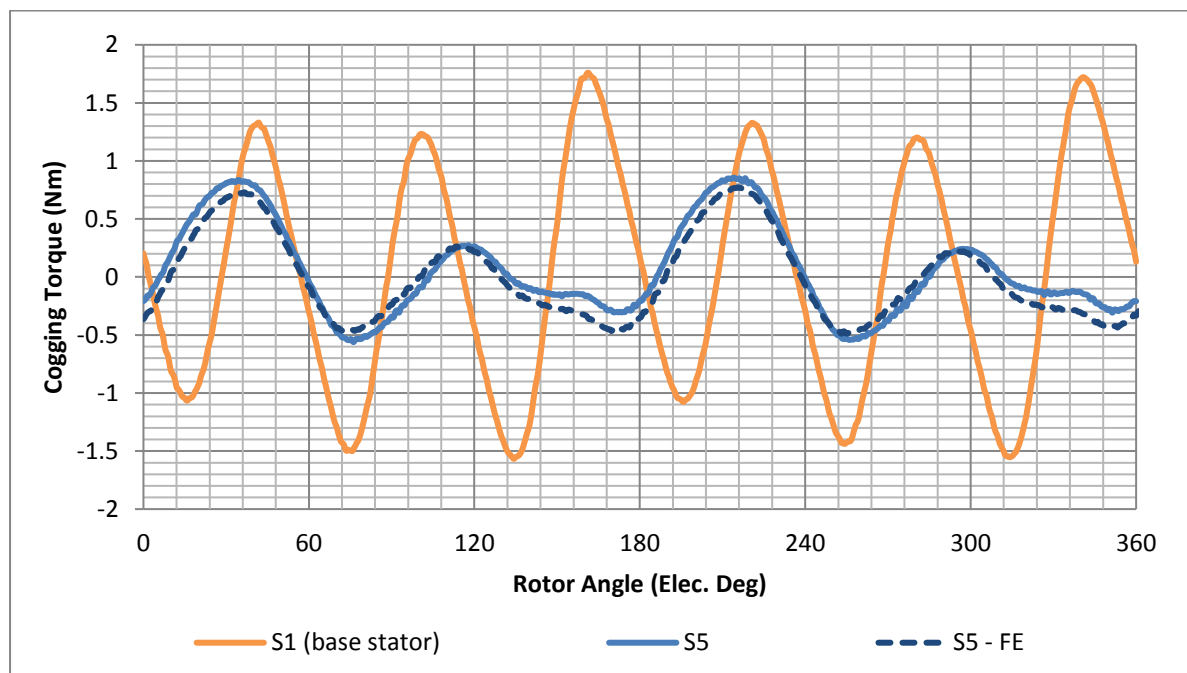


Figure 6. 8: Comparison of cogging torque waveforms for S1R1 (base model) and S5R1

S5 was tested with R4 and R5, cogging torque waveforms are shown in Figure 6.9. It is comprehensible that R4 reduces cogging torque the most. R5 also reduces the peak cogging torque compared to R1 however it introduces a higher T_{c6} compared to T_{c6} of R1. This is because of the shape of R5 pole piece as was described in section 4.4.

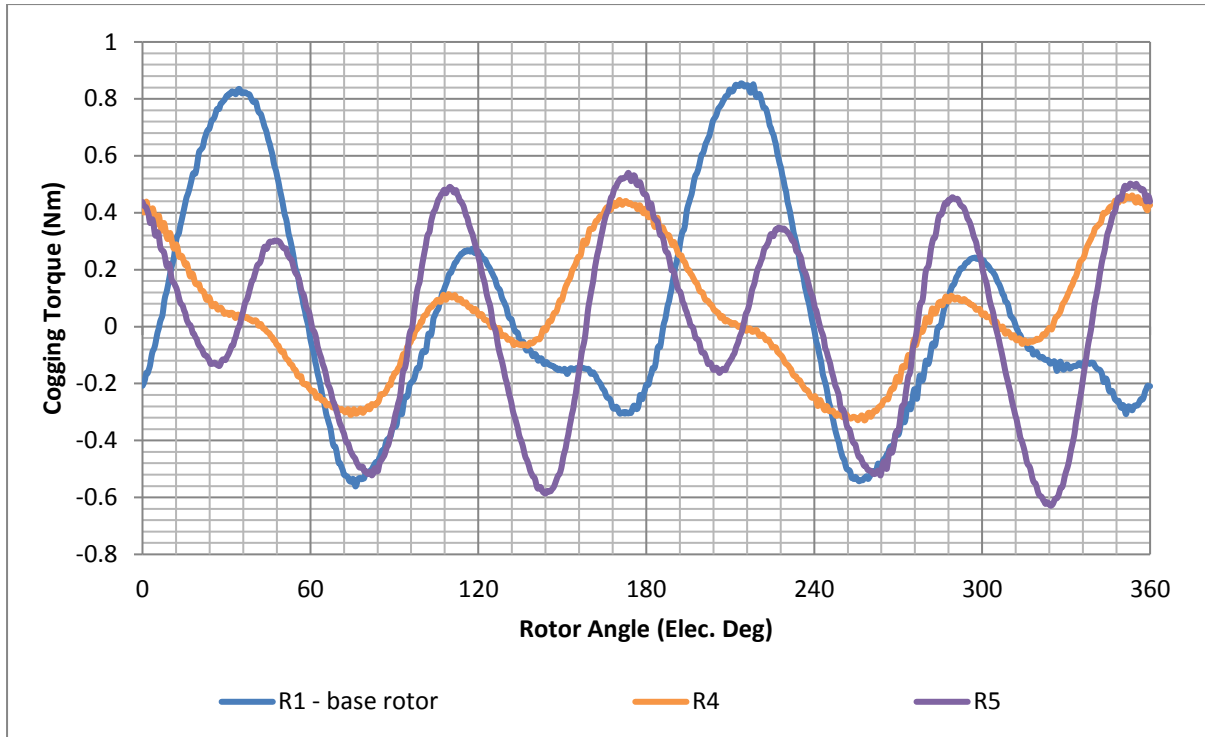


Figure 6. 9: Comparison of cogging torque waveforms for S5R1, S5R4 and S5R5

Next, S5 was tested with R2 and R3; waveforms are displayed in figure 6.10. Both of these rotors helped reduce the cogging torque in comparison with R1 however R2 introduces a higher T_{c6} and R3 establishes a higher T_{c2} .

Lastly, S7 was used with R1 to lower the mutual coupling. This was achieved as can be seen from Table 6.6. Peak cogging torque and the entire harmonic range was reduced in comparison with S1. Figure 6.11 compares these waveforms.

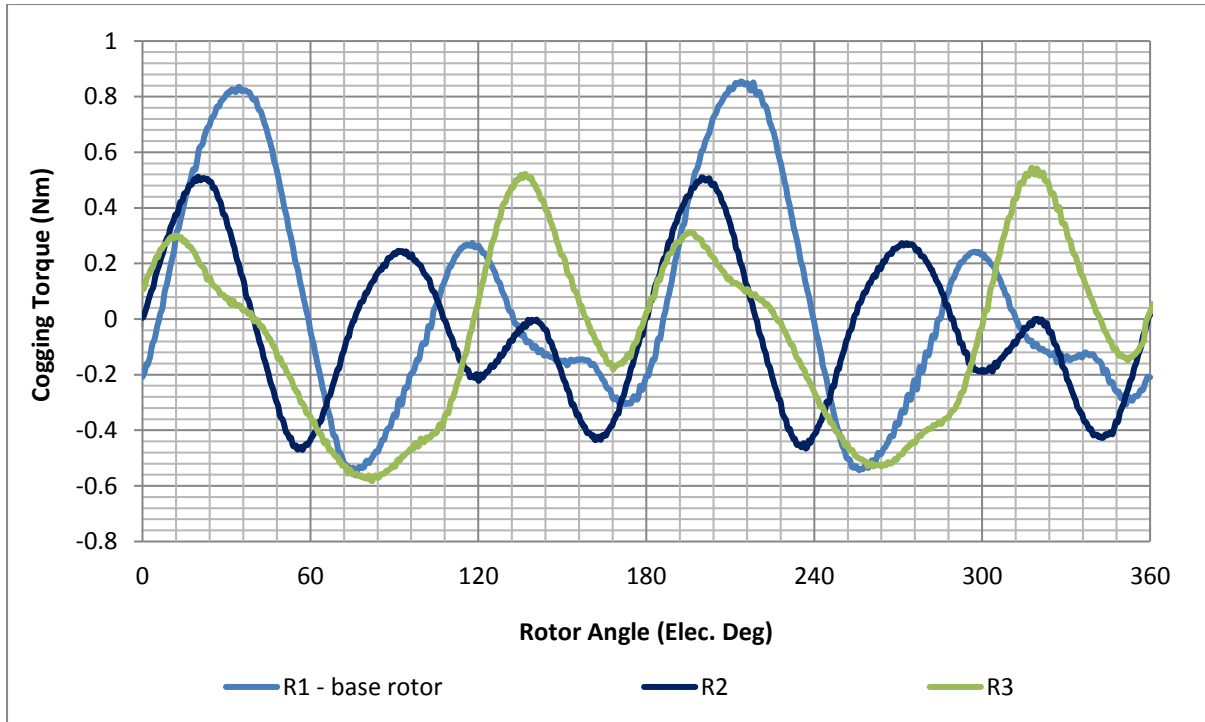


Figure 6. 10: Comparison of cogging torque waveforms for S5R1, S5R2 and S5R3

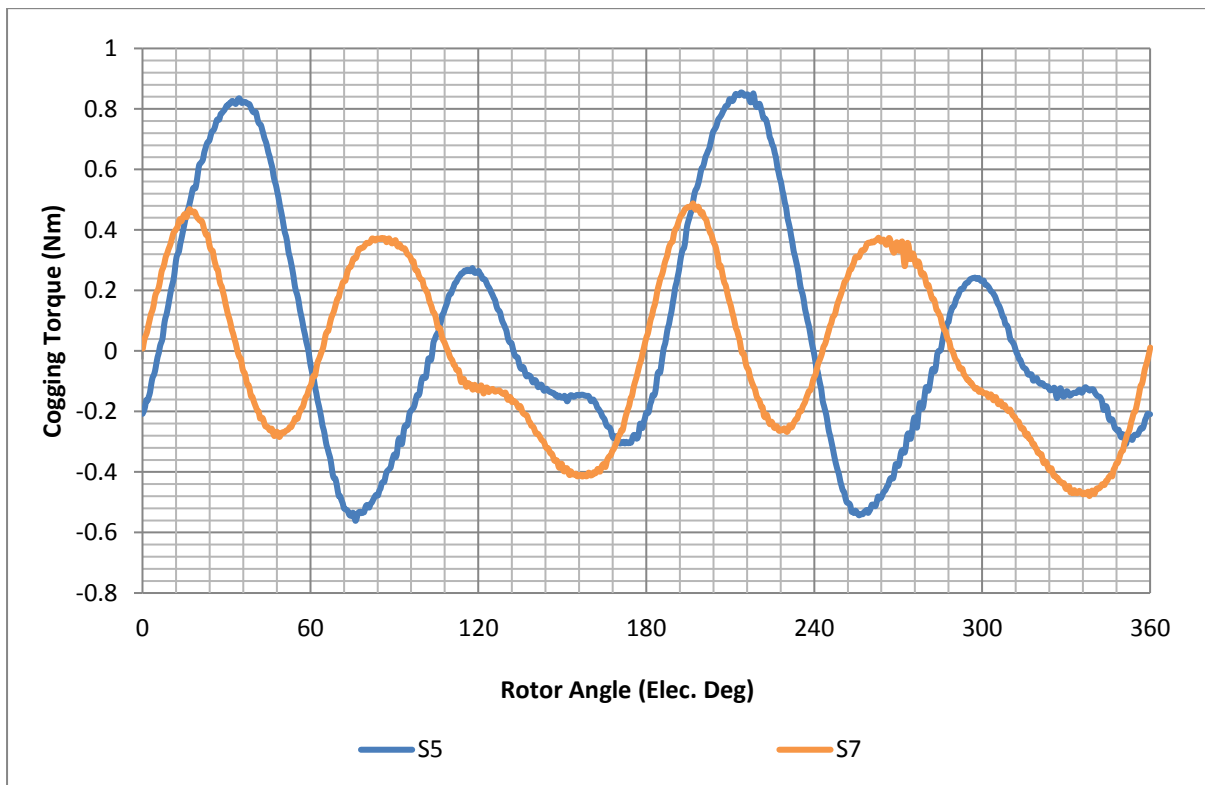


Figure 6. 11: Comparison of cogging torque waveforms for S5R1 and S7R1

To conclude, S5 was tested with five different rotor types. The aim was to reduce the peak cogging torque and ideally, all its corresponding harmonics too.

Table 6.6 presents the results; it is seen that R4 produce the least cogging torque, a reduction of 46% however its 2nd harmonic is a little higher than R1's 2nd harmonic. R2 also reduces the peak cogging torque by 34% however it increases the 6th harmonic and also increases the component count. The machine that reduces all the harmonics is with an increased inner phase stator gap with simple rotor (S7R1); peak cogging torque is reduced by 30%. It is not an ideal solution however, as increasing the phase gap will have an effect on the back EMF production and efficiency of the machine; presented in sections 6.3 and 7.2 respectively.

Table 6. 6: Comparison of Peak cogging torque and its harmonic content for S5 with five type of rotors and S7 with R1.

Motor Type	Peak Cogging Torque	2nd Harmonic	4th Harmonic	6th Harmonic	12th Harmonic
S5, R1	0.86	0.27	0.46	0.12	0.00
S5, R2	0.57	0.06	0.27	0.21	0.01
S5, R3	0.58	0.35	0.24	0.13	0.02
S5, R4	0.47	0.33	0.10	0.11	0.01
S5, R5	0.63	0.21	0.19	0.44	0.04
S7, R1	0.60	0.19	0.18	0.05	0.01

B) SMC 6th and 12th pitched Stator (S6)

S6 is compared first with S5 and then a comparison is made for this with all types of rotors used in the study. Figure 6.12 depicts the comparison of cogging torque waveforms for this new stator (S6) and S5.

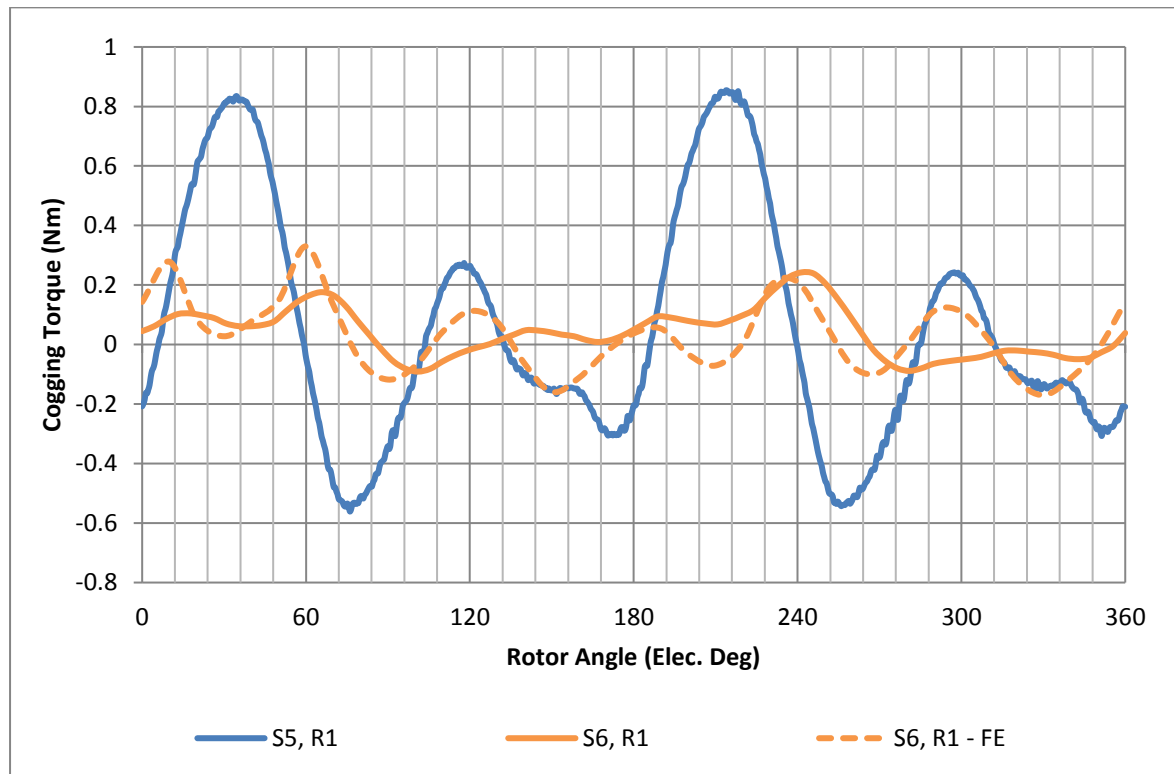


Figure 6. 12: Comparison of cogging torque waveforms for the two SMC stators

It can be seen that there is a 70% reduction in peak cogging torque for this new stator when tested with R1 producing a minor 0.25 Nm of peak cogging torque. Moreover the reductions in all the harmonics are evident too; these results are displayed in table 6.7.

S6 was then enclosed with R2, R4 and R5; figure 6.13 shows this comparison along with FE waveforms. It can be seen that although all these rotors further reduce the cogging torque, R4 provides the optimum solution. R2 and R5 also reduces the cogging torque however T_{c2} and T_{c12} for these are increased in comparison to R1.

The comparison between measured and FE results are positive and shows that the manufacturing, assembling and testing of the prototypes were of good standards.

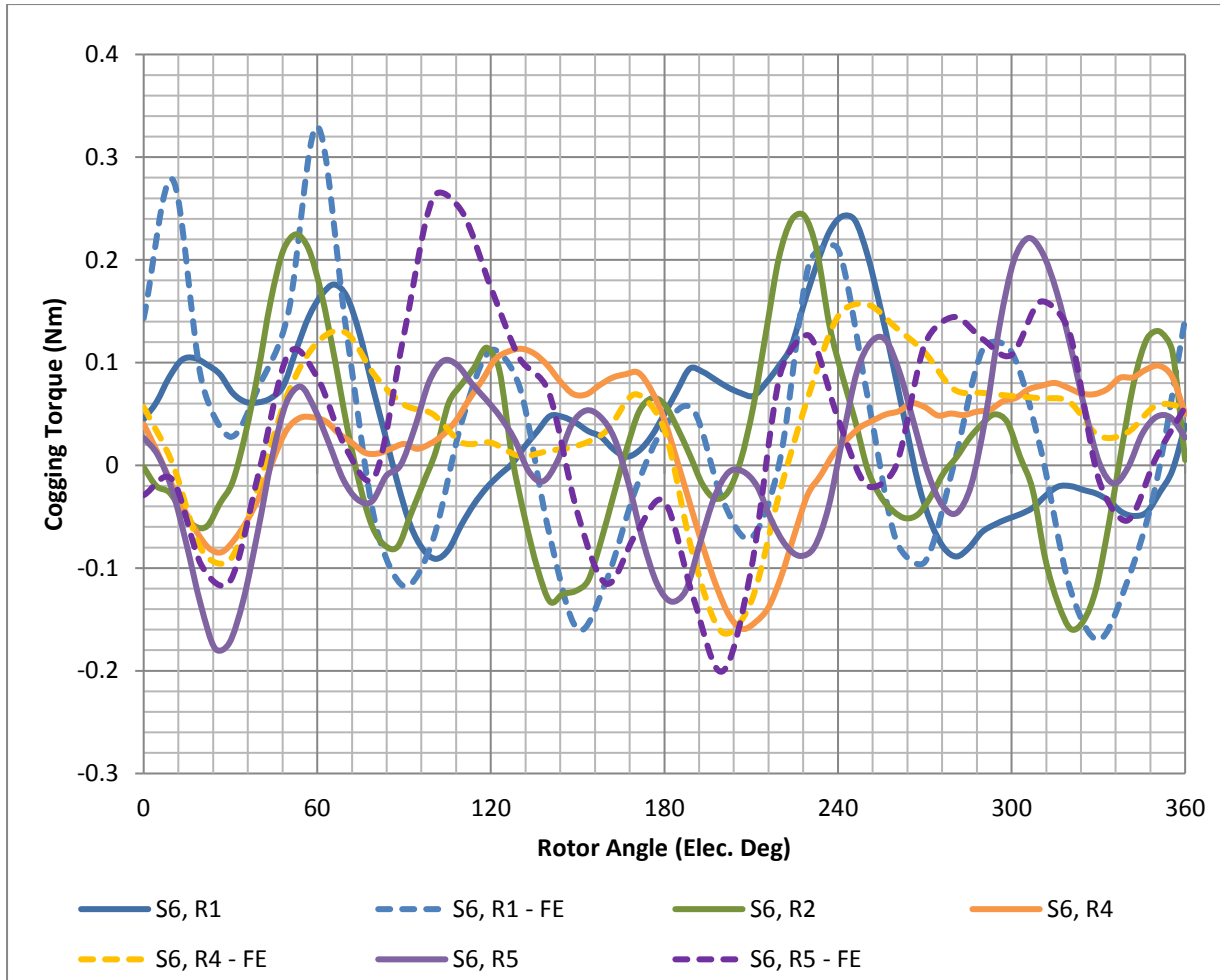


Figure 6. 13: Comparison of cogging torque waveforms for S6 with R1, R2, R4 and R5

Table 6. 7: Comparison of Peak cogging torque and its harmonic content for for S6 with R1, R2, R4 and R5

Motor Type	Peak Cogging Torque	2nd Harmonic	4th Harmonic	6th Harmonic	12th Harmonic
S6, R1	0.254	0.09	0.028	0.053	0.002
S6, R2	0.251	0.042	0.043	0.096	0.006
S6, R4	0.169	0.024	0.019	0.03	0.001
S6, R5	0.233	0.083	0.019	0.023	0.006

6.2.3 Summary Cogging Torque

The full set of cogging torque results are summarised in Figure 6.14. These results are all per unit of the base design i.e. S1R1. It is clear from this figure that all combinations of stators and rotors designs reduce the cogging torque compared to the base model.

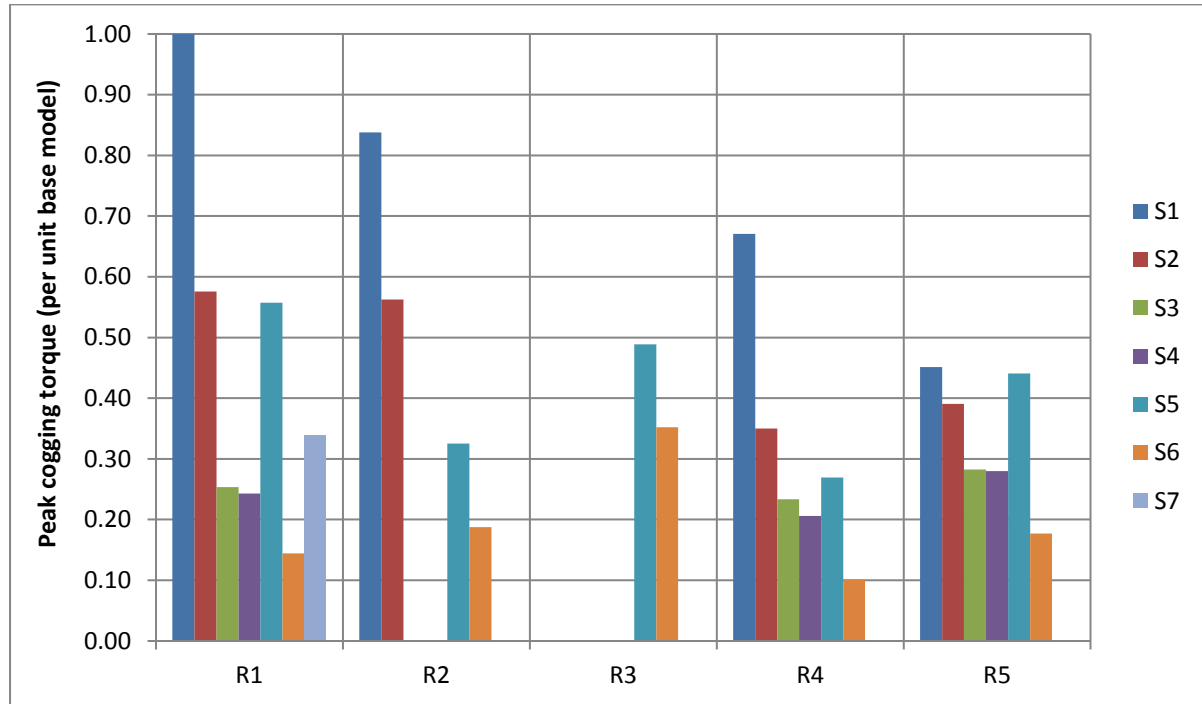


Figure 6. 14: Comparison of peak cogging torque per unit of base model for all the motors tested

For all five rotor types, S6 produces the lowest peak cogging torque; a reduction of 86%, 81%, 65%, 90% and 82% for R1, R2, R3, R4 and R5 respectively.

Except for S1, R4 proves to be the optimum rotor type for all other stators as the lowest peak torque is achieved with this. The only exception is S1 which when combined with R5 produces the lowest peak cogging torque.

The aim behind designing all these motors was not just to reduce the cogging torque but to also keep the important 2nd, 4th, 6th and 12th harmonic as low as possible. Figures 6.15 to 6.18 present a comparison of these harmonics; all results being per unit of the base motor.

It is evident from Figure 6.15 that using S1 and S2 causes a higher 2nd harmonic than the base motor. On the other hand, S4 and S6 reduce the 2nd harmonic; especially for R4 and R5. In fact the R1 in conjunction with S6 works equally as well. The worst case scenario is using S5 with R1 as it increases the 2nd harmonic three times of the base motor.

It can hence be concluded that the optimum motors to reduce the 2nd harmonic of cogging torque are S4R4 and S6R4 while S2 and S5 generally introduces a higher 2nd harmonic.

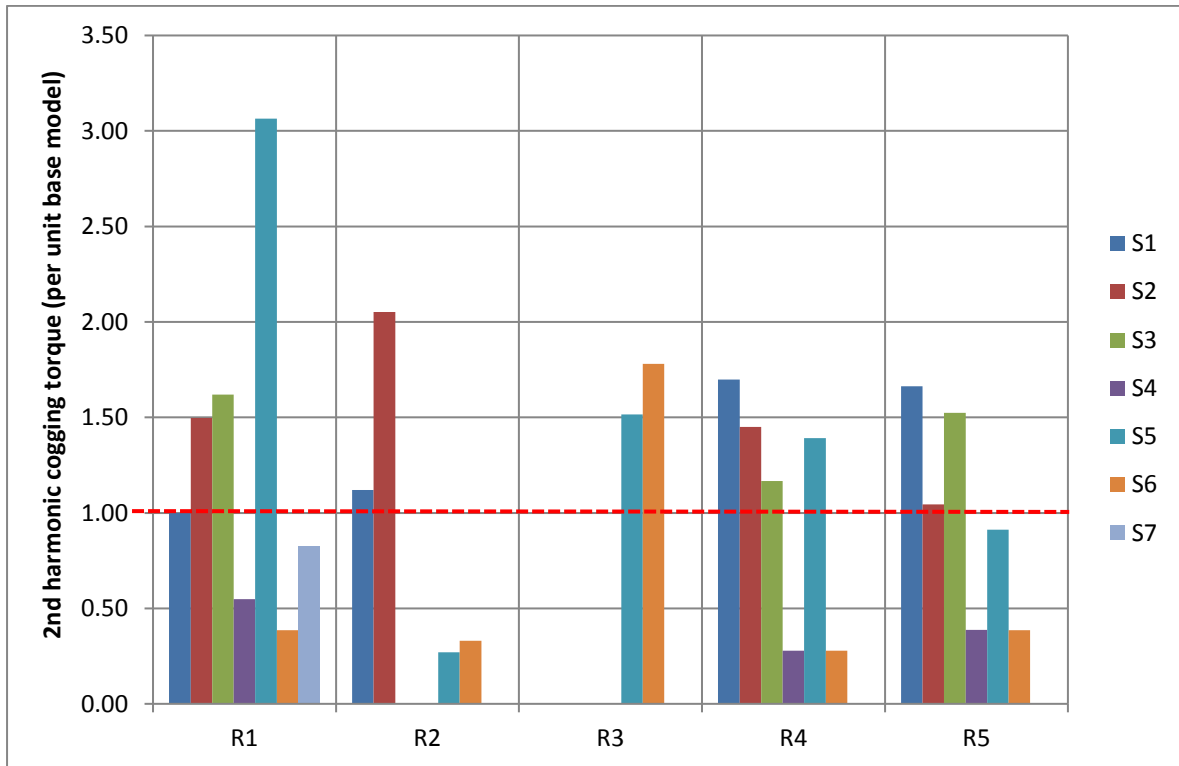


Figure 6. 15: Comparison of 2nd harmonic of peak cogging torque per unit of base model for all the motors tested

Figure 6.16 displays the 4th harmonic comparison and it is obvious that except S5, all the other stator and rotor couples reduce this harmonic. S4 and S6 combined with R4 and R5 reduce this harmonic by the largest amount too as was the case with 2nd harmonic.

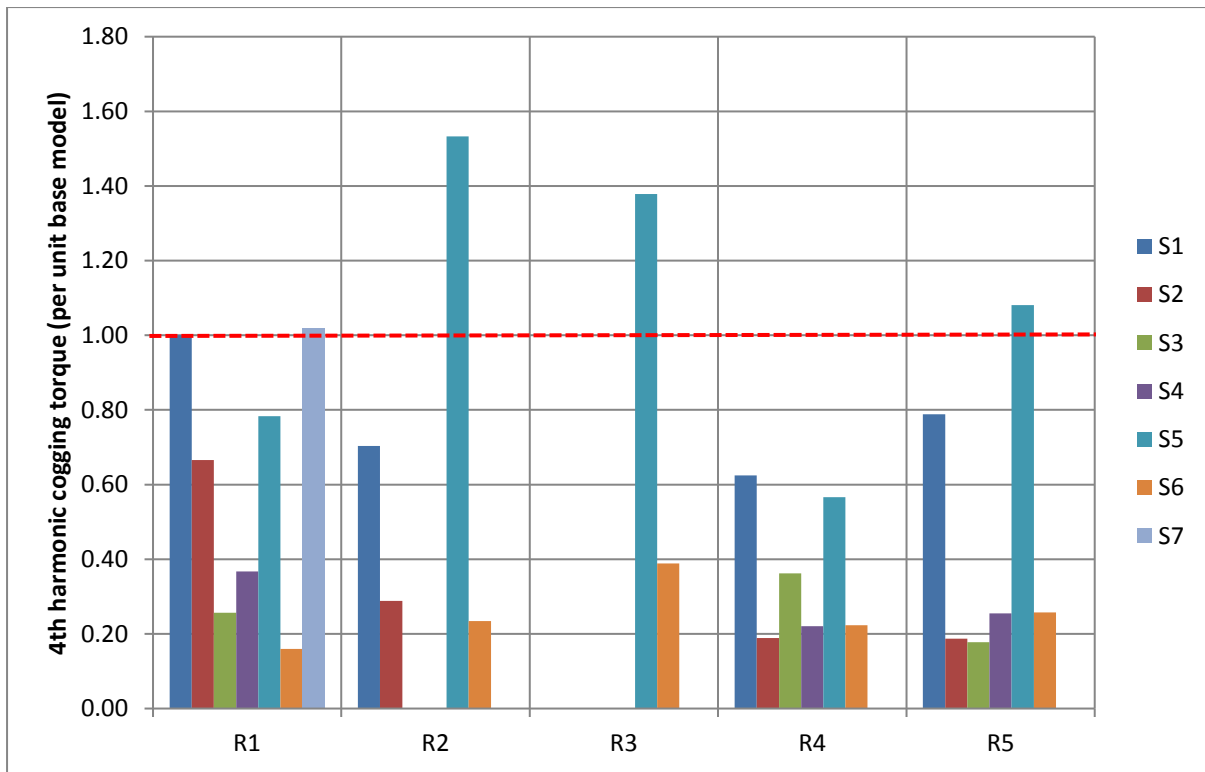


Figure 6. 16: Comparison of 4th harmonic of peak cogging torque per unit of base model for all the motors tested

Most important cogging torque harmonics in this study are the 6th and 12th as these were the main ones present in the initial base motor (S1R1). Figure 6.17 shows the comparison between the 6th harmonic of the motors tested and it can be seen that S3 works the best in minimising this unwanted harmonic. In fact all of the motors manufactured and tested have lower 6th harmonic than the base model. Equally good were the S4 and S6 when combined with R4.

Figure 6.18 presents the comparison between 12th harmonic of these motors and similar to 6th, all the motors have a lower harmonic than the base motor. S6 have the lowest 12th harmonic for all the rotors making this stator a good choice.

It can be concluded that the best motor for reducing cogging torque and its harmonics is the motor with S6 and R4. This motor, when compared with the base motor, reduces the peak cogging torque by 90%, 2nd harmonic of cogging torque by 72%, 4th harmonic by 78%, 6th harmonic by 98% and the 12th harmonic by 99% (shown in table 6.8). These percentage reductions are massive and help to reduce the vibrations in motor and give a smoother overall performance. The entire harmonic breakdown is presented in figure 6.19 for the base and optimised motor designs.

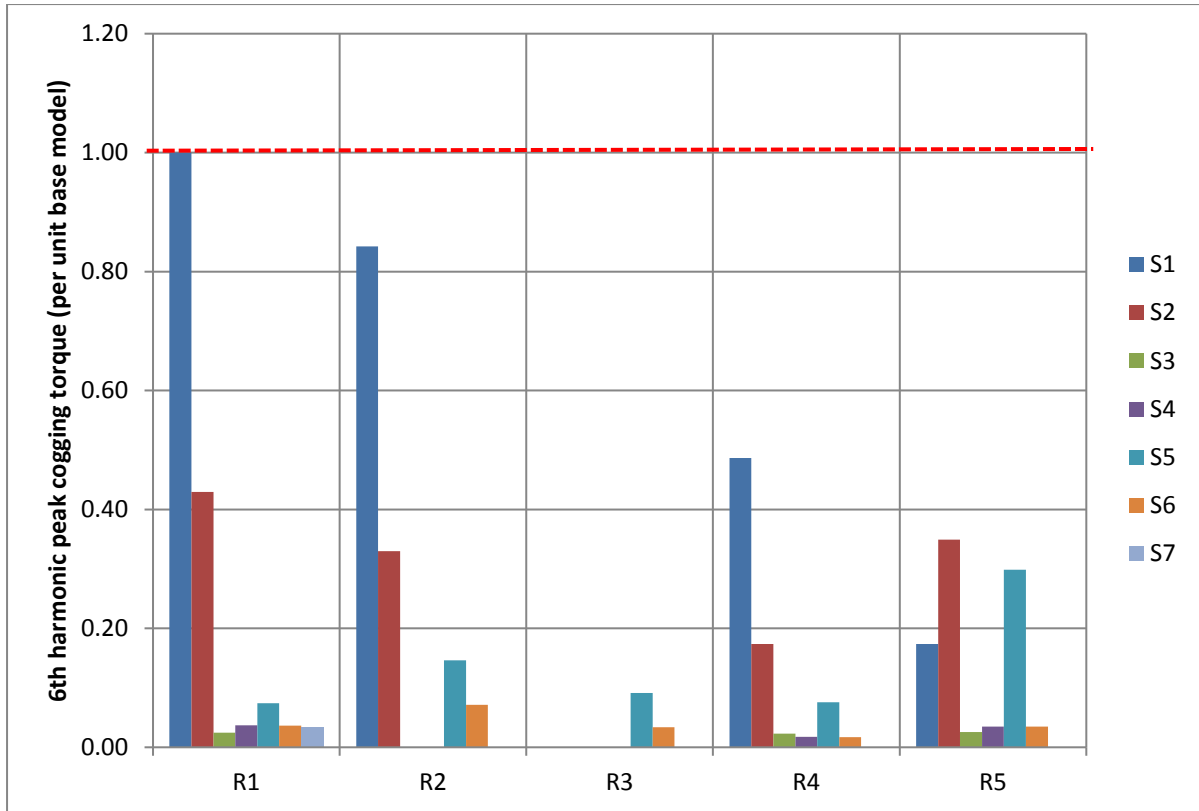


Figure 6. 17: Comparison of 6th harmonic of peak cogging torque per unit of base model for all the motors tested

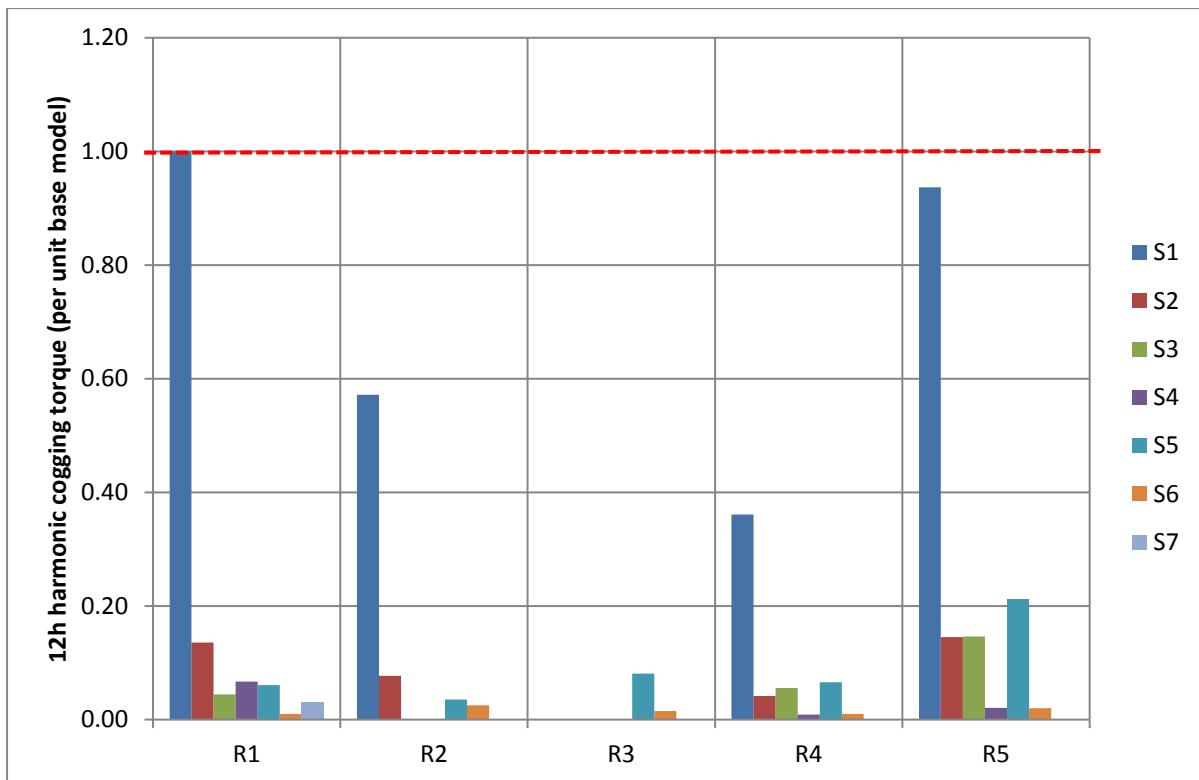


Figure 6. 18: Comparison of 12th harmonic of peak cogging torque per unit of base model for all the motors tested

Table 6. 8: Comparison of Cogging Torque of the base motor and the most optimised motor

	S1, R1 (Base motor)	S6, R4 motor	Percentage reductions
Peak Cogging Torque (Nm)	1.759	0.178	90
2nd harmonic	0.234	0.065	72
4th harmonic	0.175	0.039	78
6th harmonic	1.457	0.025	98
12th harmonic	0.198	0.002	99

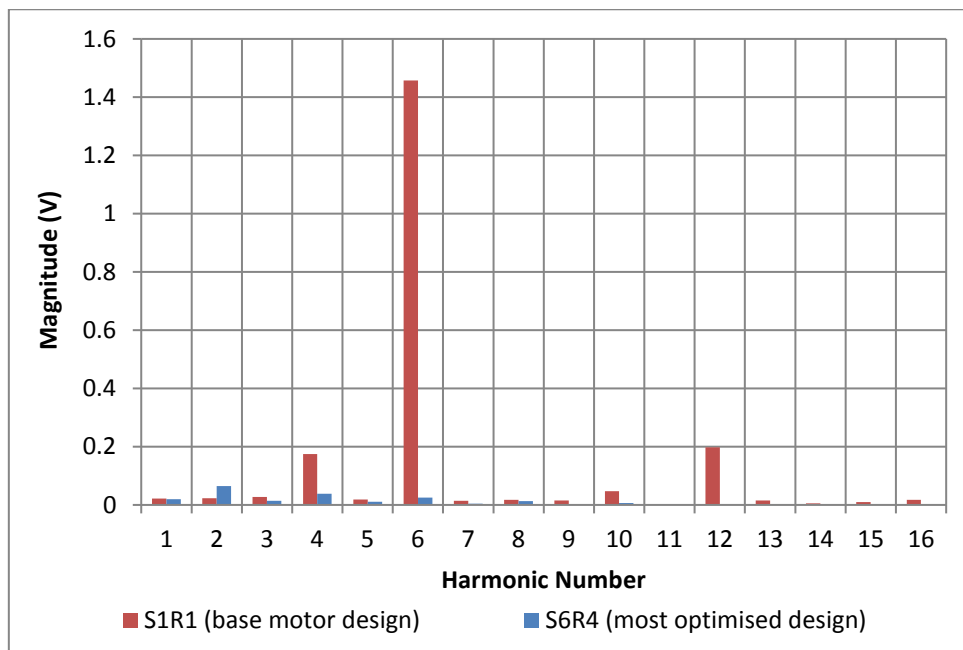


Figure 6. 19: Harmonic content for the base and optimised motor designs

However, it is vital to see how the back EMF, efficiency and torque production of this machine is compared with the base motor as well as the other motors under tests before coming to a final choice of optimum motor.

6.3 Back EMF

It was observed from Finite Element analysis that similar to the cogging torque harmonics, changes in tooth span and pitching also varies the back EMF harmonic content. This section focuses on the changes in back EMF and its harmonics observed for the two set of stator families. The test bench used for carrying out back EMF measurements was described in detail in section 6.12.

Figure 6.20 shows the comparison of central phase (B) with end phases (A and C) for S4R1. It is evident that there is very little phase misalignment while peak values for all three phases are similar too.

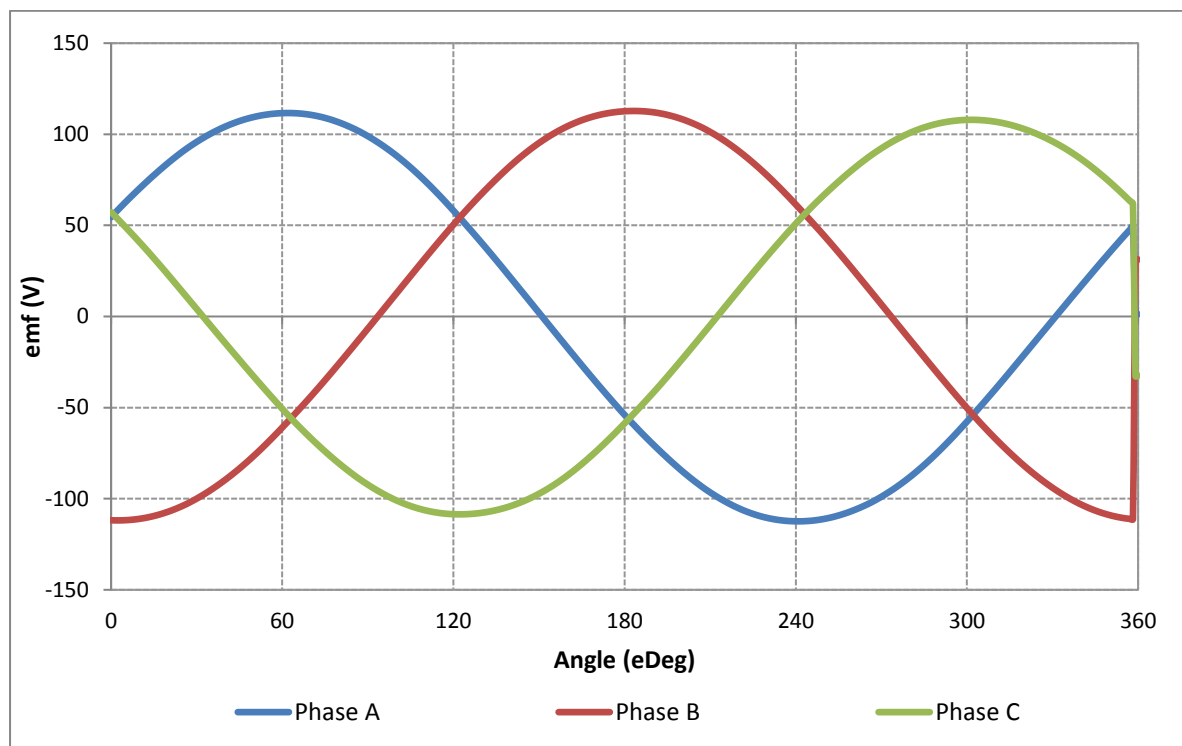


Figure 6. 20: Comparison of central and end phases of S4R1

For all the following measurements, only central phase will be used as there isn't a difference between the three phases as shown from figure 6.20.

6.3.1 Laminate Stators (S1 to S4)

Firstly, the stators manufactured from laminates are tested with R1, R2, R4 and R5.

A) Basic rotor (R1)

Figure 6.21 demonstrates the shape of the back EMF waveform for four stators in conjunction with R1; Table 6.9 displays the changes in key harmonics.

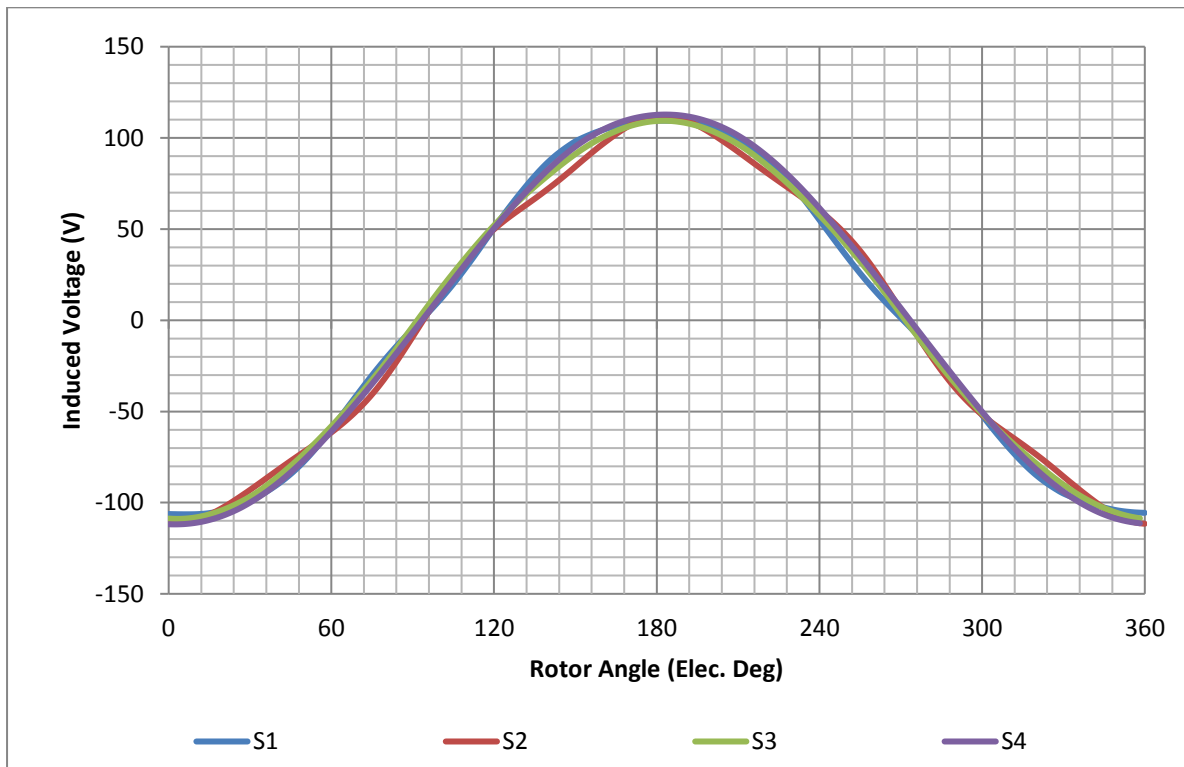


Figure 6. 21: Illustration of back EMF waveforms of phase 2 for four laminated stators with R1

S4 produces the largest fundamental harmonic, surpassing the base motor (S1) too however has a higher 7th harmonic. S3 have a lower fundamental harmonic however its 5th and 7th harmonic are lower than S1.

Table 6. 9: Harmonic content of back EMF waveform for laminated stators with R1

Motor Type with R1	Fundamental Harmonic	5th Harmonic	7th Harmonic
S1	110.57	3.20	0.86
S2	107.36	4.82	0.52
S3	108.53	0.79	0.26
S4	111.24	1.79	1.47

B) Convex Rotor (R4)

Same stators were tested with R4; waveforms are displayed in figure 6.22 while the harmonic contents are shown in table 6.10.

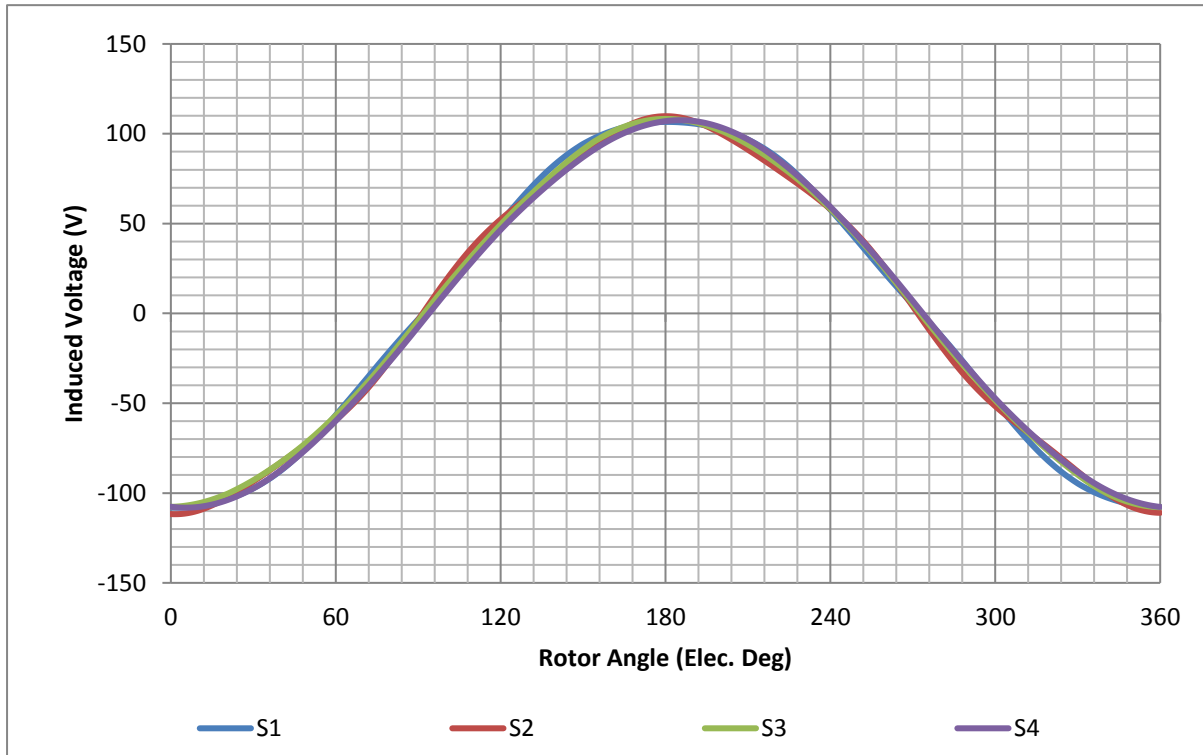


Figure 6. 22: Variation in back EMF waveforms with different laminated stators with R4

Comparing table 6.9 with 6.10, it is evident that using R4 reduces the back EMF produced by the motor, however by only 1%. There is a considerable bigger percentage difference of 3.6% for S4 when R4 is used instead of R1. The harmonic content in this stator however is quite lower when compared with S1. S2 also reduces the fundamental harmonic as well as giving rise to the 5th and 7th harmonic so is not the ideal motor to choose in terms of back EMF.

Table 6. 10: Harmonic content of back EMF waveform for laminated stators with R4

Stator types with R4	Fundamental Harmonic	5th Harmonic	7th Harmonic
S1	109.10	2.03	0.32
S2	107.59	3.56	0.36
S3	107.09	0.89	0.18
S4	107.27	0.32	0.18

C) Wave direction (R5)

R5 was used next with the four stators under test. Back EMF waveforms for these are shown in Figure 6.23 while their harmonic contents are displayed in Table 6.11.

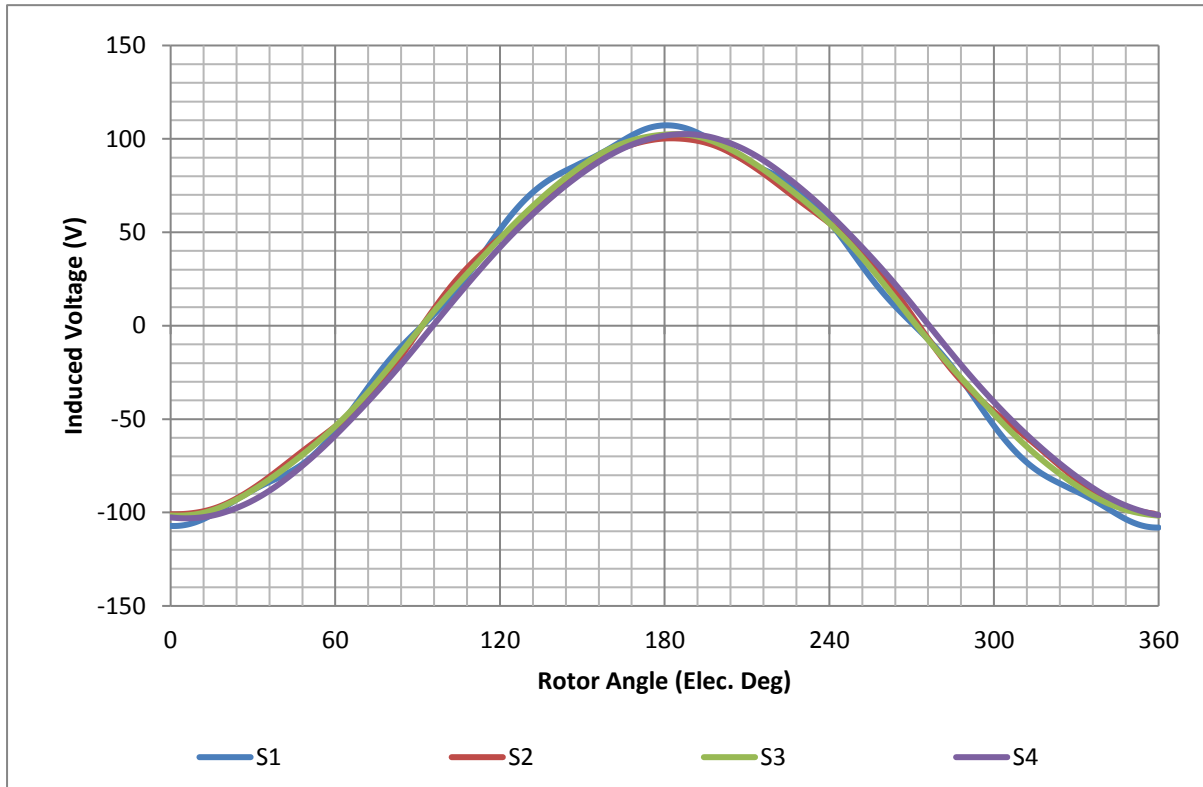


Figure 6. 23: Variation in back EMF waveform with four laminated stators and R5

Using R5 decreases the fundamental harmonic and also introduces a large 7th harmonic in back EMF with S1 as shown in table 6.11; an increase of 370 times from R1 and 1000 times from R4. The stator best suited so far being S4 still has a very minimal 5th and 7th harmonic and a good fundamental harmonic content when compared with S1R1.

A small conclusion can be derived at this point that R5 seem to reduce the back EMF for all stator types while generally introducing a high 7th harmonic.

Table 6. 11: Harmonic content of back EMF waveform for laminated stators with R5

Stator types with R5	Fundamental Harmonic	5th Harmonic	7th Harmonic
S1	105.01	0.03	3.19
S2	99.52	2.63	1.38
S3	101.49	0.74	0.45
S4	101.88	0.51	0.14

D) Split Rotor (R2)

Lastly, the split rotor is tested with the two laminated stators, S1 and S3. The waveforms are displayed in Figure 6.24 and its harmonic contents are presented in table 6.12.

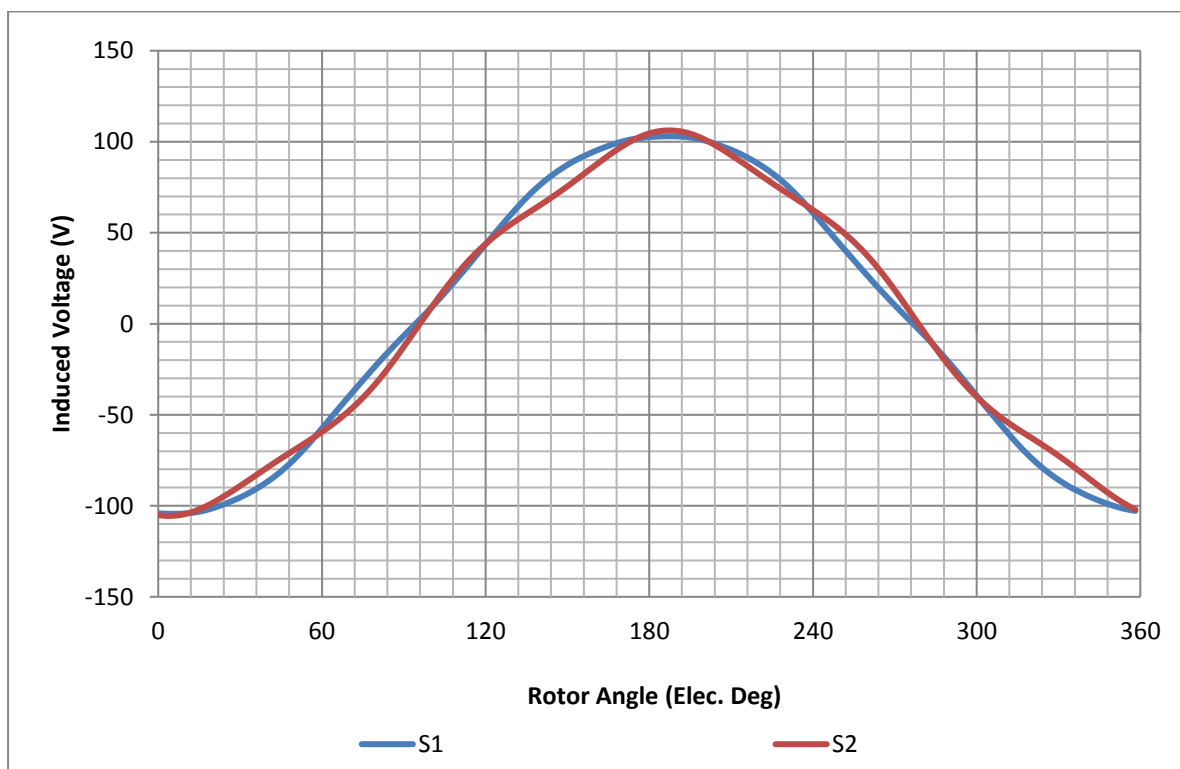


Figure 6. 24: Variation in back EMF waveform with two laminated stators and R2

Comparing Table 6.9 and 6.12, it is apparent that R2 reduces the fundamental harmonic by approximately 6% while 5th and 7th harmonic are reduced too. This means that the technique to split the rotor to reduce the cogging torque comes at a cost of 6% reduction in back EMF as

well as more components count. S2 provides the lowest fundamental harmonic while the 5th harmonic in back EMF is the largest for this motor type, making this motor choice a bad one.

Table 6. 12: Harmonic content of back EMF waveform for laminated stators with R2

Stator type with R2	Fundamental Harmonic	5th Harmonic	7th Harmonic
S1	104.10	1.99	0.68
S2	100.20	4.81	0.17

6.3.2 SMC Stators (S5 to S7)

This Section will present back EMF analysis for the three SMC manufactured stators; S5, S6 and S7.

S5 was combined with five rotors (R1 to R5) and measurements were taken for its back EMF. S7 was also tested with R1; results of cogging torque for this combination showed promising results in Figure 6.11. Figure 6.25 displays the back EMF waveforms while Table 6.13 presents the harmonic content of these motors.

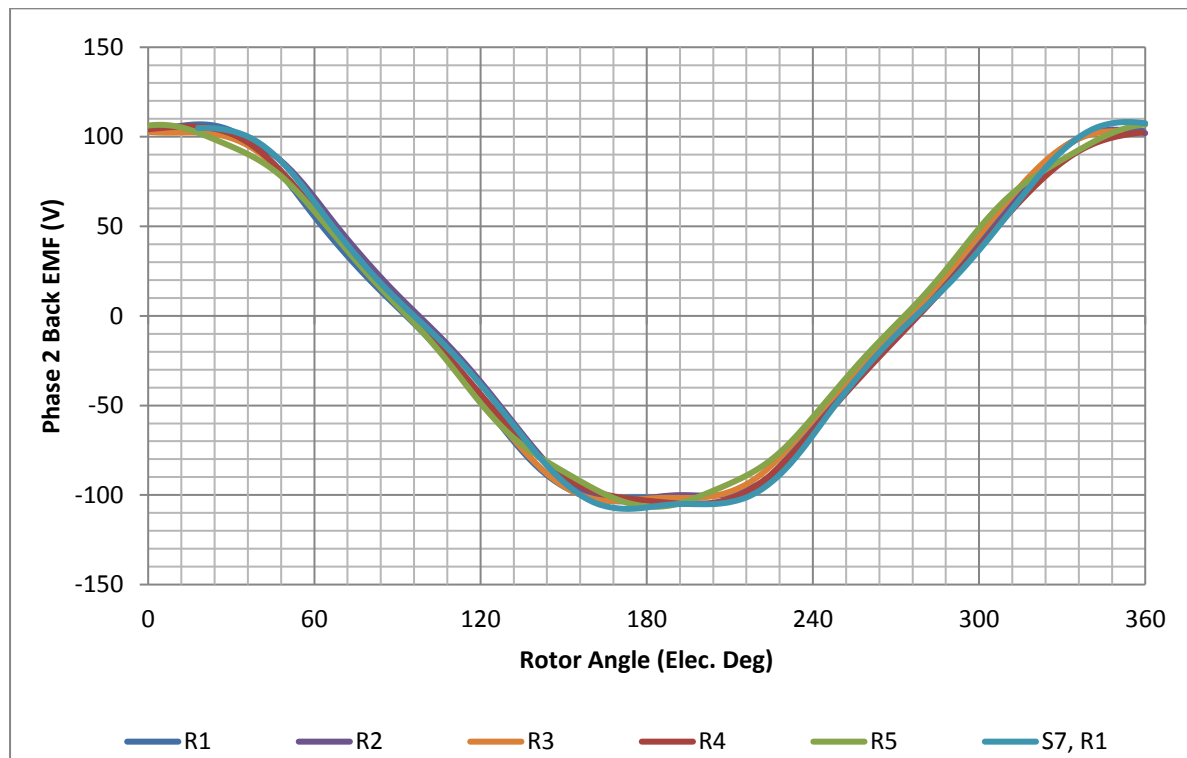


Figure 6. 25: Illustration of back EMF waveforms for S5 with different rotors

Table 6.13 shows that S7 provides the highest fundamental harmonic followed by S5R3. These prove the concept that weakening the inner phase to reduce the mutual coupling increases the back EMF however the 5th harmonic for these two motors are in the high. R4 and R5 reduce the fundamental harmonic by 1.5% however the harmonic content in these are comparatively low making it a good option. It was also seen from Table 6.6 that S5R4 and S5R5 produce the lowest cogging torque and its harmonic content are low relative to the other stator rotor combinations. It can hence be concluded that S5 combined with R4 or R5 provide the best compromise between the cogging torques and back EMF.

Table 6. 13: Harmonic content of back EMF waveform for S5 with various rotors and S7 with R1

Motor Types	Fundamental Harmonic	5th Harmonic	7th Harmonic
S5R1	108.77	5.25	0.72
S5R2	106.10	6.43	0.67
S5R3	110.13	5.74	0.91
S5R4	106.99	2.92	0.42
S5R5	106.22	0.79	1.67
S7R1	110.80	4.75	0.88

Secondly, S6 was combined with the various rotor types and tested for back EMF, waveforms are shown in Figure 6.26 whereas the harmonic contents of these are charted in Table 6.14.

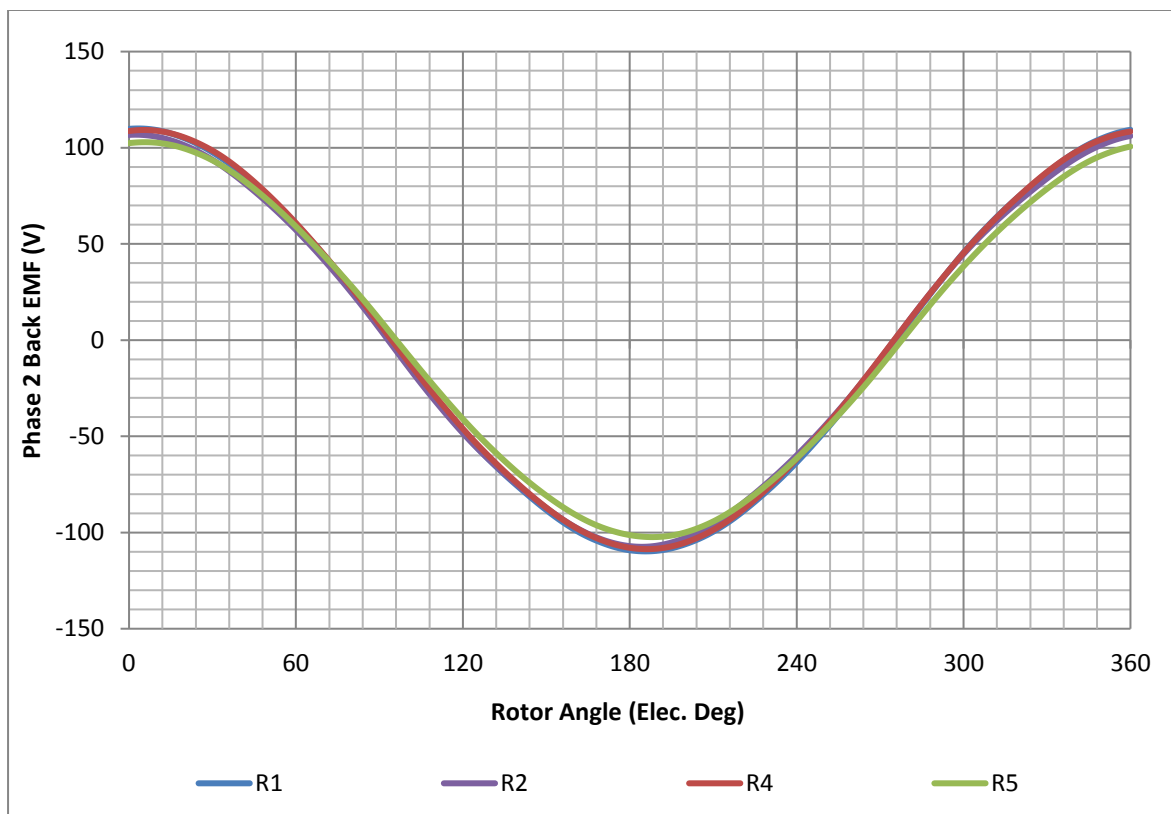


Figure 6. 26: Variations in Back EMF waveforms for S6 and four rotors

S6 combined with the R1 produces the highest back EMF while its 5th and 7th harmonics are reasonable. Combining S6 with R4 produce a very similar back EMF fundamental harmonic however the 5th and 7th harmonic content are much smaller, giving a smoother curve. Table 6.6

also showed that S6 combined with R4 deliver the best solution for cogging torque and table 6.14 backs up this motor choice further as it also has the lowest back EMF harmonic content.

Table 6. 14: Harmonic content of back EMF waveform for S6 and four rotors

Motor Type with S6	Fundamental Harmonic	5th Harmonic	7th Harmonic
S6R1	109.12	0.78	0.22
S6R2	105.76	1.07	0.20
S6R4	108.35	0.32	0.18
S6R5	101.68	0.50	0.13

6.3.3. Back EMF Summary

The mean back EMF of all the motors tested are summarised in Figure 6.27; all these are displayed as per unit of the base motor (S1R1). It can be seen that the lowest back EMF produced is by S2R5, a 9% drop while the highest back EMF is produced by S4R1, an increase of 3% compared to S1R1. S4R1 however nearly doubles the 7th harmonic when compared to the base motor as seen from Figure 6.29. A general observation can be made; modifying the rotors decrease the back EMF production while the basic rotor R1 provides a better EMF.

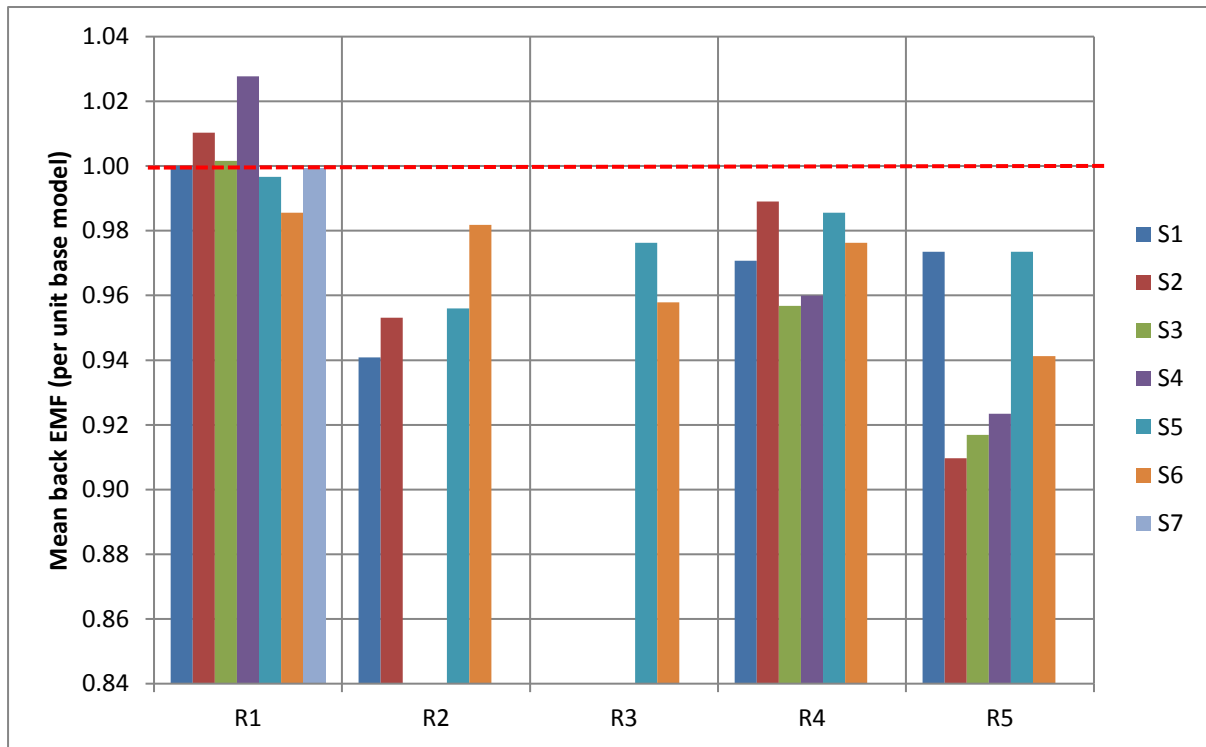


Figure 6. 27: Comparison of mean back EMF per unit of base model for all the motors tested

Table 6.15 shows the measured and FE results to be the same in most cases and approves the manufacturing, assembling and testing techniques.

Table 6. 15: Comparison of mean back EMF measured results with FE in brackets, all number per unit of base model (S1R1)

	S1	S2	S3	S4	S5	S6	S7
R1	1.00 (1.00)	1.01 (1.00)	1.00 (1.00)	1.03 (1.02)	1.00 (0.99)	0.99 (0.99)	1.00 (1.01)
R2	0.94 (0.94)	0.95 (0.95)			0.96 (0.96)	0.98 (0.98)	
R3					0.98 (0.97)	0.96 (0.96)	
R4	0.97 (0.96)	0.99 (0.97)	0.96 (0.97)	0.96 (0.96)	0.99 (0.99)	0.98 (0.98)	
R5	0.97 (0.97)	0.91 (0.93)	0.92 (0.92)	0.92 (0.93)	0.97 (0.97)	0.94 (0.94)	

Figure 6.28 shows S2 and S5 produce a relatively high 5th harmonic as compared to the S1R1. S3, S4 and S6 are a better choice as the 5th harmonic is generally low in these. It is also observed that R5 causes 5th harmonic to decrease while R1, R2 and R3 increases this unwanted harmonic.

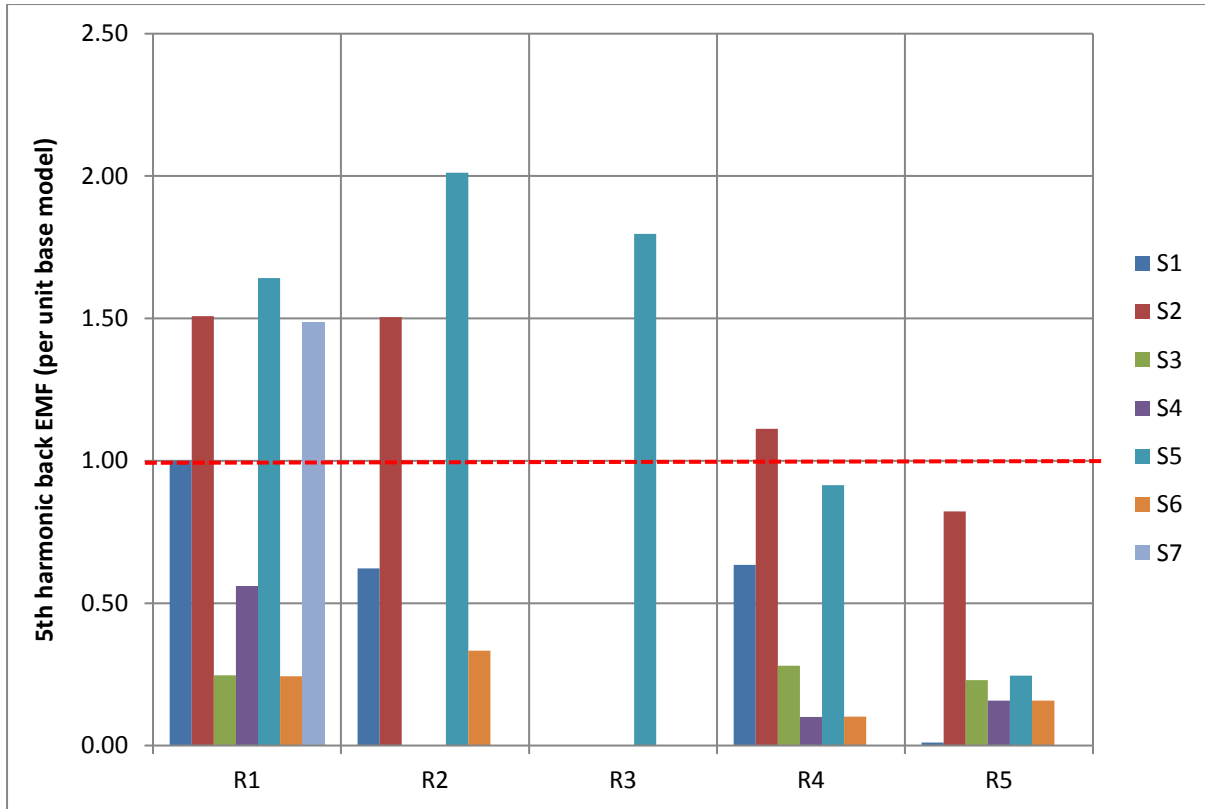


Figure 6. 28: Comparison of 5th harmonic of mean back EMF per unit of base model for all the motors tested

Similar trend is seen from Figure 6.29 where the 7th harmonic is presented for all machines type. Machines comprised of R5 generally have a high 7th harmonic while R2 and R4 diminishes the 7th harmonic.

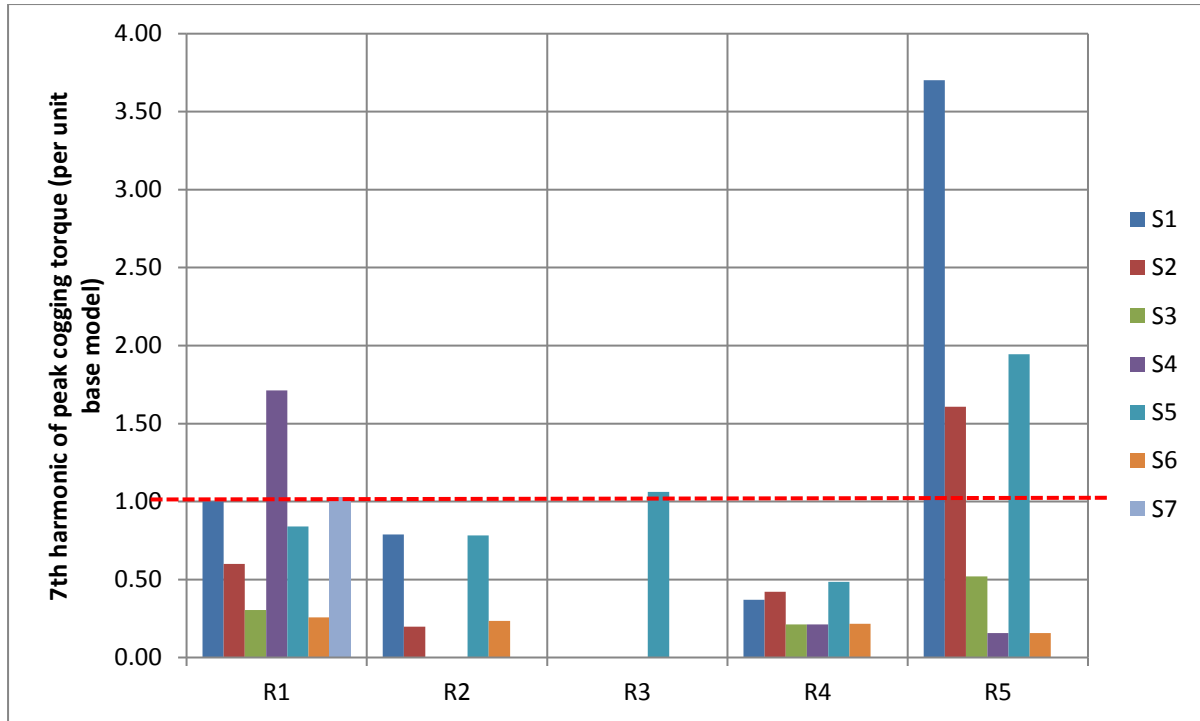


Figure 6. 29: Comparison of 7th harmonic of mean back EMF per unit of base model for all the motors tested

It can be concluded that the best solution for back EMF is provided by the motor made of S6 and R4, generating 98% of the mean back EMF while its 5th and 7th harmonic are 10% and 22% of the base motor, respectively. This is the same motor that reduced the cogging torque by 90% as seen in Table 6.8.

7. Performance measurements

This chapter presents the performance measurements (torque speed envelopes and efficiency) of the motors tested in Chapter 6. The drive setup used to carry out these tests was presented in Figure 6.12.

Performance in terms of torque-speed capability and efficiency is accessed here.

7.1. Torque Speed Envelope

This section will focus on the torque-speed characteristics for the full set of machines. All tests were carried out up to 350rpm and at a fixed voltage of 48V.

7.1.1: Laminate Stators

Figures 7.1 and 7.2 present the Torque-Speed curves for the two laminated stators that offer the lowest cogging torque and cleanest back EMF while Table 7.1 shows the maximum Torque achieved by each motor. These two stators were tested with rotors R1, R2 and R3.

S3 in conjunction with R1 provides 40.4Nm of peak torque while S4 combined with R1 outputs a peak torque of 47.18 Nm; a 17% increase.

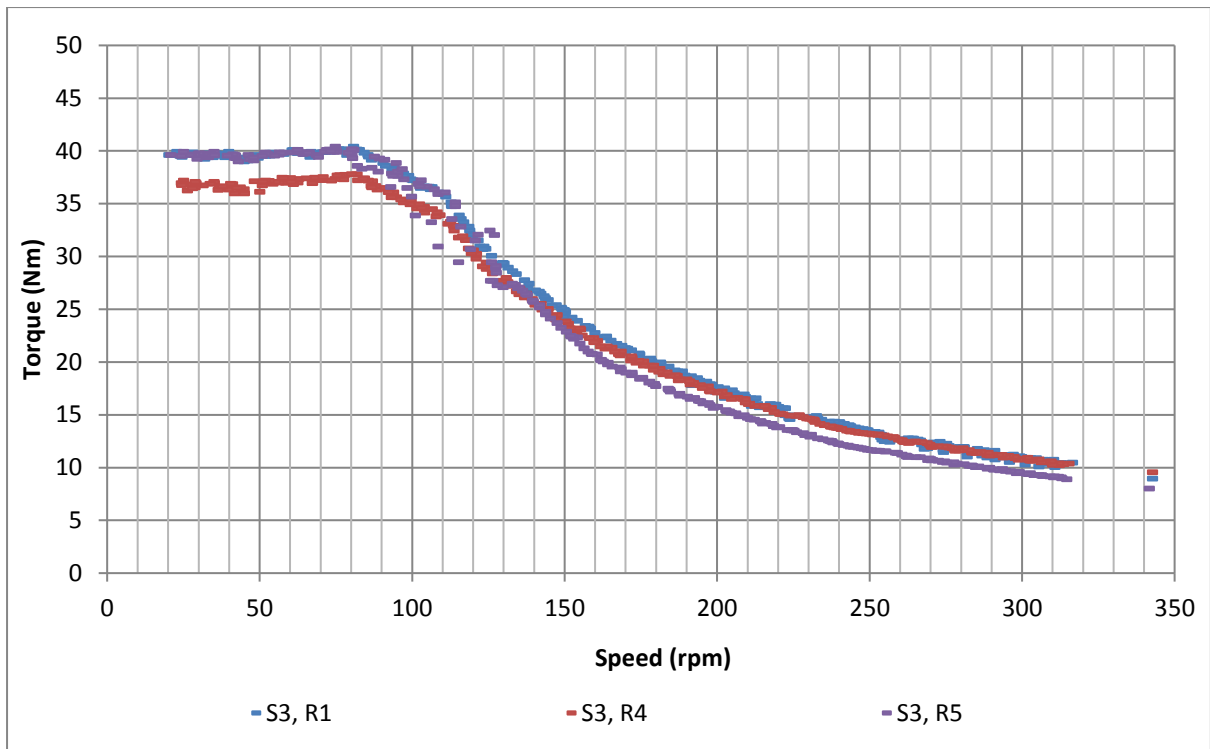


Figure 7. 1: Illustration of Torque Speed envelope for S3 with R1, R4 and R5

R4 and R5 combined with S3 and S4 reduces the peak torque produced by these motors as seen from table 7.1. S4 produces the most torque for all motors of laminated family while the lowest torque output is through using S2.

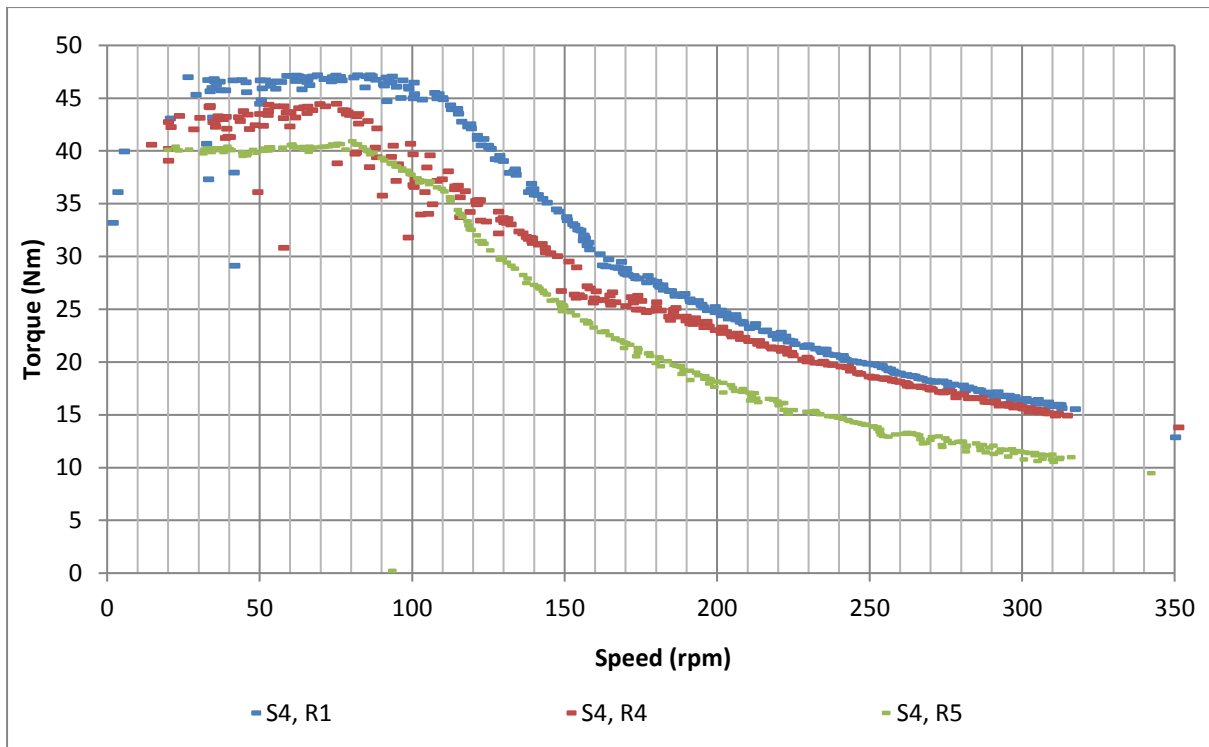


Figure 7. 2: Illustration of Torque Speed envelope for S4 with R1, R4 and R5

At present, the Höganäs e-bike motor is capable of producing a maximum of 50Nm torque under best conditions however the cogging torque is generally high at this point. These laminated family stators produce much lower torque than 50 Nm. The base motor (S1R1) used in this case study generates 40.42 Nm. Comparing all other motors with this, S2 is the worst stator type in regards to peak torque while S1 and S3 perform in similar range. S4 depicts the best performance as not only is the torque generated greater, the cogging and back EMF performance of this stator was relatively much better (as seen from chapter 6).

Table 7. 1: Peak Torque produced by each laminated motor

Stator/Rotor type	R1	R2	R4	R5
S1	40.42	38.92	38.59	39.17
S2	37.81	35.81	38.63	37.45
S3	40.40	NA	39.10	40.12
S4	47.18	NA	44.50	41.35

7.1.2 SMC Stators

The same Torque Speed envelope was created for the 2nd family of stators; the SMC components, S5, S6 and S7.

S5's torque speed envelope was measured for R1, R2, R4 and R5 while a fifth measurement was done for S7 with R1. These waveforms are presented in Figure 7.3.

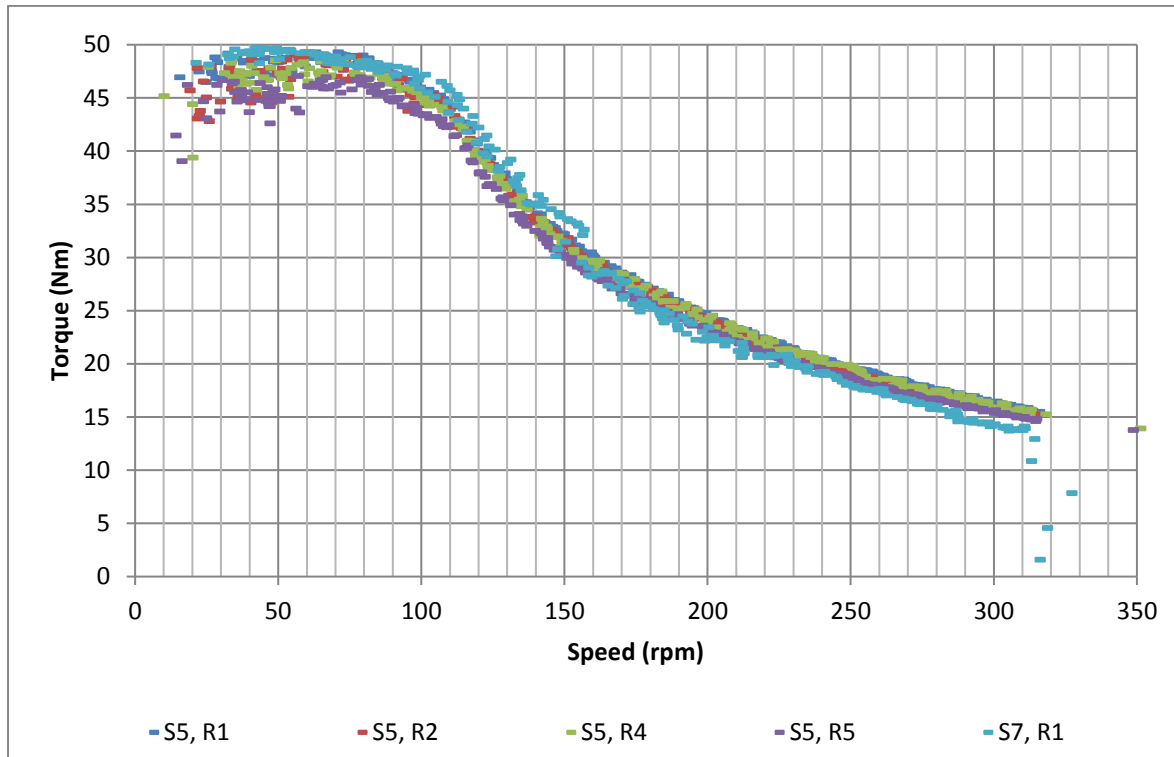


Figure 7. 3: Illustration of Torque speed curves of S5 with different rotors

This stator combined with the rotors mentioned above achieves peak torque of nearly 50 Nm, shown in table 7.2. R1 generates 49.29 Nm while R4 and R5 produce 48.7 Nm and 47.05 Nm respectively. Splitting the rotor (R2) to reduce mutual coupling also output a 49 Nm peak torque whereas increasing the inner phase gap in stator (S7) generates 48.6 Nm. This also shows that the rotor variations have a relatively low effect on the peak torque produced as the values are very similar; S5 proves to be a good option for high torque production due to chamfered teeth structure.

The Torque speed curves for S6 along with the four rotors are presented in Figure 7.4 along with the peak torque in table 7. 2.

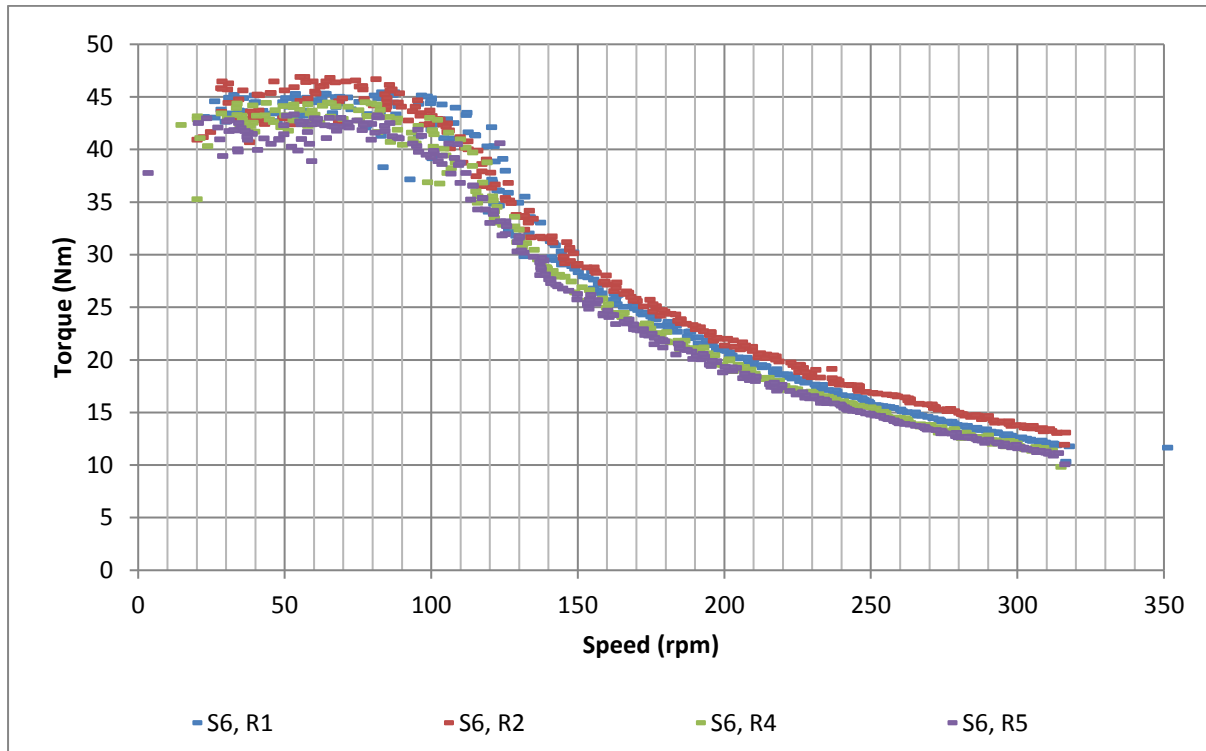


Figure 7. 4: Illustration of back Torque speed waveforms for S6 with different rotors

It was seen from figure 6.12 that using S6 reduces the peak cogging torque by 70% compared to S5. This is due to the reduction of 6th and 12th harmonic by pitching the stator which has a more detrimental effect on cogging than the chamfered teeth of S5. This comes at a price of peak torque reduction of approximately 8% between the two stators as shown in Table 7.2 for all rotor types. This means that pitching the stator for 6th and 12th reduces the peak cogging torque and its harmonics; have a similar back EMF while a small reduction in peak torque is seen compared to the SMC chamfered stator teeth.

Table 7. 2: Peak Torque produced by each SMC motor

Peak Torque (Nm)	R1	R2	R4	R5
S5	49.29	49.03	48.69	47.05
S6	45.45	46.90	44.50	43.34
S7	48.55	NA	NA	NA

7.1.3 Summary

Figure 7.5 shows the chart with a summary of peak torque of all motors per unit of S1R1. The new Höganäs brochure claims to produce motors up to 50Nm peak torque; however the base motor for this study produced 40Nm and all motors are still compared against this.

It can be seen from Figure 7.5 that the stators manufactured from SMC (S5, S6 and S7) tend to achieve higher peak torque. This is because of the isotropic and thermal properties of SMC, and its ability to produce three-dimensional flux paths that are ideal for modulated pole machines. S1 and S2 in conjunction with any of the four rotors produce lower peak torque than S1R1. Similar values are seen for S3 except S3R1 which outputs 18% more torque than the base model.

S5 produces the highest torque however the cogging for this stator was not the lowest as seen from Figure 6.14 to 6.18 nor was the 5th and 7th back EMF harmonics as seen in Figures 6.27 and 6.28. Contrary to this, S6R4 was the optimum motor in terms of lowest peak cogging torque and its harmonic as well lowest back EMF harmonic; it also produces 110% of the peak torque.

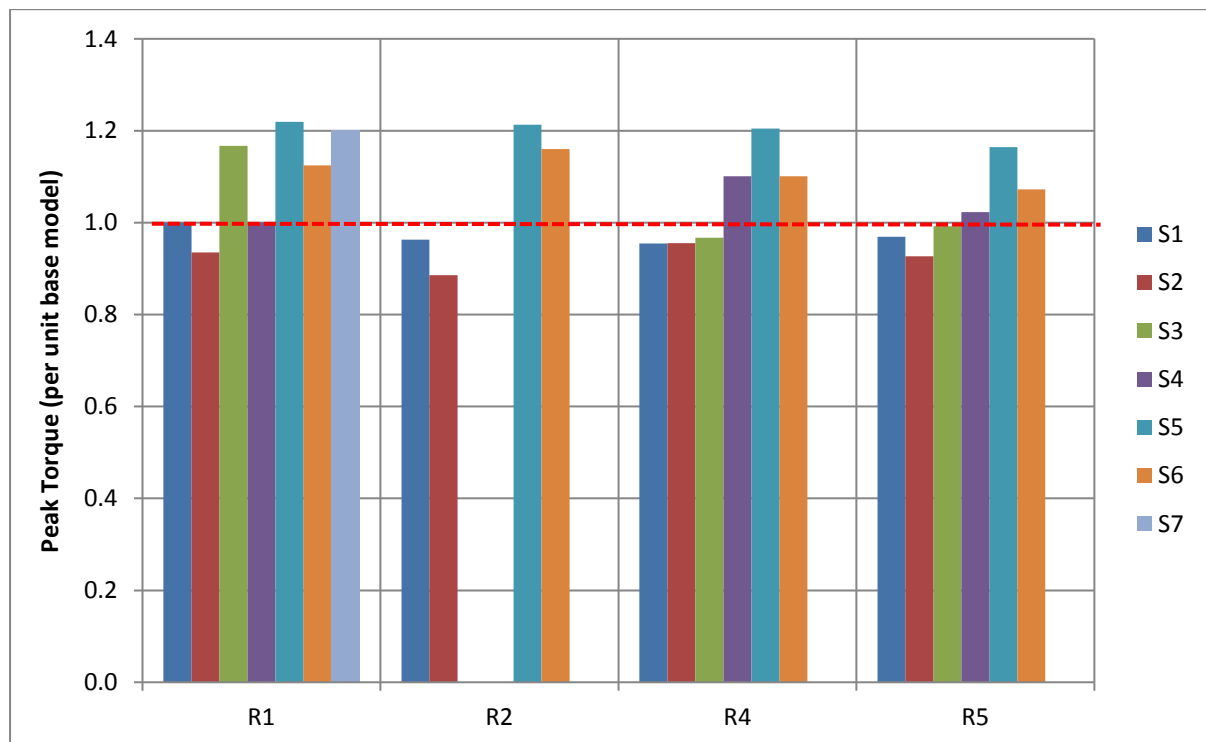


Figure 7. 5: Summary of all motors for Peak torque produced per unit of a 40 Nm motor (S1R1).

The last parameter of interest is the efficiency of the motor and the comparisons are presented in section 7.2.

7.2 Efficiency

To achieve high motor efficiency, careful attention must be paid to all sources of loss in a motor. A motor designer should take advantage of any inherent performance characteristics of different motor geometries to achieve the goal of a high efficiency motor with low material and manufacturing costs.

Motor efficiency is inversely related to the total amount of power losses in the motor. Motor losses are often divided into two major areas: conduction losses and speed-related losses. Conduction losses are the result of the motor drive current flowing in the motor coils with a finite resistance. These losses are related to the motor current squared times the motor resistance (I^2R). All of the conduction losses occur in the stator of a permanent magnet motor. The speed related losses consist of iron losses, hysteresis and eddy currents in the motor components, frictional losses from the bearings, and windage. Iron losses can occur in both the stator and the rotor of the motor. Frictional losses are all related to the rotor of the motor.

A last category of losses is other losses that depend both on torque and speed and especially occur in the extremes of motor operation. These losses are generally related to magnetic nonlinearities which increase harmonics, hysteresis and eddy current losses at a rate that is faster than predicted by normal operating conditions. Conduction losses generally dominate the efficiency performance of a motor when the motor is operated at lower speeds. Iron losses generally set the efficiency performance at high speeds. To achieve a broad flat efficiency curve, both conduction and iron losses must be addressed and kept at a low value. Motor losses are summarized in Table 7.3 below.

Table 7. 3: Motor Loss Summary [137]

Conduction losses – torque-related losses	Stator
Coil I^2R losses	
Speed losses – speed-related losses	
Iron losses – hysteresis and eddy currents	stator and rotor
Frictional losses – bearings and windage	
Other – torque and speed related	
Excess losses – hysteresis and eddy currents	stator and rotor

Efficiency of the motors in this thesis is compared against the base motor in this section, figure 7.9 presents the summary of efficiency percentages for all motors tested at 200 rpm. The test bench in section 6.12 was used for efficiency torque measurements too.

7.2.1 Laminated Stators

Figure 7.6 presents the efficiency torque waveforms for S3 and S4 combined with R1, R4 and R5. S3 has the highest efficiency with R1; of 82% at 8Nm whereas S4's highest efficiency is achieved with R4, of 86% at 9Nm. R3 and R4 combined with S3 tend to have a lower efficiency compared to when these rotors are used with S4. This shows that pitching the stator produces higher efficient motors compared to using combinations of tooth spans. This is because it is not possible to add the effect of two teeth with different spans for the points at which teeth of two differing spans intersect as was shown in Figure 4.15.

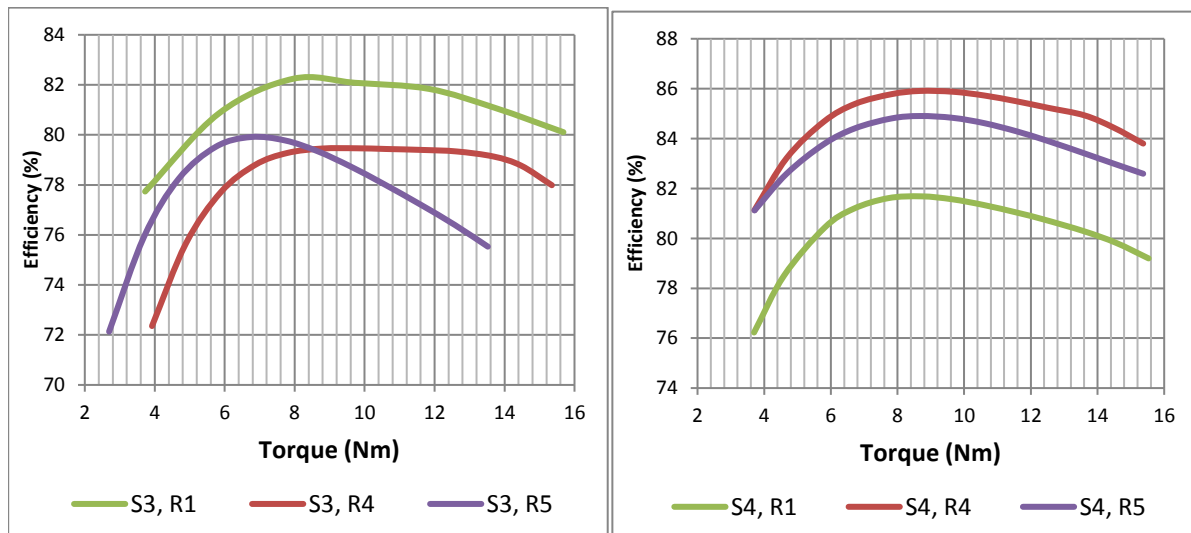


Figure 7. 6: Efficiency vs. Torque waveforms of S3 (left) and S4 (right) with R1, R4 and R5

7.2.2 SMC Stators

The same measurements were done for the SMC manufactured stators with same set of rotors. Efficiency curves for S5 and S7 are presented in Figure 7.7 while S6 is shown in 7.8.

It can be seen that the efficiency of these stators are higher than the laminated stators, an increase of 6% is seen on average. The peaks of these motors are also towards the 8 Nm marks which is similar to the laminated stators.

There is a very little difference between S5 and S6 in terms of peak efficiency achieved. S7 attain the highest efficiency of around 87% while motors with R4 and R5 have efficiencies in the range of 86% which is very good for this motor type.

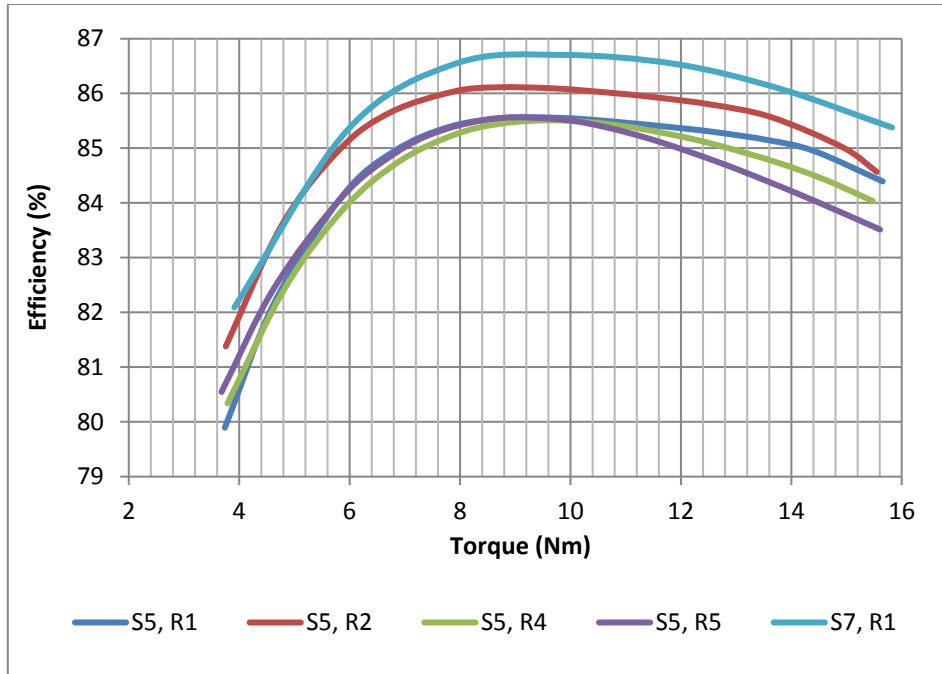


Figure 7. 7: Efficiency vs. Torque curves for S5 with R1, R2, R3, R4 and S7 with R1

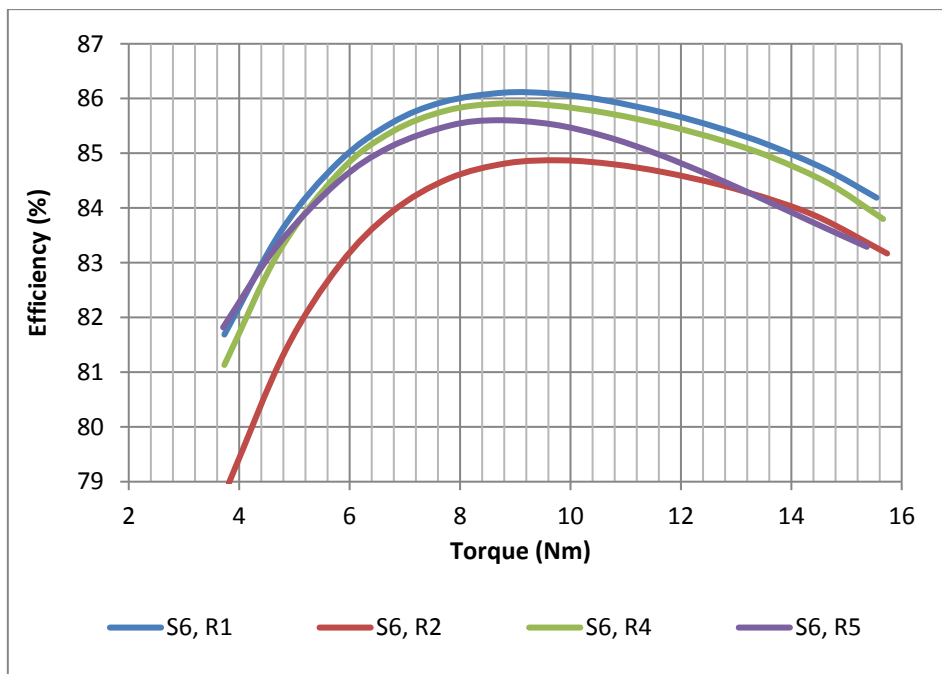


Figure 7. 8: Efficiency vs. Torque curves for S6 with with R1, R2, R3 and R4

7.2.3 Summary – Efficiency vs. Torque

The base motor in this study has an efficiency of 79%, one of the lowest. One of the highest efficiencies achieved is 86% by the motor made of S6R4. The laminated stators (S1 to S4) are generally 80% efficient while R4 and R5 increase the efficiency by 4 to 5% for S4.

It can be concluded that the efficiency is not affected greatly by the choice of rotors rather the choice of stator and material are more significant; SMC stators are more efficient as shown by figure 7.9.

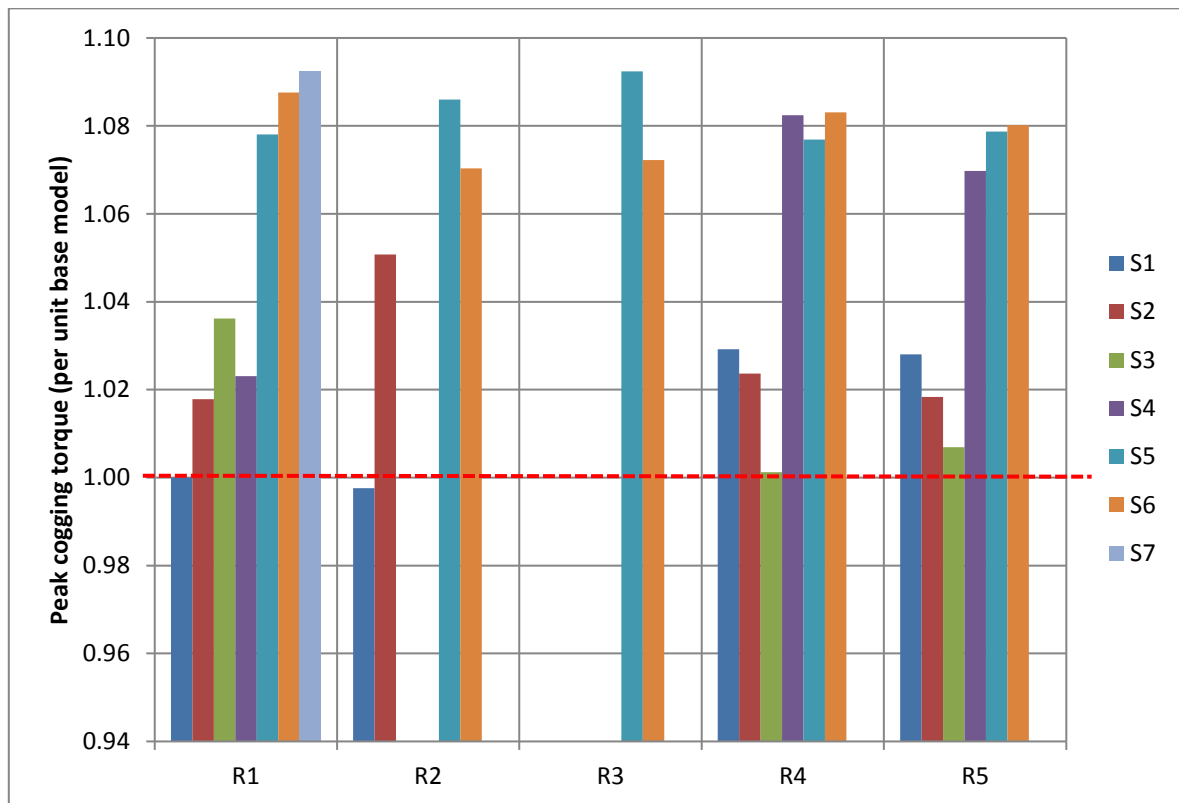


Figure 7. 9: Summary of efficiency of all motors in the study

This is due to the fact that SMC give stators isotropic and thermal properties, and ability to produce three-dimensional flux paths that are ideal for modulated pole machines. These also have a lower permeability than laminated steels mainly due to the compaction process; the non-magnetic gaps created between the adjacent iron powders that make up the composite and help in achieving higher efficiencies than laminated stators.

7.3. Conclusion

Back EMF and torque are the two major aspects for evaluating machine performance. The back EMF is highly associated with the permanent magnet performance and the relationship between the applied voltage and rotating speed. On the other hand, torque dominates the relation between the generated torque and applied current.

Hysteresis losses are directly related to frequency, and eddy current losses are proportional to frequency squared, it is important to minimize higher frequency content in the motor to achieve low losses and high efficiency [137]. Therefore, it becomes obvious that a high efficiency motor would minimize harmonic content as much as possible ultimately reducing cogging torque.

The initial study showed that the base motor design (S1R1) had high cogging torque and significant harmonic content present in the back EMF. These caused the motor's performance to be affected, causing the efficiency and peak torque to be relatively lower than expected.

Changing and combining the stator tooth span, pitching the teeth, chamfering the stator teeth, modifying the rotor pole piece shapes and weakening the inner phase were techniques tested in this chapter. It was shown that these techniques work well for some harmonics while others are worsened. For example a combination of tooth spans works well to reduce the cogging torque, however introduces high 5th harmonic in the back EMF. Similarly, using chamfered stator teeth provides high percentage efficiency and peak torque, however the 2nd and 4th harmonics in cogging torque are aggravated.

Table 7.4 presents the results for all 25 motors manufactured, assembled and tested in this project. All motors are compared against the base model (S1R1).

Table 7. 4: Measured results for all motors tested in this thesis compared against the base motor (S1R1)

COGGING TORQUE	R1	R2	R3	R4	R5
S1	1.00	0.84	-	0.67	0.45
S2	0.58	0.56	-	0.35	0.39
S3	0.25	-	-	0.23	0.28
S4	0.24	-	-	0.21	0.28
S5	0.56	0.33	0.49	0.27	0.44
S6	0.14	0.19	0.35	0.10	0.18
S7	0.34	-	-	-	-
BACK EMF	R1	R2	R3	R4	R5
S1	1.00	0.94	-	0.97	0.97
S2	1.01	0.95	-	0.99	0.91
S3	1.00	-	-	0.96	0.92
S4	1.03	-	-	0.96	0.92
S5	1.00	0.96	0.98	0.99	0.97
S6	0.99	0.98	0.96	0.98	0.94
S7	1.00	-	-	-	-
PEAK EFFICIENCY	R1	R2	R3	R4	R5
S1	1.00	1.00	-	1.03	1.03
S2	1.02	1.05	-	1.02	1.02
S3	1.04	-	-	1.00	1.01
S4	1.02	-	-	1.08	1.07
S5	1.08	1.09	1.09	1.08	1.08
S6	1.09	1.07	1.07	1.08	1.08
S7	1.09	-	-	-	-
PEAK TORQUE	R1	R2	R3	R4	R5
S1	1.00	0.96	-	0.95	0.97
S2	0.94	0.89	-	0.96	0.93
S3	1.17	-	-	0.97	0.99
S4	1.00	-	-	1.10	1.02
S5	1.22	1.21	1.05	1.20	1.16
S6	1.12	1.16	1.04	1.10	1.07
S7	1.20	-	-	-	-

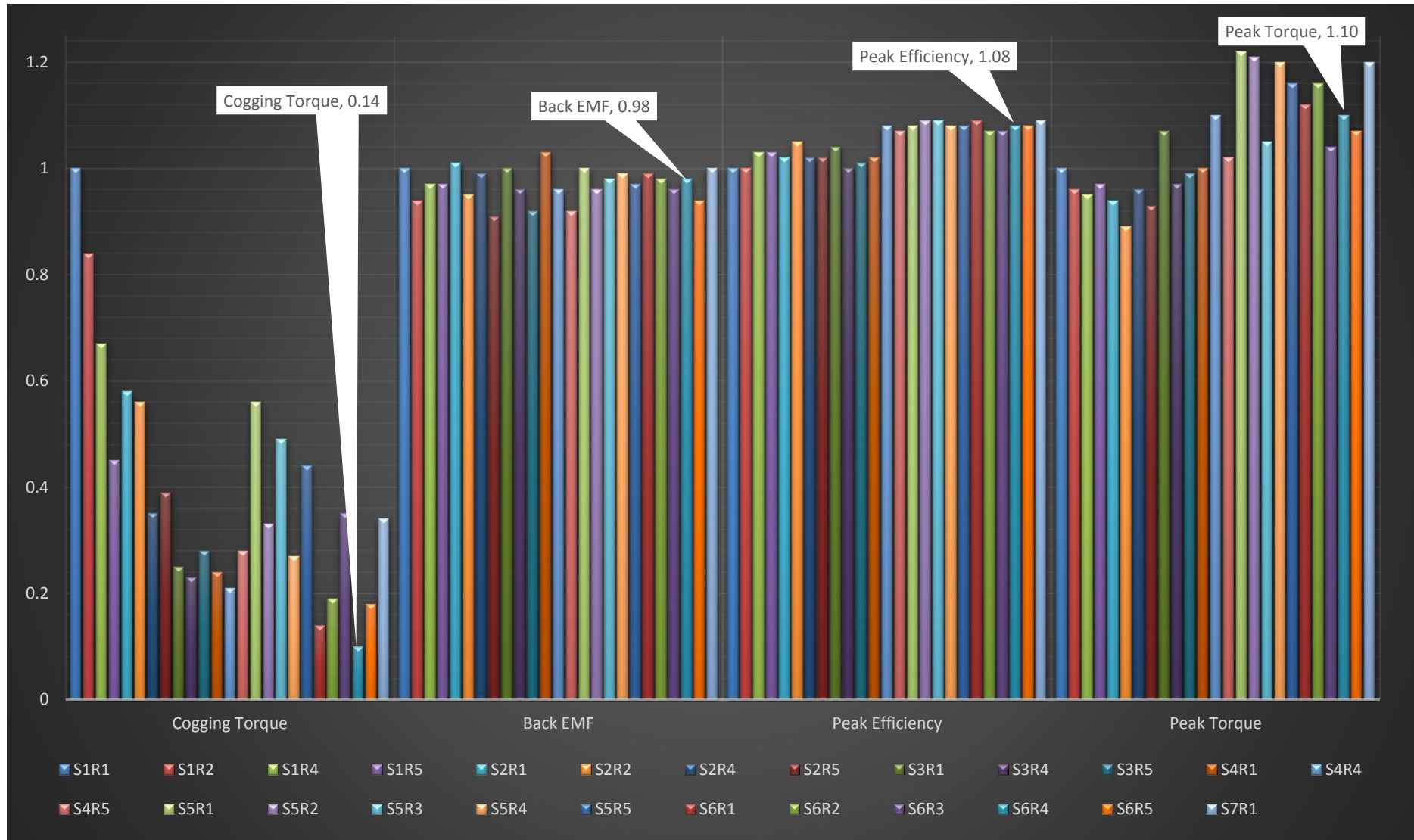


Figure 7. 10: Measured results for all motors tested in this thesis compared against the base motor (S1R1)

It was seen that techniques where pitching was introduced in the stator teeth (S3, S4 or S6) and rotors with modified pole pieces (R4 and R5) reduces the cogging torque the most, while maintains a high back EMF, peak efficiency and peak torque.

According to table 7.3, the most optimised motor is the S6R4; cogging torque is reduced by 90%, back EMF is 98% of the base motor, efficiency has increased by 8% and there is an increase of 10% in peak torque. Table 7.4 sums up the interesting comparisons between the cogging torque, back EMF, peak efficiency and peak torque for the base design motor and the chosen optimised motor.

Table 7. 5: Comparison of base design with the most optimised motor, consisting of SMC 6th and 12th pitched stator and convex pole shaped rotor pole pieces; percentage difference between the important parameters shown (2 d.p)

	Base motor (S1R1)	SMC 6th & 12 pitched stator with convex rotor (S6R4)	Percentage Difference
Peak Cogging Torque	1.76	0.18	-89.88
2nd harmonic	0.23	0.07	-72.22
4th harmonic	0.18	0.04	-77.71
6th harmonic	1.46	0.03	-98.28
12th harmonic	0.20	0.00	-98.99
Peak Back EMF	108.27	105.70	-2.37
5th Harmonic back EMF	3.20	0.33	-89.69
7th Harmonic back EMF	0.86	0.19	-77.91
Peak Efficiency	79.37	85.96	8.30
Peak Torque	40.42	44.50	+10.094

Results shown in table 7.4 depict a 90% reduction in peak cogging torque with the vital 6th and 12th harmonics nearly reduced to zero. There is a minor 2% reduction in mean back EMF however the major reductions in 5th and 7th harmonics are crucial and can compensate the effect of this 2% reduction. Lastly the peak efficiency and peak torque are improved for the optimised motor, with an increase of 8% and 10% respectively.

8. Combined Phase MPM

A combined phase modulated pole machine (CPMPM) design was introduced previously [117] where it was shown that this design provided greater torque density within a given volume as compared to the separate phase machine (SPMPM).

8.1 Combined Phase vs. Separate Phase MPM

The CPMPM and SPMPM have the same outer and inner diameters, axial length and core-back depth, identical pole numbers and coils and all material used are the same. The difference between the two designs (shown in Figure 8.1) is that the inside teeth of the separate-phase topology have been combined into sets; Teeth 1' and 2 combine to form tooth 2 of the combined-phase topology, and likewise separate-phase tooth 2' and 3 to form combined-phase

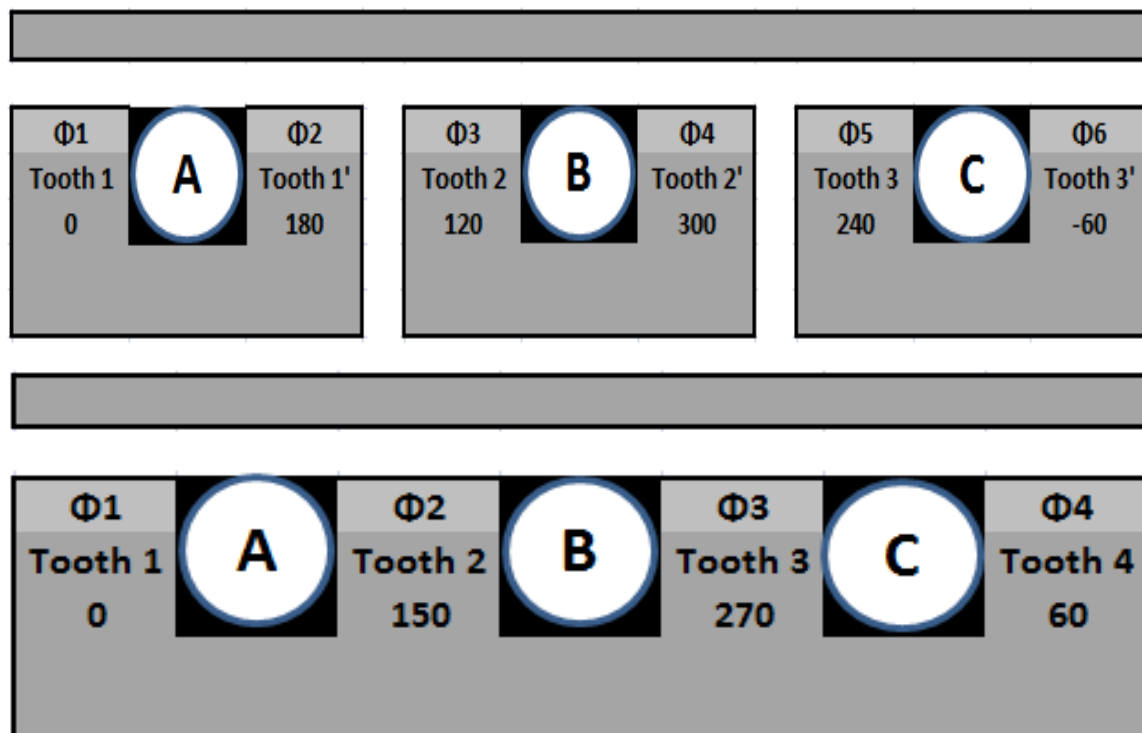


Figure 8. 1: Axial view of a separate phase MPM (top) and a combined phase MPM (bottom)

tooth 3. Hence, there are now four rather than six sets of stator teeth. Note the three coils and rotor are identical in both cases.

The method of ensuring the angular and axial locations of the four rings of stator teeth in the combined phase topology is explained in detail in [84, 106]. It was determined that if tooth 1 and tooth 4 are 1 unit long in the axial direction, tooth 2 and tooth 3 must be $\sqrt{3}$ units long. The angular position of the tooth must be 0° , 150° , 270° and 60° for teeth 1, 2, 3 and 4 respectively. Experimentation confirmed the improved performance of the combined phase machine, with a 10.3% increase in fundamental back EMF (corresponding to a 8.6% increase in RMS back EMF), a 15.0% increase in the average excitation torque, and 10.4% higher torque density when compared to the separate-phase machine [21].

In addition to the improved electromagnetic performance, the combined-phase machine offers a reduction in stator SMC components from six to four. This is clearly of benefit for commercial production, with fewer components and greater mechanical integrity of the stator.

Continuing the interest in reducing harmonic content and cogging torque of the combined-phase machine, this section aims to reduce this cogging torque without changing the machine size or the phase arrangements described. The method (of varying and combining tooth spans) applied earlier to the separate machine are now applied to the combined phase machine. The comparison of two topologies under the influence of tooth spans is investigated; results for static torque and back EMF are presented with conclusions in the following sections.

8.2 Induced back EMF

The differential of the flux waveforms yields the back EMF, shown in Figure 8.2. At 285 r/min, the rms phase back EMFs for the CP and SP machines are 28.8 and 25.8 mV per pole per turn respectively, an increase of 11.6% for the CP machines. This reflects the fact that there is some harmonic content in each of the waveforms. It is seen from Figure 8.3 that there is an increase in fundamental harmonic for CP machine when compared with SP machine.

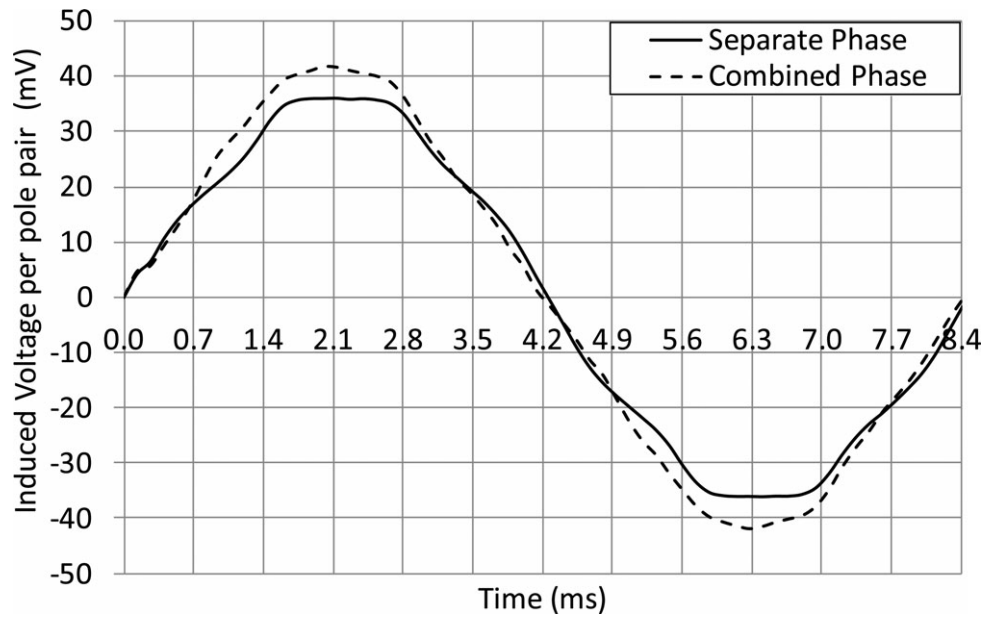


Figure 8. 2: Three dimensional FE comparison of the induced back EMF in one coil of the SP and CP machines

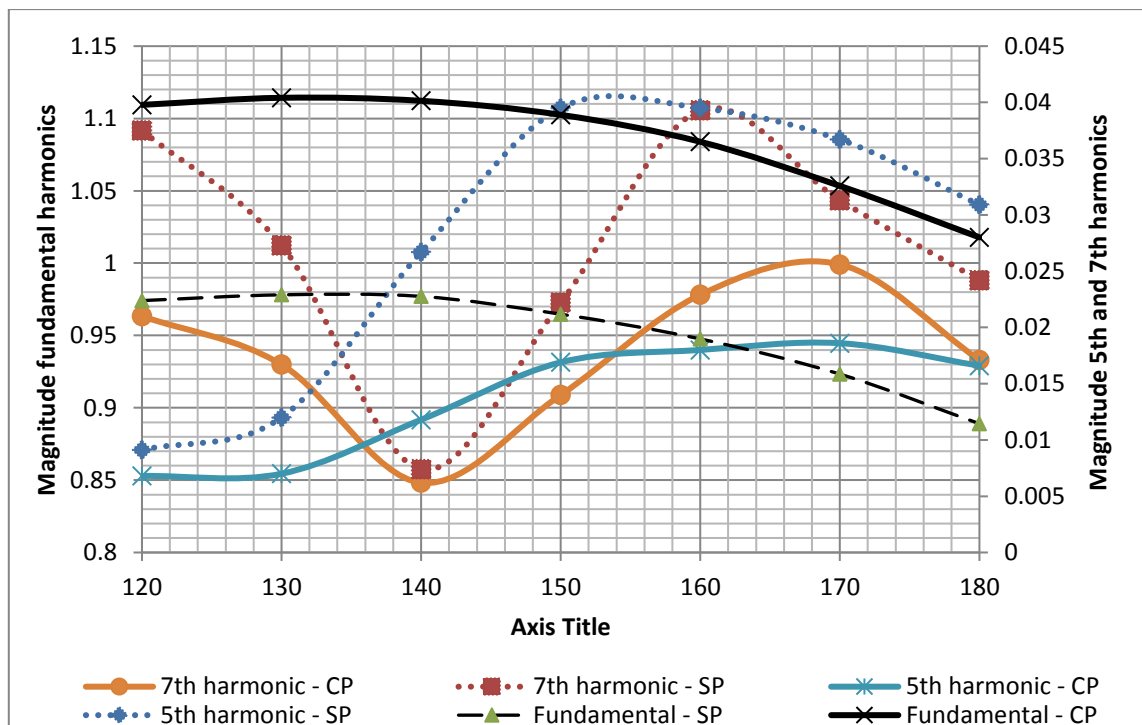


Figure 8. 3: Harmonic content of back EMF waveform with tooth span for SP and CP topologies.

The harmonic content of back EMF for a variety of tooth spans is shown in figure 8.3. It can be seen that as the tooth span changes, the harmonic magnitude is cyclic with clear minima and maxima. A 140° span coincides with the minima for the 7th harmonic while its 5th harmonic is also comparable to others and appears to be the optimal tooth width to choose with regarding keeping the harmonics in the inner phase voltage low.

Similar to SP topology, EMF induced by the central phase in CP differs from that for the outer two phases, as end leakage flux is not present here. The harmonic content of the inner and outer coil EMF was calculated and is shown in figure 8.4. It is evident that the inner coil possesses a greater 7th harmonic when compared to that for the outer coils. As with SP, tooth span alterations are investigated as a method of balancing the harmonic content of all three phases.

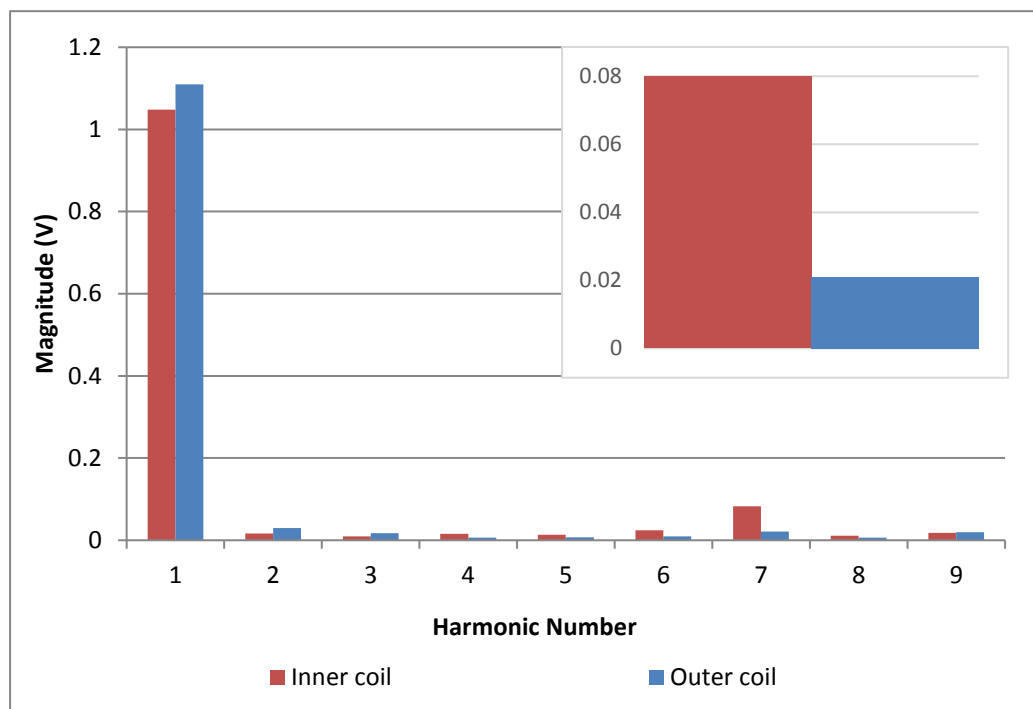


Figure 8. 4: Harmonic contents of inner and outer coils EMF (7th harmonic zoomed in)

The variation in flux linkage for the outermost phase of the SP and CP machines is shown in Figure 8.5. This was obtained by performing a series of magnetostatic simulations with the rotor stepping through a full electrical cycle. It can be seen that there is an increase of 10.7% for CP machine when compared with SP. This is because of the additional flux obtained by using a rotor that extends the full length of the stator. The additional magnet flux is provided by the magnets directly above the gap separating the phases and also some mutual fluxes due to the proximity of phases to each other.

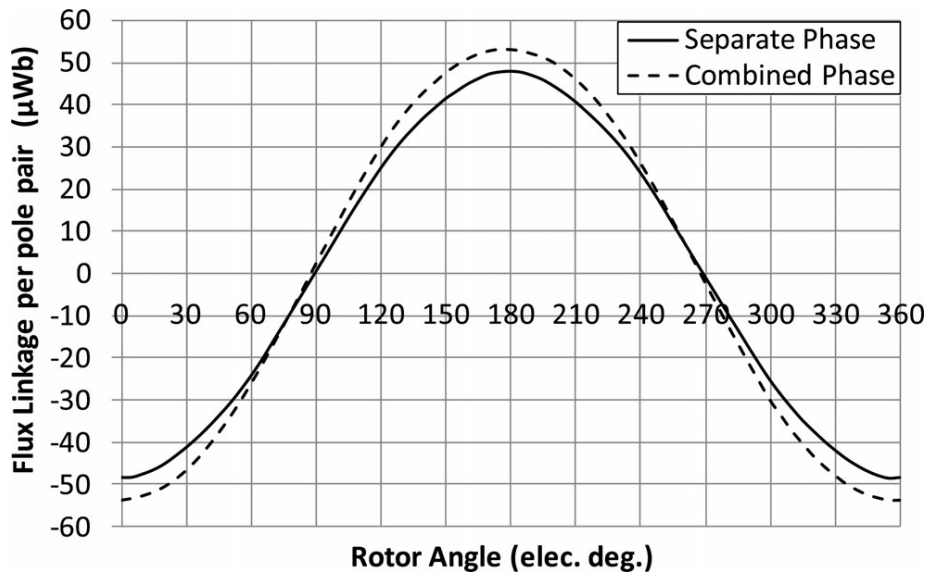


Figure 8. 5: Three dimensional FE no-load flux linkage for phase A of the SP and CP machines

8.3 Cogging Torque

Static torque characteristics of CP was simulated and compared with SP machines. Figure 8.6 shows the cogging torque (non-energised coils) for the same range of tooth spans in Figure 8.3. It can be seen that the minimal cogging occurs for tooth span of 160° , a position where the EMF harmonic content is not ideal. It also shows the change in magnitude of the important 2nd and 4th harmonics of cogging. The peak cogging torque of the base design with 120° span was found to be 5.05Nm. A trend was observed; as the tooth span increased towards 160° , the cogging torque decreased by 78% to 1.1Nm at a tooth span of 160° .

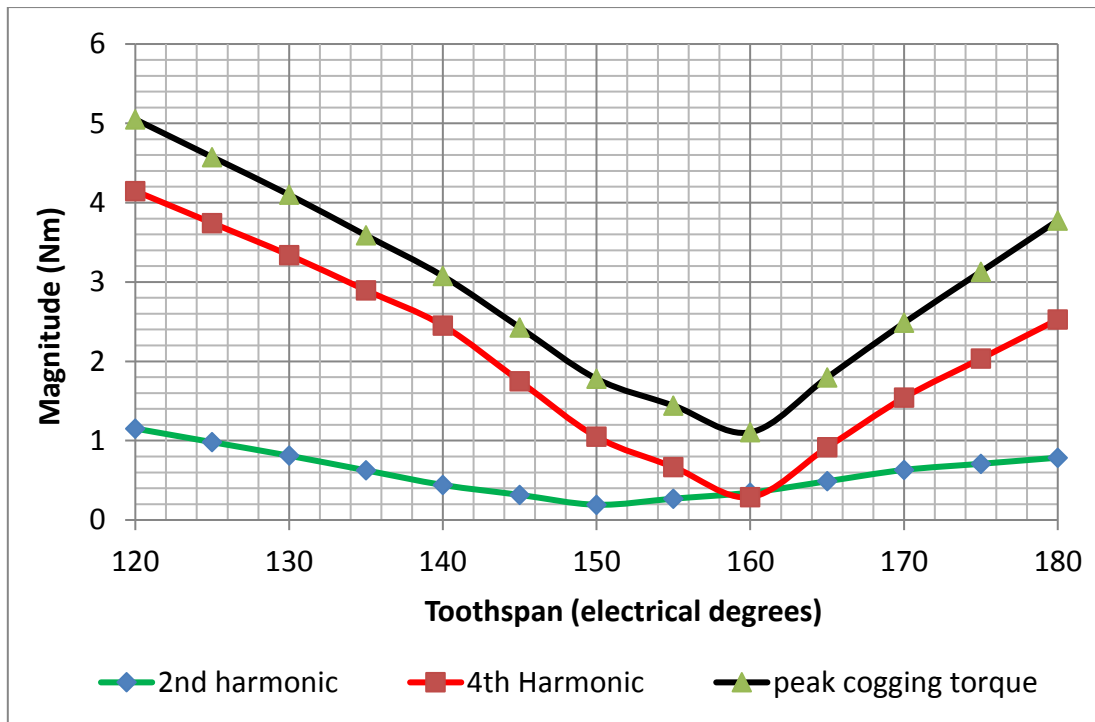


Figure 8. 6: Magnitude of cogging torque harmonics in the three-phase MPM with varying tooth span

A comparison of two topologies for peak cogging torque with varying tooth spans is shown in Figure 8.8. CP has the lowest cogging torque at 160° while SP is at 170° . For a tooth span of 165° , CP has 1.8Nm of peak cogging torque compared to 0.6Nm for SP; an increase of 300%.

Technique of combining the tooth spans was applied to see if the cogging torque can be reduced as it was for SP topology.

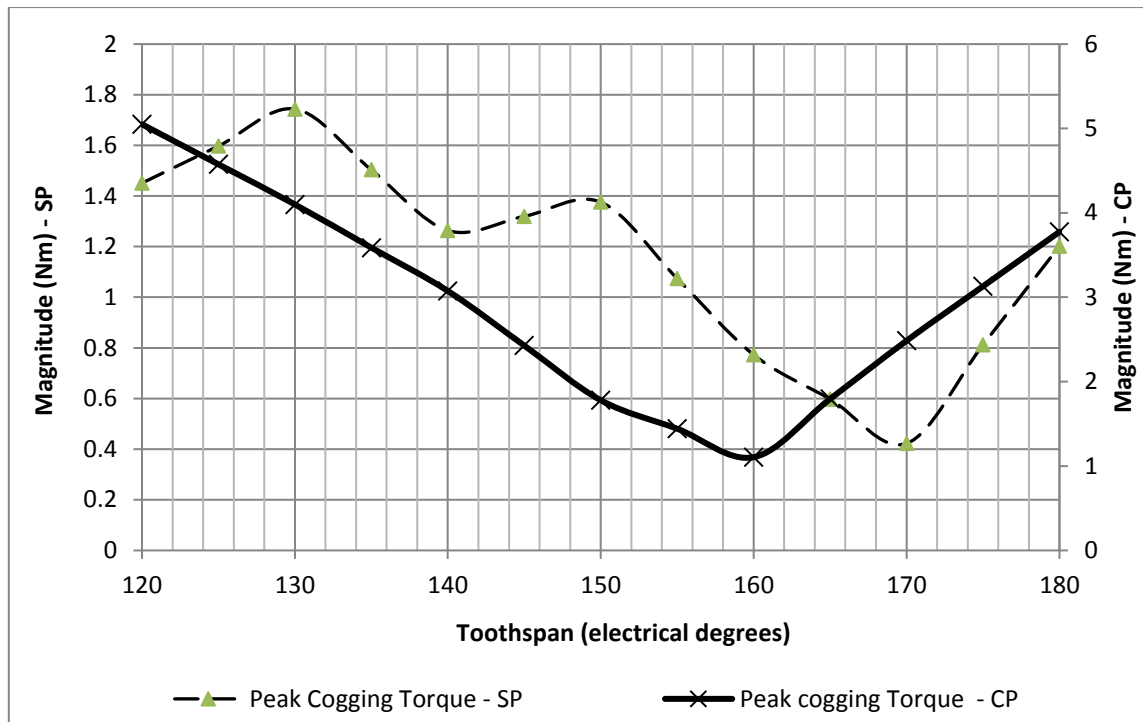


Figure 8. 7: Comparison of peak cogging torque for SP and CP topologies

8.4 Torque Ripple

A sinusoidal current with a peak value of 14.14rms was applied to the three phase machine over the range of tooth spans (120° to 180°). Torque ripple for each tooth span is shown in Figure 8.8 along with torque ripple of SP topology superimposed for comparison.

It is evident that CP topology produced a much higher torque ripple for a given tooth span compared to SP topology. For example, CP topology nearly doubles the ripple compared with SP topology for the tooth span of 130° .

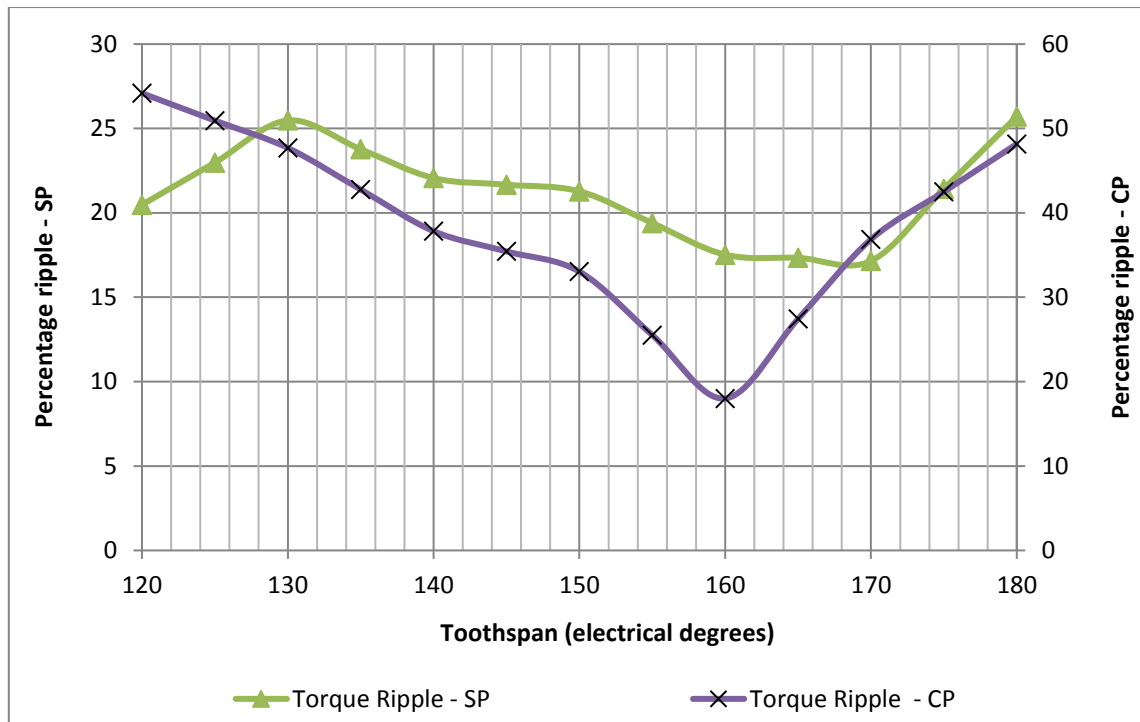


Figure 8. 8: Comparison of torque ripple for SP and CP topologies

It is seen that the a span of 160° gives the lowest torque ripple which matches to the position of lowest cogging torque found earlier (Figure 8.7). The torque ripple is reduced significantly from 54% of the average torque for 120° down to 18% for 160° ; the average torque drops by 4% as would be expected due to the drop in the fundamental component of back EMF that was seen in Figure 8.4.

8.5 Combination of tooth spans

It was proposed that the technique of combining the tooth spans can be applied to CP topology too in order to reduce EMF harmonics and cogging torque. As before, there is a possibility that the negatives of each tooth span can be used to cancel out the drawbacks in each other.

In depth study was carried out to see if this technique worked equally as well as it did in SP topology. It was seen that 120° degree span's inner phase voltage has a seventh harmonic that is in anti-phase with the 180° degree span's seventh harmonic. The two waveforms of 120° and 180° are summed as they are in anti-phase, and undergo destructive interference, reducing the resultant harmonic content leaving a much smoother waveform.

After carrying out series of simulations, it was decided that there would be 10 teeth of 120° span and 15 teeth of 180° span; this tooth layout is shown in figure 8.9.

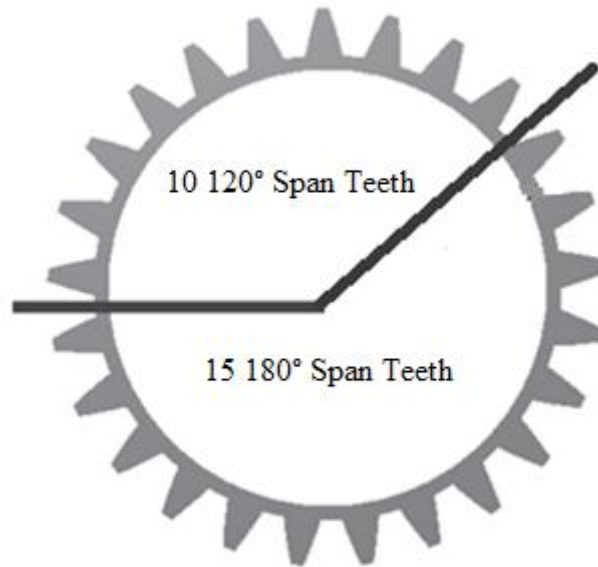


Figure 8. 9: Illustration of tooth span combinations for reducing 7th harmonic in back EMF

Figure 8.10 shows the waveform shapes for 120° and 180° spans and the resultant waveform for a machine with a combination of the two tooth spans. Accompanying this is fig 8.11 which shows the harmonic content of the three back EMF waveforms. It can be seen that the combination of spans has suppressed the seventh harmonic significantly, while all other harmonics experiences a reduction too. There is a little reduction in the fundamental component for this combination of tooth span when compared to 120° tooth span, however it is minimal when compared to the suppression of seventh harmonic.

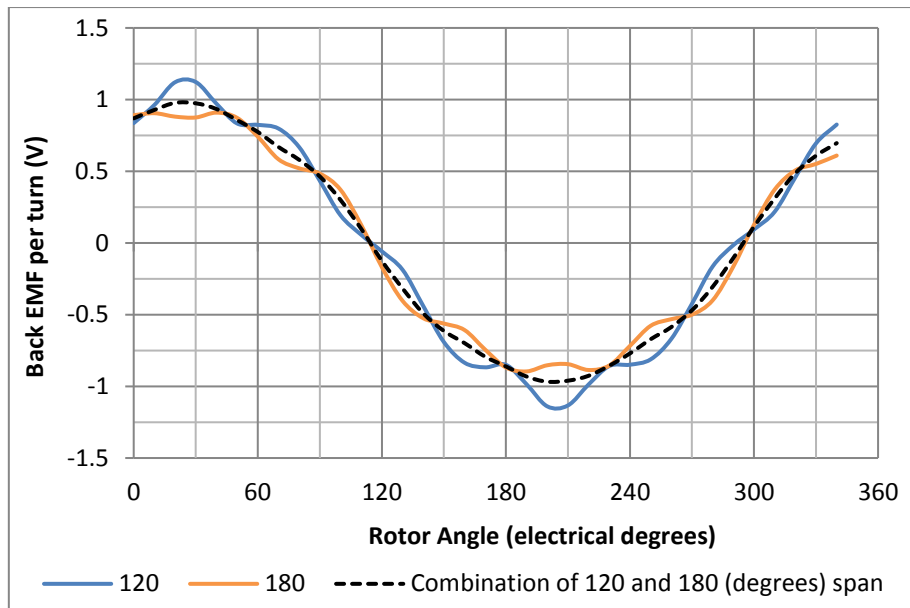


Figure 8. 10: Back EMF waveforms for 120°, 180° and the resultant waveform of summing the two together

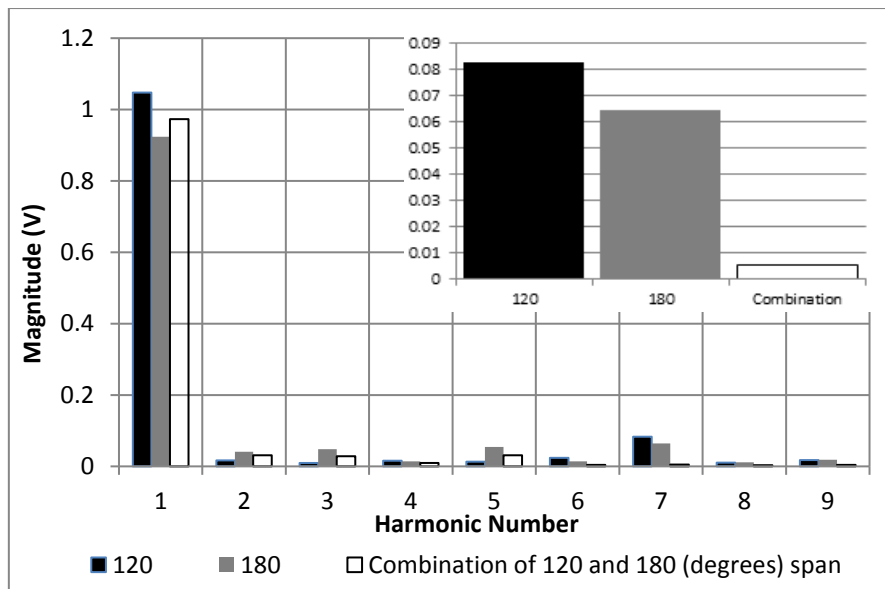


Figure 8. 11: Harmonic content of back EMF waveforms from a combination of tooth spans with 7th harmonics zoomed in

There were infinite number of tooth span combinations. However it is important to find an optimum combination that is a good compromise between reducing the seventh harmonic in back EMF, the second and fourth harmonic in cogging torque, whilst still maximising the average torque.

Combinations of tooth spans were applied, this time to minimise the cogging torque. There are many combinations of tooth spans that can reduce the cogging torque and torque ripple but only 3 (most optimised ones) are shown in Table 8.1.

It was tried to use a similar combination that works for EMF and cogging so combination B was used as it provides a good balance between the cogging torque and back EMF while combination of 3 tooth spans are easy to produce. Figure 8.12 presents the three original waveforms while it is seen from figure 8.135 that the resulting 2nd and 4th harmonics are greatly reduced using this; 2nd harmonic is down by 83% while 4th is reduced by 97% with a peak cogging torque of 0.48Nm i.e. a reduction of 90% when compared to base model of 120° span.

Table 8. 1: Tooth Combinations – Number of teeth of each span

Name	120° Tooth Span	140° Tooth Span	150° Tooth Span	180° Tooth Span
Combination A	3	3	9	10
Combination B	4	0	11	10
Combination C	0	13	0	12

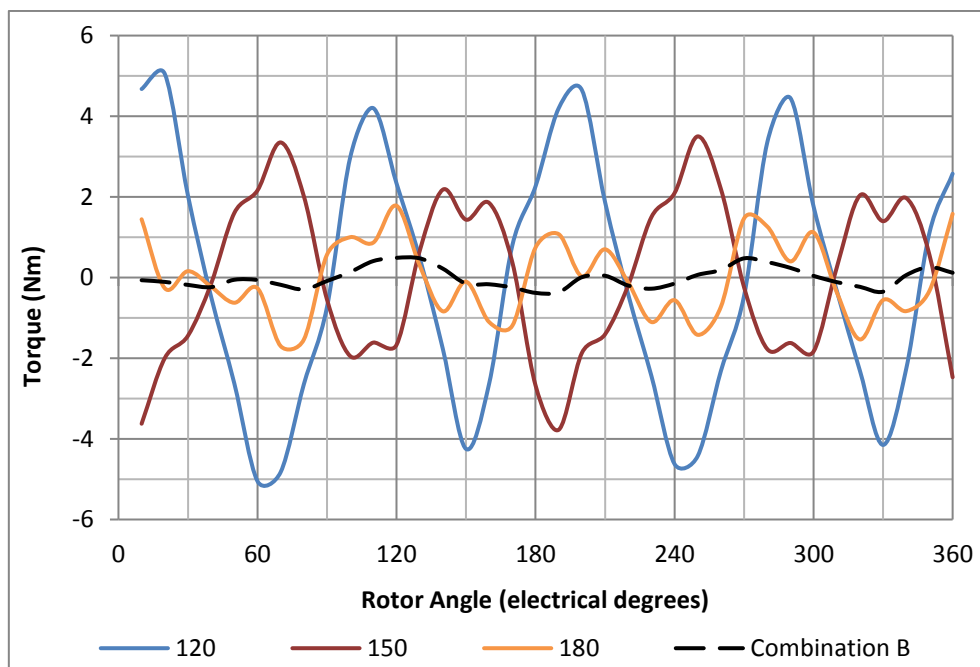


Figure 8. 12: Cogging torque waveforms for a 120°, 150°, 180° and combination of tooth span

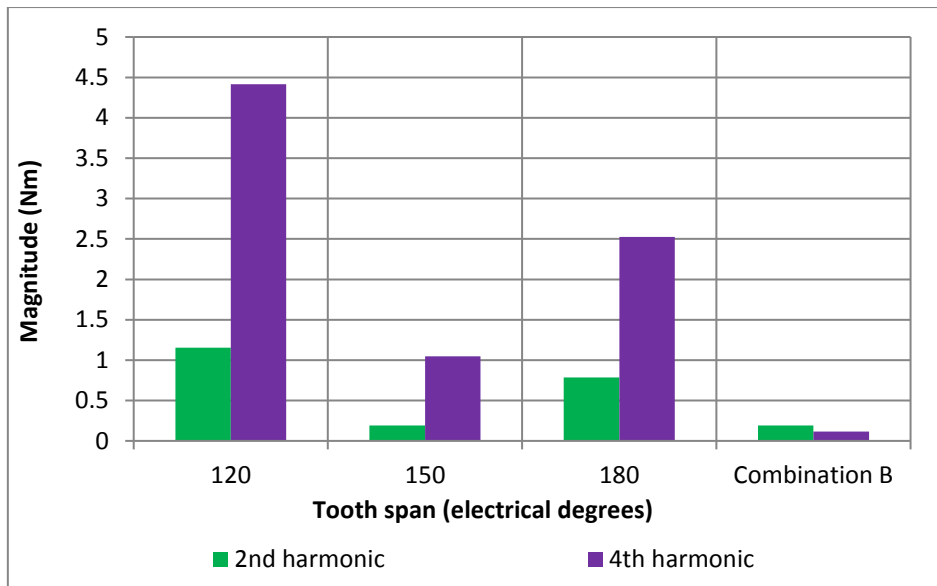


Figure 8. 13: Comparison of 2nd and 4th harmonic content of cogging torque waveforms for 120°, 150° and 180° span with combination of tooth span

Initial 3DFE analysis showed that there was a significant harmonic content present in the back EMF (7th in the inner phase) and the cogging (2nd and 4th) which were undesired. Changing the tooth span of the teeth was investigated and FE analysis showed this method to reduce the harmonic content and the cogging torque.

Table 8.2 concludes the findings; there is a reduction in average torque of 5% when using combination B. This comes from the reduction in the fundamental harmonic content of the back EMF waveform when larger tooth spans are used.

There are of course many more combinations of spans that can reduce the ripple and the cogging torque as shown in Table 8.1 though for simplicity and ease of production, the choice of different spans is kept to three.

Table 8. 2: Comparison of base model with 120° tooth span and the model using combinations of tooth span

Parameters comparison	Base Model 120° span	Combination B	Percentage reductions
Peak Cogging (Nm)	5.05	0.48	90
2 nd Harmonic	1.15	0.19	83
4 th Harmonic	4.42	0.11	98
Torque Ripple	54.18	18.73	65
Average Torque (Nm)	18.55	17.62	5
7 th Harmonic of inner phase EMF	0.083	0.006	93

A final comparison in terms of percentage changes for two topologies while using combination of tooth spans is shown in Table 8.3. It is seen that the technique works for both topologies and reduces the peak cogging torque by considerable percentage changes. Peak cogging torque is reduced by 79% in SP machine and 90% in CP at a cost of 2% and 5% reductions in average torque for SP and CP respectively.

Table 8. 3: Comparison of SP and CP machines for using combination of tooth spans technique

	SP (percentage change from base model)	CP (percentage change from base model)
Peak Cogging Torque	0.37 (79%)	0.48 (90)
Average Torque	14.72 Nm (2%)	17.62 Nm (5)

8.6 Conclusion

This section explored methods to reduce back EMF harmonics, cogging torque and torque ripple in a ‘combined’ three-phase Modulated Pole Machine. The prototype versions of separate phase and combined phase MPMs were shown in Figure 8.16.

An analysis was carried out to distinguish the optimum tooth span for the machine between 120° and 180° electrical. It was concluded that the 160° span gave the lowest cogging torque and torque ripple while a 140° provided the lowest non-fundamental harmonic content for the back EMF.

It was shown that the cogging torque and overall torque ripple could be reduced by changing a simple stator dimension, the tooth span. A simple combination was modelled and investigated; it was found that the peak cogging torque could be reduced by 90% while the torque ripple by 65% of the average torque with only a 5% reduction in the average torque.

The 2nd and 4th cogging harmonics were reduced by 83% and 98% while the 7th harmonic of inner phase EMF was reduced by 93%.

Depending on the choice of application, the final combination choice of tooth spans can be made. This method could be further expanded to tune the machine output torque with other and additional combinations.



Figure 8. 14: Assembled stator; Separate Phase MPM (left) and Combined Phase MPM (right)

A CPMPM offers 10% increase in fundamental back EMF, a 15.0% increase in the average excitation torque and 10.4% higher torque density when compared to the basic SPMPM with fewer components count [15].

9. Summary & Conclusions

The aim of this thesis was to improve the existing technology by reducing the cogging torque and back EMF harmonics in a modulated pole machine.

Techniques such as combination of stator tooth spans, pitching the stator teeth and modifying the rotor pole piece shapes were applied to reduce the unwanted harmonic contents.

Initial Finite Element investigations were carried out to find an optimum solution which was then implemented in prototypes. These prototypes were built to confirm the solutions and further improvements were made by combining the above techniques. For example, the best solution motor designed and tested consists of 6th and 12th pitched stator with convex pole pieces rotor.

Further to this, combining the tooth span technique was applied to a combined phase version of modulated pole machine and is presented in previous chapter. It was shown through Finite Element analysis that the technique works for this version of machine too and prototypes can be constructed to test this as a further work.

9.1 Background

The existing modulated pole machine was manufactured by Höganäs AB, used in electrical bicycle, provided extra propulsion to help the rider. This modulated pole machine was termed separate phase machine due to the motor made of three single phase machines, sharing the same rotor, each producing their own cogging torque which was summed on to the shaft. This project was aimed at reducing this cogging torque while maintaining the performance and size of the existing machine.

A combined phase machines was investigated by a previous EngD student sponsored by Höganäs AB, where in the machine provided higher torque density for fewer component counts and reduced rare earth magnetic material. However the cogging torque and back EMF harmonics in this machine were even greater than the separate phase machine.

This project therefore aimed to reduce the unwanted harmonics in cogging torque and back EMF firstly for separate phase machine and secondly to see if similar techniques can be used in combined phase machine.

9.2 Design and Construction

The separate phase modulated pole machine is composed of three single phase units as one unit alone cannot provide a continuous torque. This single phase is made of two sets of teeth surrounding a simple hoop coil modulating the two pole field of coil into the number of teeth that are equal to the stator teeth.

The three phase modulated pole machine consists of three axially arranged single phase units on the shaft, separated by non-magnetic separation to reduce mutual coupling and shifted by 120° electrical to complete the three phase arrangement.

The initial studies showed that the separate phase machine had a very high cogging torque which was predominantly made of 6th and 12th harmonics, while the back EMF had a high 5th and 7th harmonics. Moreover the torque ripple produced by this machine was 25% of the average torque which was quite a high number.

To reduce these unwanted harmonic contents in back EMF and cogging torque, three solutions were proposed. First one explored the effect of changing or combining the stator tooth spans while the second one looked at the effect of pitching the stator teeth. The third technique was to change the shape of the pole face directly over the air gap in a way that reduces the unwanted harmonics.

Initial Finite Element analysis showed that the optimal tooth span for reducing cogging torque was not the same for reducing back EMF harmonics and hence it was anticipated to use combination of tooth spans so a compromise between the two can be found.

Finite element analysis was conducted on these motor designs in Chapter 4 which showed that these techniques can be implemented in real world and hence prototypes were constructed as shown in Chapter 5. It was decided that two stators would be made of SMC while three stators

were made from laminates; this way a comparison could also be made between the two materials and it was seen how the cogging is affected by the choice of material.

There were five different kinds of stators manufactured which were used with four rotors one by one to test for the optimum stator rotor combination which maximised the reduction of cogging torque and back EMF harmonics. The stators consisted of laminations that were pitched, or have combination of tooth spans, or had both pitching and tooth span combinations. Rotors were either made of modified pole piece shapes, or had an increased inner phase air gap or were split to reduce the mutual coupling between the phases.

Moreover, the stators made of laminate steel allowed the easier construction of smaller parts which otherwise would have been hard to manufacture using SMC as it is harder to press them, as explained in Chapter 2. It was hence decided that larger parts which can be pressed in one piece such as the core back can be manufactured from SMC while the stator teeth can be made from laminated steel; ultimately reducing the cost and complexity of the machine.

The construction and assembling of the prototypes were shown in Chapter 5. Majority of the parameters were identical for all the motors except the pole piece shapes and the stator tooth spans and pitching angles. This made sure that the techniques to reduce the cogging torque and back EMF harmonics were compared fairly.

The prototypes were tested for their cogging torque, back EMF, efficiency and torque speed envelopes. These results for each motor were compared against each other motor and a matrix was constructed where each stator was tested with each rotor providing the best stator rotor combination that worked best for reducing the unwanted harmonics.

Chapter 6 provides the results for the testing carried out on all the prototypes; 25 motors in total. It was concluded that the stator pitched for 6th and 12th harmonic made of SMC while the rotor composed of convex type of pole pieces provided the best machine design for the separate phase topology. The benefits of this motor over the base design motor previously designed with simple stator and rotor is shown in Table 9.1.

Table 9. 1: Comparison of results of the base motor with the most optimised motor made

	Base motor	SMC 6th & 12 pitched stator with convex rotor	Percentage Difference
Peak Cogging Torque	1.759	0.178	-89.881
6th harmonic	1.457	0.025	-98.284
12th harmonic	0.198	0.002	-98.990
Peak Back EMF	108.270	105.700	-2.374
5th Harmonic back EMF	3.200	0.330	-89.688
7th Harmonic back EMF	0.860	0.190	-77.907
Peak Efficiency	79.370	85.960	+8.303
Peak Torque	40.420	44.500	+10.094

The peak cogging torque of the new motor is reduced by 90% which is a massive improvement. Almost all the harmonics in the cogging are reduced, while the vital 6th and 12th are nearly reduced by 100%.

The back EMF of the new motor was 2.4% lower than the base motor which was mainly due to the reduction in fundamental harmonics. However, the important 5th and 7th harmonics in back EMF are significantly reduced, 90% and 78% respectively. This shows that although the fundamental harmonic in back EMF is a little lower than the base motor, eliminating the 5th and 7th harmonics can have a significant effect on the torque producing capability of the machine and hence the peak torque provided by the new motor is 10% higher than the base motor.

Both machines had the same mass and volume therefore the new motor would have higher torque density and higher torque per volume. Moreover, due to crucial improvements in cogging and back EMF harmonic, the peak efficiency of the new motor was 8% higher than the base motor.

All in all, this PhD produced various novel design techniques to reduce the cogging torque and back EMF harmonic. 24 motor variants were constructed and tested to approve these techniques and ultimately one optimum motor was chosen that reduced the peak cogging torque by 90%; the efficiency and peak torque of the optimum motor is 8% and 10% higher, respectively, when compared with the base motor used in this study.

9.3 Future work recommendations

This thesis concentrated on design techniques only to reduce cogging torque and back EMF harmonics however in future, drive techniques such as introducing current harmonics to reduce unwanted harmonics could also be implemented.

Various current profiling methods have been implemented and described in literature [78-81]. Most of these conventional methods generally rely on application of Fourier Series Analysis or least square minimization methods to acquire the harmonic coefficients and optimal output torque. Approaches such as designing the permanent magnet field characteristics to match the stator excitation current for achieving optimal torque or to use excitation current design to complement the permanent magnet field characteristics to ensure optimal torque have been implemented [134].

These methods usually require significant computational time and control being impractical. In [134], C. W. Lu et al describes a novel approach where application of instantaneous power theory [135] is implemented which eliminates Fourier analysis and rather requires Park's transformation only. This method eliminates the need to assume a finite harmonic spectrum as is the case in conventional current profiling methods, and instead, instantaneous measurements are used.

Similar technique was implemented and various calculations were carried out to produce a three phase current waveforms that can be applied instead of sinusoidal currents, half the current waveform is shown in Figure 9.1.

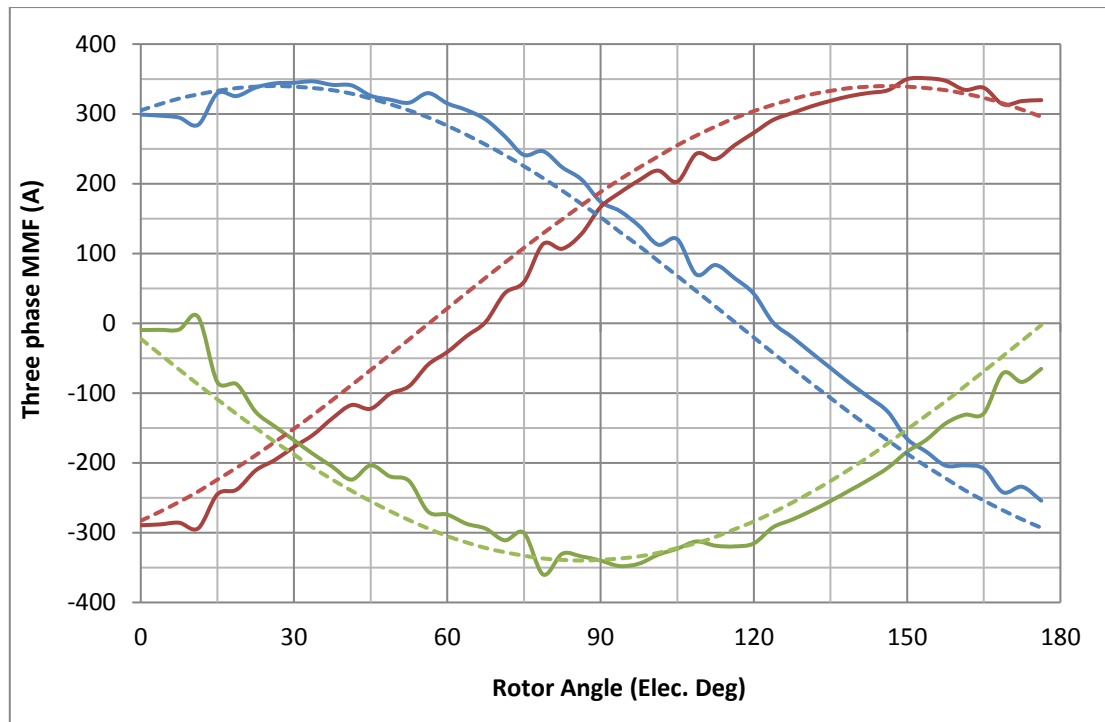


Figure 9. 1: Comparison of the optimum currents and the sinusoidal currents

Implementation of the profiled current waveforms results in reducing cogging torque harmonic contents as shown in Figure 8.2. A reduction is seen in all harmonics especially in the vital 6th and 12th harmonics, 82% and 77% respectively.

This area of current profiling along with injecting current harmonics to create torque that would oppose the cogging torque could be a very interesting future area to look into. The initial Finite Element analysis show success using these methods on separate phase machine; it will be interesting to see how this method works on combined phase topology presented in previous chapter.

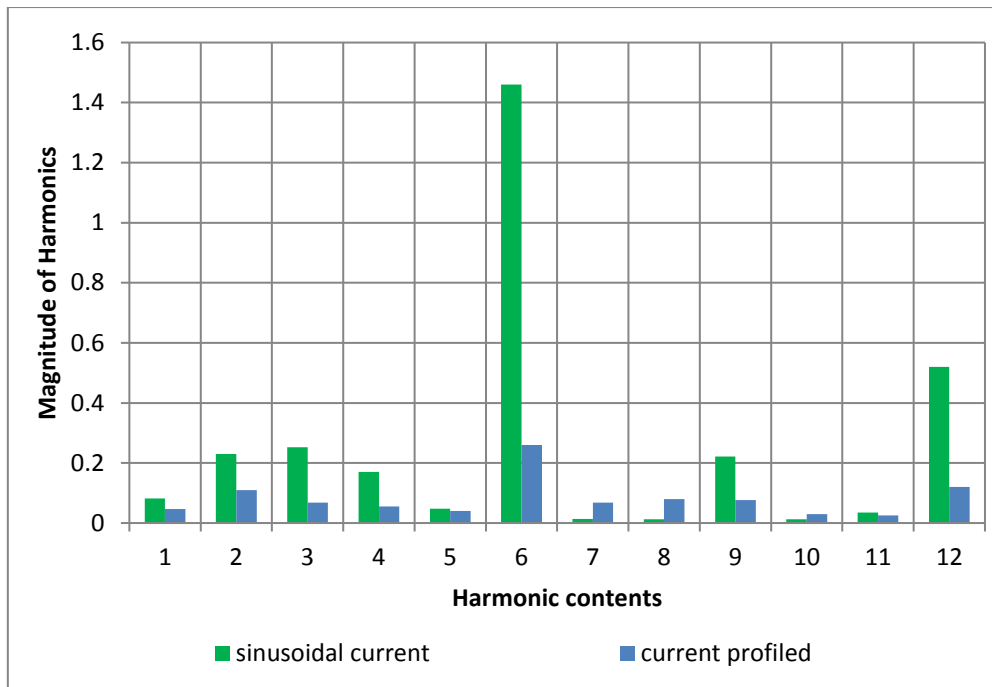


Figure 9. 2: Comparison of cogging torque harmonics for sinusoidal and profiled current waveforms shown in Figure 9.1

One of the techniques applied to reduce the cogging torque and back EMF harmonics was using combination of tooth spans. There were few simple combinations of this idea investigated however there can be significantly many more possible combinations that can be manufactured. For example a stator where 5 tooth spans are combined with introduction of a pitching angle can be manufactured as initial Finite Element analysis showed this to reduce back EMF harmonics even more. Moreover, it was shown in Chapter 7 that this technique of combining tooth spans can be implemented to combined phase modulated pole machine too and it reduces the desired harmonic content in both, back EMF and cogging torque. The next step could be to produce a prototype of this topology and compare the results.

9.4 Published work

Following is a list of published work stemmed from the research carried out during this PhD.

1. Ahmed, N; Atkinson, G. J. ; Baker, N. J. ; Sjöberg, L. **“Flux Switching Modulated Pole Machine topologies which offer greater mechanical simplicity”**, Electrical Machines and Drives Conference (IEMDC), 2013 IEEE International on, pp. 354 – 358, May 2013
2. Ahmed, N; Washington, J. ; Atkinson, G. J. ; Baker, N. J. **“Reduction of cogging torque and torque ripple in Modulated Pole Machines by geometrical changes”**, Power Electronics, Machines and Drives (PEMD 2014), 7th IET International Conference on, pp. 1 – 6, April 2014.
3. Ahmed, N; Atkinson, G. J. ; Baker, N. J. ; Sjöberg, L. **“Reduction of Cogging Torque and back EMF harmonics in Modulated Pole Machine by variations in Tooth span,”** Electrical Machines and Drives Conference (IEMDC), 2015 IEEE International on, May 2015
4. Nabeel Ahmed, Glynn Atkinson. **“Low Ripple TFM feasibility study for BAFCO”**, January 2016. The Big Ass Fan Corporation (BAFCO) requested that Newcastle University carry out a feasibility on two TFM topologies, the aim being to produce feasible designs with high efficiency and low torque ripple.
5. Nabeel Ahmed, *Cristofaro Pompermaier, Jamie Washington, Lars Sjöberg.* **“Reduction of Cogging Torque in Transverse Flux Machines by Stator and Rotor Pole Shaping”**, *IEEE Energy Conversion Congress and Expo, Sept 18-22, Milwaukee, WI, USA.*

References

1. Mordey, W. M., "Electric Generator," US Patent No. 437501, 1890.
2. H. M. Weh, H., "Achievable force densities for permanent magnet machines in new configurations," *Proc. Int. Conf. Electrical Machines (ICEM86)*, 1986. Pp. 1107-1111.
3. B. C. Mecrow, A. G. Jack, and C. P. Maddison, "Permanent Magnet Machines for High Torque, Low Speed Applications," *Proc. Int. Conf. Electrical Machines (ICEM96)*, vol. 3, pp. 461-466, 1996.
4. R. Blissenback, U. Schafer, W. Hackmann, and G. Henneberger, "Development of a transverse flux traction motor in a direct drive system," *Proc. Int. Conf. on Electrical Machines (ICEM2000), Helsinki, Finland*, vol. Volume III, pp. 1457-1460, 2000.
5. M. Dubois, H. Polinder, and J. A. Ferreira, "Effect of air gap thickness on transverse-flux permanent magnet (TFPM) machine with flux-concentration," *Proc. Int. Conf. on Electrical Machines (ICEM2002), Brugge, Belgium*, 2002.
6. C. P. Maddison, B. C. Mecrow, and A. G. Jack, "Claw Pole Geometries for High Performance Transverse Flux Machines," *Proc. Int. Conf. on Electrical Machines (ICEM98), Istanbul, Turkey*, pp. 340-345, 1998.
7. M. R. Dubois, N. Dehlinger, H. Polinder, and D. Massicotte, "Clawpole Transverse-Flux Machine with Hybrid Stator," *Proc. Int. Conf. on Electrical Machines (ICEM2006)*, 2006.
8. P. Dickinson, A. Jack, and B. Mecrow, "Improved permanent magnet machines with claw pole armatures," *Proc. Int. Conf. on Electrical Machines (ICEM2002), Brugge, Belgium*, 2002.
9. Mitcham AJ, Bolton TW. The transverse flux motor: a new approach to naval propulsion. Symposium on Motor Technology for Underwater Naval Sea Applications, Rode Island/USA, 1997; pp. 73–80.

10. Masmoudi A, Elantably A. An approach to sizing high power density TFPM intended for hybrid bus electric propulsion. *Electrical Machines and Power Systems* 2000; 28(4):341–354
11. Blissenbach R, Henneberger G, Schafer U, Hackmann W. Development of transverse flux traction motor in a direct drive system. *Proceedings of International Conference on Electrical Machines (ICEM)*, Vol. 3, Espoo/Finland, 2000; pp. 1457–1460.
12. Mecrow, B. C., Jack, A. G., Maddison, C. P., "Permanent Magnet Machines for High Torque, Low Speed Applications," *Proc. Int. Conf. Electrical Machines (ICEM96)*, vol. 3, pp. 461-466, 1996.
13. Lange A, Canders W-R, Laube F, Mosebach H. Comparison of different drive systems for a 75 kW electrical vehicle drive. *International Conference on Electrical Machines (ICEM)*, Vol. 3, Espoo/Finland, 2000; pp. 1308–1312.
14. Kastinger G. Design of a novel transverse flux machine. *International Conference on Electrical Machines (ICEM)*, Bruges/ Belgium, 2002, CD-ROM
15. M. R. Harris, G. H. Pajooman, and S. M. Abu Sharkh, "The problem of power factor in VRPM (transverse-flux) machines," in *Electrical Machines and Drives, 1997 Eighth International Conference on (Conf. Publ. No. 444)*, 1997, pp. 386-390.
16. Washington, J.G. ; Atkinson, G.J. ; Baker, N.J. ; Jack, A.G. ; Mecrow, B.C. ; Jensen, B.B. ; Pennander, L. ; Nord, G.L. ; Sjoberg, L., "Three-Phase Modulated pole machine topologies utilizing mutual flux paths," *Energy conversion, IEEE Transactions on*, vol.27, issue 3, pp.507-515, June 2012.
17. Y. G. Guo and J. G. Zhu, "Study of permanent magnet transverse flux motors with soft magnetic composite core," in *Australasian Universities Power Engineering Conference*, Brisbane, Sept. 2004.
18. Schmidt, "3-D finite element analysis of the cogging torque of a transverse flux machine," *Magnetics, IEEE Transactions on*, vol. 41, pp. 1836-1839, 2005.
19. Schmidt, "Finite element analysis of a novel design of a three phase transverse flux machine with an external rotor," *Magnetics, IEEE Transactions on*, vol. 47, pp. 982-985, 2011.
20. M. Dubois. "Optimized permanent magnet generator topologies for direct drive wind turbines", Ph.D. dissertation, Delft University of Technology, Delft, The Netherlands, 2004.

21. Polinder, H.; Mecrow, B.C.; Jack, A.G.; Dickinson, P.G.; Mueller, M.A.; , "Conventional and TFPM linear generators for direct-drive wave energy conversion," *Energy Conversion, IEEE Transactions on* , vol.20, no.2, pp. 260- 267, June 2005
22. Zhu, Z.Q.; Ruangsinchaiwanich, S.; Schofield, N.; Howe, D.; , "Reduction of cogging torque in interior-magnet brushless machines," *Magnetics, IEEE Transactions on* , vol.39, no.5, pp. 3238- 3240, Sept. 2003
23. Mecrow, B. C., Jack, A. G., Maddison, C. P., "Permanent Magnet Machines for High Torque, Low Speed Applications," *Proc. Int. Conf. Electrical Machines (ICEM96)*, vol. 3, pp. 461-466, 1996.
24. Pinguey, E., "On the design and construction of modulated pole machines," "Engineering Doctorate Thesis, Newcastle University, 2010.
25. Schmidt, E., "3-D finite element analysis of the cogging torque of a transverse flux machine," *Magnetics, IEEE Transactions on*, vol. 41, pp. 1836-1839, 2005.
26. Masmoudi, A. and Elantably, A., "An Approach to Sizing High Power Density TFPM Intended for Hybrid Bus Electric Propulsion," *Electric Power Components and Systems*, vol. 28, pp. 341 - 354, 2000.
27. Mitcham, A. J., "Transverse Flux Motors for Electric Propulsion of Ships," *Proc. IEE Colloquium on New Topologies for Permanent Magnet Machines, London UK*, 1997.
28. Kang, D. H., Chun, Y. H. and Weh, H., "Analysis and optimal design of transverse flux linear motor with PM excitation for railway traction," *Electric Power Applications, IEE Proceedings -*, vol. 150, pp. 493-499, 2003.
29. Bang, D., Polinder, H., Shrestha, G. and Ferreira, J. A., "Ring-Shaped Transverse Flux PM Generator for Large Direct-Drive Wind Turbines," *International Conference on Power Electronics and Drive Systems*, 2009.
30. Deok-je, B., Polinder, H., Shrestha, G. and Ferreira, J. A., "Comparative design of radial and transverse flux PM generators for direct-drive wind turbines," in *Electrical Machines, 2008. ICEM 2008. 18th International Conference on*, 2008, pp. 1-6.
31. Quddes, M.R., Sekino, M., Ohsaki, H., Kashima, N. and Nagaya, S., "Electromagnetic Design Study of Transverse Flux Enhanced Type Superconducting Wind Turbine Generators," *Applied Superconductivity, IEEE Transactions on* , vol.21, no.3, pp.1101-1104, June 2011.
32. Hosseini, S.; Moghani, J.S. Ershad, N.F. and Jensen, B.B., "Design, Prototyping, and Analysis of a Novel Modular Permanent-Magnet Transverse Flux Disk Generator," *Magnetics, IEEE Transactions on* , vol.47, no.4, pp.772-780, April 2011.

33. Polinder, H.; Mecrow, B.C.; Jack, A.G.; Dickinson, P.G.; Mueller, M.A.; , "Conventional and TFPM linear generators for direct-drive wave energy conversion," *Energy Conversion, IEEE Transactions on* , vol.20, no.2, pp. 260- 267, June 2005.
34. Vining, J., Lipo, T.A. and Venkataramanan, G., "Design and optimization of a novel hybrid transverse / longitudinal flux, wound-field linear machine for ocean wave energy conversion," *Energy Conversion Congress and Exposition, 2009. ECCE 2009. IEEE* , vol., no., pp.3726-3733, 20-24 Sept. 2009.
35. Mueller, M.A.; , "Electrical generators for direct drive wave energy converters," *Generation, Transmission and Distribution, IEE Proceedings-* , vol.149, no.4, pp. 446-456, Jul 2002
36. N. Tesla, "Alternating-Electric-Current Generator," United States Patent No. 447921, 1891.
37. E. F. W. Alexanderson, "High-Frequency Alternator," G. E. Company, Ed. United States Patent No. 1008577, 1911.
38. F. A. Furfari and E. L. Owen, "Rediscovering William Stanley, Jr. Part 2," *Industry Applications Magazine, IEEE*, vol. 10, pp. 10-13, 2004.
39. E. L. Owen, "Rediscovering William Stanley, Jr. Part I," *Industry Applications Magazine, IEEE*, vol. 9, pp. 9-12, 2003.
40. R. H. Bertsche, "Dynamoelectric Machine," United States Patent No. 2928963, 1960.
41. H. R. Kirchmayr, "Permanent magnets and hard magnetic materials," *Journal of Physics D: Applied Physics*, vol. 29, p. 2763, 1996.
42. Weh, H., Hoffmann, H. and Landrath, J., "New permanent magnet excited synchronous machine with high efficiency at low speed," *Proc. Int. Conf. Electrical Machines (ICEM88)*, 1988.
43. Arshad, W. M., Backstrom, T. and Sadarangani, C., "Analytical design and analysis procedure for a transverse flux machine," in *Electric Machines and Drives Conference, 2001. IEMDC 2001. IEEE International*, 2001, pp. 115-121.
44. Henneberger. G. and Bork, M., "Development of a new transverse flux motor," in *New Topologies for Permanent Magnet Machines (Digest No: 1997/090), IEE Colloquium on*, 1997, pp. 1/1-1/6.
45. M. Bork and G. Henneberger, "New transverse flux concept for an electric vehicle drive system," in *Proc. Int. Conference on Electrical Machines (ICEM)*, Vigo, Spain, 1996.

46. G. Henneberger and M. Bork, "Development of a new transverse flux motor," in *New Topologies for Permanent Magnet Machines (Digest No: 1997/090), IEE Colloquium on*, 1997, pp. 1/1-1/6.
47. Harris, M. R., Pajooman, G. H., and Sharkh, S. M. A., "Comparison of alternative topologies for VRPM (transverse-flux) electrical machines," in *New Topologies for Permanent Magnet Machines (Digest No: 1997/090), IEE Colloquium on*, 1997, pp. 2/1-2/7.
48. P. G. Dickinson, A. G. Jack, and B. C. Mecrow, "Improved permanent magnet machines with claw pole armatures," in *International Conference on Electrical Machines (ICEM)*, Brugge, Belgium, 2002.
49. F. A. Furfari and E. L. Owen, "Rediscovering William Stanley, Jr. Part 2," *Industry Applications Magazine, IEEE*, vol. 10, pp. 10-13, 2004.
50. Kang, D. H., Chun, Y. H. and Weh, H., "Analysis and optimal design of transverse flux linear motor with PM excitation for railway traction," *Electric Power Applications, IEE Proceedings -*, vol. 150, pp. 493-499, 2003.
51. Yuqi, R., Chenglin, G., and Huaishu, L., "Analytical design and modeling of a transverse flux permanent magnet machine," in *Power System Technology, 2002. Proceedings. PowerCon 2002. International Conference on*, 2002, pp. 2164-2167 vol.4.
52. Siatkowski, M. and Orlik, B., "Flux linkage in Transverse Flux machines with flux concentration," in *Optimization of Electrical and Electronic Equipment, 2008. OPTIM 2008. 11th International Conference on*, 2008, pp. 21-26.
53. Bao, G. Q., Jiang, J. Z., "A modular multiphase permanent magnet machine optimization for direct propulsion systems," *Vehicle Power and Propulsion Conference, 2008. VPPC '08. IEEE*, vol., no., pp.1-5, 3-5 Sept. 2008.
54. Ferreira da Luz, M. V., Dular, P., Sadowski, N., Carlson, R. and Bastos, J. P., "Development of analytical equations to calculate the cogging torque in transverse flux machines," in *Electric Machines and Drives Conference, 2009. IEMDC '09. IEEE International*, 2009, pp. 1612-1616.
55. Weh, H., "Transversal Flow Machine in Accumulator Arrangement," US Pat No. 5,051,641, 1988.
56. A. G. Jack, B. C. Mecrow, C. P. Maddison, and N. A. Wahab, "Claw pole armature permanent magnet machines exploiting soft iron powder metallurgy," in *Electric*

- Machines and Drives Conference Record, 1997. IEEE International, 1997, pp. MA1/5.1-MA1/5.3.*
57. C. P. Maddison, "Transverse Flux Machines for High Torque Applications," Ph.D. Thesis, University of Newcastle upon Tyne: Newcastle upon Tyne, 1999.
 58. Persson, M., Jansson, P., Jack, A. G. and Mecrow, B. C., "Soft magnetic composite materials-use for electrical machines," in *Electrical Machines and Drives, 1995. Seventh International Conference on (Conf. Publ. No. 412)*, 1995, pp. 242-246.
 59. Küppers, S., Henneberger, G. and Ramesohl, I., "The Influence of the number of poles on the output performance of a claw pole alternator," *Proc. Int. Conf. Electrical Machines (ICEM96)*, vol. 3, pp. 268-272, 1996.
 60. Seung-Bin, L., Dae-Sung, J., Ki-Chan, K., Dae-Hyun, K. and Ju, L., "Characteristic Analysis of Permanent-Magnet-Type Stepping Motor With Claw Poles by Using 3 Dimensional Finite Element Method," *Magnetics, IEEE Transactions on*, vol. 43, pp. 2519-2521, 2007.
 61. Ji-Hyun, A., Seung-Chan, P., Se-Hyun, R. and In-Sung, J., "Claw-pole shape design of permanent magnet stepping motor," in *Electrical Machines and Systems, 2005. ICEMS 2005. Proceedings of the Eighth International Conference on*, 2005, pp. 276-279 Vol. 1.
 62. Qu, R., Kliman, G. B. and Carl, R., "Split-phase claw-pole induction machines with soft magnetic composite cores," in *Industry Applications Conference, 2004. 39th IAS Annual Meeting. Conference Record of the 2004 IEEE*, 2004, pp. 2514-2519 vol.4.
 63. Jack, A. G., Mecrow, B. C., Maddison, C. P. and Wahab, N. A., "Claw pole armature permanent magnet machines exploiting soft iron powder metallurgy," in *Electric Machines and Drives Conference Record, 1997. IEEE International, 1997, pp. MA1/5.1-MA1/5.3.*
 64. Maddison, C P., Mecrow B. C., and Jack, A. G., "Claw Pole Geometries for High Performance Transverse Flux Machines," *Proc. Int. Conf. on Electrical Machines (ICEM98), Istanbul, Turkey*, pp. 340-345, 1998.
 65. Dickinson, P. G., "Application of Soft Magnetic Composites in electrical machines," PhD Thesis, Newcastle University, 2003.
 66. P. G. Dickinson, A. G. Jack, and B. C. Mecrow, "Improved permanent magnet machines with claw pole armatures," in *International Conference on Electrical Machines (ICEM)*, Brugge, Belgium, 2002.

67. Guo, Y. G., Zhu, J., Lu, H., Wang, S., and Jin, J., "Performance analysis of an SMC transverse flux motor with modified double-sided stator and PM flux concentrating rotor," in *Electrical Machines and Systems, 2007. ICEMS. International Conference on*, 2007, pp. 1553-1556.v
68. Mansouri A, Njeh A, Makni Z, Trabelsi H, Masmoudi A, Elantably A. On the torque production capability of a claw pole TFPM. *International Journal on Applied Electromagnetics and Mechanics* 2004; 19(1–4):391–394
69. B. C. Mecrow, A. G. Jack, D. J. Atkinson, P. G. Dickinson, and S. Swaddle, "High torque machines for power hand tool applications," in *Power Electronics, Machines and Drives, 2002. International Conference on (Conf. Publ. No. 487)*, 2002, pp. 644-649.
70. Y. P. Dou, Y. G. Guo, J. G. Zhu, and H. Y. Lu, "Effect of Armature Reaction of a Permanent-Magnet Claw Pole SMC Motor," *Magnetics, IEEE Transactions on*, vol. 43, pp. 2561-2563, 2007.
71. Y. G. Guo, J. G. Zhu, and H. Y. Lu, "Effects of Armature Reaction on the Performance of a Claw Pole Motor With Soft Magnetic Composite Stator by Finite-Element Analysis," *Magnetics, IEEE Transactions on*, vol. 43, pp. 1072-1077, 2007.
72. J. Cros, J. R. Figueroa, and P. Viarouge, "Analytical design method of polyphase claw-pole machines," in *Industry Applications Conference, 2004. 39th IAS Annual Meeting. Conference Record of the 2004 IEEE*, 2004, pp. 1397-1404 vol.3.
73. Jack, A. G. and Hultman, L. O., "Soft Magnetic Composites – Motor Design Issues and Applications," *PM²TEC 2004*, in Chicago, USA, 2004.
74. Hultman, L. O., Persson, M., Engdahl, P., "Soft magnetic composites for advanced machine design," *PMA_{Asia}2005 in Shanghai*, 2005.
75. Persson, M., Jansson, P., Jack, A. G. and Mecrow, B. C., "Soft magnetic composite materials-use for electrical machines," in *Electrical Machines and Drives, 1995. Seventh International Conference on (Conf. Publ. No. 412)*, 1995, pp. 242-246.
76. Jack, A. G., Pennander, L-O., "Soft Magnetic Iron Powder Materials AC Properties and their Application in Electrical Machines," *EURO PM2003*, in Valencia, Spain, 2003.
77. Jack, A. G., Mecrow, B. C., Dickinson, P. G., Jansson, P. and Hultman, L. O., "Design and testing of a universal motor using a soft magnetic composite stator," in

- Industry Applications Conference, 2000. Conference Record of the 2000 IEEE*, 2000, pp. 46-50 vol.1.
78. Jack, A. G., Krogen, Ö., "Insulated iron powder (SMC) used as a soft magnetic material in a rotating electrical machine," PM2000, in Kyoto, Japan, 2000.
79. Jack, A. G., Mecrow, B. C. and Maddison, C. P. "Combined radial and axial permanent magnet motors using soft magnetic composites," in *Electrical Machines and Drives, 1999. Ninth International Conference on (Conf. Publ. No. 468)*, 1999, pp. 25-29.
80. Jack, A. G., Mecrow, B. C., Nord, G. and Dickinson, P. G., "Axial Flux Motors Using Compacted Insulated Iron Powder and Laminations Design and Test Results," in *Electric Machines and Drives, 2005 IEEE International Conference on*, pp. 378-385, 2005.
81. Lundmark, S. K. T., "Application of 3-D Computation of Magnetic Fields to the Design of Claw-Pole Motors." Tech. Licentiate Thesis, Chalmers University of Technology, 2005.
82. Narasimhan, K. S., "More power calls sparks soft compact research," *Metal Powder Report*, vol. 58, pp. 12-16, 2003.
83. Jack, A. G., "The impact of new materials on the design of electrical machines," in *Impact of New Materials on Design, IEE Colloquium on*, 1995, pp. 1/1-1/5.
84. Hultman, L. O. and Jack, A. G., "Soft magnetic composites-materials and applications," in *Electric Machines and Drives Conference, 2003. IEMDC'03. IEEE International*, 2003, pp. 516-522 vol.1.
85. Amreiz, H. M., "Transverse Flux Switched Reluctance Motors," Ph.D. Thesis, University of Newcastle upon Tyne: Newcastle upon Tyne, 2002.
86. Hanselman, D. C., "Effect of skew, pole count and slot count on brushless motor radial force, cogging torque and back EMF," *Electric Power Applications, IEE Proceedings -* , vol.144, no.5, pp.325-330, Sept. 1997.
87. Xin, G., Guangxian, H., Zhi C., Zongpei, W., "Research of cogging torque in the brushless DC motor with fractional ratio of slots and poles," *Electrical Machines and Systems, 2005. ICEMS 2005. Proceedings of the Eighth International Conference on* , vol.1, no., pp. 76- 80 Vol. 1, 27-29 Sept. 2005.
88. Zhu, Z. Q., Ruangsinchaiwanich, S., Schofield, N., Howe, D., , "Reduction of cogging torque in interior-magnet brushless machines," *Magnetics, IEEE Transactions on* , vol.39, no.5, pp. 3238- 3240, Sept. 2003.

89. Zhu, Z. Q., Howe, D., "Influence of design parameters on cogging torque in permanent magnet machines," *Energy Conversion, IEEE Transactions on* , vol.15, no.4, pp.407-412, Dec. 2000.
90. Schuttler, J., and Orlik, B., "Analytical model describing the operation behaviour of transverse flux machines in flat magnet configuration," in *Power Electronics and Applications, 2007 European Conference on*, 2007, pp. 1-10.
91. Y. G. Guo, J. G. Zhu, and H. Y. Lu, "Accurate determination of parameters of a claw-pole motor with SMC stator core by finite-element magnetic-field analysis," *Electric Power Applications, IEE Proceedings -*, vol. 153, pp. 568-574, 2006.
92. Masmoudi A., and Elantably, A., "A simple assessment of the cogging torque in a transverse flux permanent magnet machine," in *Electric Machines and Drives Conference, 2001. IEMDC 2001. IEEE International*, 2001, pp. 754-759
93. Guo, Y. G., Zhu, J. G., Watterson, P. A. and Wu, W. "Design and analysis of a transverse flux machine with soft magnetic composite core," in *Electrical Machines and Systems, 2003. ICEMS 2003. Sixth International Conference on*, 2003, pp. 153-157 vol.1.
94. N. Bianchi and S. Bolognani, "Design techniques for reducing the cogging torque in surface-mounted PM motors," *IEEE Trans. Magn*, vol. 38, no. 5, pp. 1259–1265, Sep./Oct. 2002.
95. Y.-H. Yeh, M.-F. Hsieh, and D. G. Dorrell, "Different arrangements for dual-rotor dual-output radial-flux motors," *IEEE Trans. Ind. Appl.*, vol. 48, no. 2, pp. 612–622, Mar./Apr. 2012.
96. D. Wang, X. Wang, D. Qiao, Y. Pei, and S.-Y. Jung, "Reducing cogging torque in surface-mounted permanent magnet motors by non-uniformly distributed teeth method," *IEEE Trans. Magn*, vol. 47, no. 9, pp. 2231–2239, Sep. 2011.
97. M.-F. Hsieh, D. G. Dorrell, Y.-H. Yeh, and S. Ekram, "Cogging torque reduction in axial flux machines for small wind turbines," in *Proc. 35th IEEE Annu. Conf. Ind. Elect. (IECON)* , 2009, pp. 4435–4439.
98. Masmoudi, A. and Elantably, A., "On the analysis and reduction of the cogging torque of a claw pole transverse flux permanent magnet machine," *European Transactions on Electrical Power*, vol. 15, pp. 513-526, 2005.
99. A. Cassat, M. Williams, and D. MacLeod, Effect of skew on brushless dc motor exciting forces, Proceedings of the Annual Symposium on Incremental Motion Control Systems and Device, p. 148, 1993.

100. R. Islam, I. Hussain, A. Fardoun et al., Permanent magnet synchronous motor magnet designs with skewing for torque ripple and cogging torque reduction, Conference Record of the 2007 IEEE Industry Applications Conference – Forty second IAS Annual Meeting, pp. 1552-1559, 2007.
101. W. Hua and M. Cheng, “Cogging torque reduction of flux-switching permanent magnet machines without skewing,” in *Proc. 8th Int. Conf. Elect. Mach. Syst. (ICEMS)*, 2008, vol. 1, pp. 3020–3025.
102. M. J. Jin, Y. Wang, J.X. Shen, P.C. K. Luk, W. Z. Fei, and C. F. Wang, “Cogging torque suppression in a permanent magnet flux-switching integrated-starter generator,” *Elect. Power Appl. (IET)*, vol. 4, no. 8, pp. 647–656, 2010.
103. H. Jia, M. Cheng, W. Hua, W. Zhao, and W. Li, “Torque ripple suppression in flux-switching PM motor by harmonic current injection based on voltage space-vector modulation,” *IEEE Trans. Magn.*, vol. 46, no. 6, pp. 1527–1530, Jun. 2010.
104. Ji-Young, L., Jung-Hwan, C., Do-Hyun, K., Sung-II, K. and Jung-Pyo, H., "Tooth Shape Optimization for Cogging Torque Reduction of Transverse Flux Rotary Motor Using Design of Experiment and Response Surface Methodology," *Magnetics, IEEE Transactions on*, vol. 43, pp. 1817-1820, 2007.
105. G. R. Slemon and A. Straughen, *Electric Machines*, Addison Wesley, Reading, MA, 1980
106. Z.Q. Zhu and D. Howe, Analytical models for predicting noise and vibration in brushless permanent magnet DC motors, Proceedings of the 25th Universities Power Engineering Conference, pp. 277-280, 1990
107. Y. S. Chen, Z. Q. Zhu and D. Howe, Vibration of PM brushless machines having a fractional number of slots per pole, *IEEE Transactions on Magnetics*, 42 (10), 3395 – 3397, 2006
108. Joao S. D. Garcia, Joao Pedro A. Bastos, “Transverse Flux Machines: What for?,” *IEEE Multidisciplinary engineering education magazine*, Vol. 2, No. 1, March 2007
109. C.C. Hwang, S.B. John, and S.S. Wu, “Reduction of cogging torque in spindle motors,” *IEEE Trans. Magn.*, vol. 34, no. 2, pp. 468-470, Mar. 1998.
110. W. Xiuhe, Y. Yubo, and F. Dajin, “Study of cogging torque in surface-mounted permanent magnet motors with energy method,” *J. Magn. Mater.*, vol. 267, no. 1, pp. 80-85, Nov. 2003.
111. Zhu Z.Q, HOWE D., “Influence of design parameters on cogging torque in permanent machines,” *IEEE Trans. Energy Convers.*, vol. 15, no. 4, pp. 407-412, 2000.

112. R. Lateb, N. Takorabet, and F. Meibody-Tabar, "Effect of magnet segmentation on the cogging torque in surface mounted permanent-magnet motors," *IEEE Trans. Magnet*, vol. 42, no. 3, pp. 442-445, Mar. 2006.
113. R. Lateb, N. Takorabet, and F. Meibody-Tabar, "Effect of magnet segmentation on the cogging torque in surface-mounted permanent-magnet motors," *IEEE Trans. Magn.*, vol. 42, no. 3, pp. 442-445, Mar. 2006.
114. K. Abbaszadeh, F. Rezaee Alam, S.A. Saied, "Cogging torque optimization in surface-mounted permanent-magnet motors by using design of experiment," *Energy Conversion and Management*, vol. 52, pp. 3075-3082, 2011.
115. N. Bianchi and S. Bolognani, "Design techniques for reducing the cogging torque in surface-mounted PM motors," *IEEE Trans. Magn*, vol.38, no. 5, pp. 1259–1265, Sep./Oct. 2002.
116. X. T. Jiang, X. W. Xing, Y. Ling, and Y. P. Lu, "Theoretical and simulation analysis of influences of stator tooth width on cogging torque of BLDC motors," *IEEE Trans. Magn.*, vol. 45, no. 10, pp. 4601–4604, Oct. 2009.
117. L. Zhu, S. Z. Jiang, Z. Q. Zhu, and C. C. Chan, "Analytical methods for minimizing cogging torque in permanent magnet machines," *IEEE Trans. Magn.*, vol. 45, no. 4, pp. 2023–2030, Apr. 2009
118. Y. Yang, X. Wang, R. Zhang, T. Ding, and R. Tang, "The optimization of pole arc coefficient to reduce cogging torque in surface-mounted permanent magnet motors," *IEEE Trans. Magn.*, vol. 42, no. 4, pp. 1135–1138, Apr. 2006
119. Y. Yang, X. Wang, R. Zhang, C. Zhu, and T. Ding, "Research of cogging torque reduction by different slot width pairing permanent magnet motors," in *2005 Proc. ICEMS 2005 Conf.*, pp. 367–370.
120. Y. Wang, M. J. Jin, W. Z. Fei, and J. X. Shen, "Cogging torque reduction in permanent magnet flux-switching machines by rotor teeth axial pairing," *Elect. Power Appl. (IET)*, vol.4, no. 7, pp. 500-506, Jun. 2010.
121. Z. Q. Zhu and D. Howe, "Influence of design parameters on cogging torque in permanent magnet motors," *IEEE Trans. Energy Convers.*, vol. 15, no. 4, pp. 407–412, 2000. 1585
122. W. Hua and M. Cheng, "Cogging torque reduction of flux switching permanent magnet machines without skewing," in *Proc. 8th Int. Conf. Elect. Mach. Syst. (ICEMS)*, 2008, vol. 1, pp. 3020-3025.

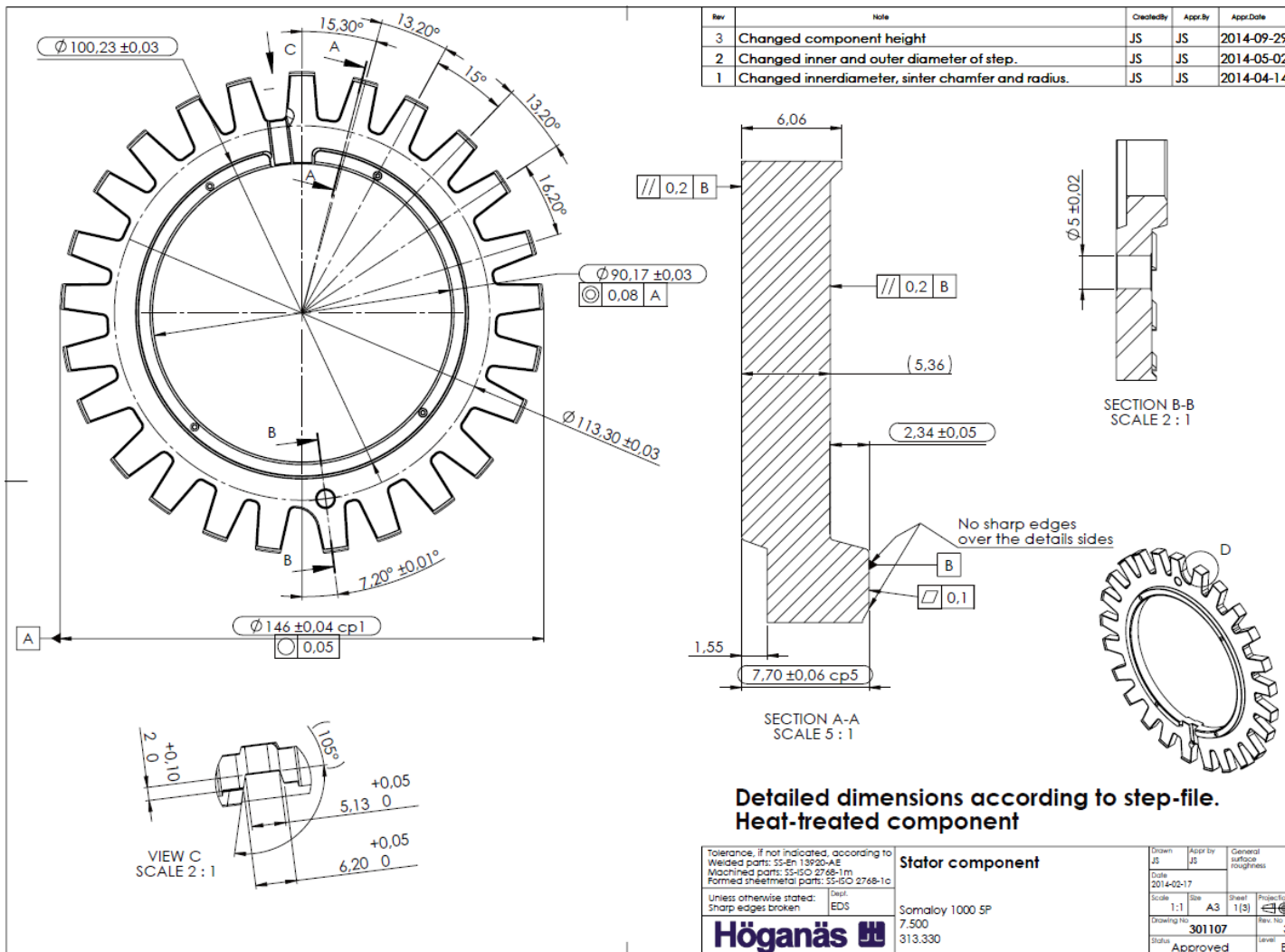
123. M. j. Jin, Y. Wang, J. x. Shen, P. C.K. Luk, W.Z. Fei, and C.F. Wang, "Cogging torque suppression in a permanent magnet flux-switching intergrated-starter generator," *Elect. Power Appl. (IET)*, vol. 4, no, 8, pp. 647-656, 2010.
124. Daohan Wang, Xiuhe Wang, and Sang-Yong Jung, "Reduction of coring torque in Flux-Switching Permanent Machine by Teeth Notching Schemes," *IEEE Trans. Magn.*, vol. 48,no. 11, pp. 4228-4231, 2012.
125. Z. Q. Zhu, A. S. Thomas, J.T. Chen, and G. W. Jewell, "Cogging torque in flux-switching permanent magnet machines," *IEEE Trans. Magn.*, vol. 45, no. 10, pp. 4708-4711, 2009.
126. Li Hao; Mingyao Lin; Xu, D.; Wei Zhang; Nian Li, "Rotor design techniques for reducing the cogging torque in a novel dual-rotor axial field flux-switching permanent magnet machine," in *Electrical Machines and Systems (ICEMS), 2014 17th International Conference on* , vol., no., pp.1581-1586, 22-25 Oct. 2014
127. Favre E, Cardoletti L, Jufer M. Permanent-magnet synchronous motor: a comprehensive approach to cogging torque suppression. *IEEE Transactions on Industry Applications* 1993; 1A-29(6):1141–1149
128. De La Ree J, Boules N. Torque production in permanent-magnet synchronous motors. *IEEE Transactions on Industry Applications* 1989; 1A-25(1):107–112.
129. Keyhani A, Studer CB, Sebastian T, Murthy SK. Study of cogging torque in permanent magnet machines. *Electrical Machines and Power System* 1999; 27(7):665–678.
130. Zhu ZQ, Howe D. Influence of design parameters on cogging torque in permanent magnet machines. *IEEE Transactions on Energy conversion* 2000; EC-15(4):407–412.
131. Huang S, Luo J, Lipo TA. Analysis and evaluation of the transverse flux circumferential current machine. *Proceedings of IEEE IAS Annual Meeting, New Orleans/USA, 1997*; pp. 241–247.
132. Masmoudi A, Elantably A. The sizing of TFPM machines for bus and truck hybrid vehicle applications. *16th Electric Vehicle Symposium (EVS), Beijing/China, 1999, CD-ROM.*

133. Washington, J., "A Modulated Pole Machine Topology exploiting mutual flux paths," Engineering Doctorate Thesis, Newcastle University, 2012.
134. M. S. Islam, S. Mir, T. Sebastian, and S. Underwood, "Design considerations of sinusoidally excited permanent-magnet machines for low torque- ripple applications," *IEEE Trans. Ind. Appl.*, vol. 41, no. 4, pp. 955–962, Jul./Aug. 2005.
135. M. Dai, A. Keyhani, and T. Sebastian, "Torque ripple analysis of a PM brushless DC motor using finite element method," *IEEE Trans. Energy Convers.*, vol. 19, no. 1, pp. 40–45, Mar. 2004.
136. Z. Azar and Z. Q. Zhu, "Influence of Electric loading and Magnetic Saturation on Cogging Torque, Back EMF and Torque Ripple of PM Machines," *IEEE Trans. Magnetics*, Vol. 48, No. 10, October 2012.
137. Z. Q. Zhu and D. Howe, "Influence of design parameters on cogging torque in permanent magnet machines," *IEEE Trans. Energy Convers.*, vol. 15, no. 4, pp. 407–412, Dec. 2000.
138. T. Li and G. Slemon, "Reduction of cogging torque in permanent magnet motors," *IEEE Trans. Magn.*, vol. 24, no. 6, pp. 2901–2903, Nov. 1988.
139. K. H. Kim, D. J. Sim, and J. S. Won, "Analysis of skew effects on cogging torque and BEMF for BLDCM," in *Proc. IEEE Industry Applications Soc. Annu. Meeting*, 1991, vol. 1, pp. 191–197.
140. D. C. Hanselman, "Effect of skew, pole count and slot count on brushless motor radial force, cogging torque and back-emf," in *Proc. IEEE Electric Power Appl. Conf.*, 1997, vol. 144, pp. 325–330.
141. Z. Q. Zhu, S. Ruangsinchaiwanich, N. Schofield, and D. Howe, "Reduction of cogging torque in interior-magnet brushless machines," *IEEE Trans. Magn.*, vol. 39, no. 5, pp. 3238–3240, Sep. 2003.
142. R. Islam, I. Husain, A. Fardoun, and K. McLaughlin, "Permanent magnet synchronous motor magnet designs with skewing for torque ripple and cogging torque reduction," *IEEE Trans. Ind. Appl.*, vol. 45, no. 1, pp. 152–160, Jan./Feb. 2009.
143. T. M. Jahns and W. L. Soong, "Pulsating torque minimization technique for permanent magnet AC motor drive—A review," *IEEE Trans. Ind. Electron.*, vol. 43, no. 3, pp. 321–330, Apr. 1996.
144. T. M. Jahns and W. L. Soong, "Pulsating torque minimization techniques for permanent magnet ac motor drives—A review," *IEEE Trans. on Power Electronics*, vol. 43, no. 2, pp. 321–330, 1996.

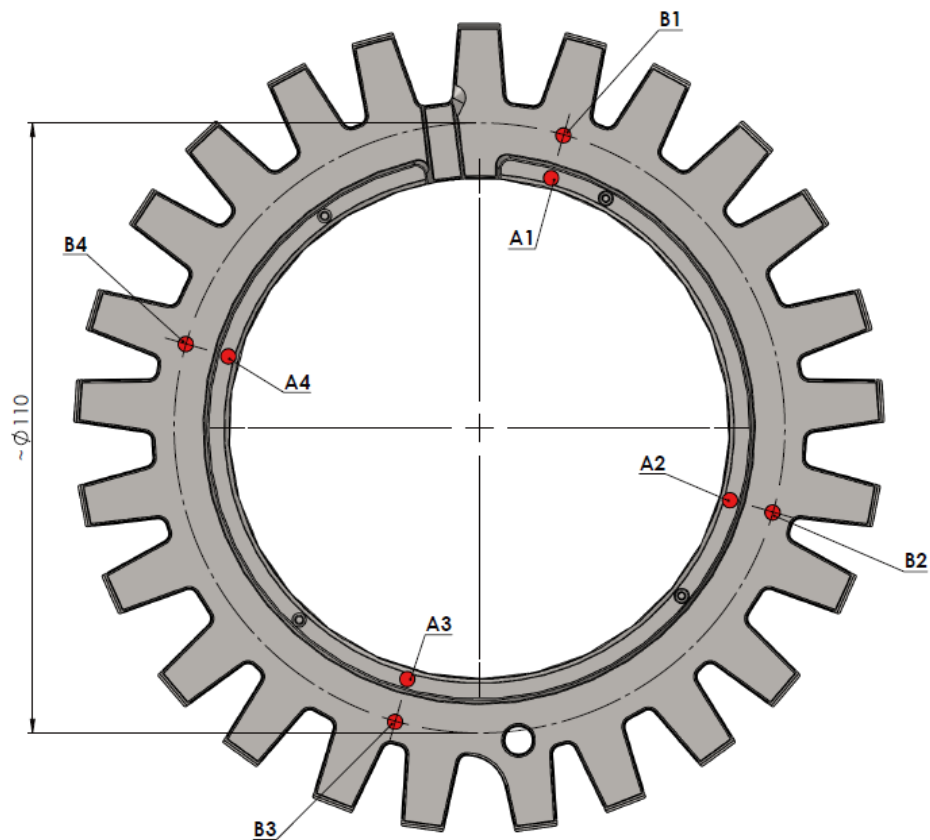
145. J. De La Ree and N. Boules, "Torque production in permanent magnet synchronous motors," *IEEE Trans. on Industry Applications*, vol. 25, no. 1, pp. 107–112, 1989.
146. R. P. Deodhar, D. A. Staton, T. M. Jahns, and T. J. E. Miller, "Prediction of cogging torque using the flux-mmF diagram technique," *IEEE Trans. on Industry Applications*, vol. 32, no. 3, pp. 569–576, 1996.
147. Z. Q. Zhu and D. Howe, "Effect of slot and pole number on cogging torque in permanent magnet machines," in *Proc. of 2nd Chinese Int. Conf. on Electrical Machines*, Hangzhou, 1995, pp. 390–394.
148. T. Li and G. Slemon, "Reduction of cogging torque in permanent magnet motors," *IEEE Trans. on Magnetics*, vol. 24, pp. 2901–2903, 1988.
149. H. Jia, M. Cheng, W. Hua, W. Zhao, and W. Li, "Torque ripple suppression in flux-switching PM motor by harmonic current injection based on voltage space-vector modulation," *IEEE Trans. Magn.*, vol. 46, no. 6, pp. 1527–1530, Jun. 2010.
150. D. Wang, X. Wang, D. Qiao, Y. Pei, and S.-Y. Jung, "Reducing cogging torque in surface-mounted permanent magnet motors by non-uniformly distributed teeth method," *IEEE Trans. Magn.*, vol. 47, no. 9, pp. 2231–2239, Sep. 2011.
151. M.-F. Hsieh, D. G. Dorrell, Y.-H. Yeh, and S. Ekram, "Cogging torque reduction in axial flux machines for small wind turbines," in *Proc. 35th IEEE Annu. Conf. Ind. Elect. (IECON)*, 2009, pp. 4435–4439.
152. Wei Hua, Ming Cheng, Z.Q. Zhu, et al, "Analysis and Optimization of Back-EMF Waveform of A Novel Flux-Switching Permanent Magnet Motor", *Proc. IEEE International Electric Machines and Drives Conference*, 3-5 May, 2007, pp. 1025-1030.
153. Y. Wang, M. J. Jin, W. Z. Fei, and J. X. Shen, "Cogging torque reduction in permanent magnet flux-switching machines by rotor teeth axial pairing," *Elect. Power Appl. (IET)*, vol. 4, no. 7, pp. 500–506, Jun. 2010.
154. W. Hua and M. Cheng, "Cogging torque reduction of flux-switching permanent magnet machines without skewing," in *Proc. 8th Int. Conf. Elect. Mach. Syst. (ICEMS)*, 2008, vol. 1, pp. 3020–3025.
155. D. Wang; X. Wang; Sang-Yong Jung; , "Reduction on Cogging Torque in Flux-Switching Permanent Magnet Machine by Teeth Notching Schemes," *Magnetics, IEEE Transactions on* , vol.48, no.11, pp.4228-4231, Nov. 2012

156. Chandan Sikder, Iqbal Husain, Wen Ouyang, "Cogging Torque Reduction in Flux Switching permanent magnet machines by rotor pole shaping", IEEE Transactions on Industry Applications, Vol. 51, No. 5, September/October 2015.
157. C. W. Lu, B. J. Chalmers, A. C. Renfrew and S. Huang, "Novel Approach to Current Profiling for AC Permanent Magnet Motors," IEEE Trans. on Energy Conversion, vol. 14, No. 4, pp. 1294-1299, December 1999.
158. H. Akagi, Y. Kanazawa, and A. Nabae, "Instantaneous reactive power compensators comprising switching devices without energy storage", IEEE Trans. On Industry Applications, vol. 20, issue 3, pp. 625-630, May 1984.
159. Infolytica Live Documents (Magnet user guide). [Online]. Available: <http://www.infolytica.com/>.
160. John Petro, "Achieving High Electric motor efficiency", EEMODS 2011 – Paper 060, Nova Torque, Inc.

Appendix A – Stator component



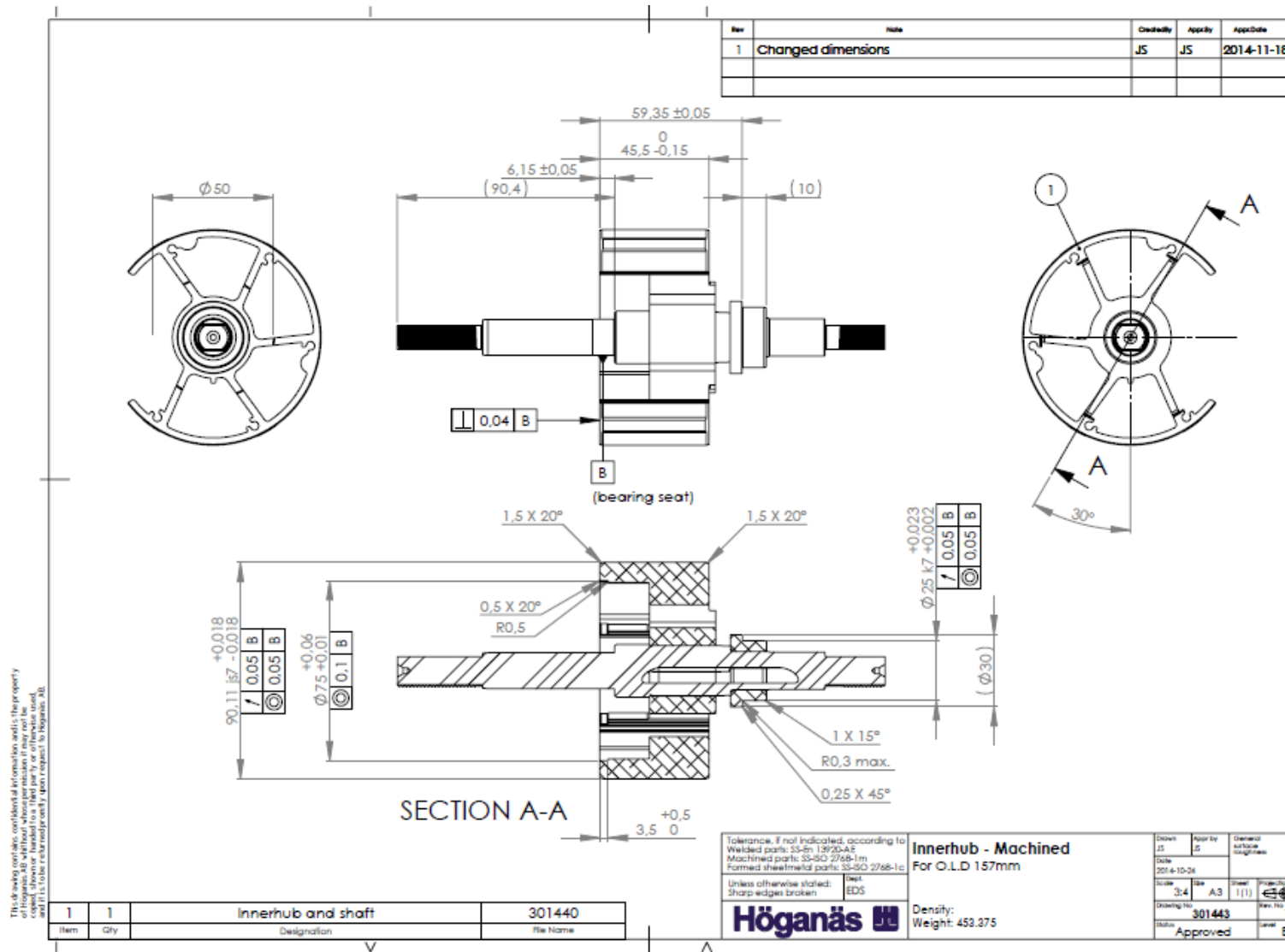
Rev	Note	CreatedBy	Appr.By	Appr.Date
3	Changed component height	JS	JS	2014-09-29
2	Changed inner and outer diameter of step.	JS	JS	2014-05-02
1	Changed innerdiameter, sinter chamfer and radius.	JS	JS	2014-04-14



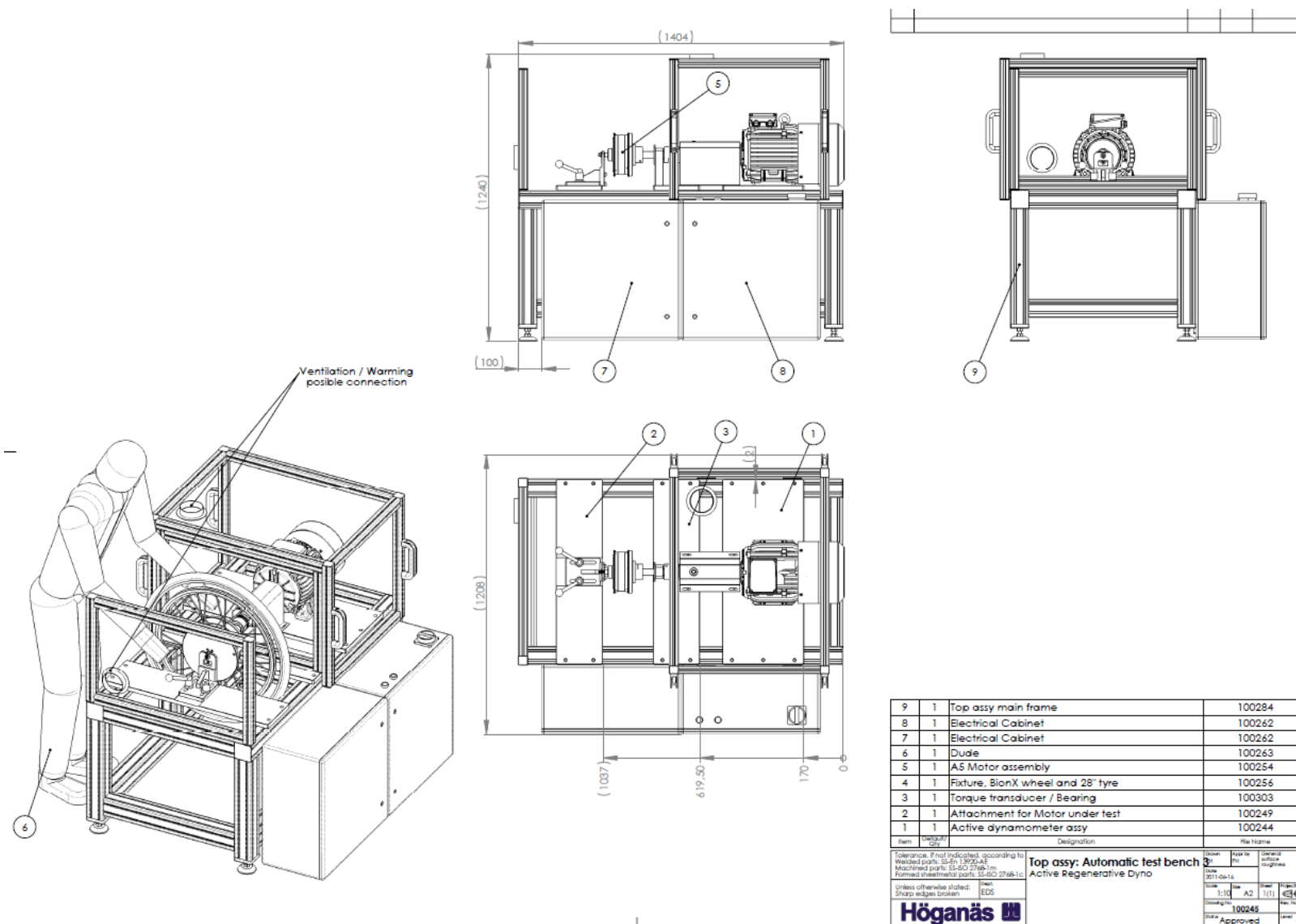
Measure points

Tolerance, if not indicated, according to Welded parts: SS-En 13920-AE Machined parts: SS-ISO 2768-1m Formed sheetmetal parts: SS-ISO 2768-1c		Stator component		Drawn JS	Appr by JS	General surface roughness			
Unless otherwise stated: Sharp edges broken				Dept. EDS	Somaloy 1000 5P 7.500 313.330		Code 2014-03-20	Scale 4:3	Size A3
				Drawing No 301107	Rev. No 3	Status Approved		Level B	

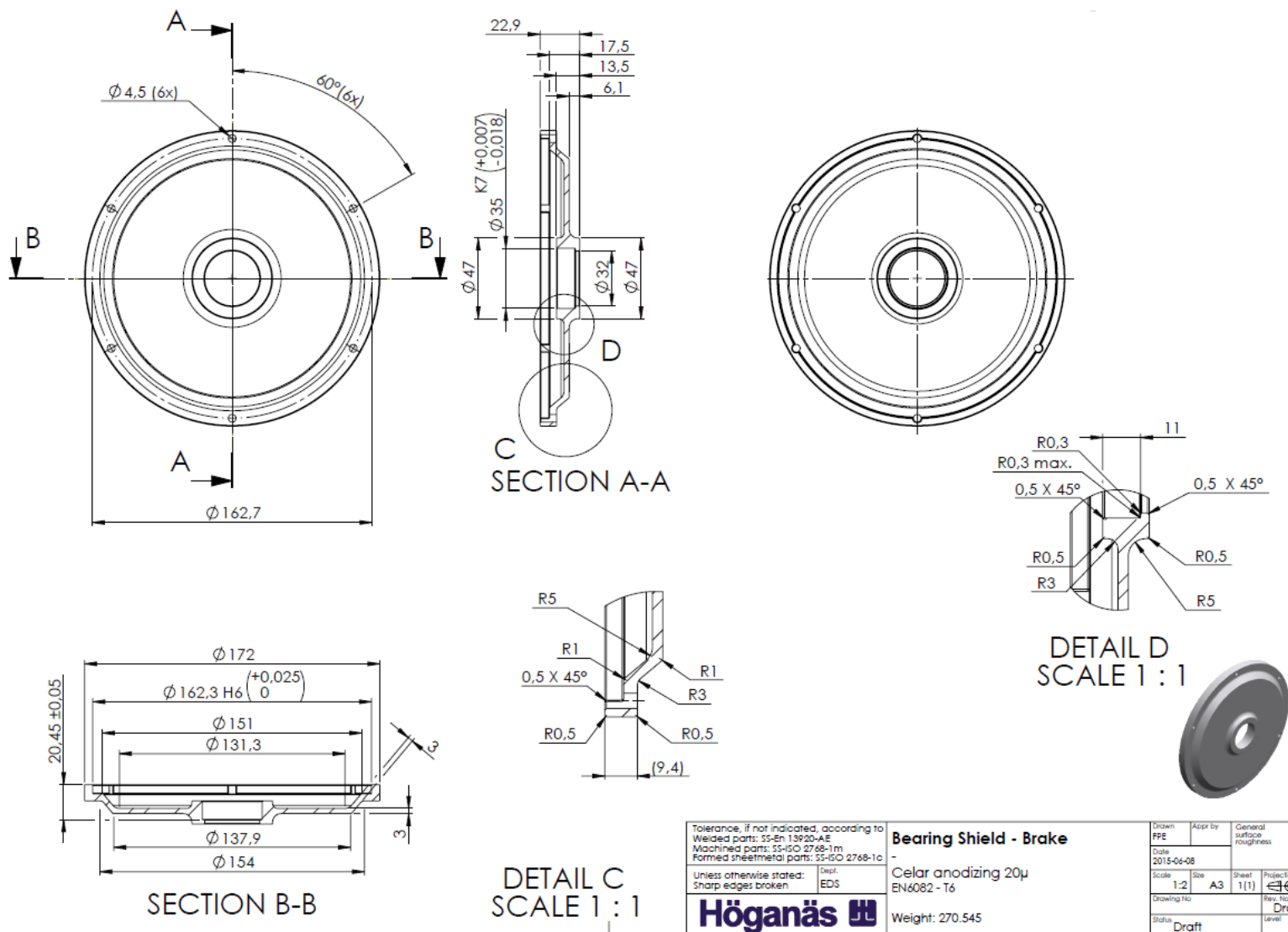
Appendix B – The Shaft



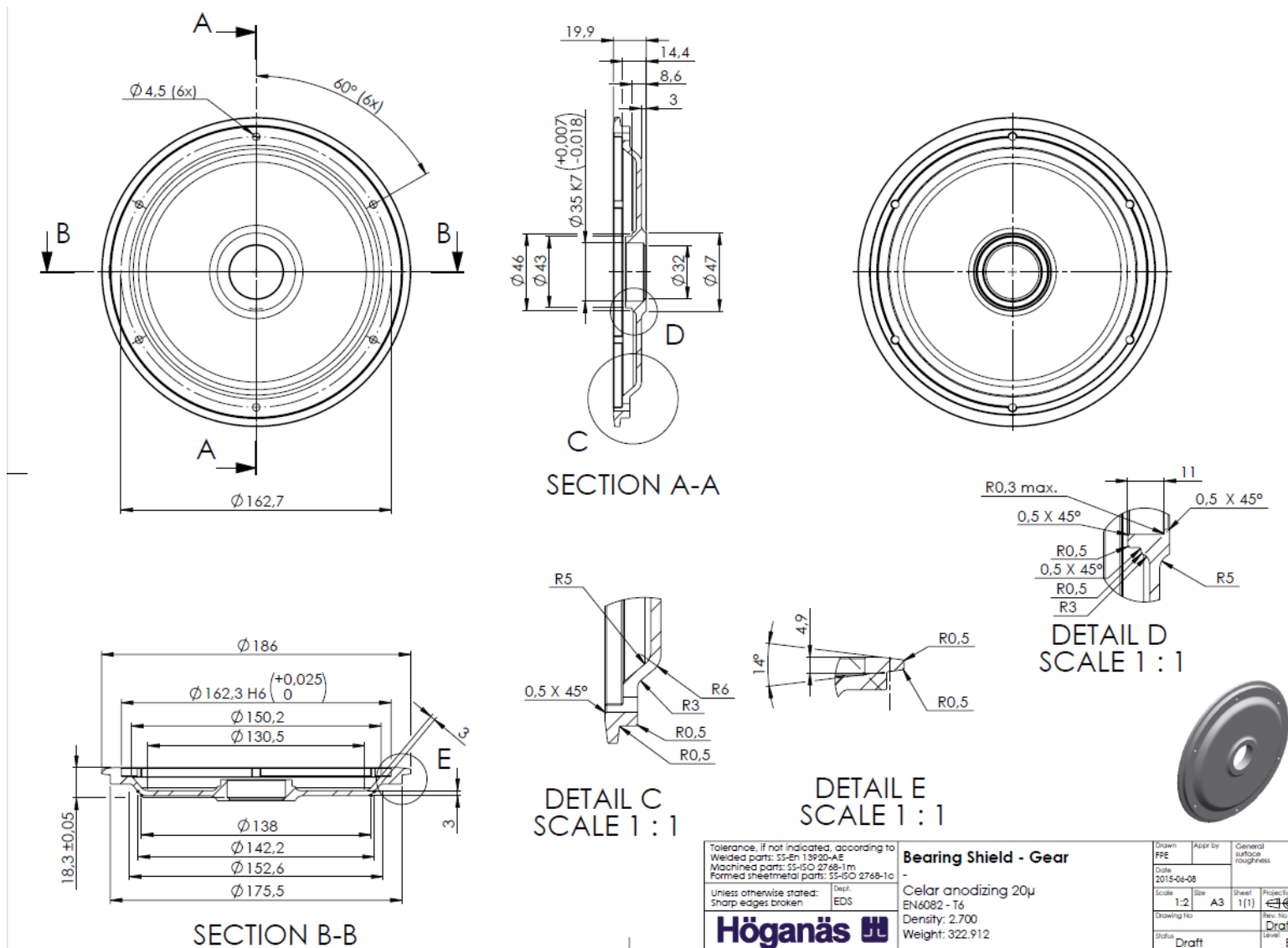
Appendix D – Motor Test Bench Rig drawings



Bearing Shield - Cable Side



Bearing Shield - Coupling Side



Pole piece designs

